



NVE

EKSTERN RAPPORT NR. 9 / 2024

Åknes rock-slope failure hydrogeology

Åknes rock mass characterization, January-July 2020

SKREVET AV Clara Sena, Alvar Braathen and Ioannis Papadimitrakis

NVE Ekstern rapport nr. 9/2024

Åknes rock-slope failure hydrogeology : final report

Åknes rock mass characterization, January-July 2020

Published by: The Norwegian Water Resources and Energy Directorate
Authors: Åknes rock-slope failure hydrogeology: Clara Sena and Alvar Braathen
Åknes rock mass characterization: Ioannis Papadimitrakis
Cover photo: Sunnlyvsfjorden seen from Åknes. Photo: Gustav Pless/NVE

ISBN: 978-82-410-2292-0
ISSN: 2535-8235
Case number: 202103882

Summary: To understand the rock slope hydrology at Åknes a collaboration between NVE and UiO was initiated where Clara Sena and Alvar Braathen lead the project. Several master theses at UiO were a part of this project which is summarized in the report. The rock mass characterization work by Ioannis Papadimitrakis is shown in the second document containing the presentation slides.

Keywords: Åknes, Drenering, Grunnvann, Hydrologi, Hydrogeologi, Fjellskred

The Norwegian Water Resources and Energy Directorate
Middelthuns gate 29
P.O. Box 5091 Majorstuen
N-0301 Oslo

Telephone: 22 95 95 95
E-mail: nve@nve.no
Internet: www.nve.no

Mars 2024

Forord

Norges Vassdrags- og Energidirektoratet (NVE) vedtok i 2017 å utrede grunnvannsforholdene på Åknes nærmere, for å utrede muligheten av å stabilisere det ustabile fjellpartiet gjennom drenering av grunnvann. I denne sammenheng har Universitetet i Oslo (UiO) og NVE inngått et samarbeid for å videre undersøke de hydrogeologiske forholdene ved Åknes, og utvikle en numerisk grunnvannsmodell. Denne rapporten oppsummerer resultatene oppnådd fra mai 2017 til desember 2020.

Borehullsdata, grunnvann og meteorologiske data innhentet av NVE, er grundig undersøkt i dette prosjektet. I tillegg ble det gjennomført flere feltkampanjer 2017 til 2019 av UiO-ansatte og studenter. Disse feltkampanjene ga viktige datasett relatert til grunnvannspåfyllings- og utslippsrater.

Resultatene fra datainnsamlingen ble samlet i en tredimensjonal numerisk modell som simulerer steady-state forholdene til grunnvannsstrømmen i Åknes, i vannmettet sone, for en gjennomsnittlig årlig nedbørsrate på 1352 mm/år (normalperiode 1960-1990). Den numeriske modellen stemmer godt overens med observerte grunnvannsnivåer, og utslippssoner for grunnvann (kilder).

Resultatene som er oppnådd i den numeriske modellen for grunnvannsstrømning i Åknes bekrefter to hovedhypoteser: (1) infiltrasjonen i baksprekken er mye høyere enn i resten av den ustabile skråningen; og, (2) sprekkesett forårsaket av forskyvning av den ustabile massen genererer "grunnvannsbarrierer" som opprettholder et relativt høyt grunnvannsspeil i øvre deler av det ustabile fjellpartiet.

Overflateavrenningen som infiltrerer i baksprekken er en viktig kilde til oppsamling av grunnvann til massen som beveger seg raskest. Avskjæring av denne tilførselen vil forventes å ha en positiv effekt på stabiliseringen av den raskest bevegelige massen, og borehullene som allerede er på plass gjør at vi kan vurdere virkningen av denne handlingen.

Oslo, mars 2024

Gustav Pless
senioringeniør
Skredseksjonen

Dokumentet sendes uten underskrift. Det er godkjent i henhold til interne rutiner.

Åknes rock-slope failure hydrogeology

Final report

By Clara Sena and Alvar Braathen



UiO : Universitetet i Oslo

Final report on the collaboration project between the Department of
Geosciences, University of Oslo (UiO) and the Norges vassdrags- og
energidirektorat (NVE)

March 2021

Abstract

In 2017, the Norges Vassdrags- og Energidirektorat (NVE) decided to study in more detail the groundwater conditions in Åknes in order to assess the feasibility of a drainage operation that seeks to increase the rockslide stability. In this context, the University of Oslo (UiO) and NVE joined a collaboration in order to further investigate the hydrogeological conditions at Åknes rock-slope and develop a groundwater flow numerical model. This is the final report produced in the frame of this collaboration agreement, compiling the results achieved from May 2017 to December 2020.

Borehole data (rockmass properties and fracture frequency), groundwater and meteorological monitoring data acquired and archived by NVE have been thoroughly investigated in this project. Moreover, several field-campaigns were done in the spring and autumn of the years 2017 to 2019 by UiO staff and students. These field-campaigns supplied crucial complementary datasets related to the groundwater recharge and discharge rates.

The results of the data harvesting were integrated in a three-dimensional numerical model that simulates the steady-state conditions of the groundwater flow in Åknes, in the water-saturated zone of the rock slope, for an average annual precipitation rate of 1352 mm/yr (Normal period 1960-1990). This numerical model agrees well with the range of observed groundwater levels, and location of the main springs (i.e. groundwater discharge zones).

The results obtained in the numerical model of groundwater flow in Åknes confirm two major hypotheses: (1) the recharge rate in the backscarp is much higher than in the rest of the unstable slope, due to the infiltration of surface runoff originated from the mountain ridge; and, (2) tension fractures caused by the displacement of the unstable rockmass generate “groundwater barriers” which sustain a relatively high water table at high elevation in the unstable rock slope.

The surface runoff infiltrating in the backscarp is a major source of groundwater recharge to the fastest moving rock mass. Cutting-off this supply to the groundwater in Åknes would expectedly have a positive effect on the stabilization of the fastest moving rock mass, and the boreholes already in place allow us to assess the impact of this action. Tension fractures generating natural groundwater barriers should be the second most preferred targets after the backscarp, in a drainage operation that seeks the improved stabilization of the slope.

Acknowledgements

We would like to thank NVE staff for the technical support at Åknes and Stranda, and the UiO master students Frida Biørn-Hansen, Stig Runar Ringstad and Halvor Bruun for their enthusiasm and commitment during the field-campaigns in Åknes, and the work they have done in each of their master theses. Thanks also to Pierre-Etienne Privat, who made an internship at UiO, and Malan Ellefsen, a PhD candidate at NTNU, who joined a field-campaign in August 2019.

Ioannis Papadimitrakis is also acknowledged by his work on the processing and analysis of the time-series of groundwater levels and meteorological data from the instrumentation installed in Åknes; and the analysis and integration of the borehole data (lithology, fracture frequency from data geological logging and optical televiewer logging) which were subsequently integrated into fracture facies and litho-structural classification.

All the data collected, processed and analysed by the abovementioned people was crucial for the development of the three-dimensional model of the rockmass domains and fracture corridors, and ultimately, the conceptual and numerical models of the groundwater flow in Åknes.

We acknowledge the thorough revision of this report done by Carlos Miraldo Ordens which greatly contributed to improve its content.

Notation

°C. Celsius degrees	mm/yr. Millimeters per year
BSS. Basal Sliding Surface	MSH. Middle Spring Horizon
Comma (,) is the thousands separator	NE. Northeast
EC. Electrical conductivity	NNE. North Northeast
ERT. Electrical Resistivity Tomography	P+SM. Bulk Precipitation and Snowmelt
ES. Eastern Stream	PET. Potential Evapotranspiration
FFM. Fracture frequency, number of fractures per meter	pH. Acid-base measure, negative of the base 10 logarithm of the concentration of the hydrogen cation
GW. Groundwater	Point (.) is the decimal separator
GPR. Ground Penetrating Radar	QGIS. Free and Open Source Geographic Information System
l/s. Litres per second	SR. Surface Runoff
LES. Lower Eastern Stream	SSW. South Southwest
LSH. Lower Spring Horizon	SW. Southwest
masl. Meters above mean sea-level	UES. Upper Eastern Stream
mbg. Meters below ground	USH. Upper Spring Horizon
mbTOC. Meters below top of casing of the borehole	
mm/d. Millimeters per day	

List of Contents

Abstract	i
Acknowledgements.....	ii
Notation	iii
List of Contents.....	iv
List of Figures.....	v
List of Tables.....	vii
1. Introduction.....	1
1.1. Context and motivation.....	1
1.2. Aim and goals	1
1.3. Location of Åknes unstable slope.....	2
1.5. Overview of the project timeline	3
2. Data harvesting	5
2.1. Data managed by NVE	5
2.2. Previous work on the Åknes unstable rock-slope	8
2.3. Previous work on Åknes hydrogeology	11
2.4. Field-campaigns led by UiO	13
2.5. Field-work and data collection challenges	17
2.6. Geographical Information System.....	18
3. Results and discussion.....	21
3.1. Rockmass characterization	21
3.1.1. Borehole data	21
3.1.2. Conceptual model of the fractured rockmass	26
3.2. Time-series	30
3.2.1. Groundwater levels and meteorological data	30
3.2.2. Multi-level data from KH-02-17	35
3.3. Groundwater chemistry	38
3.3.1. Physico-chemical parameters and springs' discharge	38
3.3.2. Major elements	40
3.4. Groundwater recharge	41
3.4.1. Conceptual model of the groundwater recharge	41
3.4.2. Estimation of the average groundwater recharge rate	44

3.5.	Three-dimensional numerical model of groundwater flow	51
3.5.1.	Boundary conditions and numerical grid	51
3.5.2.	Hydraulic parameterization of the modelled rockmass.....	54
3.5.3.	Numerical model results	59
3.5.4.	Refinement of the conceptual model informed by the numerical modelling ...	65
3.5.5.	Model evaluation	66
4.	Other project outputs	68
5.	Limitations and future work.....	69
6.	Concluding remarks and recommendations	71
7.	References.....	73
	Appendix.....	77

List of Figures

Figure 1.	Location of Åknes unstable rock-slope, and photo of the slope seen from Oaldsbygda (Grøneng et al., 2010). Unstable area: white line, Sliding planes: red lines (Ganerød et al., 2008). Maps modified from Google maps.	2
Figure 2.	Monitoring instrumentation in Åknes. The location of the streams is from Frei (2008), and interpretation of the backscarp and sliding planes is from Ganerød et al. (2008).....	7
Figure 3.	Conceptual hydraulic potential field with visually interpolated equipotential lines and flow lines beginning at the tracer injection points (Frei, 2008).....	12
Figure 4.	Location of the hydrogeology and structural geology monitoring points on a hillshade map. LSH, MSH & USH: Lower, Middle and Upper Spring Horizons; LES, UES: Lower and Upper Eastern Stream. Data source: water monitoring (Biørn-Hansen, 2019); structural geology stations (Ringstad, 2019; Bruun, 2019)	16
Figure 5.	Illustration of the procedure to measure the flow-rate in the point LS1 (images (a) and (b)); and, LS6 (image c), both located in the Lower Spring Horizon. The arrow indicates: in (a) the point where the bucket with a volume scale is inserted; in (b) the top of the cloth fixed with stones; and in (c) the fixation of a small cloth when the flow-rate is relatively low.....	18
Figure 6.	Lithological units logged in core photographs (from Papadimitrakakis, 2020). Borehole code is on top of each log. “KH” was removed from the borehole code for simplicity. Boreholes are aligned according to their elevation in the unstable slope. References: ⁽¹⁾ NGI (2020a); ⁽²⁾ Elvebakk (2008), and Elvebakk and Pless (2018); ⁽³⁾ NGI (2020b).....	22
Figure 7.	Fracture frequency (FFM, number of fractures per meter) for the five boreholes with the two logging data sets: geological and optical televiewer (Papadimitrakakis, 2020).	24

Figure 8. Workflow for the correction of the fracture frequency data for the boreholes without optical televiewer log.	24
Figure 9. Fracture frequency classes (FFM, number of fractures per meter) for the twelve boreholes drilled in Åknes (from Papadimitrakakis, 2020). Borehole code is on top of each log. “KH” was removed from the borehole code for simplicity. Boreholes are aligned according to their elevation in the unstable slope. ⁽¹⁾ NGI (2020a); ⁽²⁾ Elvebakk (2008), and Elvebakk and Pless (2018); ⁽³⁾ NGI (2020b).	25
Figure 10. Seismic refraction profile, interpreted fractured bedrock and fracture zones from Tassis and Rønning (2019) with projection of the fracture frequency classes: Borehole data are either intersected or projected into the cross-section. Location of the profile is shown in the inserted aerial photograph.	27
Figure 11. Main sub-vertical structures in Åknes, as depicted from the integration of field-observations, borehole and geophysical data. Seismic and ERT-interpreted zones are from Tassis and Rønning (2019). Location of streams is from Frei (2008) and Biørn-Hansen (2019).	28
Figure 12. Three-dimensional model of the shear zones in Åknes (not to scale). Depth (in mbg) of: the shear zones in red; the highest water-table in blue; and, the water-table after drilling in green. In parenthesis, water-table elevation in masl. Shear zones’ depth from NGI (2020a) and water-table after drilling from NGI (2020b).	29
Figure 13. Time-series of the groundwater level measured in the boreholes KH-01-05, KH-02-06, KH-04-05, KH-03-06, precipitation and air temperature.	33
Figure 14. Time-series of the groundwater level measured in the boreholes KH-01-06, KH-01-12, KH-02-17, precipitation and air temperature.	34
Figure 15. Time-series of selected pressure sensors from the multi-level borehole KH-02-17. Borehole sketch for location of the pressure sensors (red dots) and packers (black lines). FFM is shown for characterization of the fractured rockmass.	37
Figure 16. Flow-rate, EC, pH and temperature in each spring horizon; and, daily precipitation and air temperature at the Åknes meteorological station, for the spring-summer of 2018 and 2019.	39
Figure 17. Piper diagram for the water samples collected at Åknes (from Biørn-Hansen, 2019).	41
Figure 18. Identification of groundwater recharge processes (a) between the mountain ridge and backscarp, and (b) downslope from the backscarp. Blue arrows and dashed line indicate the surface water divide that runs along the mountain ridge. Elevation contours (in masl) in black, and hydrogeology monitoring points in red.	43
Figure 19. Identification of the backscarp properties that contribute to groundwater recharge. Dashed lines: red – graben; blue – open fractures; black – rocky cliff, 10 to 20 m high.	44
Figure 20. Groundwater recharge rates estimated for the three sub-areas in the unstable slope, with an average bulk precipitation and snowmelt of 1352 mm/yr (Normal period 1960-1990). White dashed line delimits the fastest moving rockmass.	50

Figure 21. Boundary conditions and grid discretization of the 3D numerical model of groundwater flow. The orientation of the numerical grid axes (I, J, K) is given in blue.	53
Figure 22. Calibrated values of the horizontal hydraulic conductivity (K_i , in m/d). This is the hydraulic conductivity parallel to the slope dip direction. Purple dots on the map view of Layer 1 indicate “drain” boundary condition.	56
Figure 23. Calibrated values of the anisotropy factor between the two horizontal hydraulic conductivities (K_i/K_j , dimensionless). An anisotropy of one means isotropic. Note how the higher anisotropy (lower values of K_i/K_j , between red and green in the colour scale) was assigned to the backscarp area and other areas dominated by tension fractures. Purple dots on the map view of Layer 1 indicate “drain” boundary condition.	57
Figure 24. Calibrated values of the vertical hydraulic conductivity (K_v , in m/d). Purple dots on the map view of Layer 1 indicate “drain” boundary condition.....	58
Figure 25. Computed hydraulic head for the three layers of the model domain. The hydraulic head in Layer 1 corresponds to the (unconfined) water-table. In the map view of Layer 1, the location of the Upper and Lower Eastern Stream (UES, LES), and Middle and Lower Spring Horizons (MSH, LSH) is shown.....	60
Figure 26. WSW-ENE cross-sections at two elevations in the slope showing computed water table slightly above the terrain in the Upper and Lower Eastern Stream (UES and LES, respectively).	61
Figure 27. Comparison between computed water-table (i.e., the computed hydraulic head in Layer 1) and the range measured in seven boreholes.	63
Figure 28. Corrected fracture frequency for the boreholes without televiewer log (2005 to 2006) and the average fracture frequency for the boreholes with both datasets (2012 to 2018).	78
Figure 29. Borehole KH-01-17 sketch, and time-series of the pressure sensors.	79
Figure 30. Borehole KH-01-18 sketch, and time-series of the pressure sensors.	80
Figure 31. Borehole KH-02-18 sketch, and time-series of the pressure sensors.	81
Figure 32. Time-series of daily precipitation, from November 2004 to September 2019, at the Åknes meteorological station.	82
Figure 33. Time-series of average daily air temperature, from November 2004 to September 2019, at the Åknes meteorological station.	82

List of Tables

Table 1. Timeline of the project work plan, and deliverable reports.	3
Table 2. Properties of the Åknes unstable rock-slope compiled from previous works.	10
Table 3. Overview of the field-campaigns done throughout the project duration.	14
Table 4. Summary of the time-series of groundwater levels at Åknes.	31
Table 5. Summary of the estimated natural hydraulic gradient of the water-table in Åknes.	35

Table 6. Ranges of the field-parameters (pH, temperature and EC) and flow-rate measured in the main springs and Eastern Stream at Åknes, in the spring-summer of 2018 and 2019.	40
Table 7. Average monthly precipitation (from www.xgeo.no) and potential evapotranspiration, estimated for Åknes using the Thornthwaite method (Biørn-Hansen, 2019).	45
Table 8. Estimation of the surface runoff generated between the mountain ridge and the backscarp that infiltrates in the unstable rock mass, $C = (A/1000) \times B$	46
Table 9. Calculation of the groundwater recharge rate for the three sub-areas defined in the unstable slope, with an average bulk precipitation and snowmelt of 1352 mm/yr (Normal period 1960-1990).....	48
Table 10. Estimated monthly discharge rate (in l/s, unless another unit is mentioned) at the main springs of the unstable slope; Middle Spring Horizon (MSH), Lower Spring Horizon (LSH), and Upper Eastern Stream (UES).	64

1. Introduction

1.1. Context and motivation

Norwegian rock-slope failures have been studied systematically the last 15 years, meeting public demands to address natural hazards for the local population. A comprehensive mapping program (step 1) and subsequent monitoring (step 2) of selected, hazardous slope-failures have brought the Norwegian geoscience and engineering community to the international forefront in this type of studies; as of today, in many aspects Norway is leading this field of science. Expertise is found within NVE (responsible government department), Geological Survey of Norway (NGU), institutes (NGI, Sintef) and private engineering companies, whereas some related research is undertaken at the universities in Tromsø and Oslo.

At this stage, a new Research and Development (R&D) avenue on rock-slope-failures is under developed; hydrogeology (step 3), as a fundamental knowledge that sustains the feasibility assessment of water drainage activities with the purpose of increasing stability and reduce risk for slope-failure. In 2017, NVE decided to study in more detail the groundwater conditions in Åknes in order to assess the feasibility of a drainage operation that seeks to increase the rock-slope stability. Therefore, Åknes is the first site to be investigated in Norway for this purpose (Blikra, 2012), and will with time form the baseline for similar studies elsewhere.

With a focus on the Åknes rock-slope failure, the UiO and NVE joined collaboration in 2017 in order to further investigate the hydrogeological conditions at Åknes rock-slope, and develop a hydrogeological numerical model. The work presented here is the final report of this collaboration.

1.2. Aim and goals

The research and development work developed at UiO on the Åknes rock-slope hydrogeology seeks to fill knowledge gaps on the specific hydrogeological conditions at Åknes, and develop new numerical modelling methods that suit the specific characteristics of rock-slope hydrogeology, such as steep topographic surface, highly heterogeneous fractured and porous media, and perched aquifers. This also contributes in NVE's attempt to assess a design of drainage operations, targeted on lowering porewater pressure in the unstable rock-slope.

The specific goals of this report are to:

- 1) Characterize the rockmass properties and integrate fracture frequency data for the definition of the hydraulic conductivity properties of Åknes rock-slope
- 2) Analyse the groundwater conditions from time-series data since 2007
- 3) Quantify groundwater recharge and discharge in the catchment of the unstable area
- 4) Present and discuss the results of the three-dimensional (3D) numerical model that simulates the groundwater flow in Åknes, under steady-state conditions

1.3. Location of Åknes unstable slope

Åknes is a mountain slope located in the Sunnysfjord, in northern West Norway. It is situated fifteen kilometres south of Stranda municipality and 15 kilometres northwest of the end of the Geirangerfjord, which is an important touristic attraction in Norway.

The mountain slope, with its ridge at 1500 meters above sea-level (masl), dips on average 35° towards SSE, and continues into the fjord for that reaches 300 m depth, as shown in Figure 1. Talus fan aprons can be seen on the seafloor below Åknes and other sites in the fjord system (Blikra et al. 2005), attesting to pre-historic rock avalanches. The unstable area of this slope has a toe zone at 100 masl, and a backscarp at 700 to 900 masl. To the west, the unstable slope is delimited by a steep NNE-SSW trending fracture zone along which runs an ephemeral stream, called the Western Gully. This fracture zone detaches the rock-slope failure from intact rock farther west. To the east, the unstable slope is bounded by a pre-existing fault dipping $35-45^\circ$ to the west, where the ephemeral Eastern Stream runs (Ganerød et al., 2008).

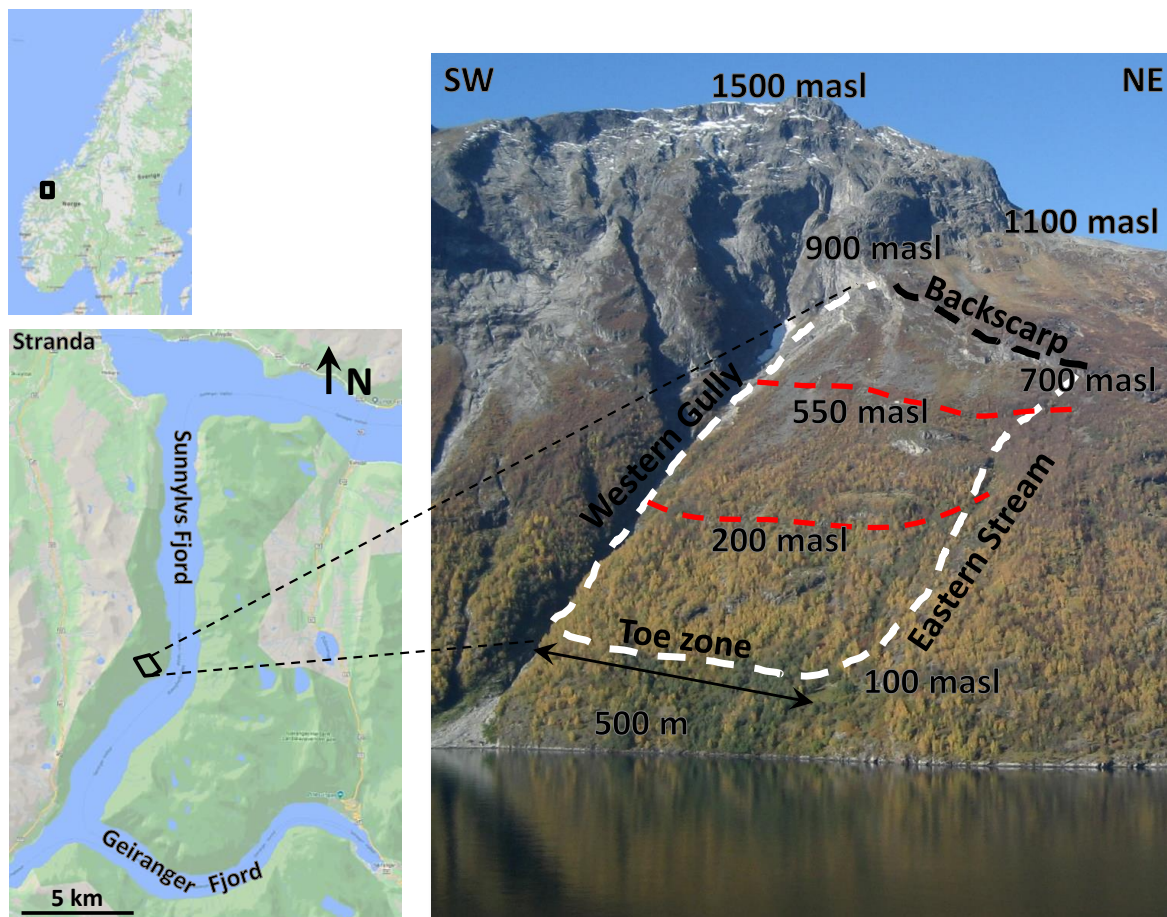


Figure 1. Location of Åknes unstable rock-slope, and photo of the slope seen from Oaldsbygda (Grøneng et al., 2010). Unstable area: white line, Sliding planes: red lines (Ganerød et al., 2008). Maps modified from Google maps.

1.5. Overview of the project timeline

This project was split in three main phases: data harvesting; data processing and analysis; and, numerical modelling of the groundwater flow in Åknes (Table 1). Data harvesting included collecting and integrating data managed by NVE and previous published work; and, conducting specific field-campaigns to collect complementary data on the groundwater conditions at Åknes. Data processing and analysis focused on the data in previous published work; the time-series of meteorological data and groundwater levels; the borehole data (such as geological logging, fracture frequency, and groundwater flow-meter data); and, the data collected in the field-campaigns led by UiO. The development of the numerical model of groundwater flow in Åknes consisted in estimating the rate of groundwater recharge, assessing the groundwater discharge as measured in the field-campaigns, defining the conceptual model for the hydrogeological parameterization of the fractured rockmass, defining the most suitable numerical modelling code, implementing and calibrating the model.

During the project duration, besides the 1st and 2nd progress reports, several output indicators were produced which are listed in section 1. Of these, three master projects at the UiO (Biørn-Hansen, 2019; Bruun, 2019; Ringstad, 2019) and the internal report by Papadimitrakakis (2020) significantly contributed to the goals of this project.

Table 1. Timeline of the project work plan, and deliverable reports.

	2017		2018			2019			2020			2021	
Tasks:	2 nd sem.		1 st sem.		2 nd sem.	1 st sem.		2 nd sem.	1 st sem.		2 nd sem.	1 st sem.	
Data harvesting													
Software solutions													
Rock facies descriptions													
Water balance of the rock-slope													
Hydrogeological model: Baseline and sensitivity tests													
Final Hydrogeological model													
Deliverables:													
Report 1													
Report 2													
Final Report													

2. Data harvesting

2.1. Data managed by NVE

Widening of the backscarp and displacement of different parts of the unstable rockmass have been monitored since 1986. In 2004 an automated monitoring system was installed by NVE (Figure 2). This system includes extensometers placed in tension fractures, fixed-station GPS on the ground, and inclinometers installed every meter along deep boreholes (between 150 and 300 m deep).

From the instrumentation installed in Åknes and earlier geological and geophysical field campaigns, the following datasets were included in this project (see Figure 2 for location of the different monitoring instruments):

- Air temperature and precipitation, recorded on a daily basis since 2004
- Groundwater levels from six open boreholes, recorded on a daily basis since 2007
- Groundwater levels of four packer-isolated multi-level boreholes, recorded on a daily basis since 2018
- Outcrop data from rock-slope failure area (summary in Ganerød et al. 2008)
- Electrical resistivity and seismic refraction profiles reported in Tassis and Rønning (2019)
- Drill core lithology, fracture frequency and televiewer recordings from the twelve boreholes installed in Åknes (Elvebakk, 2008; Elvebakk, 2013; Ganerød et al., 2007; Ganerød, 2013; Storrø and Gaut, 2008; Elvebakk and Pless, 2018)
- Differential Monitoring System of displacement data along four boreholes; KH-02-06, KH-03-06, KH-02-17, KH-01-12. The two last digits in the code of each borehole indicate the year of construction
- Multi-tracer tests reported in Frei (2008)

Time series of groundwater level and meteorological data were integrated into the conceptualization of the groundwater flow in Åknes. To do so, it was decided to analyse the recorded data from October 2007 to August 2020. At present, these are the available time series of daily groundwater levels from the boreholes installed in Åknes:

- Oct/2007 to Jan/2017: KH-01-05
- Oct/2009 to Jan/2017: KH-04-05
- Oct/2007 to Jul/2013: KH-01-06
- Sep/2015 to present: KH-02-06
- Sep/2015 to present: KH-03-06
- Jun/2014 to present: KH-01-12
- Oct/2018 to present: KH-01-17, KH-02-17, KH-01-18, KH-02-18 (multi-level boreholes)

The monitoring data from the boreholes KH-01-05 and KH-04-05, constructed in 2005, was discontinued in January 2017. Nonetheless, the boreholes KH-02-06 (located close to KH-01-05) and KH-03-06 (located close to KH-04-05), constructed in 2006, collect data since September 2015. The overlapping measurements between the boreholes from 2005 and 2006 indicate very similar groundwater levels, and therefore the 2006 boreholes can be considered a continuation of the time series obtained by the 2005 boreholes.

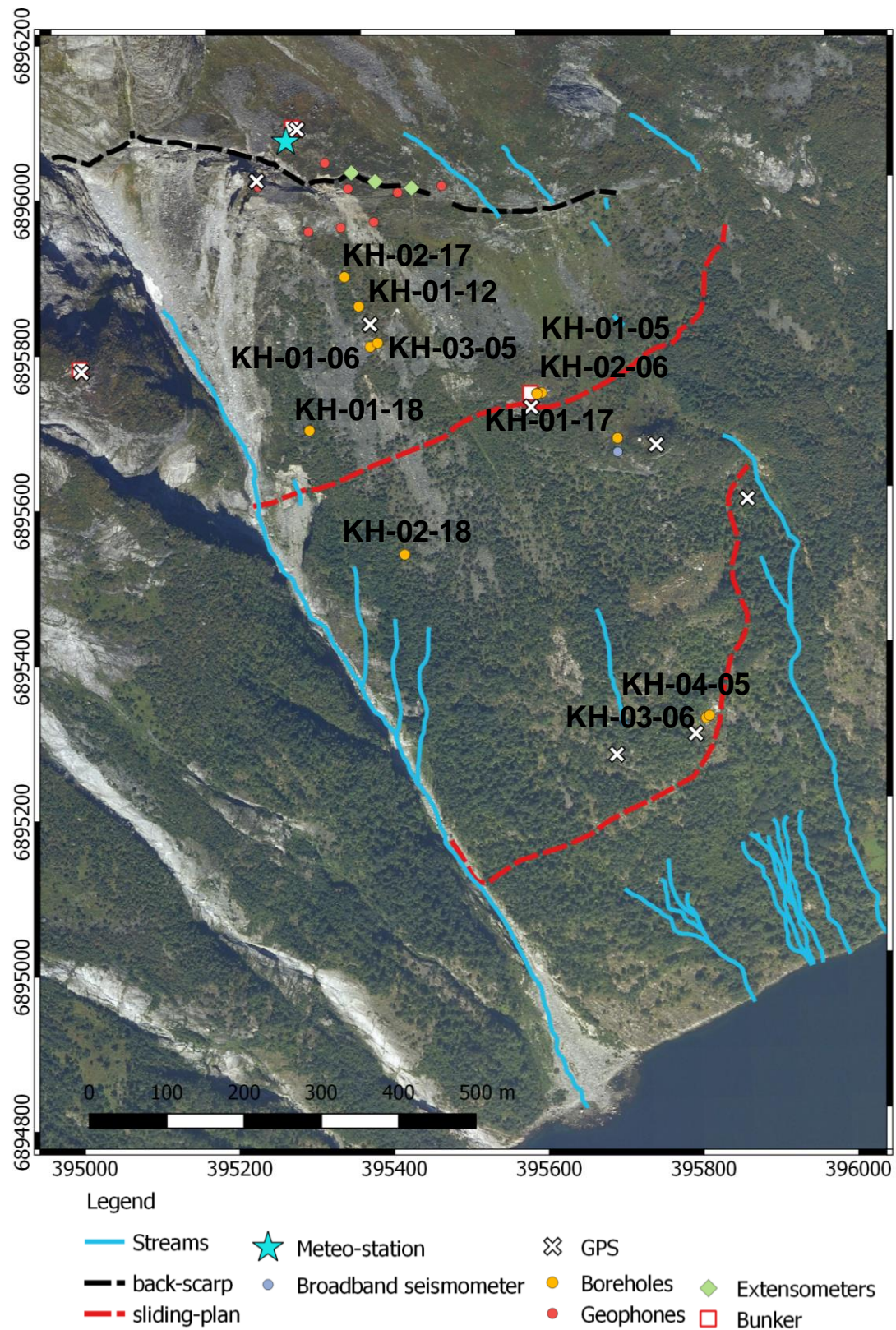


Figure 2. Monitoring instrumentation in Åknes. The location of the streams is from Frei (2008), and interpretation of the backscarp and sliding planes is from Ganerød et al. (2008).

2.2. Previous work on the Åknes unstable rock-slope

Åknes rock-slope is predominantly made up of granitic gneisses which were altered and reworked during the Caledonian Orogeny. These vary from white to light pink medium grained granitic gneiss to a dark grey biotite bearing granodioritic gneiss, and further to a subordinate white to light grey, hornblende to biotite bearing, medium grained dioritic gneiss. There are also laminae, and up to 20 cm-thick layers of biotite schistose gneiss (Braathen et al., 2004; Ganerød et al., 2008 and references therein). Sub-vertical joints form predominantly in the granitic gneiss while undulating foliation surfaces, which are sub-parallel to the mountain slope, prevail in the biotite schistose gneiss (Ganerød et al., 2008 and Oppikofer et al., 2011).

Since 2008, several publications have described the geomorphological, lithological, structural and stability properties of the Åknes unstable rock-slope (Ganerød et al., 2008, Nordvik et al., 2009, Grøneng et al., 2009, Grøneng, et al., 2010, Jaboyedoff et al., 2011, Oppikofer et al., 2011). Åknes is known as the most hazardous rockslide area in Norway at present, and is among the most investigated rockslides in the world, representing an exceptional natural laboratory. This study focuses on structural geology and the usage of geophysical methods to interpret and understand the structural geometry of the rockslide area. The interpretations are further used to build a geological model of the site. This is a large rockslide with an estimated volume of 35-40 million m³ (Derron et al., 2005) defined by a back scarp, a basal shear zone at about 50 m depth and an interpreted toe zone where the sliding surface daylights the surface. The rockslide is divided into four sub-domains, experiencing extension in the upper part and compression in the lower part. Structural mapping of the area indicates that the foliation of the gneiss plays an important role in the development of this rockslide. The upper boundary zone of the rockslide is seen as a back scarp that is controlled by, and parallel to, the pre-existing, steep foliation planes. Where the foliation is not favourably orientated in regard to the extensional trend, the back scarp follows a pre-existing fracture set or forms a relay structure. The foliation in the lower part, dipping 30° to 35° to S-SSE, seems to control the development of the basal sliding surface with its subordinate low angle thrust surfaces, which daylights at different levels. The sliding surfaces are sub-parallel to the topographic slope and are located along mica-rich layers in the foliation. Geophysical surveys using Ground Penetrating Radar (GPR), refraction seismic and 2D electrical resistivity profiling, give a coherent understanding of undulating basal sliding surface in the subsurface. The geophysical surveys map the subsurface in great detail to a depth ranging from 30-40 m for GPR to approximately 125 m for refraction seismic and 2D resistivity profiling. This gives a good control on the depth and lateral extent of the basal sliding surface, and its subordinate low angle thrusts. Drill cores and borehole logging add important information with regard to geological understanding of the subsurface. Fracture frequency, fault rock occurrences, geophysical properties and groundwater conditions both in outcrops and/or drill cores constrain the geometrical and kinematic model of Åknes rockslide.

An attempt is made here to summarize the findings attained in these works (Table 2). This information is crucial to constrain the hydrogeological conceptual and numerical model of

Åknes rock-slope since the majority of the geomorphological, lithological and structural features that delimit and constitute the unstable rock mass have hydrogeological implications.

Table 2. Properties of the Åknes unstable rock-slope compiled from previous works.

Publication	Limits of unstable area	Total unstable volume (10 ⁶ m ³)	Depth of basal sliding surface, BSS (mbg)	Dip angle of basal sliding surface (°)	Dip angle of slope (°)	Number of secondary sliding surfaces	Fastest moving rock mass (cm/yr)
Ganerød et al., 2008	Back scarp (800 to 900 masl); Basal shear zone; Eastern Boundary (fault dipping 35-45° west); Western Boundary (NNW-SSE trending strike slip fault)	35-40	35-65	30-35	30-35	4 (mica-rich layers)	14 (NW Subdomain)
Nordvik et al., 2009	Sc A: same as Ganerød et al. (2008) Sc B (most likely): same as Ganerød et al. (2008), but lower boundary coincides with the Lower Spring Horizon	Sc A: 20 Sc B: 43	40-55 (Sc A) 105-115 (Sc B)	-	30-35	Sc A: 4 Sc B: 5	-
Grøneng et al., 2009	Same as Ganerød et al. (2008)	30-40 (Derron et al., 2005)	25-60	-	35	-	-
Grøneng, et al., 2010	Same as Nordvik et al. (2009), Sc B	43	105-115	-	30-35	2	-
Jaboyedoff et al., 2011	Same as Ganerød et al. (2008), but with a stepped basal sliding surface (Fig. 9)	30-40	-	27-34 (Kveldsvik et al. 2006)	30-35	2	15 (NW Subdomain)
Oppikofer et al., 2011	Same as Ganerød et al. (2008), but with a stepped morphology for the basal sliding surface: (i) undulating (biotite-rich) foliation surfaces which are folded, and interrupted by (ii) sub-vertical joints (steps) of granitic gneiss Curved shape of the BSS is unlikely in hard rock-slope failure	Sc 2(var.): 85.7 Sc 3: 11.6	Sc 2(var.): 144.5 Sc 3: 63.5	Foliation: 32.5 Step: 72.3	30-40	-	-

Note: mbg: meters below ground; Sc: scenario

2.3. Previous work on Åknes hydrogeology

In the frame of the Åknes/Tafjord Beredskap investigation, monitoring and early-warning project, several research projects, including PhD and Master theses were undertaken focusing among other aspects on the Åknes hydrogeology. These are:

- Groundwater Flow at the Åknes Rockslide Site (Norway): Results of a Multi-Tracer Test, MSc thesis by Frei (2008)
- Dynamic fluid electric conductivity logging for identification and characterization of preferential groundwater flow in the Åknes rockslide (Norway), MSc thesis by Thoeny (2008)
- Geological model of the Åknes rockslide , western Norway, scientific article by Ganerød et al. (2008)
- Meteorological effects on seasonal displacements of the Åknes rockslide, western Norway, scientific article by Grøneng et al. (2011)

In 2008, Frei identified 22 springs and/or groundwater discharge zones in Åknes rock-slope. According to their altimetry, they were grouped in Upper, Middle and Lower Spring Horizons. From the flow rate measurements done in August-October 2007, the highest flow rate was found in the Lower Spring Horizon. Here, only in spring SN2a water is discharged through a clear fracture in the bedrock. The remaining springs are diffuse discharge areas, covered by pebbles and cobbles, which makes it difficult to identify the exact area where groundwater is discharged. In this work, the tracer Eosin, injected in a fracture located in the Western area of the backscarp, close to the Åknes meteorological station (Klimastasjon), was detected at the Middle (S29, S30, S31) and Lower (SN2b, SN3b, SN5, SN6, SN8) Spring horizons, while the tracer Sulphorodamine-B, injected in the borehole KH-01-06, was detected in the Middle (S30) and Lower (SN2b, SN6, SN8) Spring horizons. This tracer showed the fastest flow path compared to all other tracers.

The subsurface peak flow velocities estimated in Frei (2008) from the tracer tests reached up to 17.4 m/h and reflect very high values compared to the runoff with 30-31 m/h, measured in the stream that runs along the Western Gully. In what concerns the groundwater flow patterns, flow systems at different depths may exist, since flow directions of some tracers crossed each other (Figure 3).

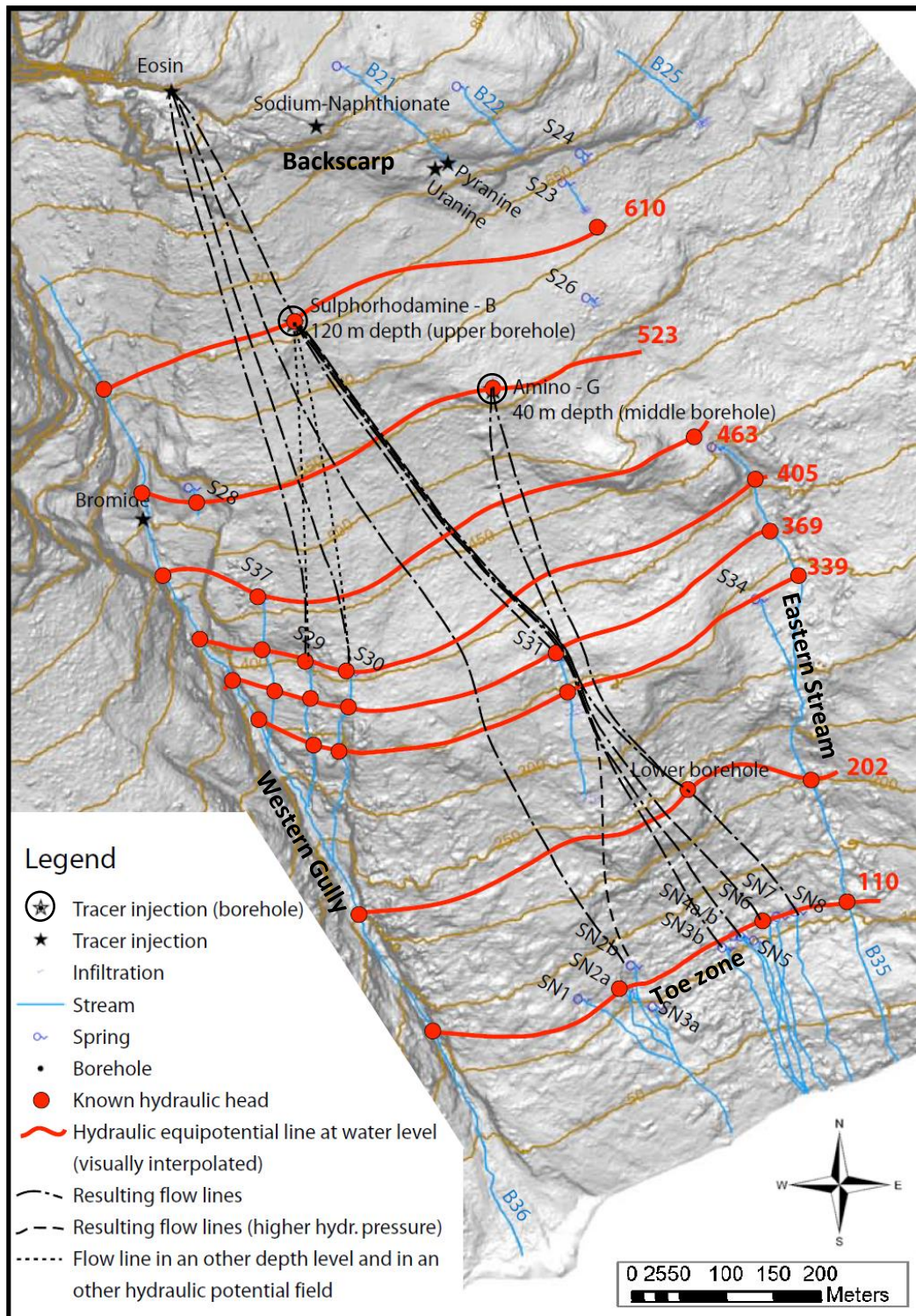


Figure 3. Conceptual hydraulic potential field with visually interpolated equipotential lines and flow lines beginning at the tracer injection points (Frei, 2008).

The subsurface peak velocities attained in Frei (2008) are clearly higher than the values typically observed in fully water-saturated fractured or porous media with laminar water flow. Therefore, the groundwater flow in Åknes rockslide seems to be that of a subsurface laminar

to turbulent flow, partially occurring along the unsaturated zone, i.e. above the water table. Besides the properties of the rock mass, made up of fractures and crushed rock that are the prevailing permeable features, the considerable steepness of Åknes rockslide also contributes to enhance the occurrence of a high-velocity subsurface flow.

Ganerød et al. (2008) classified Åknes as a complex groundwater system fed by precipitation directly on the unstable area and in the catchment area upslope. Several seasonal streams flow into the backscarp. Runoff from snowmelt in the springtime brings significant volumes of water into the unstable area. The springs observed at the site indicate groundwater seepage along the observed sliding surfaces. The area beneath the toe zone reveals abundant springs. In the lower part of the rockslide area, towards the fjord, the groundwater table is close to the surface. The water chemistry in these springs indicates short retention time in sub-domain 2 (i.e. Upper Spring Horizon), while springs from sub-domain 3 and 4 (i.e. Middle and Lower Spring Horizons, respectively) seemingly have longer retention times. The Lower Spring Horizon, beneath the toe zone, indicates the longest retention time. Based on groundwater borehole data, these authors also concluded that the water table fluctuates seasonally, increasing by as much as 5 m during snowmelt. The data indicate a complex groundwater system, with several inflows and outflows at different depths and possibly perched groundwater aquifers. In addition, the results attained in Ganerød et al. (2007), Langeland (2013) and Thoeny (2008), indicate that the most likely water conductive features intersected by borehole drilling at different depths in the unstable rock mass are:

- Fractured to highly fractured rock mass (granitic or biotitic gneiss, and/or pegmatite)
- Crushed rock (with little clayey matrix)
- Rock with intense fracturing parallel to foliation

By comparing displacement data from the backscarp with meteorological data from the Åknes station from November 2004 to August 2008, Grøneng et al. (2011) identified snow and ice melt water in Spring and large temperature fluctuations around the freezing point in Spring, Autumn, and early Winter to be the most important meteorological factors affecting the activity in the tension crack (i.e., the backscarp). The records show less acceleration phases in the measured distance across the tension crack in the second half of the analysed period even though annual displacements are increasing, indicating that other processes, like disintegration of irregularities along unfilled joints and disintegration of intact rock bridges in the sliding plane have become more important.

2.4. Field-campaigns led by UiO

Throughout the project duration eight field campaigns were done in Åknes by UiO staff, master (MSc) students and other project members with a focus on the groundwater recharge and discharge processes of the whole mountain slope (from the lake Instevatnet to the fjord), and the structural geology, stability, and groundwater recharge pathways in the area above the backscarp (Table 3, Figure 5, and Figure 4).

Table 3. Overview of the field-campaigns done throughout the project duration.

Year	2017		2018				2019	
Period	12 Jun	05-08 Sep	04-09 Jun	16 Jul to 06 Aug	07-24 Aug	03-15 Sep	23-27 Apr	05-09 Aug
Field-work	Hydrogeology in the whole slope		Structural geology above backscarp		Hydrogeology in the whole slope		Hydrogeology in the whole slope	
CS	✓ + LK, KM	✓ + LK, GP, PR	✓				✓	✓ + PEP, ME
FLBH			✓	✓		✓ + GP	✓	
SRR				✓	✓			
HB					✓			
AB					✓			
MM					✓			
Assistant				✓		✓		

Note: UiO staff: CS Clara Sena, MM Mark Mulrooney, AB Alvar Braathen; UiO MSc students: FLBH Frida Liv Biørn-Hansen, SRR Stig Runar Ringstad, HB Halvor Bruun. ME Malan Ellefsen (NTNU); PEP Pierre-Etienne Privat (internship MSc student at UiO). NVE staff: LK Lene Kristensen, KM Knut Magne, GP Gustav Pless, PR Pål Røssevold.

In the hydrogeology field campaigns, the following tasks were conducted:

- Location, mapping and characterization of springs and streams, and establishment of a procedure for taking flow-rate measurements in the boulder and unstable terrain that characterizes Åknes
- In situ measurement of pH, electrical conductivity (EC) and temperature of the water in the springs and streams, and collection of water samples for inorganic hydrochemical characterization
- Characterization of soil cover, vegetation and fractured rock surfaces which contribute to temporary water retention, evapotranspiration, and groundwater recharge
- Monitoring of groundwater discharge rates in the Summer-Autumn 2018

In the structural geology field campaigns, the following tasks were conducted:

- Collection of a large database on fracture distribution and fracture intersections in the field stations shown in Figure 4
- Collection of field data to assess fracture distribution facies and geometry
- Drone campaign with photo coverage for photogrammetric analysis

For each station, the fracture strike and dip, fracture frequency, cross-cutting relationships and continuity, fracture termination and other notable features were taken. The outcomes of this work can be found in two master theses; Ringstad (2019), and Bruun (2019).

The location of the hydrogeology sampling points and structural geology stations of the field-campaigns is shown in Figure 4.

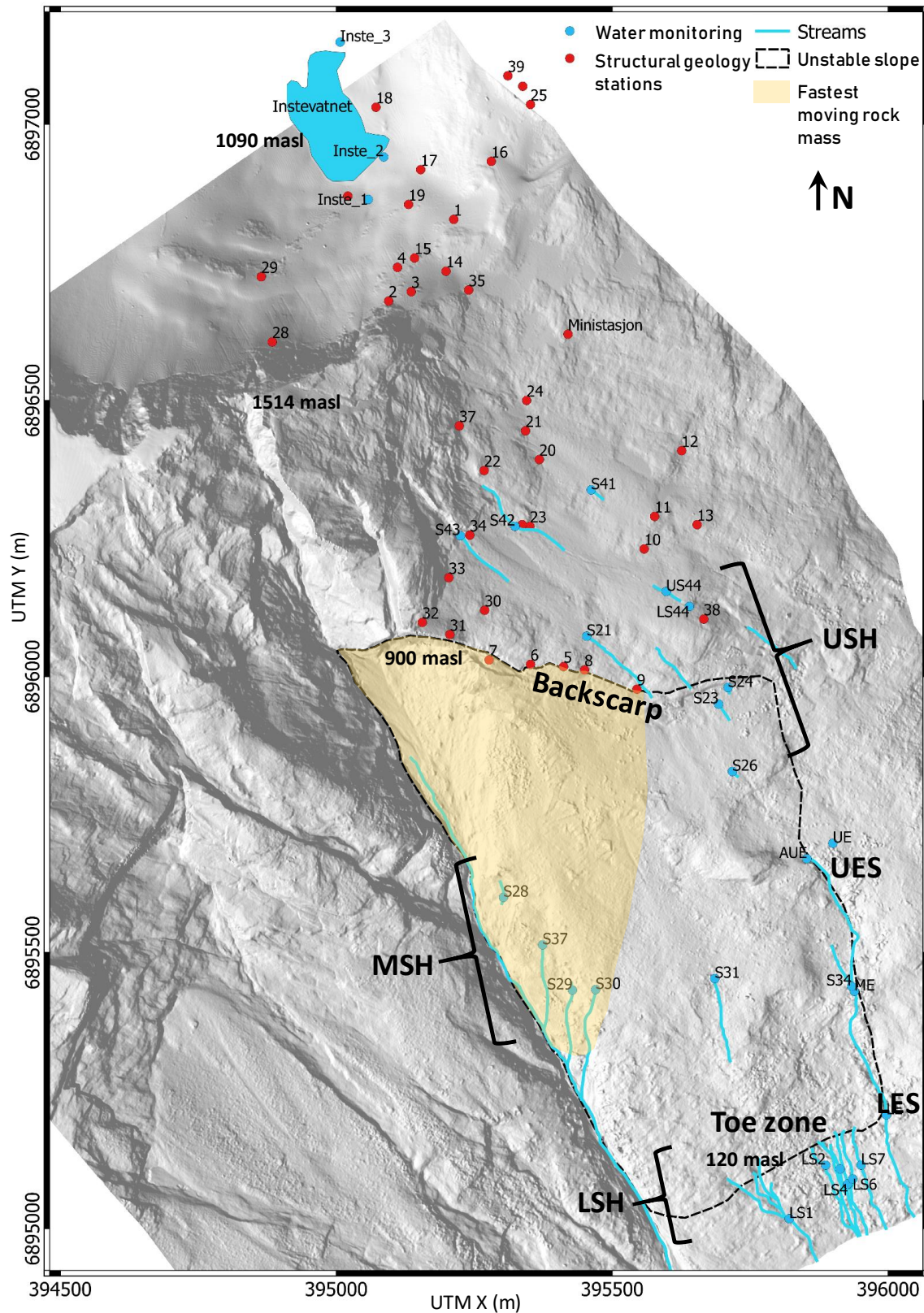


Figure 4. Location of the hydrogeology and structural geology monitoring points on a hillshade map. LSH, MSH & USH: Lower, Middle and Upper Spring Horizons; LES, UES: Lower and Upper Eastern Stream. Data source: water monitoring (Biørn-Hansen, 2019); structural geology stations (Ringstad, 2019; Bruun, 2019)

2.5. Field-work and data collection challenges

The terrain in Åknes is very steep (with an inclination of 35° on average, and many areas of 60°), and the bouldery deposits that cover all the springs are dragged and re-distributed every winter-spring due to snow accumulation, creeping and melting. This has a significant impact on how we access the springs' water in the field. In most cases, we cannot access the outcropping groundwater in discrete fractures of the rockmass, as this is hidden by rock debris, soil and vegetation. In the field, we listen to the sound of the water flowing downslope from this outcrop underneath the bouldery terrain. As soon as we can access a certain running water, we map it and mark it in the field, so that we can come back to the exact same location in subsequent field campaigns.

Due to the inherent field conditions, a manual flow-rate measurement procedure had to be established, entailing light weight equipment to facilitate the mobility of staff along the mountain slope, and adaptable to different flow-rate regimes in order to cover high and low flow-rates. By June 2018, this procedure was established, with acceptable associated errors. It entails placing an impermeable cloth fixed on the stream bed with stones available in the stream bed in order to direct ideally all the running water into a point in the cloth where a water bucket with a volume scale can be placed and the time needed to fill a certain volume can be taken (Figure 5). In each measuring point, at least three measurement replicas were taken, and each measurement took at least 5 to 10 seconds. A detailed analysis of the outcomes of the hydrogeology field-campaigns can be found in the master thesis by Biørn-Hansen (2019).



Figure 5. Illustration of the procedure to measure the flow-rate in the point LS1 (images (a) and (b)); and, LS6 (image c), both located in the Lower Spring Horizon. The arrow indicates: in (a) the point where the bucket with a volume scale is inserted; in (b) the top of the cloth fixed with stones; and in (c) the fixation of a small cloth when the flow-rate is relatively low.

2.6. Geographical Information System

A georeferenced database has been generated throughout this project, integrated in a Geographical Information System (GIS) project that was built using the software QGIS (<https://qgis.org/en/site/>). The datum used is the WGS84, and the projected coordinate system is the UTM Zone 32N. All maps shown in this report are framed with these coordinate values. In all the maps of this report north is upwards. This GIS was built by creating new files, and adding files from previous works and available data:

- 1) Existing files and data related to previous projects, namely elevation contours (1 and 5 meters equidistance), fjord bathymetry, aerial photo, shaded relief map of Åknes
- 2) Public topographic maps and digital elevation models available at <https://kartkatalog.geonorge.no/search>
- 3) Aerial photos of Åknes and surrounding areas available at <https://www.norgebilder.no/> through the UiO-Norgebilder agreement

4) Aerial photo and digital elevation model from a drone campaign held in 2020, and made available by NVE to the project members

5) New shapefiles created:

- a. From the analysis and interpretation of the previously existing maps and files, namely Tassis and Rønning (2019)
- b. From the conversion of tables presented in previous projects into shapefiles
- c. By digitizing specific features shown in maps of previous published work, namely from Frei (2008), Thoeny (2008) and Ganerød et al. (2008)

Whenever needed, output files from this GIS project were shared with project members through the NVE ftp for the Åknes project.

3. Results and discussion

3.1. Rockmass characterization

3.1.1. Borehole data

From 2005 to 2018, twelve boreholes were drilled in the unstable rockmass of Åknes with depths between 150 and 300 m. They are located at several elevations, from 240 masl (KH-04-05 and KH-03-06) close to the toe zone, to 734 masl (KH-01-17) close to the backscarp (Figure 2 and Figure 6). Rock cores recovered during drilling, geophysical logging and groundwater flow meter logging are described and analysed in the reports by the Geological Survey of Norway (NGU) (Elvebakk, 2008; Elvebakk, 2013; Ganerød et al., 2007; Ganerød, 2013; Storrø and Gaut, 2008; Elvebakk and Pless, 2018).

Taking into account the colour of the rocks intersected by the drilled boreholes (in the photographs of the drill cores), three lithological units were defined (Ganerød et al., 2007, and Papadimitrakakis, 2020):

- Granitic gneiss and pegmatite occur as white to light-grey
- Dioritic gneiss occurs as dark-grey
- Biotitic gneiss occurs as black

Granitic gneiss and pegmatite are the dominant lithology, covering 62% of the total recovered drill cores. 23% are biotitic gneiss, while the remaining 15% is made-up of dioritic gneiss. From what can be seen in Figure 6, there is no evident pattern on the occurrence of the different lithological units in depth nor along the slope dip, reflecting the disordered aspect of the rockmass lithology. This is probably due to the different folding phases that reworked these rocks during the Caledonian Orogeny for several tens of million years.

Strings of inclinometers (DMS-tubes) were installed in eight boreholes, as shown in Figure 6. Deformation of these DMS-tubes locates zones of shear in the subsurface, seen as sharp changes in the displacement. Four of these sharp changes in inclinometer data are not confirmed by lithological properties observable in the core log (dashed green lines in Figure 6), whereas eight of these are confirmed by local intense fracturing and occurrence of crushed material in the core log (dashed red lines in Figure 6; NGI, 2020a), in so-called fracture corridors.

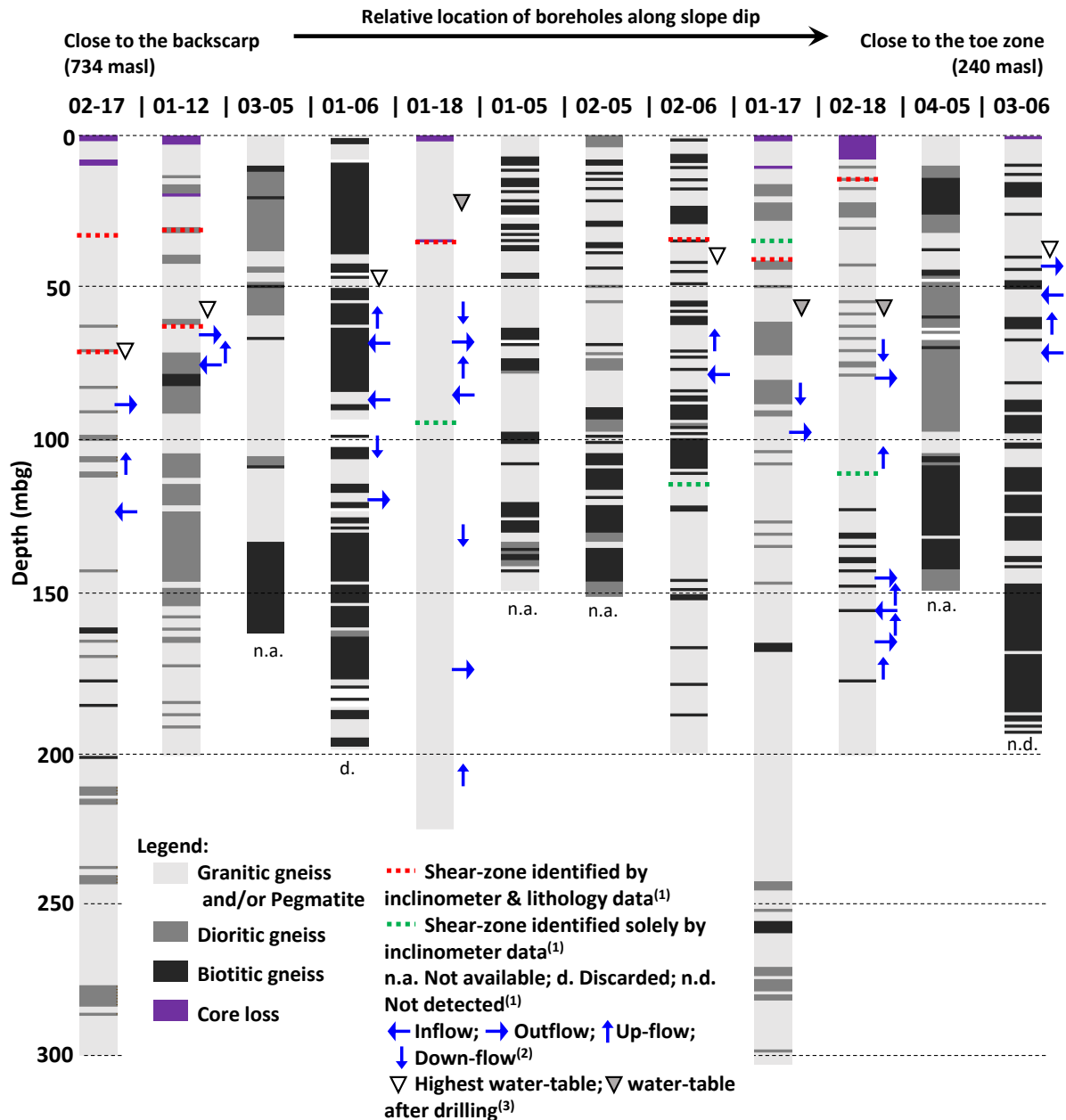


Figure 6. Lithological units logged in core photographs (from Papadimitrakakis, 2020). Borehole code is on top of each log. “KH” was removed from the borehole code for simplicity. Boreholes are aligned according to their elevation in the unstable slope. References: ⁽¹⁾NGI (2020a); ⁽²⁾Elvebakk (2008), and Elvebakk and Pless (2018); ⁽³⁾NGI (2020b).

Regarding the groundwater conditions, the highest water-table recorded since 2007 is in most boreholes below the deepest shear-zone meaning that the identified shear-zones are mostly dry throughout the hydrological year (Figure 6). However, during rain events or snow melt, the water percolating downwards has to pass through these shear-zones before reaching the water-table.

Borehole KH-01-18 is an exception, as the water-table is quite high and clearly above the shallowest shear-zone. This borehole is located close to the western boundary of the unstable rockmass where the topography becomes very steep, allowing the occurrence of several groundwater springs (Figure 2). For the three boreholes in which a reliable groundwater time series is not available (KH-01-17, KH-01-18, KH-02-18) the water-table measured after drilling is plotted instead of the highest recorded value (Figure 6).

Flow-meter data recorded after drilling, under open borehole conditions, reveal a clear stratification of the hydraulic head in the fractured rockmass as indicated by outflow and inflow of groundwater and vertical flow between these locations (Figure 6). Upward hydraulic gradients are registered close to the water-table in four boreholes (KH-02-17, KH-01-12, KH-01-06, KH-02-06), and at depth in two boreholes (KH-01-18, KH-02-18). Downward hydraulic gradients are registered close to the water table in three boreholes (KH-01-17, KH-01-18, KH-02-18), and between 100 and 150 mbg in two boreholes (KH-01-06, KH-01-18).

The intensity of fracturing, described in terms of fracture frequency of the rockmass in Åknes has been analysed from two borehole datasets; geological logging and optical televiewer logging. Geological logging of fracture frequency is done manually from the visual analysis of the drilled core (Ganerød et al., 2007; Ganerød, 2013), while optical televiewer logging of fracture frequency is undertaken automatically through computer-based inspection of the image retrieved from the geophysical logging along the open borehole (Elvebakk, 2013; Elvebakk and Pless, 2018). The former dataset is available for all (twelve) boreholes in Åknes, while the latter is available for the five most recent boreholes (KH-01-12, KH-01-17, KH-02-17, KH-01-18, KH-02-18).

Fracture frequency obtained from geological logging is likely an overestimation of the actual value, as drilling-induced fractures increase the fracturing of the retrieved drill core (Ganerød et al., 2007). On the other hand, optical televiewer-based fracture frequency is likely underestimating the actual value due to the limitation imposed by the televiewer image resolution, and the automatic method for fracture identification and counting (Elvebakk, 2013). For the five boreholes in Åknes which have both datasets, the fracture frequency estimated from the geological log is on average between 2.0 (borehole KH-01-12) and 4.1 (borehole KH-01-18) times higher than that estimated from the optical televiewer log (Figure 7).

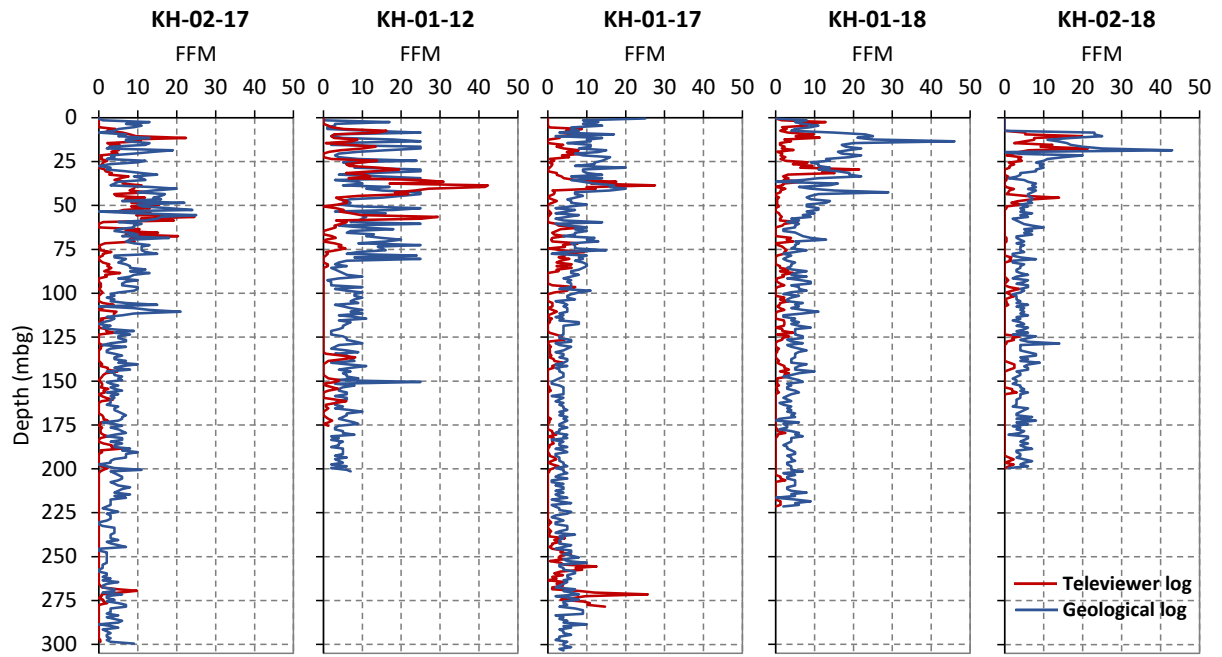
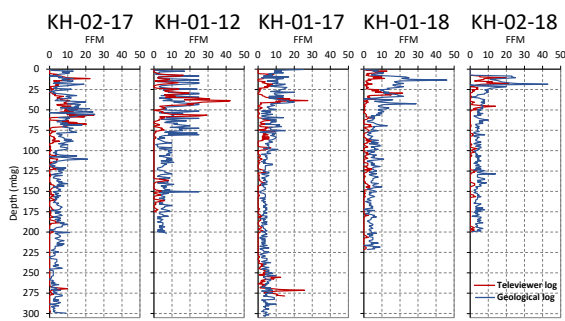


Figure 7. Fracture frequency (FFM, number of fractures per meter) for the five boreholes with the two logging data sets: geological and optical televiewer (Papadimitrakakis, 2020).

In this report we, therefore, assume that the actual value of fracture frequency is the average of both data sets, except for the boreholes without televiewer log (KH-01-05, KH-02-05, KH-03-05, KH-04-05, KH-01-06, KH-02-06, KH-03-06). For these, a correction factor was applied which was determined from the boreholes with both datasets (Figure 8; Papadimitrakakis, 2020).

Five boreholes with the two datasets (FFM, fracture frequency from televiewer & geological log):



Moving average of both datasets every 30 meters depth.

Correction factor (CF) for every 30 meters:

$$CF = \frac{\text{Average FFM}}{\text{Geological log FFM}}$$

Corrected FFM every 30 meters depth (FFM_{cor}) for those boreholes without televiewer log:

$$FFM_{cor} = (\text{Geological log FFM}) \times CF$$

Figure 8. Workflow for the correction of the fracture frequency data for the boreholes without optical televiewer log.

The corrected fracture frequency for the boreholes without televiewer log and the average fracture frequency for the boreholes with both datasets are shown in Figure 28, in the Appendix. These data were classified into three classes intended to reflect the aquifer versus aquitard potential of the fractured rockmass (Figure 9). A rockmass with a fracture frequency equal to or above five fractures per meter is considered to have a high aquifer potential, while less than three fractures per meter refer to aquitards.

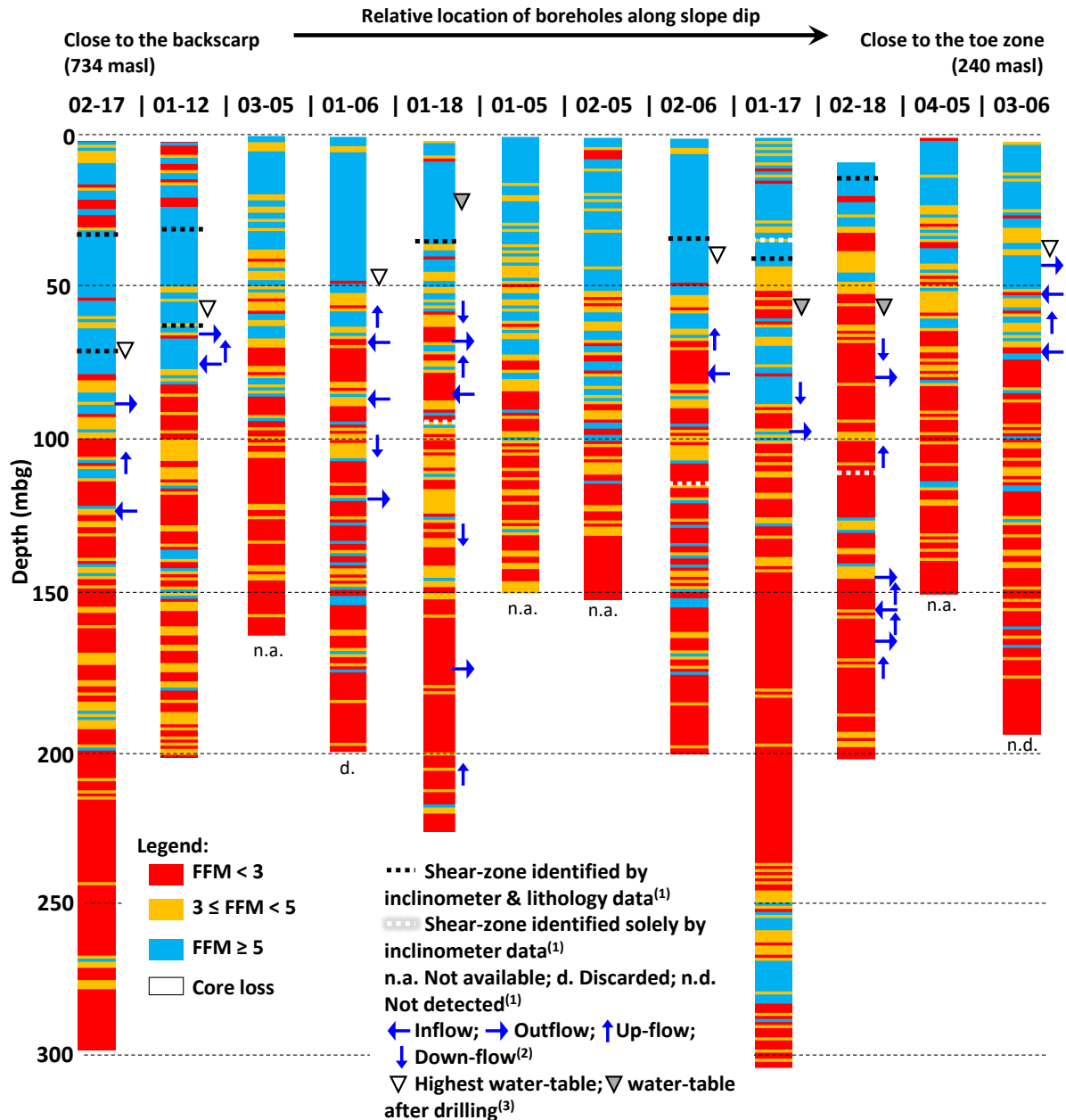


Figure 9. Fracture frequency classes (FFM, number of fractures per meter) for the twelve boreholes drilled in Åknes (from Papadimitrakakis, 2020). Borehole code is on top of each log. “KH” was removed from the borehole code for simplicity. Boreholes are aligned according to their elevation in the unstable slope. ⁽¹⁾NGI (2020a); ⁽²⁾Elvebakk (2008), and Elvebakk and Pless (2018); ⁽³⁾NGI (2020b).

In general, higher fracture frequency (5 or more fractures per meter) prevails close to the ground level, domineering to 30 meters below ground (mbg) (in KH-02-18) but present as deep as 90 mbg (in KH-02-17) and sporadically deeper. The overall tendency is for a progressive predominance of aquitards (FFM less than 3) below 100 mbg, except in KH-01-17 where high FFM areas occur at three depths, bounded by aquitards. These high FFM domains occur at 0 to 42, 62 to 87, and 251 to 279 mbg (Figure 9).

The location of the water-table is clearly within the high fracture frequency domain, and, with some exceptions, most of the inflows and outflows registered by flow-meter measurements coincide with higher fracture frequency locations in the boreholes (Figure 9).

3.1.2. Conceptual model of the fractured rockmass

In Figure 10, the fracture frequency classes along selected boreholes are overlain on a seismic refraction profile that runs along the western part of the unstable slope. The high fracture frequency areas close to the ground level coincide with the three lowermost seismic velocity classes (purple to green areas) revealing a good match between the two datasets. The seismic refraction profile shows the extension of the unstable fractured bedrock and the location of possible fracture zones that penetrate to depths of at least 120 mbg.

Sharp sub-vertical boundaries exist between the low-seismic velocity areas interpreted as fracture zones and the rockmass immediately downslope (Figure 10). This can be clearly seen in the backscarp area where a red-coloured sub-vertical area bounds downslope the low-seismic velocity area (in blue). This pattern reflects the rockmass properties and geometry of pull-apart structures that characterize tension fractures such as the backscarp, and the other sub-vertical fracture zones interpreted in this profile.

Rockmass areas dominated by tension fractures should have a significant hydrogeological role in the groundwater flow and storage at Åknes. These are sub-vertical open fractures perpendicular to the main groundwater flow direction which roughly follows the slope dip. In these tension fractures, the horizontal hydraulic conductivity along slope dip should be much lower than its perpendicular horizontal counterpart. These structures store and divert laterally the groundwater, generating what we designate here as “groundwater barriers” (Figure 10). For this reason, and since they will be integrated in the groundwater flow numerical model of Åknes, we defined the main sub-vertical structures in Figure 11. The sub-vertical structures defined in dark red (as normal faults) are interpreted as areas dominated by tension fractures that form perpendicular to the downslope movement of the adjacent rockmass.

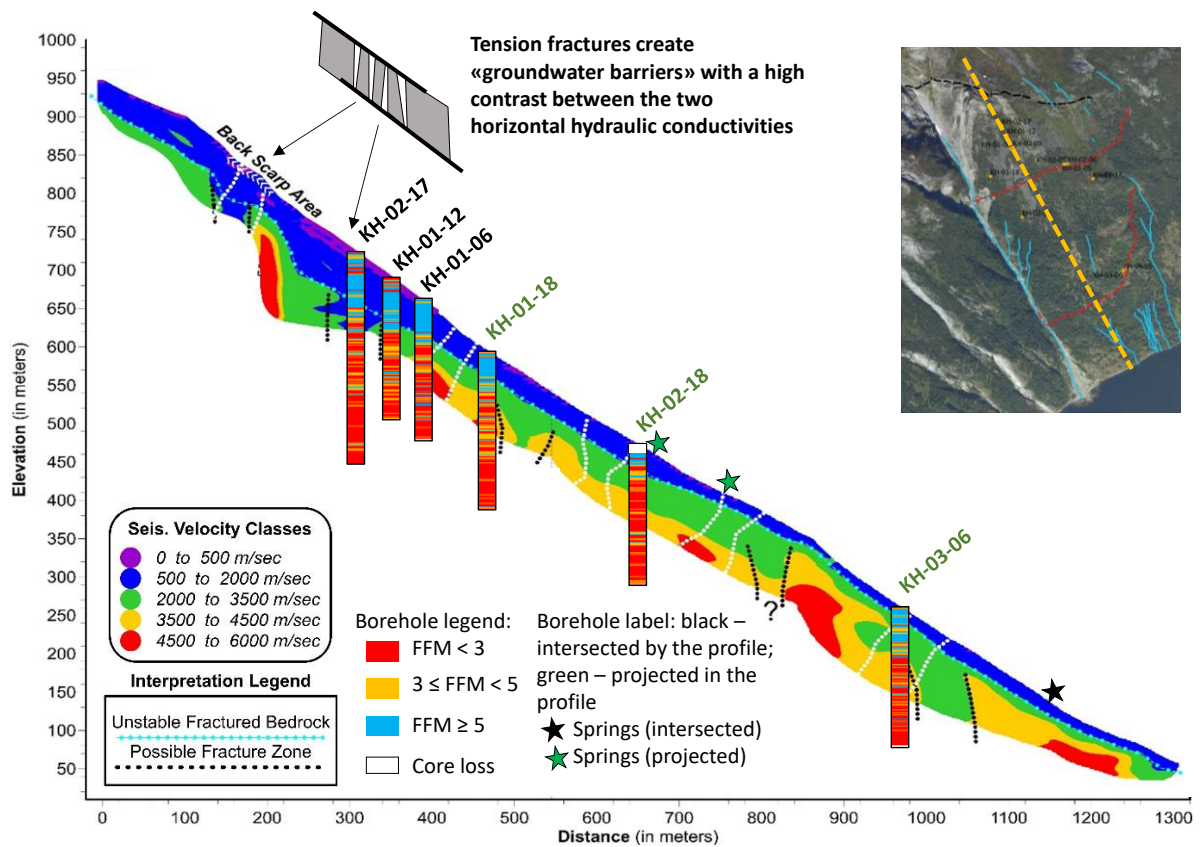


Figure 10. Seismic refraction profile, interpreted fractured bedrock and fracture zones from Tassis and Rønning (2019) with projection of the fracture frequency classes: Borehole data are either intersected or projected into the cross-section. Location of the profile is shown in the inserted aerial photograph.

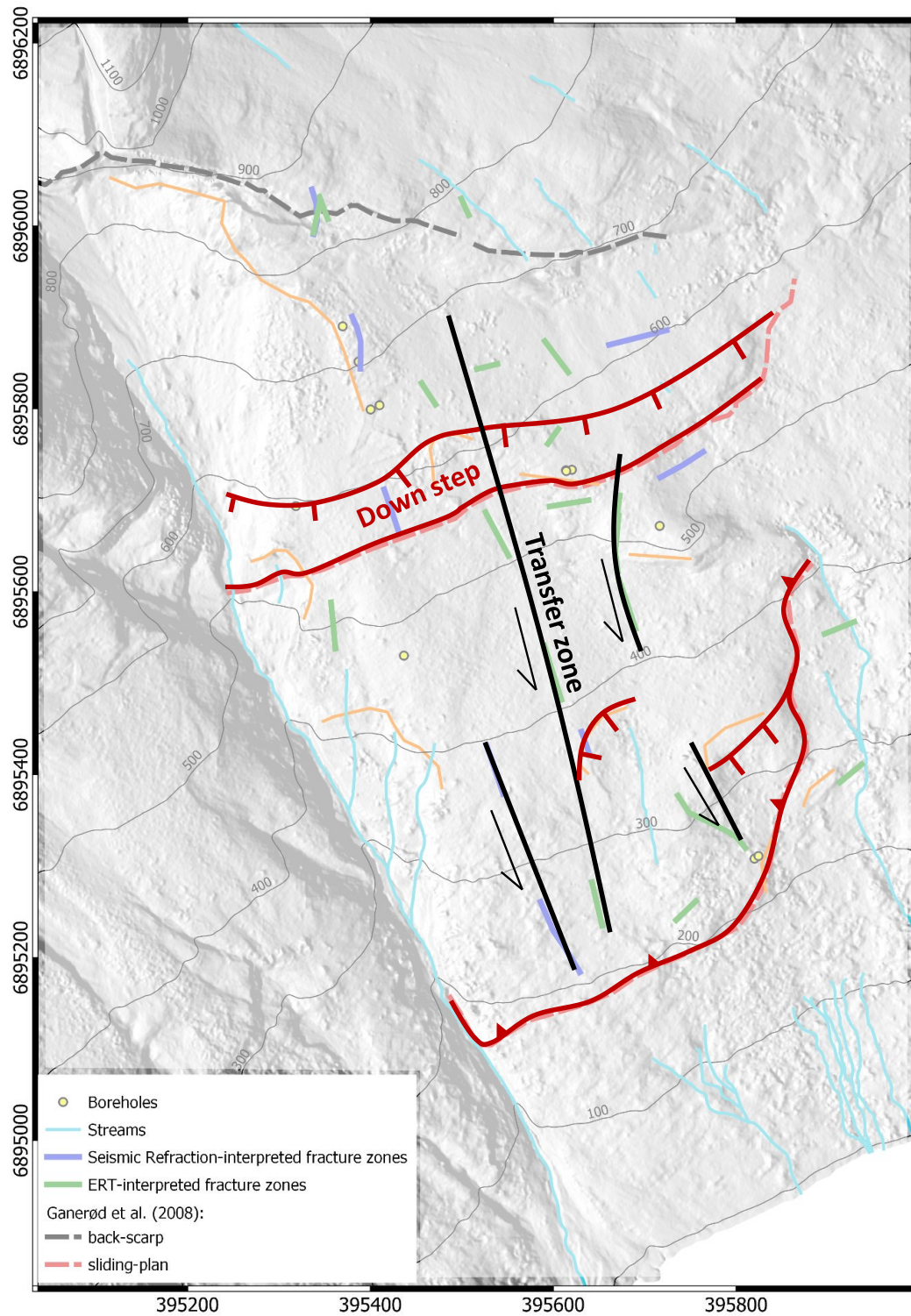


Figure 11. Main sub-vertical structures in Åknes, as depicted from the integration of field-observations, borehole and geophysical data. Seismic and ERT-interpreted zones are from Tassis and Rønning (2019). Location of streams is from Frei (2008) and Biørn-Hansen (2019).

In Figure 12, we define the three-dimensional model of the main shear zones in Åknes. Two main shear zones are interpreted; one at 31 to 35 mbg and second one, deeper, located between 63 and 115 mbg. The shallowest shear zone surfaces in a rock overhang, at the toe zone, and is located near the surface (or surfaces) in the Wester Gully. The configuration of the deepest shear zone towards the toe zone is still unclear. The shallowest shear zone is located above the water-table while the deepest one is mostly below it.

The backscarp is the main tension fracture, and it is much wider to the West where a local graben has formed, than to the East where it becomes tighter and crops out as a 20 meter high rocky cliff. As previously mentioned, similar underground tension fractures are believed to occur downslope in the unstable rockmass (coinciding with the fracture zones interpreted by Tassis and Rønning, 2019), and they are likely related to steps on the underlying shear zones, as suggested in the model by Oppikofer et al. (2011).

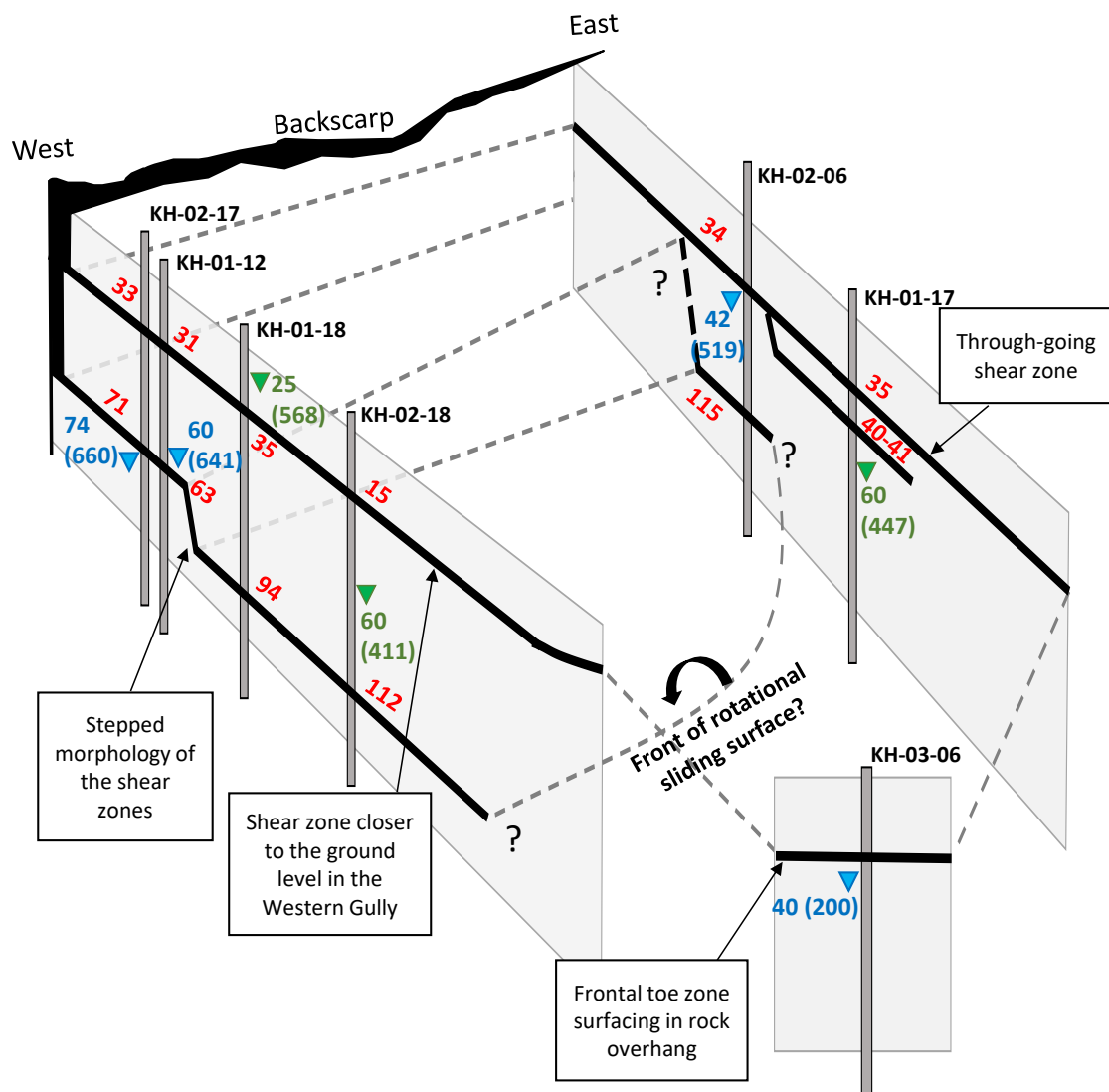


Figure 12. Three-dimensional model of the shear zones in Åknes (not to scale). Depth (in mbg) of: the shear zones in red; the highest water-table in blue; and, the water-table after drilling in green. In parenthesis, water-table elevation in masl. Shear zones' depth from NGI (2020a) and water-table after drilling from NGI (2020b).

3.2. Time-series

3.2.1. Groundwater levels and meteorological data

Time-series of measured groundwater levels at Åknes were analysed for the ten boreholes with data. The four most recent (installed in 2017 and 2018) are multi-level boreholes with inflatable packers isolating each section containing a water pressure sensor, while the remaining six (installed in 2005, 2006 and 2012) are open boreholes with one pressure sensor. From the four multi-level boreholes, KH-01-17, KH-01-18, KH-02-18 were discarded from the analysis of the time-series because the monitored time interval is too short (October to December 2019) and the data obtained is difficult to relate to precipitation events, pointing to the possibility of leakage of the installed packers. The data is shown in Figure 29 to Figure 31, in the Appendix.

For the time-series analysis, the hydrological year is set to start on October 1st, and end on September 30th of the following year. According to data availability, the time-series of groundwater-levels starts on the 1st of October 2007 and ends on the 30th of September 2019. The time-series of meteorological data, precipitation and air temperature, selected for this project is from the 11th November 2004 to the 30th of September 2019.

Regarding the daily precipitation, the wettest months are from September to December, while the driest are from April to June. Fifteen events with the highest daily precipitation (50 to 62 mm/d) occurred between August and December, and three occurred in March, April and June. There is a slight decreasing trend of the daily precipitation of -0.07 mm/day, every year (Figure 32 in the Appendix). The average annual precipitation registered in Åknes is 1618 mm/year.

The average daily air temperature in Åknes is 3.0°C, with a minimum of -14.0°C (February 2010) and maximum of 23.4°C (July 2019). The coldest months, from December to March, have an average daily temperature of -2.5°C, while the warmest months, from June to August, have an average daily temperature of 9.9°C. There is a slight increasing trend of the daily temperature of 0.07°C, every year (Figure 33 in the Appendix).

The whole time-series of groundwater levels in Åknes show a decreasing trend of -0.11 m/year close to the upper Eastern Stream and close to the backscarp (boreholes KH-01-05 and KH-02-17, respectively). Close to the backscarp, but lower in the topography, an increasing trend of 0.55 m/year is observed in borehole KH-01-06. At the toe zone, a nearly null trend is observed in borehole KH-04-05 (Table 4, Figure 13, and Figure 14).

Table 4. Summary of the time-series of groundwater levels at Åknes.

Borehole code, KH-	TOC (masl)	Time-series interval	Groundwater levels variation				
			Trend for the time-series interval (m/year)	Minimum annual amplitude (m; year)	Maximum annual amplitude (m; year)	Annual minima occur in:	Annual maxima occur in:
01-05	561.9	Oct/2007 to Jan/2017	-0.11	0.6 (2013/14)	2.7 (2007/08)	Mar to May	Sep to Nov
04-05	239.8	Oct/2009 to Jan/2017	0.01	2.0 (2011/12)	3.6 (2010/11)	Jan to Mar	Oct to Dec, Mar to Apr
01-06	658.3	Oct/2007 to Jul/2013	0.55	2.5 (2009/10)	8.8 (2007/08)	Mar to Apr	Sep to Nov
02-06	560.9	Sep/2015 to Sept/2019	0.04	1.0 (2015/16)	1.6 (2018/19)	Feb to Apr, and Ago	Ago to Nov
03-06	239.9	Sep/2015 to Sept/2019	0.25	2.6 (2016/17)	3.1 (2017/18)	Feb to Apr	Sep to Dec, Feb to Apr
01-12	701.1	Jun/2014 to Sept/2019	0.04	1.1 (2015/16)	3.2 (2017/18)	Feb to Apr	Sep to Nov
02-17 (sensor at 78 mbg)	733.8	Oct/2018 to Sep/2019	-0.11	2.8 (only one year of data)	-	Dec, and Ago	Oct, May, and Sep
02-17 (sensor at 101 mbg)	733.8	Oct/2018 to Sep/2019	-0.11	14.7 (only one year of data)	-	Apr	Oct to Nov

Close to the backscarp, the annual variation of groundwater levels is from 1.1 m (in KH-01-12) to 8.8 m (in KH-01-06). However, the largest annual variation of groundwater levels was recorded in the multi-level borehole KH-02-17: 14.7 m, at 101 mbg. This borehole is the closest to the backscarp, and the data obtained here is of major importance for the assessment of the groundwater conditions at Åknes. Therefore, a detailed analysis of this time-series is given in the following subsection. The highest peak observed in KH-01-12 is 641.6 masl on the 9th October 2017 (Figure 14). This is most likely due to the drilling and installation of borehole KH-02-17 that is located 40 meters upslope. The highest peak observed in KH-01-06 (608.6 masl, on the 1st September 2012) could also be related to the drilling and installation of KH-01-12, as this is 54 meters upslope KH-01-06.

KH-01-05 and KH-02-06 are six meters apart, stand at about 560 masl, close to the upper Eastern Stream. Here, the groundwater levels vary between 0.6 and 2.7 meters over the year (Table 4 and Figure 13).

KH-04-05 and KH-03-06, located five meters apart, stand lowest in the topography, close to the toe zone. Although there is a temporary drop of 1.5 m in the groundwater levels measured in KH-04-05 that coincides with a data gap, hindering its interpretation, it seems to recover from 2016 onwards (Figure 13). The data from these two boreholes indicate that at the toe zone, the groundwater levels have a seasonal variation between 2.0 and 3.1 meters, and their overall trend is almost null (Table 4).

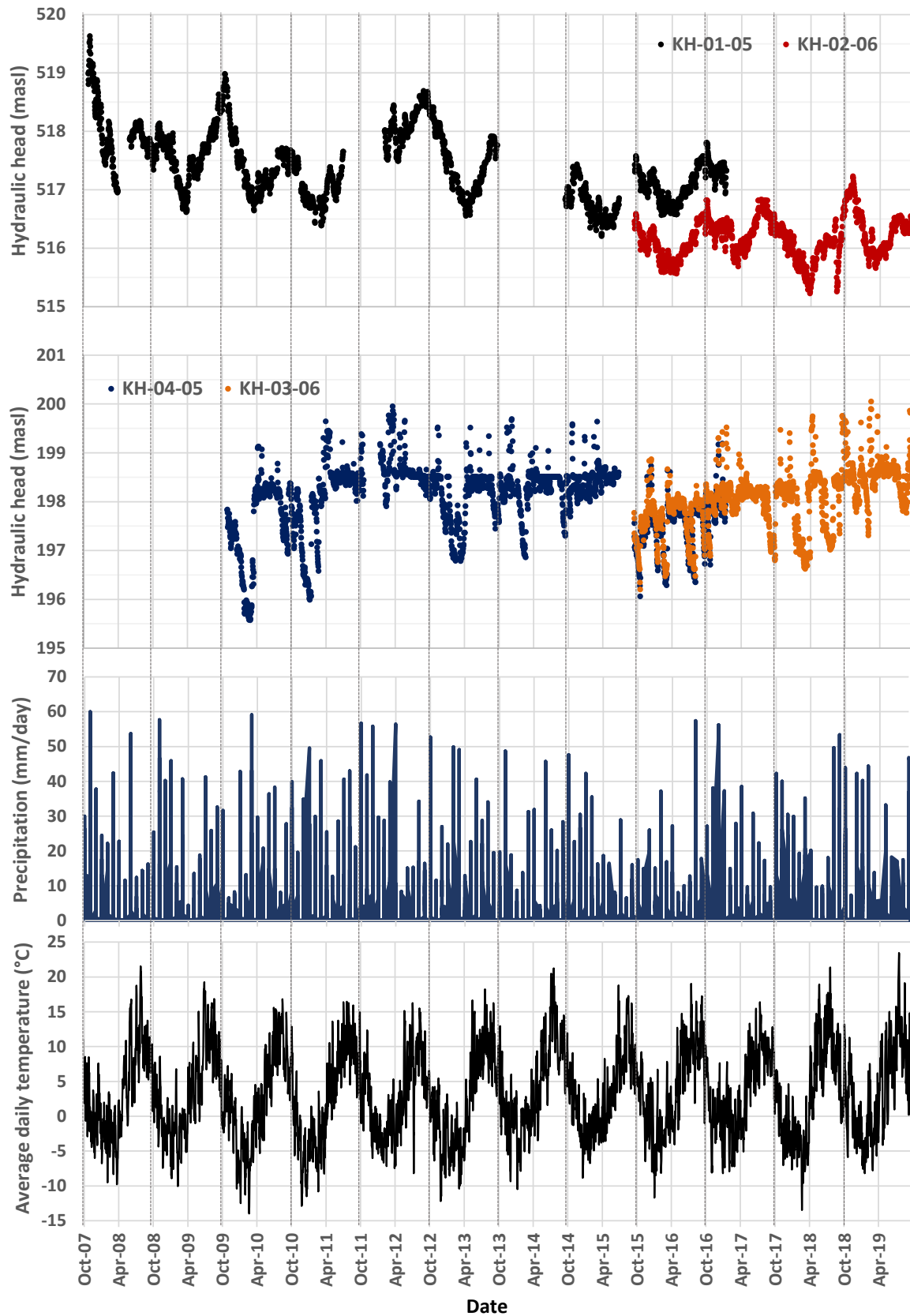


Figure 13. Time-series of the groundwater level measured in the boreholes KH-01-05, KH-02-06, KH-04-05, KH-03-06, precipitation and air temperature.

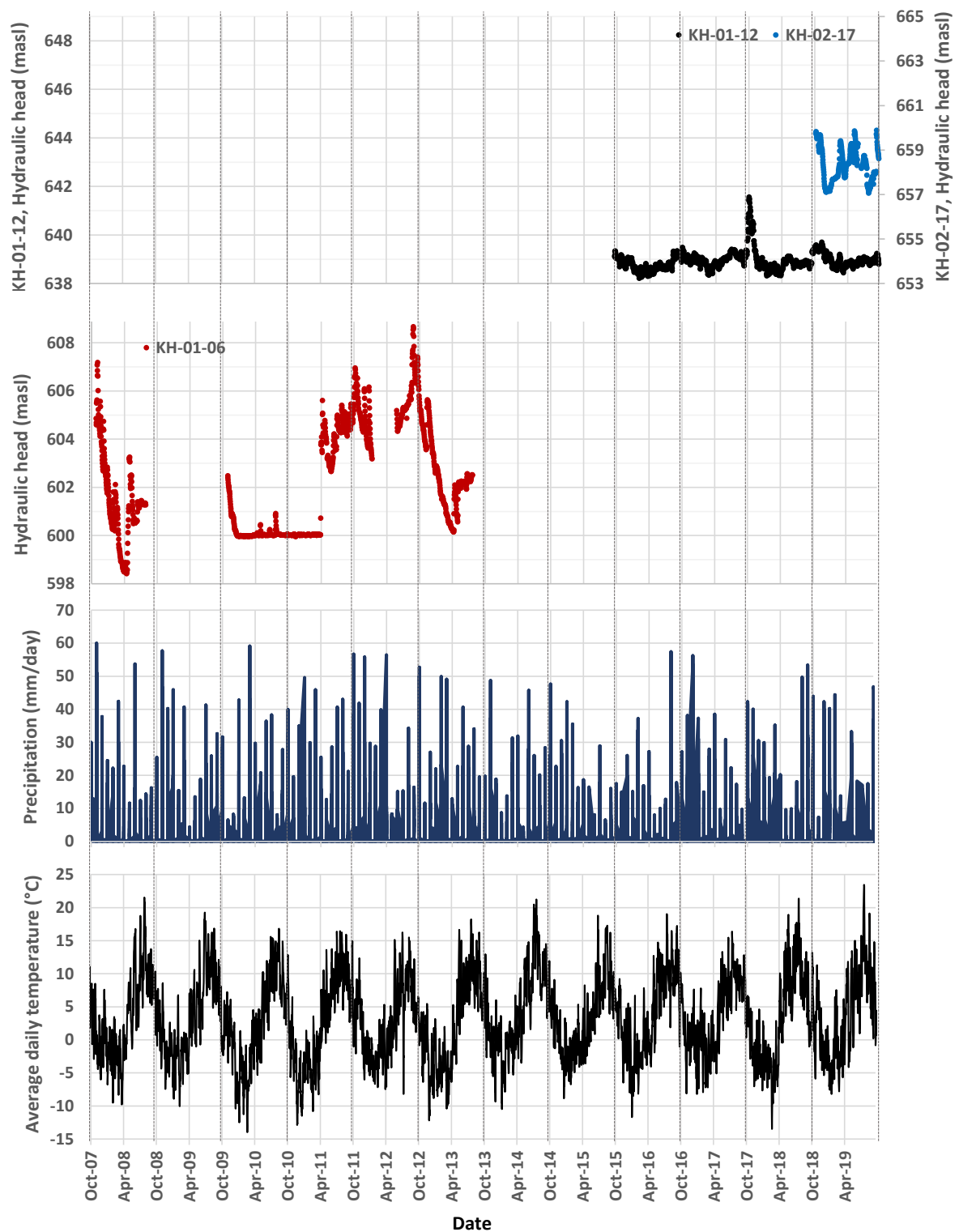


Figure 14. Time-series of the groundwater level measured in the boreholes KH-01-06, KH-01-12, KH-02-17, precipitation and air temperature.

The natural hydraulic gradient of the unconfined water-table has been assessed in Åknes through triangulation of borehole data for the high levels (November) and the low levels (March, Table 5). For the boreholes KH-01-17, KH-01-18, and KH-02-18 instead of using the groundwater level registered in the days specified in Table 5, we have used the water-table position after drilling the borehole, as the groundwater level data in these boreholes is not reliable (Figure 29 to Figure 31, in the Appendix).

The whole slope has an average hydraulic gradient between 0.42 and 0.44 m/m, which is quite high, and reflects the steepness of the terrain. The backscarp area has the highest hydraulic gradient, while the mid-height area has the lowest hydraulic gradient. The changing hydraulic gradient along the slope reflects the heterogeneity of the fractured rockmass and its permeability. The highest hydraulic gradient at the backscarp area supports the hypothesis of a natural “groundwater barrier” in the area dominated by tension fractures (shown as the down-step in Figure 11).

Table 5. Summary of the estimated natural hydraulic gradient of the water-table in Åknes.

Area of the slope	Backscarp	Mid-height	Toe zone	Average for the whole slope
Boreholes used in the calculation	KH-02-17 KH-01-12 KH-01-18	KH-01-17 KH-02-06 KH-02-18	KH-01-17 KH-03-06 KH-02-18	
Average hydraulic gradient (m/m), on the 17/11/2018	0.57	0.29	0.45	0.44
Average hydraulic gradient (m/m), on the 24/03/2019	0.56	0.29	0.41	0.42

3.2.2. Multi-level data from KH-02-17

The multi-level borehole KH-02-17 is located closest to the backscarp and penetrates down to 300 mbg. Eleven sections are isolated with inflatable packers, ten of which have a water pressure sensor installed (Figure 15). As previously shown, it intersects two shear zones, at 33 and 71 mbg.

The topmost sensor is located 24 mbg. It is mostly dry throughout the year, with some short period peaks reaching up to 13 m of water pressure, after which it drains within 15 to 30 days. Some peaks coincide with precipitation events and snowmelt in winter when the air temperature oscillates around 0° Celsius (Figure 15). The sensors installed in the five sections just below this (between 32 and 67 mbg) show continuously dry conditions, meaning that the

intermittently water-bearing section at 24 mbg is likely a perched aquifer that drains relatively quickly. Perched aquifers were also intersected closer to the Upper Easter Stream during the drilling of KH-02-06 and KH-01-05, as there was a sudden loss of pressure at 194 mbg (Biørn-Hansen, 2019).

The sensor at 78 mbg is most likely capturing the (unconfined) water-table located between 656 and 660 masl. It responds to precipitation and snow-melt events, but its amplitude is narrower than in the sections beneath it. Its seasonal variation is very subtle or inexistent.

The sensor at 88 mbg shows very clear peaks coinciding with precipitation and snow-melt events, and it also shows the characteristic seasonal variation with a groundwater level decline during Winter, when the frozen water in the shallowest fractures and soil prevents groundwater recharge, and, the annual high during autumn. The high groundwater levels reached in autumn are due to the cumulative effect of the long recharge period that starts with the snowmelt in early spring, and continues with the rainfall during summer and autumn. The sensor at 101 mbg has a pronounced seasonal variation (amplitude of 14 to 18 m) with few and smoothed short-period peaks. This hydrograph reveals a clear semi-confined to confined behaviour of the fractured rockmass at this depth (Figure 15). The seasonal variation of the hydraulic head measured at 101 mbg is also observed in the open boreholes KH-02-06 and KH-01-12 but with a much lower amplitude (maximum amplitude of 1.6 and 3.1 m, respectively).

The multi-level data obtained so far in KH-02-17 indicates a clear stratification of the hydraulic heads in the fractured rockmass with upward hydraulic gradient in autumn, and downward gradient in winter. The relatively high annual amplitude registered at 101 mbg reflects the seasonal storage of a considerable amount of groundwater, at high elevation in the slope, and very close to the backscarp (122 m). This could be due to the presence of tension fractures which act as natural “groundwater barriers”, as mentioned in section 3.1.2 and illustrated in Figure 10.

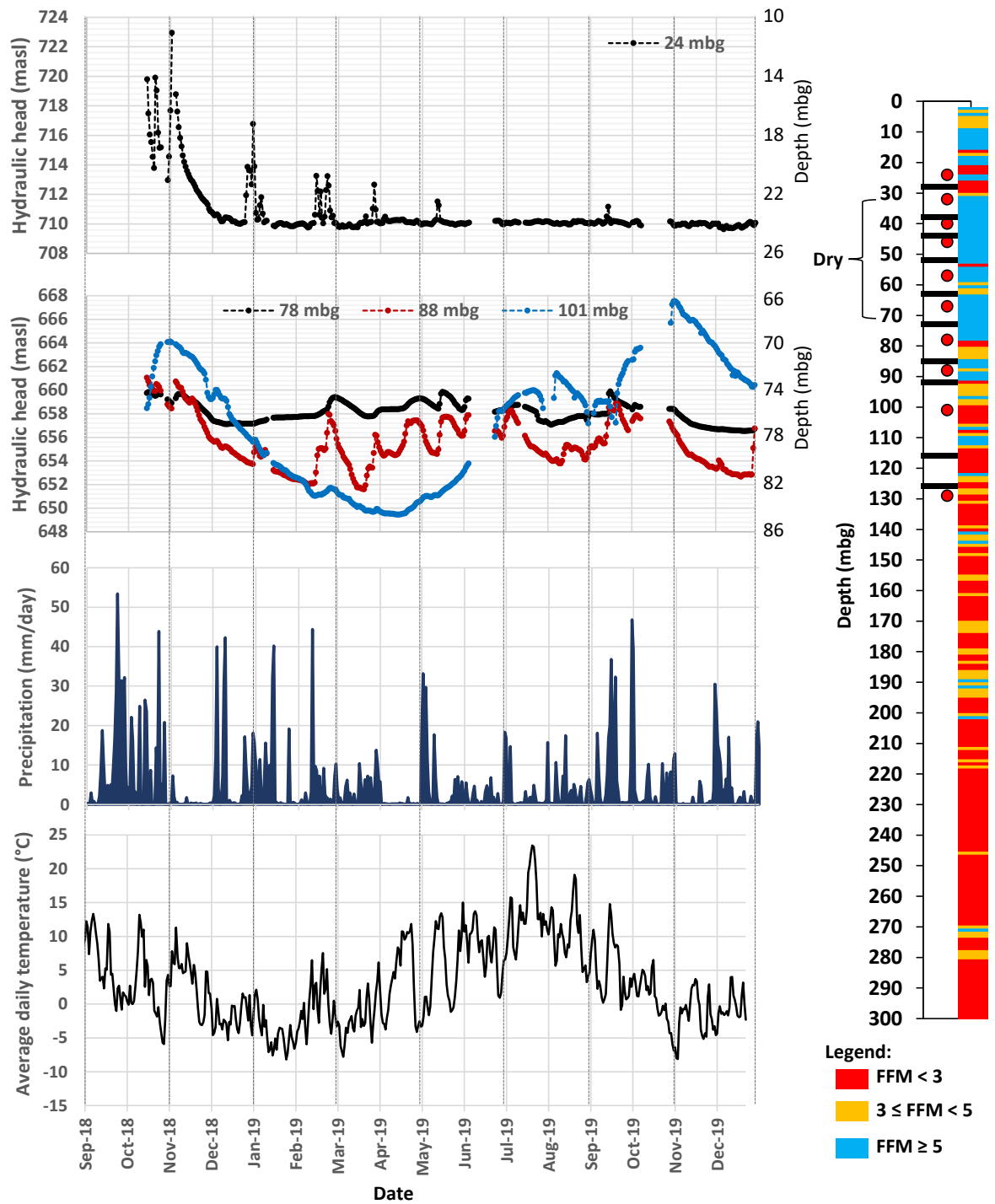


Figure 15. Time-series of selected pressure sensors from the multi-level borehole KH-02-17. Borehole sketch for location of the pressure sensors (red dots) and packers (black lines). FFM is shown for characterization of the fractured rockmass.

3.3. Groundwater chemistry

3.3.1. Physico-chemical parameters and springs' discharge

For the study of the physico-chemical composition of the groundwater and quantification of the natural groundwater discharge rate, field-campaigns were conducted in the spring-summer of 2018 and 2019. Measurement of field-parameters and groundwater sampling took place in the springs that occur at the Upper, Middle and Lower spring horizons (USH, MSH and LSH, respectively). In addition, the Upper Eastern Stream (UES), Lower Eastern Stream (LES), lake Instevatnet, and the rain (at 900 masl) were also sampled (see Figure 4 for location of sampling sites).

In all the field-campaigns of the spring-summer 2018, the flow-rate of the springs increases going downslope; with an average of 0.8 l/s in the Upper Spring Horizon (USH), 1.3 l/s in the Middle Spring Horizon (MSH), and 4.7 l/s in the Lower Spring Horizon (LSH) (Figure 16 and Table 6). This agrees with the findings by Ganerød et al. (2008) and Frei (2008). The lowest registered flow-rates occurred in the beginning of June and mid-July 2018 which were extremely hot and dry months. The MSH and LSH had measurable groundwater discharge (0.4 and 3.4 l/s, respectively) while the UES was almost dry (flow-rate too low to measure). This indicates the presence of a groundwater reservoir with an important storage capacity feeding the MSH and LSH, while the USH and Easter Stream are ephemeral. The highest flow-rates were registered in September 2018 which was characterized by intense rainfall events.

At the beginning of the spring-summer 2019 (in April), the flow-rate at the Lower Eastern Stream (LES) was extremely high (170 l/s) reflecting the considerable amount of surface runoff collected in the Eastern Stream due to the snowmelt contribution. This is also evidenced by the lowest EC value registered at the LSH in this month. In August 2019, the Lower Eastern Stream was dry, reflecting its strong dependency on precipitation and snowmelt (Figure 16).

pH varies from circum-neutral at the Lower Spring Horizon (7.4) to more acidic in the Upper Spring Horizon and Lower Eastern Stream (6.3 and 5.6, respectively). More acidic groundwater, i.e. closer to rainwater pH (5.8, on 11/09/2018), is characteristic of a short residence time, while circum-neutral pH in a granitic-gneissic setting reveals dissolution of feldspar by the naturally occurring carbonic acid in the infiltrating rainwater and snowmelt. As higher the residence time of the groundwater in the rock-slope, higher the content of dissolved solids, and therefore, higher is the Electrical Conductivity (EC). This is clearly seen by the higher EC values recorded in the LSH and MSH throughout the sampling campaigns (Figure 16 and Table 6), and agrees with the findings by Ganerød et al. (2008), and Frei (2008). The downslope increase of the groundwater temperature also sustains the increasing residence time.

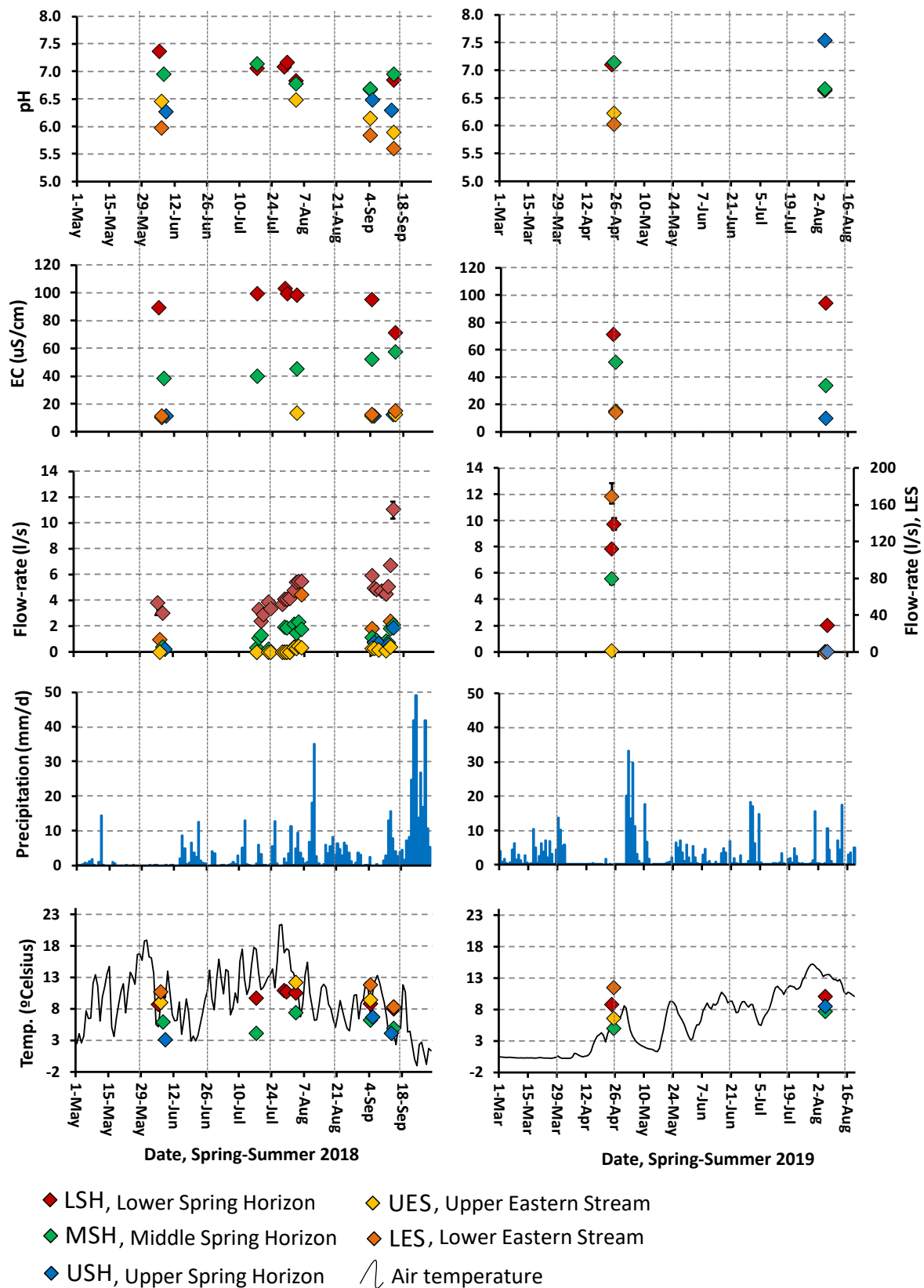


Figure 16. Flow-rate, EC, pH and temperature in each spring horizon; and, daily precipitation and air temperature at the Åknes meteorological station, for the spring-summer of 2018 and 2019.

Table 6. Ranges of the field-parameters (pH, temperature and EC) and flow-rate measured in the main springs and Eastern Stream at Åknes, in the spring-summer of 2018 and 2019.

Spring Horizon	pH range	Temperature range (°C)	EC range (µS/cm)	Peak flow rate (l/s; month/year)	Lowest flow rate (l/s; month/year)
Upper Spring Horizon	6.3 to 7.5	3.1 to 6.7	10 to 12	2.07; Sep/19	0.13; Aug/19
Middle Spring Horizon	6.7 to 7.1	4.1 to 7.7	34 to 57	5.9; Apr/19	0.02; Aug/19
Lower Spring Horizon	6.9 to 7.4	8.0 to 10.9	71 to 103	11.7; Sep/18	2.0; Aug/19
Upper Eastern Stream	5.9 to 6.5	6.6 to 12.3	10 to 15	0.5; Aug/18	0; Jul/18
Lower Eastern Stream	5.6 to 6.0	8.3 to 11.8	11 to 15	170; Apr/19	0; Aug/19

3.3.2. Major elements

Major cations and anions were analysed by ion chromatography at the University of Oslo. Alkalinity was measured through acid titration, either in the laboratory at the University of Oslo within seven days after sampling (first field-campaign), or in the field in the same day of sampling in the field, for the remaining campaigns (Biørn-Hansen, 2019).

The rainwater in Åknes is a highly diluted, slightly acidic, sodium-chloride water. The groundwater in Åknes has low mineralization (EC usually below 100 µS/cm, Figure 16) and very low alkalinity (Biørn-Hansen, 2019), reflecting the granitic rockmass composition and the relatively short residence time that is imposed by the occurrence of wide underground openings, a connected fracture network, and a steep topographic slope.

The predominant anion is either chloride in the Upper Spring Horizon (USH) and Upper Eastern Stream (UES), or sulphate in the Middle and Lower Spring Horizons (MSH and LSH, respectively; Figure 17). As previously mentioned, the first two are highly dependent on rainwater (and snowmelt), and therefore their major elements composition reflects that of rainwater (they plot together on the anions diagram in Figure 17). The reason for the predominance of sulphate at the MSH and LSH is still unsure, but it could be due to the presence of pyrite in the rockmass, and dry deposition influenced by the marine character of the water in the fjord.

Calcium is the predominant cation in the LSH, and in sample S31 of the MSH, which is located at mid width of the slope in this spring horizon. The magnesium fraction is slightly higher than sodium in the western part of the MSH (sample S30), in the USH and in the UES (Figure 17). The predominance of calcium and magnesium in these waters reflects the dissolution of minerals such as plagioclase, amphibole and biotite present in the granitic to dioritic rockmass.

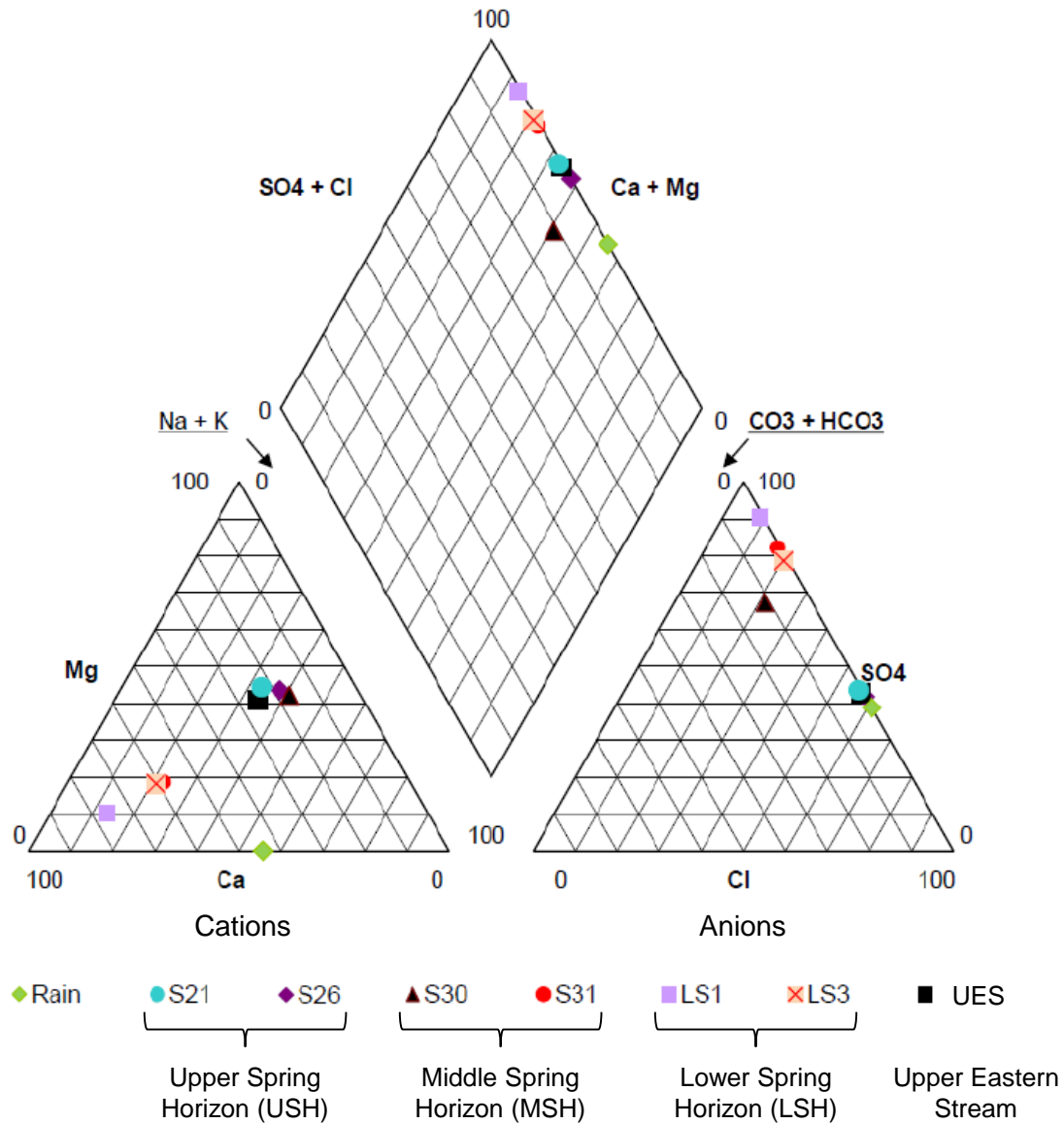


Figure 17. Piper diagram for the water samples collected at Åknes (from Biørn-Hansen, 2019).

3.4. Groundwater recharge

3.4.1. Conceptual model of the groundwater recharge

The groundwater recharge and discharge have been assessed for the purpose of the steady-state numerical model of groundwater flow in Åknes. The identification and characterization of the groundwater recharge and discharge processes are based on field observations, measurement of springs' discharge, and analysis of borehole data. The quantification of groundwater recharge is based on the estimation of the potential evapotranspiration and surface runoff, which depend on empirical equations; the Thornthwaite equation (Thornthwaite, 1948) and the Curve Number method (Dingman, 2015), respectively. Other methods exist to estimate groundwater recharge, namely the chloride mass balance, the

water table fluctuation, numerical methods and other methods based on empirical equations such as the Penman-Monteith (Healy, 2010). The chloride mass balance is most likely not applicable in Åknes, as the amphibole minerals present in the rockmass contain chloride (see Biørn-Hansen (2019) for further details). The other alternative methods could not be tested in the frame of this project, but surely deserve to be tested in a future project concerning the groundwater recharge at Åknes.

The quantification of groundwater discharge, on the other hand, is based on the calibration of the numerical model of groundwater flow against borehole data and the location of the main springs and streams in the slope.

At the beginning of this project, previous hydrogeological studies had raised the possibility that the lake Instevatnet, located at a higher elevation and on the opposite side of the mountain ridge with respect to the unstable slope, could be a source of groundwater recharge. To investigate this hypothesis, two master theses were conducted in this part of the mountain with extensive fieldwork to characterize the fracture network and detect possible groundwater recharge pathways (Bruun, 2019; Ringstad, 2019). The outcomes of these theses indicate that the fracture network, without trough-going fracture zones from the lake to the slope, offer limited capability for groundwater recharge to the unstable slope. The observation of the water level, the inflows to and outflows from Instevatnet, further indicate that this surface water body is not connected to the groundwater body in the unstable slope (Biørn-Hansen, 2019). On the other hand, some large open fractures up-dip from the backscarp suggest the movements in the slope involve higher terrain than reported, suggesting that the unstable slope gradually expands upslope (Ringstad, 2019). These tentatively growing, open fractures represent infiltration paths in the area that feeds the backscarp by surface runoff of snowmelt and rain water. In any case, based in the observations and reasoning around mentioned data, the area located on the opposite side of the mountain slope draining into the Instevatnet catchment, is discarded from the estimates of groundwater recharge to the unstable slope (Figure 18a).

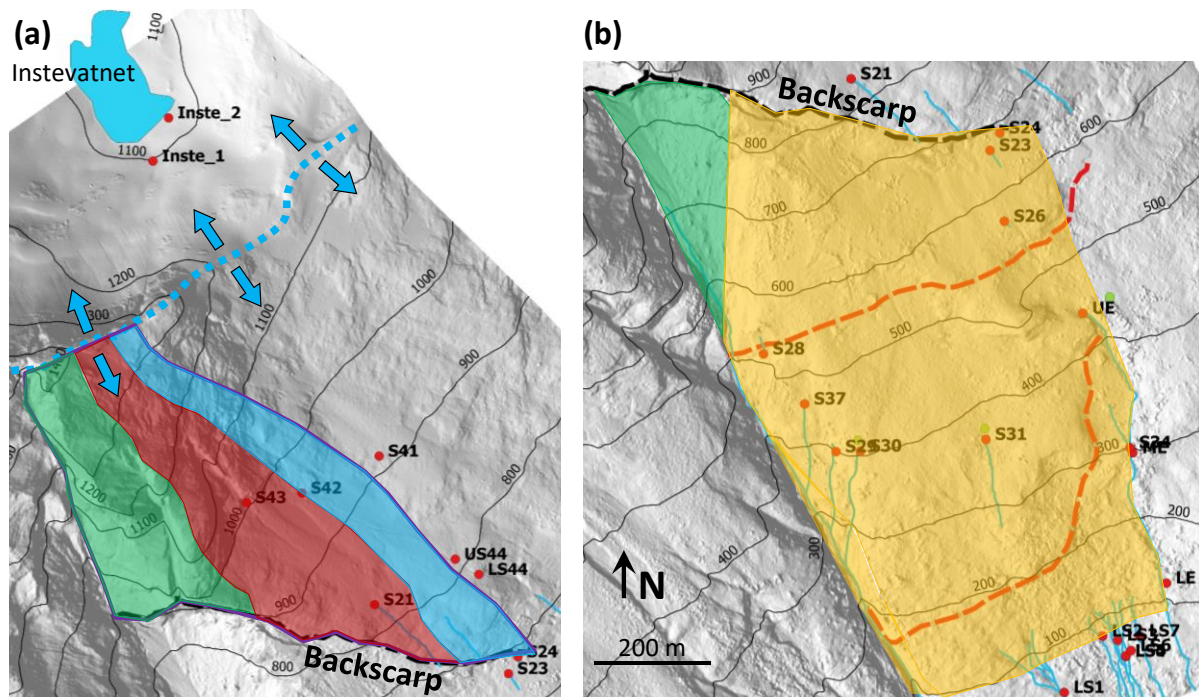
The results attained in this project indicate that the groundwater recharge in the unstable rockmass occurs in three distinct ways (Figure 18):

- (1) Focused and (2) dispersed infiltration of surface runoff originated from the mountain ridge. From the surface water divide (i.e., the mountain ridge) to the backscarp, the scarcity and tightness of the fractures indicate that precipitation and snowmelt lead primarily to evapotranspiration and surface runoff (Biørn-Hansen, 2019) (a). This surface runoff infiltrates (i) as focused infiltration in the graben and open fractures that occur in the west part of the backscarp (immediately downslope the red area in Figure 18a); and, (ii) below the closed section of the backscarp (which is a 10-20 m high cliff) as dispersed infiltration (downslope the blue area in Figure 18a).

- (3) Infiltration of precipitation and snowmelt falling directly on the unstable slope. From the backscarp to the toe zone, the portion of the precipitation and snowmelt that falls directly on the unstable rockmass, left after evapotranspiration and surface runoff, infiltrates and recharges groundwater (yellow area in Figure 18b)

The fraction of the slope highlighted in green in Figure 18 indicates the areas where precipitation and snowmelt lead solely to surface runoff and evapotranspiration, meaning that no groundwater recharge occurs in this part of the slope. This is mainly due to the high steepness of the slope and its location at the upper part of the Western Gully which is a deep crevasse in the terrain that collects rock avalanches and loose boulders, surface runoff from snowmelt and precipitation, and groundwater discharge from the neighbouring springs.

The green, red and blue areas in Figure 18a, are catchment areas that were defined by drawing their boundaries perpendicular to the elevation contour lines, in QGIS.



Groundwater recharge processes (modified after Biørn-Hansen, 2019):

- Surface runoff that feeds surface runoff in the Western Gully (no groundwater recharge)
- Surface runoff that feeds focused infiltration in the backscarp (graben and open cracks)
- Surface runoff that bypasses the backscarp cliff infiltrating diffusely further downstream
- Direct infiltration of rain and snowmelt

Figure 18. Identification of groundwater recharge processes (a) between the mountain ridge and backscarp, and (b) downslope from the backscarp. Blue arrows and dashed line indicate the surface water divide that runs along the mountain ridge. Elevation contours (in masl) in black, and hydrogeology monitoring points in red.

The backscarp is more open to the west, and progressively closes to the east. The graben located on the west is 20 to 30 m deep, 20 to 30 m wide and 150 m long. In the middle part of the backscarp, c. 350 m-long open fractures partially filled with disintegrated rock, penetrate at least 60 m deep. To the east, a 10 to 20 m high rocky cliff runs along for 240 m (Figure 19). During the field-campaigns, water was not seen accumulating in the graben, indicating that this is a relatively permeable zone. Further to the east, during the snowmelt period and rainfall events, temporary streams either infiltrating just above the backscarp or bypassing the rocky cliff as thin waterfalls were observed. In addition, the bouldery terrain that occurs at the foot of the open fractures and rocky cliff contains running water during these periods. Ephemeral springs occur mainly along the foot of the eastern cliff.

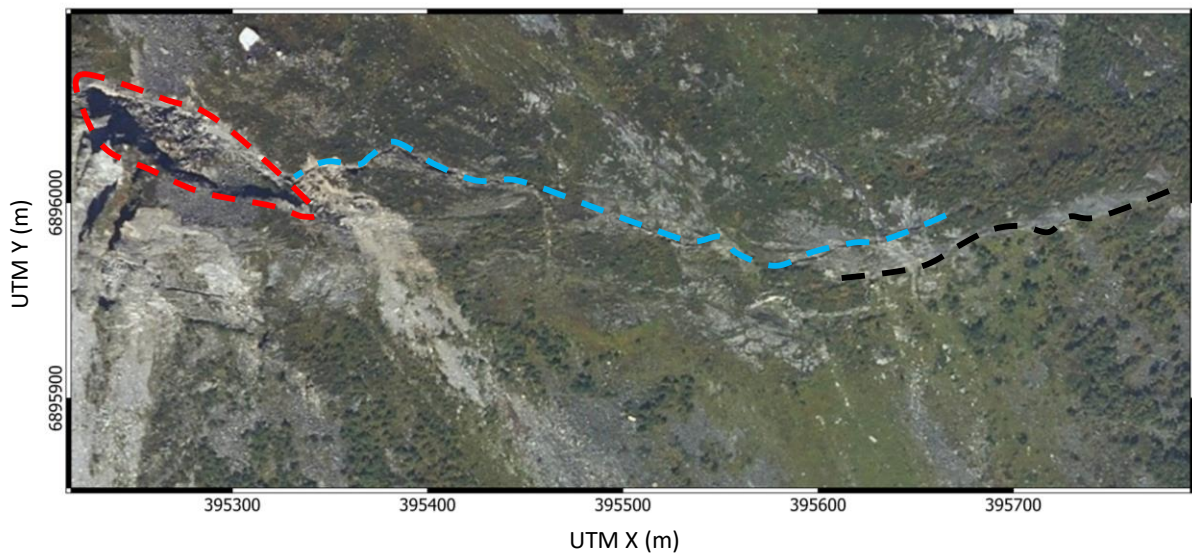


Figure 19. Identification of the backscarp properties that contribute to groundwater recharge. Dashed lines: red – graben; blue – open fractures; black – rocky cliff, 10 to 20 m high.

3.4.2. Estimation of the average groundwater recharge rate

The estimation of the average groundwater recharge rate was conducted for the average annual precipitation and snowmelt rates. For the period between 11th November 2004 and 30th of September 2019, the average annual precipitation registered in the Åknes meteorological station is 1618 mm/year. Since the recorded period is shorter than 30 years, for the purpose of the water balance and numerical model of groundwater flow in Åknes, we decided to use simulated data based on the nearest meteorological stations for which a period of 30 years, from 1st October 1960 to 30th September 1990, is available (XGEO, 2018). The simulated dataset and the Åknes measured dataset show a Pearson correlation factor of 0.92, and 0.71 for the temperature and precipitation, respectively (see Biørn-Hansen (2019) for details). For the 30-years simulated dataset (1960-1990), the average annual precipitation is 1352 mm/yr, and the average temperature is 3°C.

For the purpose of this project, and since it is subject to high uncertainty in its parameterization, we did not estimate the actual evapotranspiration, and therefore, the estimation of groundwater recharge is based on the estimated potential evapotranspiration, using the Thornthwaite method (Table 7). The so estimated annual potential evapotranspiration is 13.6% of the bulk precipitation and snowmelt, which corresponds to 184 mm/yr (Biørn-Hansen, 2019). Due to the scarcity and tightness of the fractures occurring in the area between the mountain ridge and the backscarp, and the high inclination of the slope (35° on average, and one third of the area above 60°), the remaining 86.4% of the bulk precipitation and snowmelt are converted into surface runoff and subsurface flow that infiltrates in the backscarp area, leading to groundwater recharge in the unstable slope (Biørn-Hansen, 2019). This corresponds to 1168 mm/yr of surface and subsurface runoff produced from the mountain ridge to the backscarp, for the normal period 1960-1990.

Table 7. Average monthly precipitation (from www.xgeo.no) and potential evapotranspiration, estimated for Åknes using the Thornthwaite method (Biørn-Hansen, 2019).

Month	Precipitation (mm/month)	Potential Evapotranspiration (mm/month)
Oct	160	15
Nov	157	0
Dec	170	0
Jan	133	0
Feb	101	0
Mar	100	0
Apr	74	10
May	54	34
Jun	64	29
Jul	86	42
Aug	93	31
Sep	160	23
Annual (mm/year)	1352	184

The 1168 mm/yr of surface and subsurface runoff generated between the mountain ridge and the backscarp will naturally flow downslope, eventually reaching the backscarp. Here, due to the depressed topography and wide openings, the water can easily infiltrate. How much of the infiltrated water reaches the water table (recharging the groundwater) and how much is diverted to surface streams is unknown. For the purpose of this study, we assume the worst case scenario, i.e. all of the surface and subsurface runoff water generated from the mountain ridge to the backscarp is assumed to infiltrate and recharge the groundwater. Therefore, we multiply 1168 mm/yr by the red and blue areas shown in Figure 18a, to obtain the annual

volume of water generated above the backscarp and infiltrated in the unstable zone (Table 2 and Figure 4):

- $0.145 \times 10^6 \text{ m}^3/\text{yr}$, as focused infiltration of surface runoff in the graben and open fractures of the backscarp
- $0.118 \times 10^6 \text{ m}^3/\text{yr}$, as dispersed infiltration of surface runoff between the backscarp and the Upper Eastern Stream.

Table 8. Estimation of the surface runoff generated between the mountain ridge and the backscarp that infiltrates in the unstable rock mass, $C = (A/1000) \times B$.

Type and location of infiltration in the unstable rock mass	(A) Annual average surface runoff generated between the mountain ridge and the backscarp (mm/year), normal period 1960-1990	(B) Area above the backscarp where surface runoff is generated (m^2)	(C) Annual volume of surface runoff that infiltrates in the unstable rock mass ($10^6 \text{ m}^3/\text{year}$)
Focused infiltration in the graben and open fractures of the backscarp	1168	124,195 (red area in Figure 18a)	0.145
Dispersed infiltration from the backscarp to the upper part of the Eastern Stream	1168	101,173 (blue area in Figure 18a)	0.118

In the area between the backscarp and the toe zone, the 1352 mm/year of bulk precipitation and snowmelt are distributed into:

- 184 mm/year of evapotranspiration (13.6% of the bulk precipitation and snowmelt)
- 965 mm/year of surface runoff which is channelled along the streams, and therefore does not infiltrate (71.4% of the bulk precipitation and snowmelt)
- 203 mm/year of direct infiltration contributing to groundwater recharge (15.0% of the bulk precipitation and snowmelt)

As previously mentioned, the evapotranspiration was estimated using the Thornthwaite method, while the split between surface runoff and direct infiltration was done using the Curve Number method from the United States Soil Conservation Service (Dingman, 2015). For this purpose, we consider the area between the backscarp and the seawater level to be, on average, covered by a forested soil with a curve number of 38.7, which is between type A (curve number of 25) and type B (curve number of 58). Type A soil is excessively drained and has a high minimum infiltration capacity, while type B soil is moderately drained and has a moderate minimum infiltration capacity. These values should be regarded as a first assessment of the infiltration of direct precipitation and snowmelt in the unstable rockmass. As they are dependent on empirical formulations they lead to uncertainties in the parameterization of the groundwater recharge rate. Assessing the consequences of these

uncertainties in the overall water balance of Åknes and corresponding numerical model goes beyond the scope of this project, and therefore they will not be analysed in this report.

In order to estimate the distribution of groundwater recharge in Åknes, the area above the seawater level (i.e., the fjord water) was split into three sub-areas depending on their groundwater recharge processes (Table 9 and Figure 20):

- Focused infiltration of surface runoff plus infiltration of direct precipitation and snowmelt
- Dispersed infiltration of surface runoff plus infiltration of direct precipitation and snowmelt
- Exclusively infiltration of direct precipitation and snowmelt

The average groundwater recharge rate in the area exclusively with infiltration of direct precipitation and snowmelt is 203 mm/yr, while for the remaining two sub-areas the infiltration of surface runoff from the mountain ridge must be added. In order to do so, we first express the groundwater recharge rate in mm/yr, by dividing the annual volume of surface runoff infiltrating by their corresponding areas (columns A, B and C, in Table 9). Then, we add the 203 mm/year to each of these areas, as shown in Table 9.

Table 9. Calculation of the groundwater recharge rate for the three sub-areas defined in the unstable slope, with an average bulk precipitation and snowmelt of 1352 mm/yr (Normal period 1960-1990).

Groundwater recharge process	Annual volume of infiltrating surface runoff (10^6 m ³ /year)	Area (m ²)	Annual rate of surface runoff infiltration (mm/yr)	Annual rate of infiltration of direct precipitation and snowmelt (mm/yr)	Annual rate of groundwater recharge (mm/yr)	Groundwater recharge (10^6 m ³ /yr)	% of total groundwater recharge to the unstable slope	Dimensionless recharge rate
	A	B	$C=(A/B)*1000$	D	$E=C+D$	$F=(E/1000)*B$	$G=[F/Sum(F)]*100$	$H=E/(1352\text{mm/yr})$
Focused infiltration of surface runoff and infiltration of direct precipitation and snowmelt	0.145	9,092	15,955	203	16,158	0.147	37	11.95
Dispersed infiltration of surface runoff and infiltration of direct precipitation and snowmelt	0.118	64,254	1,839	203	2,042	0.131	33	1.51
Infiltration of direct precipitation and snowmelt	0	583,901	0	203	203	0.118	30	0.15

The so obtained groundwater recharge rates reveal a very uneven distribution of the groundwater recharge in the unstable slope, with a much higher rate in the graben and open fractures of the backscarp (16,158 mm/yr), less between the backscarp and the Upper Eastern Stream (2,042 mm/yr), and much less in the rest of the slope (203 mm/yr). According to our estimations, the highest groundwater recharge rate is located at the upper part of the fastest moving rockmass (Figure 20). This has, of course, very important implications when it comes to an eventual groundwater drainage operation that seeks the increased slope stabilization.

These values are also expressed in terms of dimensionless recharge rate (last column of Table 9) which can be directly applied as a factor to any value of bulk precipitation and snowmelt. These results indicate that in a drainage operation seeking the increased stabilization of the unstable slope, the backscarp should be a prioritized target.

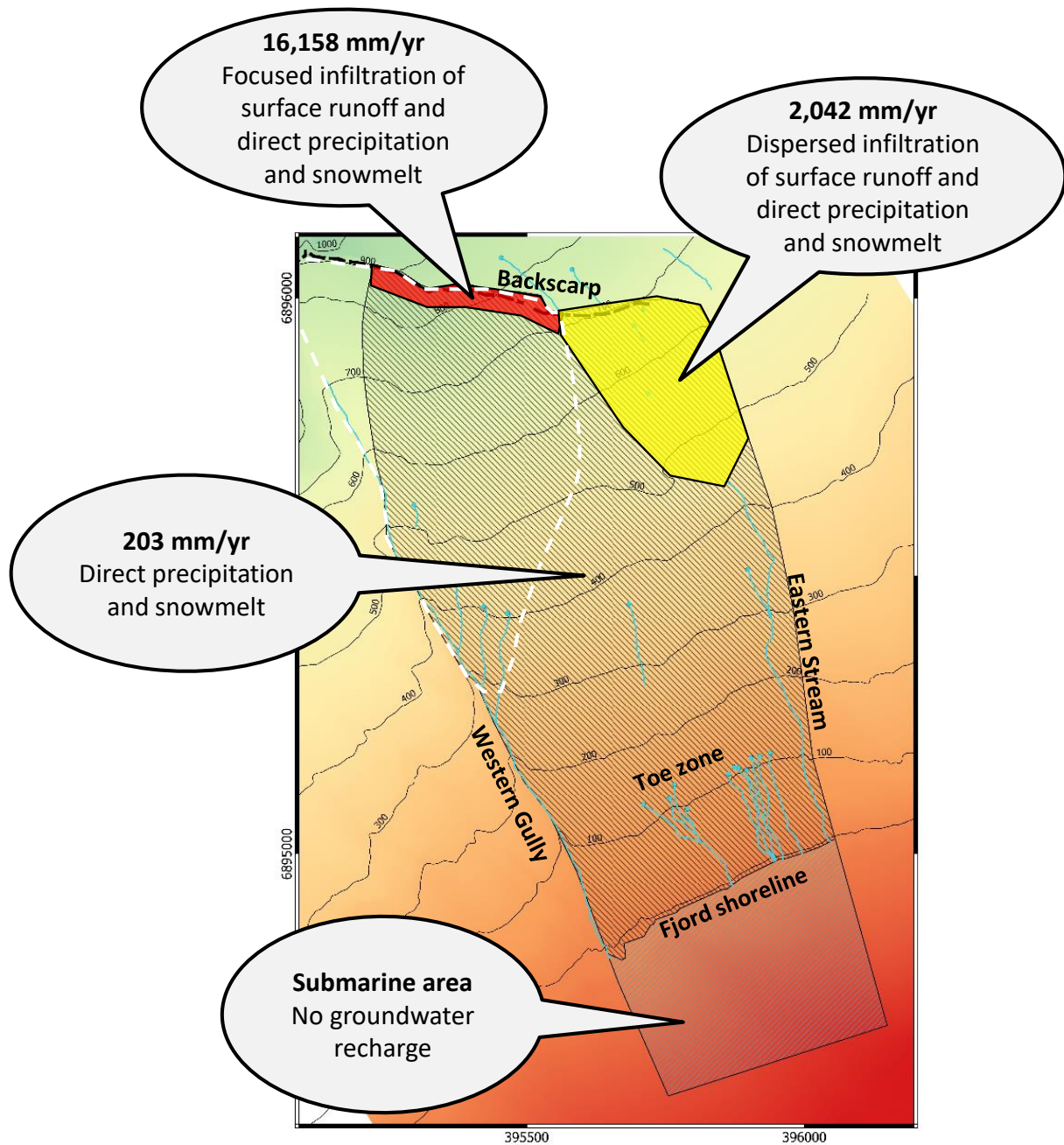


Figure 20. Groundwater recharge rates estimated for the three sub-areas in the unstable slope, with an average bulk precipitation and snowmelt of 1352 mm/yr (Normal period 1960-1990). White dashed line delimits the fastest moving rockmass.

3.5. Three-dimensional numerical model of groundwater flow

3.5.1. Boundary conditions and numerical grid

In order to test the estimated groundwater recharge rates and the conceptual model of the fractured rockmass, we built a three-dimensional (3D) numerical model that simulates the groundwater flow in Åknes, using the equivalent porous media approach. This was done by using the finite-differences numerical modelling code MODFLOW from the United States Geological Survey (Harbaugh, 2005) and the graphical user interface GMS-Groundwater Modelling System, from Aquaveo (Aquaveo, 2019).

This is a steady-state numerical model of groundwater flow in the Åknes unstable slope for an average bulk precipitation and snowmelt of 1352 mm/yr (Normal period 1960-1990). In order to reflect the effect of decreasing fracture frequency with depth on the hydraulic conductivity of the rockmass, the numerical model was divided in three layers. The top of the grid coincides with the topography while the bottom is located between 185 mbg, under the fjord, and 245 mbg, at the backscarp.

The location of the bottom of the grid was defined taking into account the decreasing fracture frequency with depth, with a predominance of less than three fractures per meter between 150 and 200 mbg. This implies a decreased hydraulic conductivity of the fractured rockmass at this depth. As seen in section 3.1.1, borehole KH-01-17 did intersect a zone with higher fracture frequency (equal or higher than five fractures per meter) at 250-280 mbg, which may play a role in the groundwater flow, but the lack of reliable hydraulic head data in this borehole hinders any conclusion. For the sake of simplicity, we decided to neglect this observation in the numerical model of groundwater flow in Åknes.

Given the purpose of this project, we use the MODFLOW package that computes the groundwater flow equation for fully water-saturated media, and therefore neglects the water flow in the unsaturated zone. With this premise, the topmost layer has to contain the computed water-table in order to avoid too many computed dry cells. Since the measured position of the water-table in Åknes deepens from the toe zone (41 mgb at KH-03-06) towards the backscarp (76 mgb at KH-02-17), the thickness of the topmost layer is from 30 m (under the fjord) to 90 m (at the backscarp).

In order to be able to express in the numerical model the overall pattern of the fracture frequency and consequently the changing hydraulic conductivity with depth, the thickness of the middle and bottom layers is 55 and 100 m, respectively. The horizontal spatial discretization is 10 m × 10 m. This means that we are not explicitly simulating any discrete fracture in the groundwater flow model, and neither the perched aquifer that occurs in Åknes. Instead, we are simulating the hydraulic behaviour of the fractured rockmass using the equivalent porous media approach.

Taking into account the optimization of the computed groundwater flow equation in each grid cell, the orthogonal grid was rotated 15 degrees counter clockwise about the K (vertical) axis in order to assure that the majority of the computed groundwater velocity vectors are parallel to the orthogonal grid. The boundary conditions of this numerical model are (Figure 21):

- Impermeable boundaries:
 - Vertical face of all layers along the Backscarp
 - Vertical face of all layers along the eastern boundary that was defined perpendicular to the elevation contour lines, and located approximately 40 m east of the Eastern Stream
 - Vertical face of all layers along the Western Gully
 - Bottom face of the numerical grid which coincides with the bottom of Layer 3
- Specified recharge rate in Layer 1, in the three sub-areas shown in Figure 21, according to the estimation done in section 3.4.2
- Specified head with a value of 0 masl in Layer 1, in the submarine area of the aquifer
- “Drain” (special sub-type of the Cauchy boundary condition where only outflow from the model domain is allowed if the computed hydraulic head is above the topography) in the location of the main springs, in Layer 1

The submarine area of the modelled domain has a constant hydraulic head of 0 masl, prescribed on the top face of the cells located under the fjord in Layer 1. The fjord water has a salinity close to that of sea-water, and one could expect a density correction for the prescribed hydraulic head here. Nonetheless, since the average hydraulic gradient within the freshwater zone of the modelled aquifer (0.43 m/m) is much higher than in normal coastal aquifers (0.0001 to 0.001 m/m), and the area of interest for this numerical model is located between 100 to 900 meters above the saline water of the fjord, we decided not to implement any density correction. In the submarine area, the underlying layers 2 and 3 indirectly discharge to the fjord since they are hydraulically connected to the topmost Layer 1 through their corresponding vertical hydraulic conductivities.

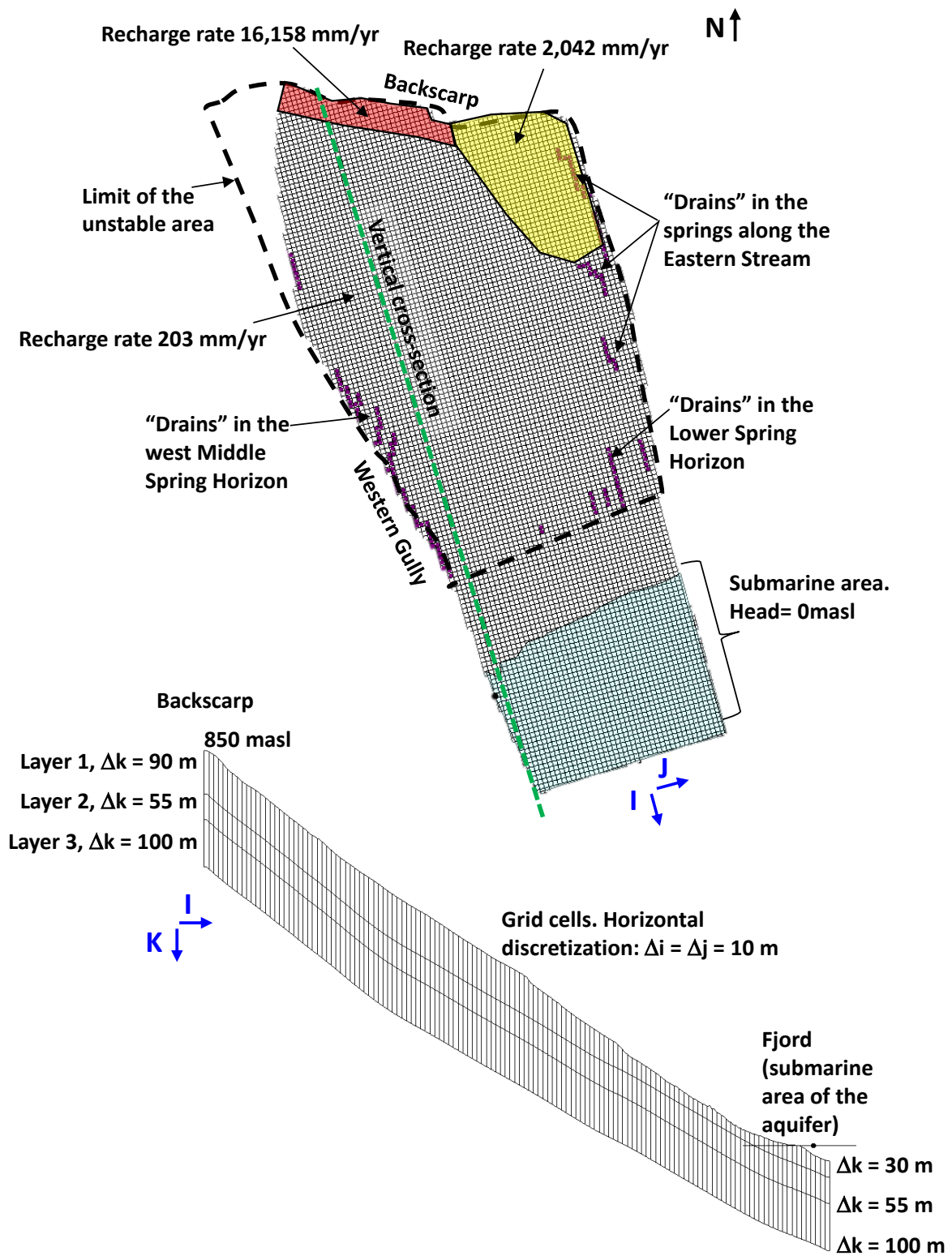


Figure 21. Boundary conditions and grid discretization of the 3D numerical model of groundwater flow. The orientation of the numerical grid axes (I, J, K) is given in blue.

3.5.2. Hydraulic parameterization of the modelled rockmass

Since this is a steady-state groundwater model, the hydraulic conductivity along the three grid axes (I, J, K) is the only parameter needed, besides the hydraulic conductance related to the “Drain” (Cauchy) boundary condition. When assigning the hydraulic conductivity to the three model layers, the results attained in the Lugeon tests performed in three boreholes in Åknes, with investigated depths between 41 and 271 mbg were taken into account. These reveal a hydraulic conductivity range of 0.003 to 0.345 m/d, with an average of 0.109 m/d (NGI, 2020b). Therefore, the premises for the hydraulic parameterization of the modelled rockmass are:

- The hydraulic conductivity range of the whole modelled domain falls within the measured range. The so obtained range is from 0.001 to 0.400 m/d
- Where tension fractures prevail (see section 3.1.2, and Figure 11), a high anisotropy factor is set between the two horizontal hydraulic conductivities (K_i/K_j), where K_i (hydraulic conductivity parallel to slope dip) is set lower than K_j
- Where tension fractures are not dominant, and in order to reflect the higher persistence of slope parallel fractures (i.e. exfoliation fractures) with respect to vertical fractures, the vertical hydraulic conductivity (K_k) is equal or lower than the horizontal (along slope dip) hydraulic conductivity (K_i)

With these premises, we defined sub-domains of the rockmass in each of the three model layers to differentiate tension fracture-dominated areas from the rest of the rockmass. Calibration of the numerical model was done manually by trial and error, targeting a computed hydraulic head that falls inside the range of the groundwater levels measured in five out of seven boreholes with these data; KH-01-05, KH-01-06, KH-02-06, KH-01-12, KH-02-17. We decided to do manual calibration of the hydraulic conductivity values, instead of automatic calibration, since this is not the only unknown parameter. The compartmentalization of different rockmass domains, geometry of the fracture corridors, location of recharge and discharge zones on the surface and underground, and the hydraulic connectivity to the fjord need also to be calibrated. Such a thorough calibration is out of the scope of this project, but should definitely be pursued in future groundwater numerical models of Åknes.

The calibration of the anisotropy factor between the two horizontal hydraulic conductivities (K_i/K_j) resulted in values between 0.03 and 0.3 in Layers 1 and 2, respectively, in the backscarp and the next tension fracture dominated area located downslope (red and green areas in the map view of Layers 1 and 2, in Figure 23). Values between 0.1 and 0.8 were assigned to other parts of Layer 1, based on the location of sub-vertical structures (Figure 11) and expert judgement during model calibration. Layer 3, i.e. the rockmass below 145 mbg (in the backscarp area) and 85 mbg (under the fjord water), is considered isotropic within the horizontal directions of the hydraulic conductivity.

The calibrated hydraulic conductivity values and anisotropy factors assigned to the model domain are shown from Figure 22 to Figure 24.

The “Drain” boundary condition was assigned along eleven curvilinear features that coincide with the main groundwater springs identified and monitored in the field (Middle and Lower Spring Horizons, and springs occurring along the Eastern Stream, Figure 21). Three additional curvilinear features located along the Western Gully, which do not coincide with springs observed in the field, were defined as “drain” boundary condition during model calibration. This is further discussed in section 3.5.4. The hydraulic conductance assigned to all the “Drains” is between 1 and 5 ($\text{m}^2/\text{d}/\text{m}$), which is regarded as the hydraulic conductivity times the width of each curvilinear feature, per unit flow length (Harbaugh, 2005).

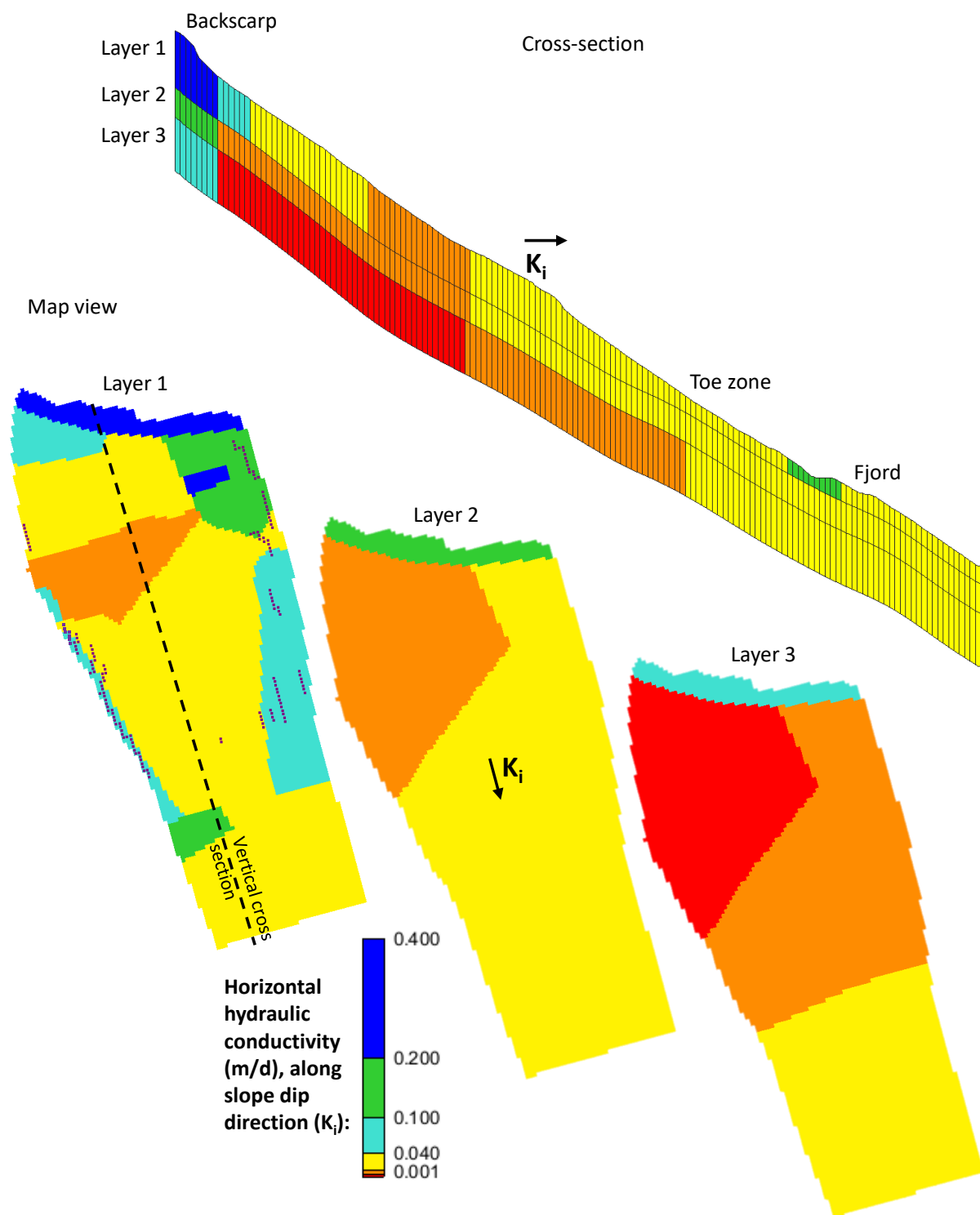


Figure 22. Calibrated values of the horizontal hydraulic conductivity (K_i , in m/d). This is the hydraulic conductivity parallel to the slope dip direction. Purple dots on the map view of Layer 1 indicate "drain" boundary condition.

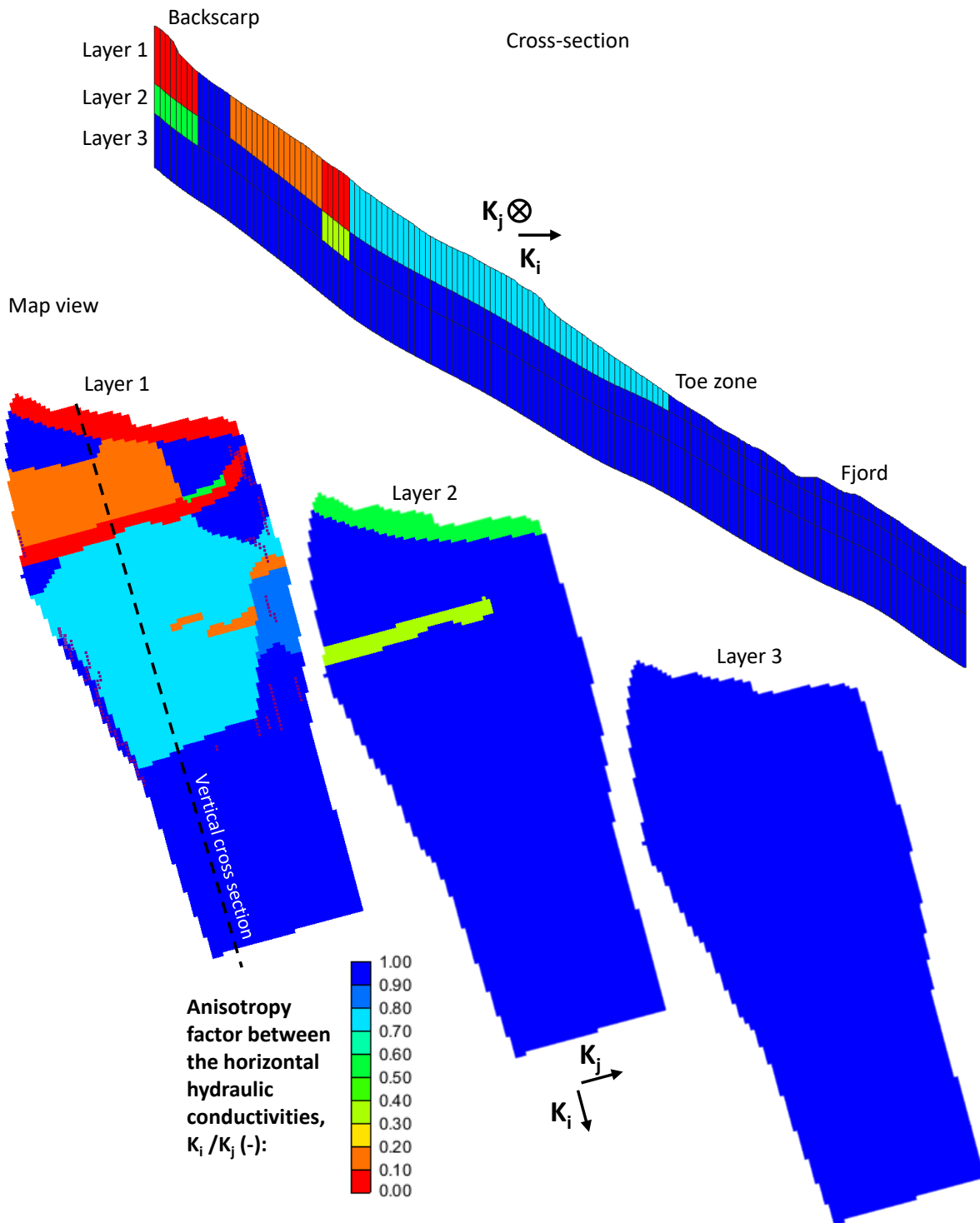


Figure 23. Calibrated values of the anisotropy factor between the two horizontal hydraulic conductivities (K_i/K_j , dimensionless). An anisotropy of one means isotropic. Note how the higher anisotropy (lower values of K_i/K_j , between red and green in the colour scale) was assigned to the backscarp area and other areas dominated by tension fractures. Purple dots on the map view of Layer 1 indicate "drain" boundary condition.



Figure 24. Calibrated values of the vertical hydraulic conductivity (K_k , in m/d). Purple dots on the map view of Layer 1 indicate "drain" boundary condition.

3.5.3. Numerical model results

The computed hydraulic heads for the three model layers are shown in Figure 25. They decrease downslope in all layers, ranging from 850 masl in the backscarp (NW corner in Layer 3) to 0 masl in Layer 1, in the area under the fjord water, where the prescribed head of 0 masl is defined. The hydraulic head computed for Layer 1 corresponds to the unconfined water-table.

In the NW corner of the model domain, the computed water-table falls below the bottom of Layer 1 which is at 90 mbg (non-coloured cells, in the NW of the map view of Layer 1, Figure 25). Nonetheless, Layer 2 is computed overpressured, i.e. with a hydraulic head higher than the top of Layer 2 which coincides with the bottom of Layer 1. The hydraulic head computed in the overpressured part of Layer 2 is between 708 and 682 masl (i.e. between 62 and 107 mbg; white-dotted cells in the NW, in Layer 2, Figure 25). Since vertical connection between the rockmass layers in this part of the backscarp is likely to occur, this means that the unconfined water-table could be between 62 and 107 mbg, which is an acceptable estimation, taking into account the measured hydraulic heads in the nearest multi-level borehole KH-02-17, and the fact that accumulating (or ponding) water was not yet observed in this part of the backscarp. The same downward increase of the hydraulic heads is computed between Layer 2 and Layer 3 in the NW corner, with an overpressured Layer 3 further north (more clearly seen in the map view of Layer 3).

The area with computed downwards increase of hydraulic heads in the backscarp extends downslope into the area where borehole KH-02-17 is located, and this downwards increase of the hydraulic heads is seen in the multi-level data obtained here (shown in section 3.2.2), providing confidence on the model results.

A second area with computed downwards increase of hydraulic heads is located at the toe zone (cross-section, in Figure 25). Here, there is no multi-level borehole data to ground proof the computed result, nonetheless, downwards increase of hydraulic heads are often seen at the foot zone of mountainous steep slopes like Åknes.

One larger middle zone is computed with a downwards decrease of hydraulic heads (cross-section, Figure 25). This is consistent with the loss of water pressure during the drilling of boreholes KH-01-05 and KH-02-06, located closer to the Eastern Stream.

Between the terrain elevation 615 and 620 masl, the computed unconfined water-table is relatively high compared to its downslope neighbouring cells (cross-section view, Layer 1, Figure 25). This water-table high coincides with an area dominated by tension fractures that are numerically simulated with a high anisotropy of the horizontal hydraulic conductivities. These structures obstruct the groundwater flow, the reason for which we designate them as “groundwater barriers”. During model calibration, it was seen that without these areas of high anisotropy, which coincide with the tension fractures-dominated areas, the computed hydraulic heads would fall unrealistically below 100 mbg.

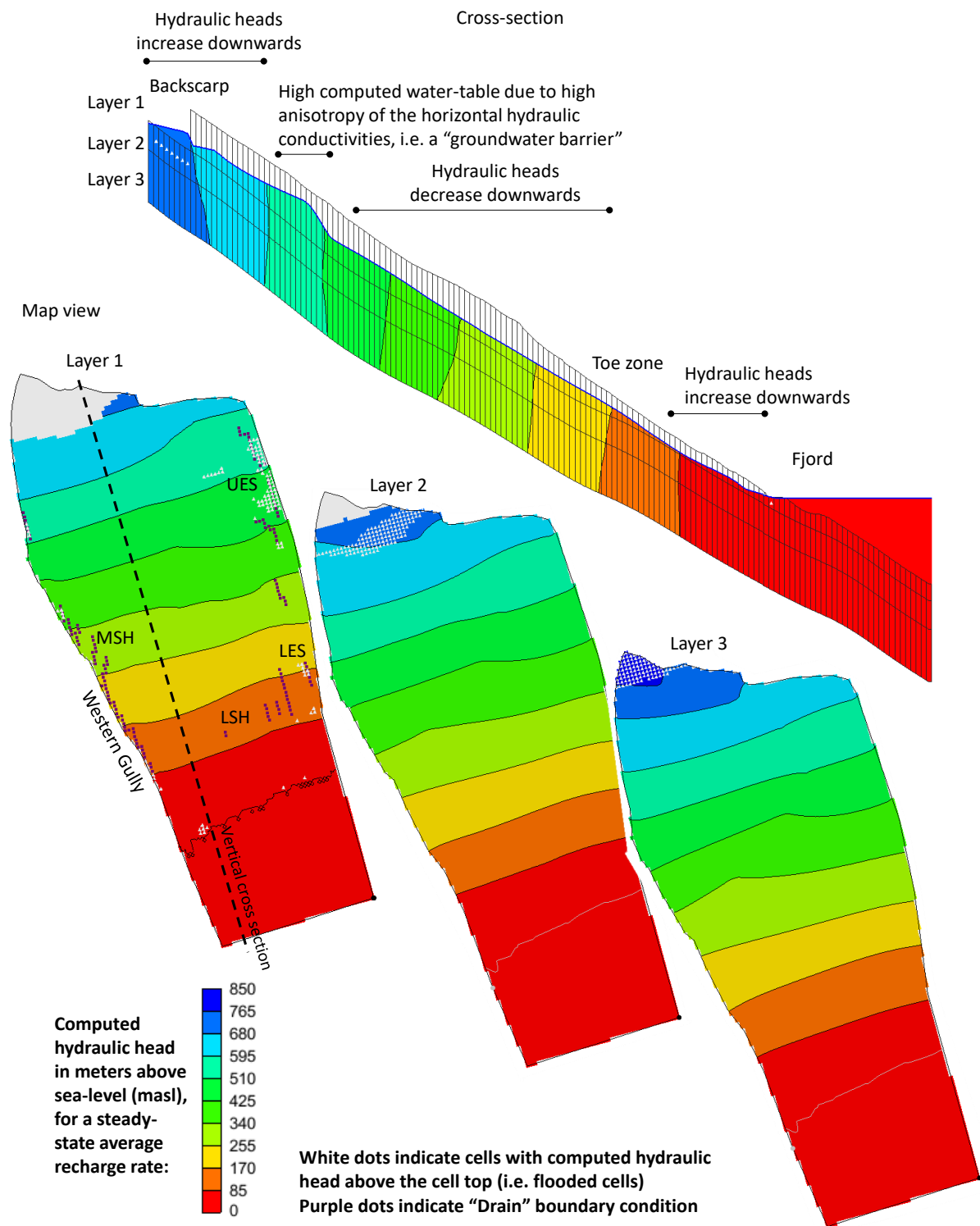


Figure 25. Computed hydraulic head for the three layers of the model domain. The hydraulic head in Layer 1 corresponds to the (unconfined) water-table. In the map view of Layer 1, the location of the Upper and Lower Eastern Stream (UES, LES), and Middle and Lower Spring Horizons (MSH, LSH) is shown.

In Layer 1, some cells along the eastern and western boundaries, and close to the shoreline, have a computed water-table above the topographic surface, which reflects errors in the

parameterization of the numerical model and/or in the geometry and type of boundary conditions that could not be investigated further during this project. The excess height of the computed water table relative to the topographic surface is (Figure 26):

- Less than 2 m in most cells, reaching a maximum of 3 m in four cells in the Upper and Lower Eastern Stream (UES, LES, respectively)
- Less than 2 m close to the shoreline (i.e., the fjord)
- Less than 2 m in most cells, reaching a maximum of 5 m in two cells close to the Western Gully

In the Eastern Stream and Western Gully the topography, and therefore the top of the grid cells, drops dramatically, hindering the parameterization of a steep hydraulic gradient with a 10 m × 10 m spatial resolution (Figure 26). It should be noted however that during the field-campaigns of September 2017, September 2018, and April 2019, the Upper Eastern Stream, and several downstream sections of the Eastern Stream were flooded, swampy and with considerable surface run-off. If these flooded and run-off areas observed in the terrain are an outcropping water-table or a pond above and detached from it, still needs to be clarified. The Western Gully offers a steep slope in the topography, with several springs where the water-table is likely to crop-out.

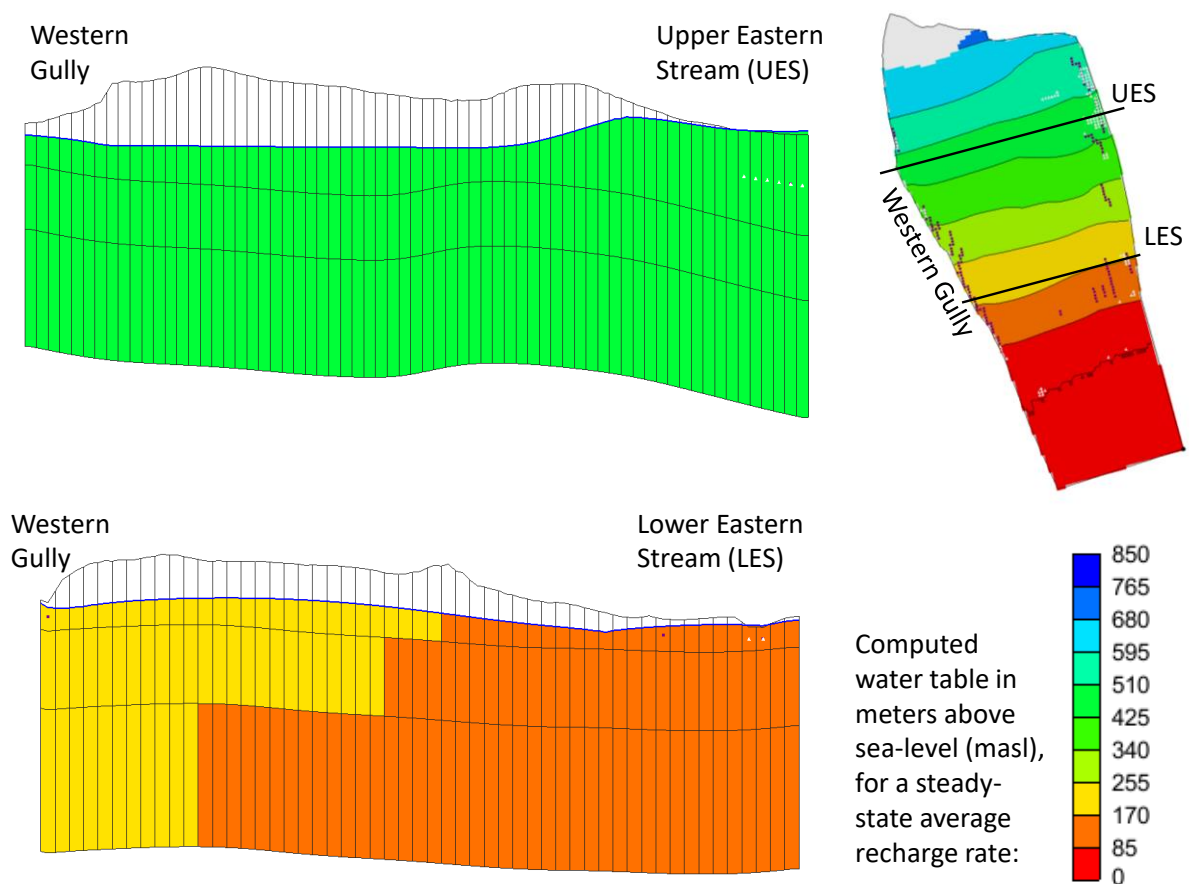


Figure 26. WSW-ENE cross-sections at two elevations in the slope showing computed water table slightly above the terrain in the Upper and Lower Eastern Stream (UES and LES, respectively).

In Figure 27, the comparison between computed and measured water-table is shown. The computed value falls within the range measured in the boreholes KH-01-05, KH-01-06, KH-02-06, KH-01-12, and KH-02-17, which is a fairly good match between computed and measured water-table.

In the boreholes KH-04-05 and KH-03-06 (5 m apart from each other), the manual calibration did not provide a good result, as the computed hydraulic head is 12 m above the maximum measured value (200 masl). These are open boreholes, and therefore what they actually measure is the groundwater level that has equilibrated as a consequence of the hydraulic connectivity created between the fractures intersected by the borehole. The actual water-table could be higher or lower than the measured value. Since these boreholes are located closest to the toe zone, where hydraulic heads likely increase with depth (also confirmed by the numerical results, Figure 25), the undisturbed water table could actually be higher than what we are measuring here. In addition, as these boreholes are so close to each other, interference between them should also be considered.

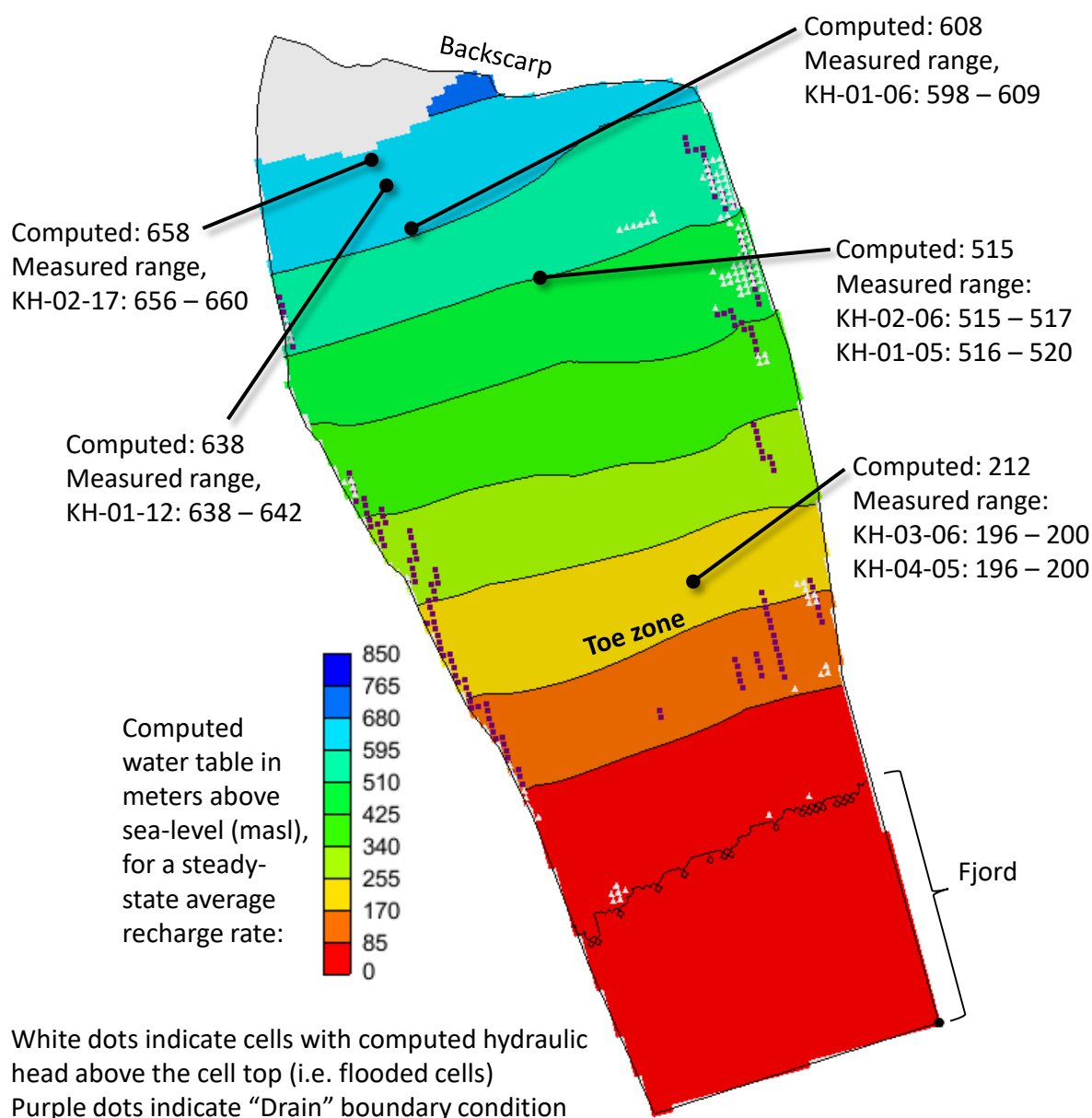


Figure 27. Comparison between computed water-table (i.e., the computed hydraulic head in Layer 1) and the range measured in seven boreholes.

The computed groundwater discharge is 51% ($561 \text{ m}^3/\text{d}$) to the springs modelled as "drains", and 49% ($548 \text{ m}^3/\text{d}$) to the submarine part modelled as prescribed head equal to 0 masl. The actual submarine discharge is very difficult to assess, hindering the discussion of this value. Regarding the computed groundwater discharge at the springs, an attempt is made here to compare with measured data. As seen in section 3.3.1, there is no full-year time-series of groundwater discharge at the springs. In addition, the springs' discharge can change abruptly from day to day during a period with precipitation events. Therefore, we decided to select the lowest measured value that represents the base flow (flow rate in February-March, representative of low groundwater levels), and the highest measured flow that represents the

period when the groundwater levels are highest (October-November). Then, we made a linear interpolation between these values to produce an estimated annual hydrograph of the main springs (Table 10). Based on this approach, we obtain an estimated annual discharge at the main springs in Åknes of 736 m³/d, which is in the same order of magnitude as that computed in the numerical model (561 m³/d).

Table 10. Estimated monthly discharge rate (in l/s, unless another unit is mentioned) at the main springs of the unstable slope; Middle Spring Horizon (MSH), Lower Spring Horizon (LSH), and Upper Eastern Stream (UES).

Month	Measured in:	MSH	LSH	UES
Oct	Highest value, Sep/2018	2.39	11.66	0.5
Nov	Highest value, Sep/2018	2.39	11.66	0.5
Dec		1.85	9.31	0.37
Jan		0.77	4.62	0.12
Feb	Lowest value, Aug/2018	0.23	2.28	0
Mar	Lowest value, Aug/2018	0.23	2.28	0
Apr		0.41	3.05	0.04
May		0.77	4.61	0.12
Jun		1.13	6.18	0.21
Jul		1.49	7.74	0.29
Ago		1.85	9.33	0.37
Sep		2.21	10.90	0.45
Annual average		1.31	6.97	0.25
Annual average (m ³ /d)		113	602	21
Annual Total (m ³ /d)		736		

The overall trend of the distribution of the hydraulic heads obtained in the numerical model is in relatively good agreement with observed borehole data and field observations. The hydraulic parameterization of the fractured rockmass, with hydraulic conductivity values that fall within the measured range, and with the explicit simulation of the rockmass areas dominated by tension fractures, is also a good achievement of this numerical model. The uneven distribution of the groundwater recharge rate applied in the numerical model, with a focused recharge rate of 16,158 mm/yr in the west and mid part of the backscarp, is in accordance to our conceptualization of the groundwater recharge to the unstable slope. The actual numbers of the recharge rate should be further investigated, and the computed flooded cells in Layer 1 indicate that this could be less than what we have estimated now, especially for the eastern part of the modelled domain.

3.5.4. Refinement of the conceptual model informed by the numerical modelling

During the calibration of the numerical model of groundwater flow in Åknes the conceptual model previously defined was put at test, and therefore, refined. In the numerical model, the computed annual springs' discharge is split into:

- 5.6 l/s along the Eastern Stream (86% of total computed springs' discharge), with 3.55 l/s in the Upper Eastern Stream
- 0.05 l/s in the Middle Spring Horizon (1% of total computed springs' discharge)
- 0.18 l/s in the Lower Spring Horizon (3% of total computed springs' discharge)
- 0.67 l/s along the "drain" boundary condition added during model calibration along specific sectors of the Western Gully (10% of total computed springs' discharge)

The computed annual discharge rates at the Upper Eastern Stream (UES), Middle and Lower Spring Horizons (MSH, LSH) differ significantly from what we have estimated based on field measurements; 0.25, 1.31 and 6.97 l/s in the UES, MSH, and LSH, respectively (Table 10). Field observations and monitoring data, indicate that the Eastern Stream is more of a surface runoff and (perched) subsurface water collector than a groundwater collector. Therefore, the computed results indicate that either one or a combination of these refinements of the conceptual model need to be tested:

- 1) The groundwater recharge rate of 2,042 mm/yr applied between the backscarp and the Upper Eastern Stream is likely lower. An unknown fraction of this water is likely diverted along the way without ever reaching the groundwater. It feeds, instead, perched aquifers and streams that are channelled into the Eastern Stream
- 2) The Eastern Stream is not a physical boundary of the groundwater flow. Therefore, the impermeable vertical boundary defined in the numerical model should either be moved further East, or allowed some discharge (whose value is unknown) along it
- 3) Additional heterogeneities exist in the rockmass that divert the groundwater from the eastern part to the middle and western part of the modelled aquifer

During model calibration, additional sectors with the "drain" boundary condition had to be implemented in the Western Gully in order to avoid a computed water table unrealistically located above the topographic surface. If these are actual groundwater discharge areas is still not known. This could be investigated in the field. Alternatively, there might be a lateral groundwater transfer, whose value is unknown, between the unstable slope and neighbouring rockmass to the West.

In the field, we have observed some groundwater discharge at a spring located in the middle of the slope, at an elevation of 370 masl (S31 in Figure 4). This spring has an intermittent (ephemeral) discharge pattern (Biørn-Hansen, 2019) revealing its dependence on precipitation and snowmelt. Nonetheless, the multi-tracer test by Frei (2008) and the hydrochemistry of the water sampled here (Biørn-Hansen, 2019) indicates a clear contribution

from groundwater. As the computed water table in this part of the modelled domain is relatively deep (34 mbg), we decided not to simulate it as a “drain” boundary condition because it would lead to an even deeper computed water table. This indicates that the groundwater contributing to the springs’ discharge is likely related to a local groundwater barrier imposed by the geometry of the fracture network located immediately upslope the main springs in Åknes, forcing the water table upwards until it crops out at the ground surface.

3.5.5. Model evaluation

Following the methodology proposed by Nordstrom (2012) we make here an evaluation of the numerical model of groundwater flow of Åknes:

1. Have the principles of sound science been applied during model development?

Yes. Prior to the development of the numerical model, we have developed a conceptual model of the fractured rockmass and of the groundwater recharge and discharge, based on borehole and field data. This raised two major hypotheses that were tested and confirmed by the numerical model. The refinement of the conceptual model informed by the numerical model was also done. Future work is identified in sections 1 and 6 that can overcome the present-day limitations and narrow uncertainties.

2. How is the choice of model supported by the quantity and quality of available data?

Good. In a fractured media such as Åknes one would expect a finite elements numerical model to simulate the groundwater flow. The goal of our modelling approach was to test the estimated annual groundwater recharge rates and the tension fractures-dominated areas in the rockmass, which means we are not interested in the groundwater flow in discrete fractures. For this reason, we used the equivalent porous media approach, using the finite-differences modelling code MODFLOW.

3. How closely does the model approximate the real system of interest?

Not so close. A discrete fracture network is needed to inform on a higher resolution groundwater model of Åknes that simulates the flow in the unsaturated and saturated zones. Despite this, the groundwater flow model developed here computes hydraulic heads that are within the measured range of five (out of seven) boreholes located at different heights along the slope. The computed annual discharge rate for all the springs in Åknes compares well to the estimation based on field-data. The distribution of the computed discharge rate between the Middle and Lower Spring Horizons, and Upper Eastern Stream does not agree with the values estimated from field-data.

4. How does the model perform the specified task while meeting the objectives set by the project?

Very well. The model helps understanding the hydrogeological system better, and allows for providing advice on management strategies. The main goal of this project was to build-up knowledge on the hydrogeology of Åknes and inform on an eventual groundwater drainage operation that seeks to increase the rock slope stability. With the conceptual and numerical models developed here we were able to point to the possibility of a much higher recharge rate in the backscarp than in the rest of the unstable slope, making it a preferred target in a drainage operation. The identification of the tension fractures-dominated areas as groundwater barriers (confirmed by the numerical model) make these a second most preferred target in a drainage operation.

4. Other project outputs

Throughout the project duration, the following project outputs were produced:

- 1st November 2018, Geofaredagen 2018:
 - The hydrogeology of Åknes: Results from field campaigns. Poster by Frida Liv Biørn-Hansen
 - Structural geological mapping of Åknes for stability and fracture network assessment: field-work results. Poster by Stig Runar Ringstad and Halvor R. Brunn
 - Discrete fracture network model of Åknes rockslide. Oral presentation by Halvor R. Brunn
- January 2019, NGF Vinterkonferanse 2019:
 - Åknes rockslide hydrogeology. Oral presentation by Clara Sena
 - The influence of structural discontinuities on the stability of the Åknes rockslide. Poster by Stig Runar Ringstad
 - Discrete fracture networks in crystalline rock as water conduits at Åknes rockslide. Poster by Halvor R. Brunn
- 14th March 2019. Lunch-talk at the Norwegian Geotechnical Institute (NGI). Assessing the natural groundwater discharge in the Åknes unstable rock-slope. Oral presentation by Clara Sena
- 2019. Three Master theses at UiO, with the corresponding link to the pdf document in the reference list: Biørn-Hansen (2019); Bruun (2019); and Ringstad (2019)
- January 2020, NGF Vinterkonferanse 2020. Groundwater recharge and discharge in the Åknes rockslide – constraining uncertainties for the development of a groundwater flow model. Oral presentation by Clara Sena

5. Limitations and future work

The characterization of the rockmass in Åknes was done based on borehole data. This revealed an overall fracture frequency decrease with depth, but also the presence of discrete high fracture frequency sections at depth (e.g., at 275 mbg in KH-01-17). The equivalent porous media approach used in this work for modelling the groundwater flow in Åknes was useful to test the estimated groundwater recharge rates and the rockmass conceptualization, but it definitely cannot inform on the groundwater flow in the discrete fractures and fracture corridors. In addition, the local groundwater barriers that are likely controlling the location of the main springs in Åknes was also not possible to implement in the 10 m × 10 m spatial resolution of the numerical grid. Therefore, a clear step forward is needed to establish a static discrete fracture network of Åknes that will inform higher resolution groundwater models.

The quantification of evapotranspiration, surface and subsurface runoff, and infiltration (that leads to groundwater recharge) are inevitably linked to high uncertainties as they cannot be measured directly, and need to be estimated based on empirical equations. Here, we have used only two methods to estimate these fluxes (Thornthwaite and the Curve Number methods). As there are alternative methods for the quantification of these fluxes, a stochastic approach should be pursued in order to provide a probabilistic answer to the rates and aerial distribution of groundwater recharge at Åknes, with associated uncertainties.

Åknes has already in place a thorough instrumentation to monitor the groundwater levels and meteorological variables. Additional instrumentation and/or sampling campaigns focusing on environmental groundwater tracers could be tested in order to reduce the uncertainties related to groundwater recharge at Åknes. Such additional work would inform not only the Åknes hydrogeology but also other similar geomorphological settings worldwide.

Discerning the relative amount of groundwater and surface/subsurface water in the water discharged at each spring was not yet done. However, Biørn-Hansen (2019) elaborates a thorough qualitative assessment of this problem based on the hydrogeochemistry of the springs' water. Future work on this matter will narrow the uncertainty on the groundwater flow paths and discharge at Åknes, and improve the calibration of the numerical model of groundwater flow. Implementing particle tracking tools in future groundwater models of Åknes and test it against the results attained by Frei (2008) will also contribute to narrow the uncertainties.

6. Concluding remarks and recommendations

The groundwater flow in Åknes is laminar to turbulent, partially occurring along perched aquifers above the local water table. The high-velocity flow regime, with an average hydraulic gradient of 0.43 m/m, is controlled by the occurrence of wide underground openings, a connected fracture network, and a steep topographic slope. Perched aquifer conditions were detected close to the upper part of the ephemeral Eastern Stream (KH-01-05, KH-02-06) and closer to the backscarp (KH-02-17).

Groundwater recharge occurs through focused and dispersed infiltration of surface runoff and subsurface flow, originated from the mountain ridge, in the backscarp, and infiltration of direct precipitation and snowmelt in the whole unstable slope. Our calculations indicate that the surface runoff infiltrating in the backscarp is a major source of groundwater recharge to the unstable slope, and especially to the fastest moving rockmass.

The groundwater recharge rates and processes presented in this report support that draining or deviating the surface (and subsurface) runoff infiltrating in the backscarp could be a relatively feasible drainage operation that can be properly monitored with the boreholes already installed in Åknes. Cutting the groundwater recharge supply, instead of draining the aquifer itself, is likely to induce a drop of the water table close to the backscarp, and therefore lower the hydraulic gradient down slope. By doing so, the water pressure is likely to decrease in the water-saturated sections of the aquifer, and so is the groundwater flow velocity. Both effects would contribute to increase the stability of the unstable rockmass.

Groundwater discharge occurs at three main spring horizons; Lower, Middle and Upper. The discharge regime and water chemistry reveal a groundwater reservoir with an important storage capacity (therefore, longer residence time) discharging at the bottom of the fastest moving rock mass (West part of the Middle Spring Horizon). An even larger groundwater reservoir feeds the Lower Spring Horizon, at the rockslide's toe zone.

The recently installed multi-level borehole KH-02-17 indicates a clear and significant stratification of the groundwater flow, with downwards increase of the hydraulic heads during autumn-winter (October to January), and downwards decrease during winter-spring (February to June).

The numerical model of groundwater flow should be seen as a first step in the numerical modelling of the water balance and groundwater flow in Åknes. It has provided us a numerical framework that proves two major hypotheses:

- 1) The recharge rate in the backscarp is much higher than in the rest of the unstable slope, due to the infiltration of surface runoff originated from the mountain ridge
- 2) Tension fractures caused by the displacement of the unstable rockmass generate "groundwater barriers" that sustain a relatively high water table at high elevation in the unstable rock slope

This report presents many results but also identifies data and knowledge gaps. New steps in numerical, hydrogeological modelling could prove or disprove the findings in this first numerical model of the groundwater flow in Åknes. Further, complementary field-data and estimation methods would narrow the range of uncertainty. This is our suggested future work:

- Develop and test new field methods to better constrain:
 - the groundwater recharge rate, and its distribution in the mountain
 - the groundwater discharge rate in the main springs and streams
 - the evapotranspiration along the elevation change covered in this mountain, 1000 to 0 masl
- Install a camera capturing images of the western part of the backscarp to check snow accumulation and eventual subsurface discharge during snowmelt and rain events
- Check if the three multi-level boreholes KH-01-17, KH-01-18 and KH-02-18 can become functional with well isolated sections, and therefore provide reliable hydraulic head data
- Develop and test new mathematical formulations to estimate infiltration, evapotranspiration, surface runoff and groundwater recharge in the geomorphological and climatic setting that characterizes Åknes
- Develop a static discrete fracture network model of Åknes for advancement of the hydrogeological and rockslide stability modelling
- Develop a new numerical model of groundwater flow that explicitly simulates the main fracture zones in Åknes, and the perched aquifer conditions that occur during groundwater recharge events
- History-match the novel ground water model to seasonal variations in recharge and discharge of groundwater, and subsequently apply this model in assessment of various groundwater drainage scenarios
- In a calibrated numerical model of the groundwater flow in Åknes, test anticipated changes in the groundwater recharge rates due to climate change

7. References

- Aquaveo (2019). <https://www.aquaveo.com/software/gms-learning>. Page visited on September 2019
- Biørn-Hansen, F. (2019). The Hydrogeochemistry and Water Balance of Åknes Rock Slope. Master thesis. University of Oslo. <http://urn.nb.no/URN:NBN:no-73743>
- Blikra, L. H. (2012). Evaluering av drenering som risikoreduserende tiltak ved Åknes. Åknes/Tafjord Beredskap, Energikonsernet Tafjord. (893).
- Braathen A., Blikra L.H., Berg S.S., Karlsen F. (2004) Rock-slope failures in Norway; type, geometry, deformation mechanisms and stability. Norwegian Journal of Geology, Vol. 84, pp. 67-88
- Bruun, H. (2019). An analysis of bedrock fracture networks based on outcrop data to establish a baseline discrete fracture network model – Åknes rock slope in western Norway. Master thesis. University of Oslo. <http://urn.nb.no/URN:NBN:no-73136>
- Derron, M.H., Blikra, L.H., Jaboyedoff, M., (2005). High resolution digital elevation model analysis for landslide hazard assessment (Åkneset, Norway). In: Senneset, K., Flaate, K., Larsen, J.O. (Eds.), Landslide and avalanches ICFL 2005 Norway. Taylor & Francis Group, London.
- Dingman S. L. (2015) Physical Hydrology. 3rd Edition. Waveland Press Inc.
- Elvebakk, H. (2008). Borehullslogging, Åknes, Stranda kommune. The Geological Survey of Norwegian. NGU report 2008.030
- Elvebakk, H. (2013). Borehullslogging i KH-08, Åknes, Stranda kommune, Møre og Romsdal. The Geological Survey of Norwegian. NGU report 2013.032
- Elvebakk, H. and Pless, G. (2018). Borehullslogging Åknes, Stranda kommune, 2017 – 2018. The Geological Survey of Norwegian. NGU report 2018.026
- Frei, C. (2008) Groundwater Flow at the Åknes Rockslide Site (Norway) Results of a Multi-Tracer Test. MSc thesis, ETH Zurich, Switzerland
- Ganerød, G. V., Grøneng, G., Rønning, J. S., Dalsegg, E., Elvebakk, H., Tønnesen, J. F., Kveldsvik, V., Eiken, T., Blikra, L. H., & Braathen, A. (2008). Geological model of the Åknes rockslide, western Norway. Engineering Geology, 102(1–2), 1–18. <https://doi.org/10.1016/j.enggeo.2008.01.018>
- Ganerød, G.V. (2013). Geological logging of drill cores from borehole KH-08-12 at Åknes, Møre and Romsdal, Western Norway. The Geological Survey of Norwegian. NGU report 2013.039
- Ganerød, G.V., Grøneng, G., Aardal, I.B., Kveldsvik, V. (2007). Logging of drill cores from seven boreholes at Åknes, Stranda municipality, Møre and Romsdal County. The Geological Survey of Norwegian. NGU report 2007.020
- Grøneng, G., Lu, M., Nilsen, B., & Jenssen, A. K. (2010). Modelling of time-dependent behavior

- of the basal sliding surface of the Åknes rockslide area in western Norway. *Engineering Geology*, 114(3–4), 414–422. <https://doi.org/10.1016/j.enggeo.2010.05.017>
- Grøneng, G., Nilsen, B., & Sandven, R. (2009). Shear strength estimation for Åknes sliding area in western Norway. *International Journal of Rock Mechanics and Mining Sciences*, 46(3), 479–488. <https://doi.org/10.1016/j.ijrmms.2008.10.006>
- Harbaugh, A.W., 2005, MODFLOW-2005, The U.S. Geological Survey modular groundwater model – the Groundwater Flow Process: U.S. Geological Survey Techniques and Methods 6- A16
- Healy, R.W. 2010. Estimating groundwater recharge. Cambridge University Press. <https://doi.org/10.1017/CBO9780511780745>
- Jaboyedoff, M., Oppikofer, T., Derron, M.-H., Blikra, L. H., Böhme, M., & Saintot, A. (2011). Complex landslide behaviour and structural control: a three-dimensional conceptual model of Åknes rockslide, Norway. *Geological Society, London, Special Publications*, 351(1), 147–161. <https://doi.org/10.1144/sp351.8>
- NGI (2020a). Åknes rock slope. Monitoring of displacements. Norwegian Geotechnical Institute report number 201080662-05-R
- NGI (2020b). Åknes rock slope. Hydrogeological report. Norwegian Geotechnical Institute report number 201080662-06-R.
- Nordstrom, K. 2012. Models, validation and applied geochemistry: issues in science, communication and philosophy. *Applied Geochemistry*, 27: 1899–1919.
- Nordvik, T., Grøneng, G., Ganerød, G. V., Nilsen, B., Harding, C., & Blikra, L. H. (2009). Geovisualization, geometric modelling and volume estimation of the Åknes rockslide, Western Norway. *Bulletin of Engineering Geology and the Environment*, 68(2), 245–256. <https://doi.org/10.1007/s10064-009-0198-x>
- Oppikofer, T., Jaboyedoff, M., Pedrazzini, A., Derron, M. H., & Blikra, L. H. (2011). Detailed DEM analysis of a rockslide scar to characterize the basal sliding surface of active rockslides. *Journal of Geophysical Research: Earth Surface*, 116(2), 1–22. <https://doi.org/10.1029/2010JF001807>
- Papadimitrakakis, I. (2020). Åknes rock mass characterization rockmass characterization. Internal report, UiO NVE collaboration project
- Ringstad, S.R. (2019). The influence of structural discontinuities on the stability of the Åknes rockslide. Master thesis. University of Oslo. <http://urn.nb.no/URN:NBN:no-73149>
- Storrø, G. and Gaut, S. (2008). Sporstofforsøk på Åkneset, Stranda commune – Møre og Romsdal fylke. The Geological Survey of Norway. NGU report 2008.091
- Tassis G., Rønning J.S. (2019). Reprocessing of Refraction Seismic data from Åknes, Stranda Municipality, Møre & Romsdal County. The Geological Survey of Norway. NGU report 2019.004
- Thornthwaite (1948). An Approach toward a Rational Classification of Climate. *Geographical*

Review, Vol. 38, No. 1, pp. 55-94

XGEO (2018). URL <http://www.xgeo.no>. Accessed: 2018-10-01.

Appendix

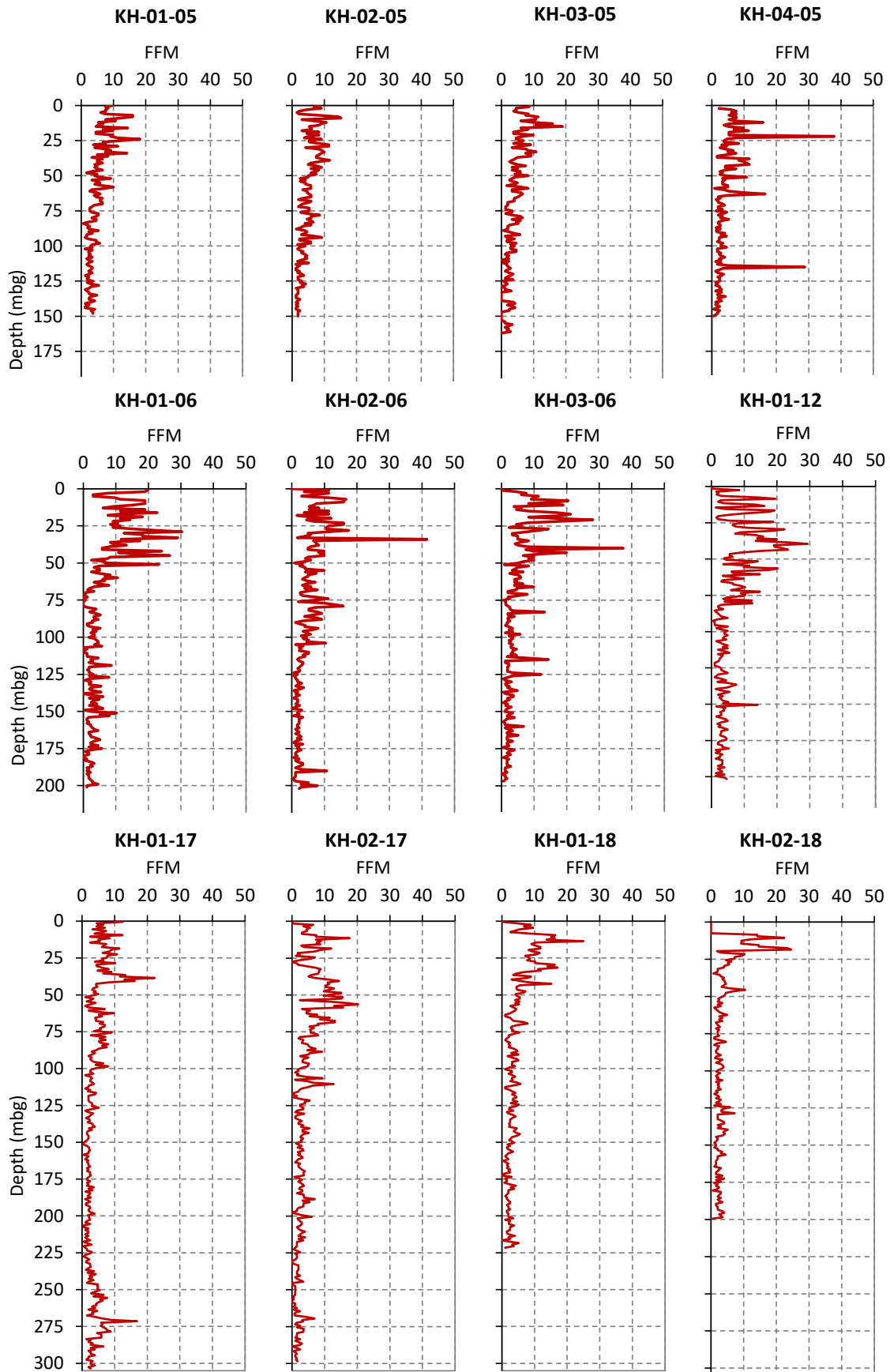


Figure 28. Corrected fracture frequency for the boreholes without televiewer log (2005 to 2006) and the average fracture frequency for the boreholes with both datasets (2012 to 2018).

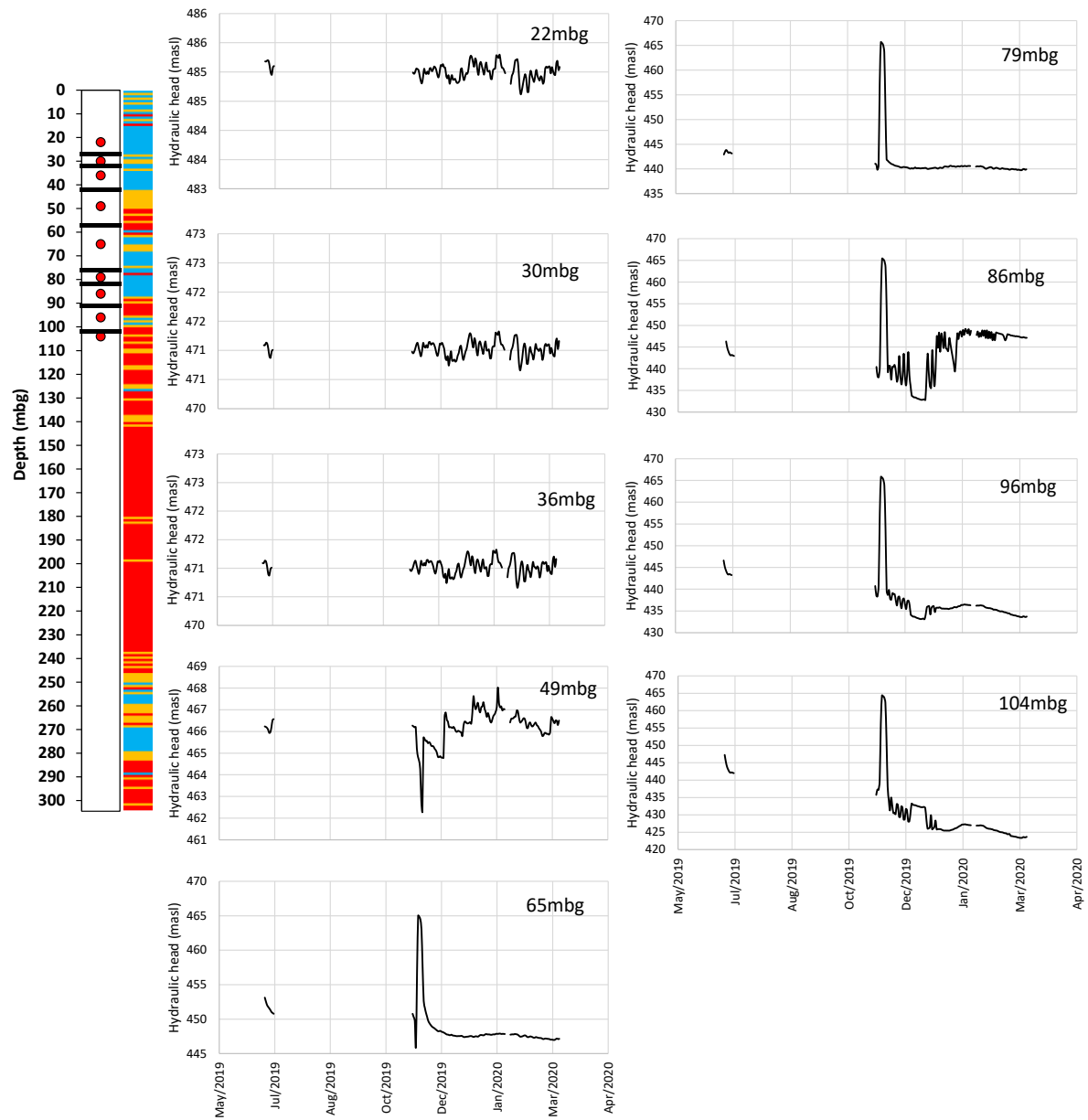


Figure 29. Borehole KH-01-17 sketch, and time-series of the pressure sensors.

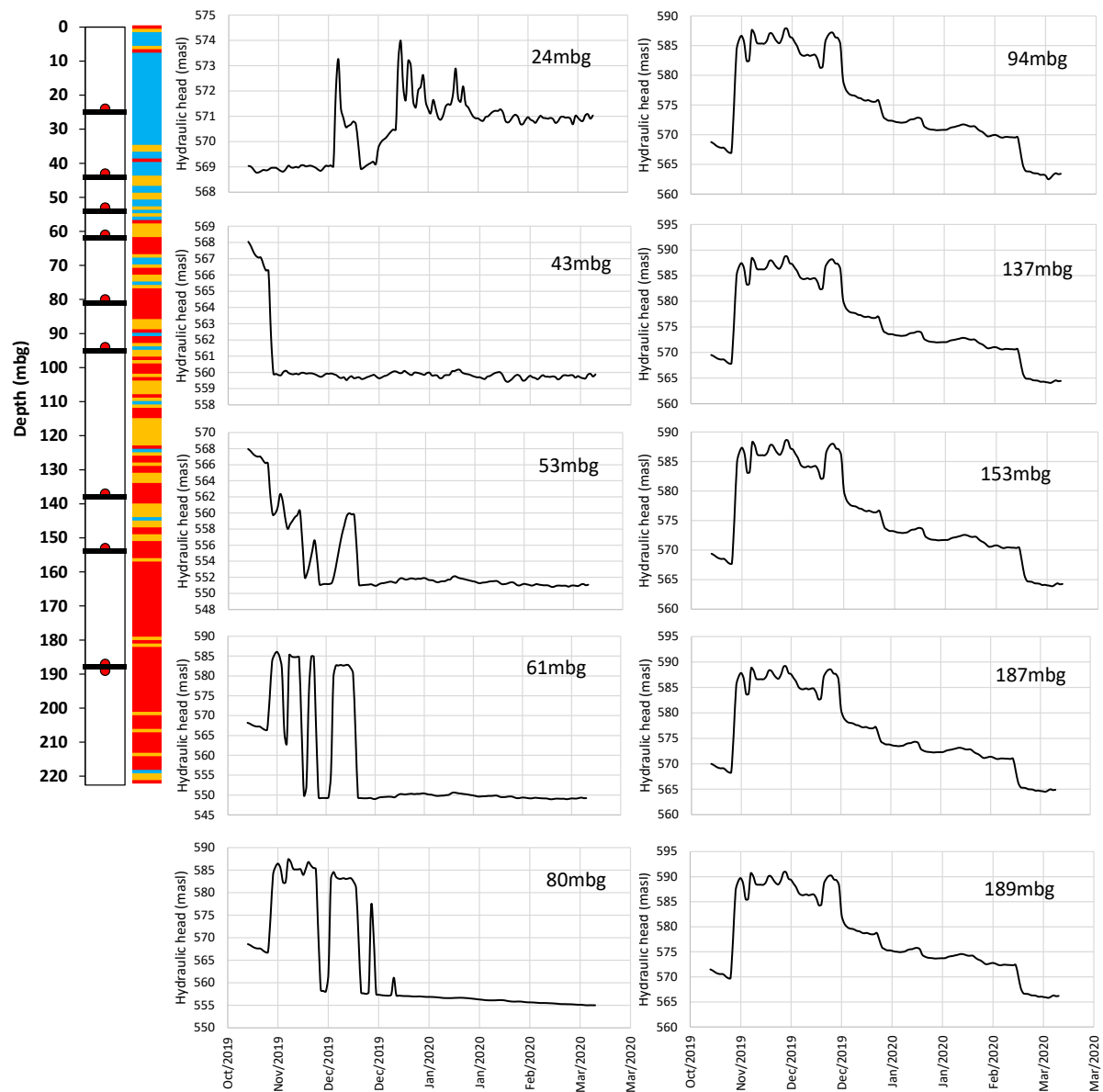


Figure 30. Borehole KH-01-18 sketch, and time-series of the pressure sensors.

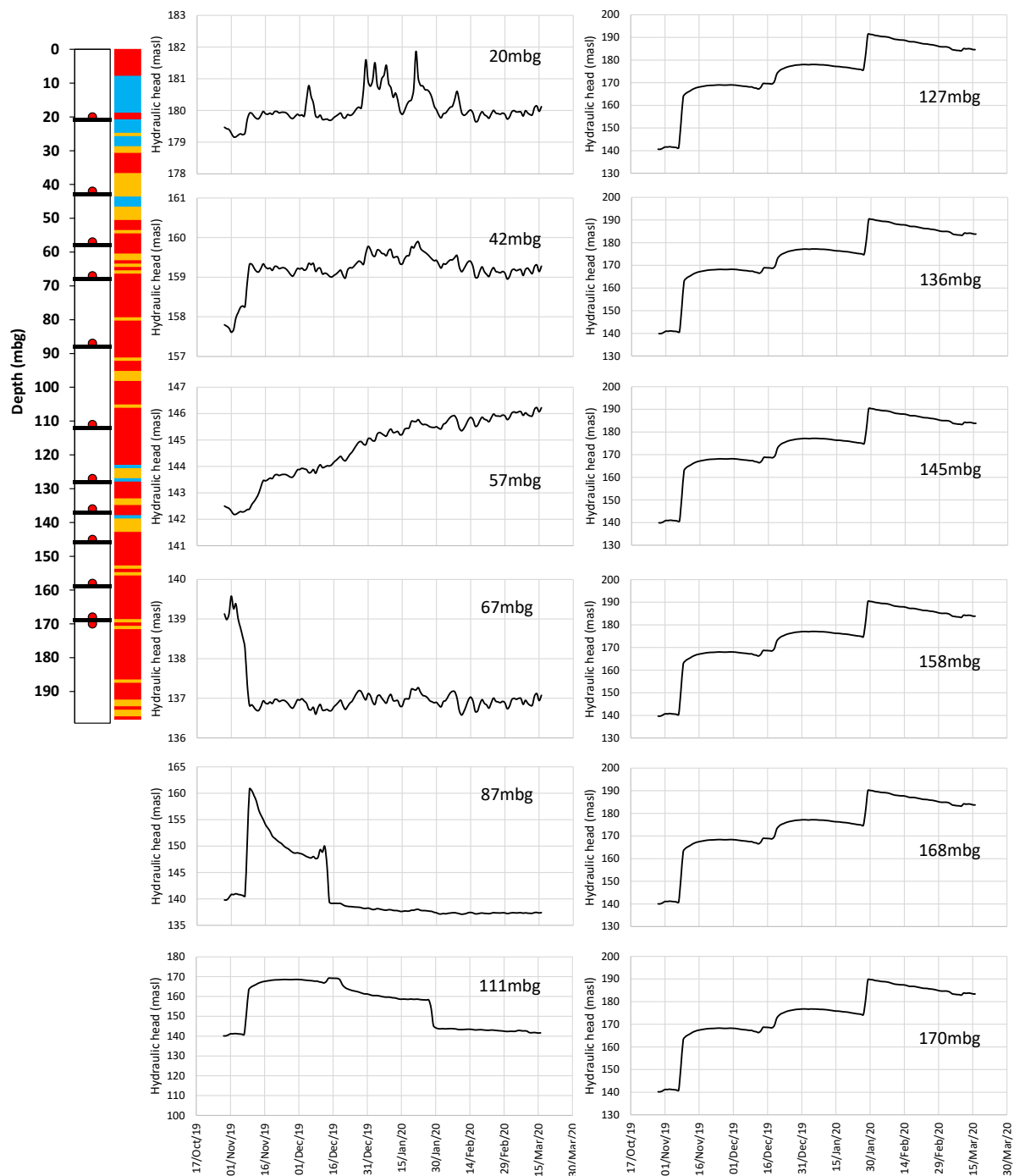


Figure 31. Borehole KH-02-18 sketch, and time-series of the pressure sensors.

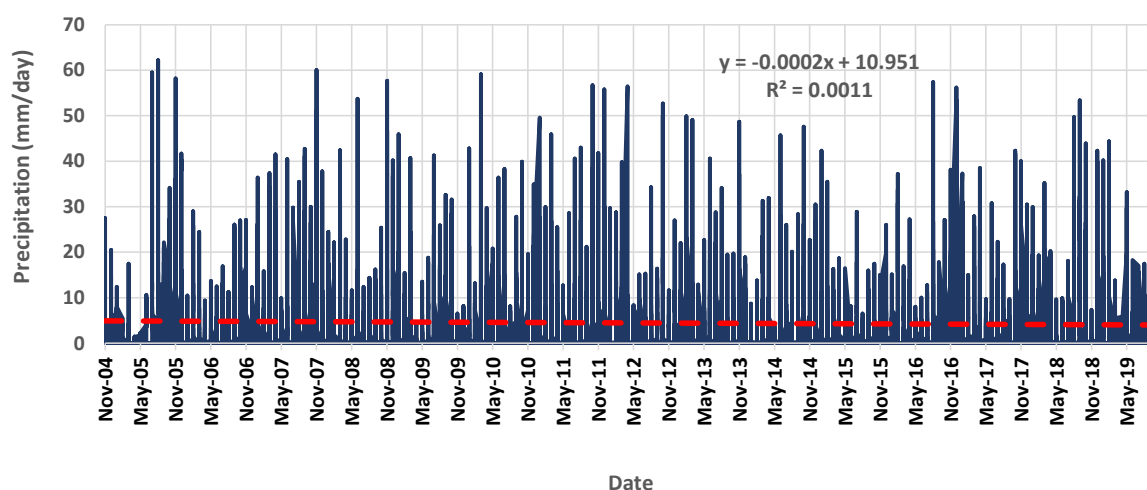


Figure 32. Time-series of daily precipitation, from November 2004 to September 2019, at the Åknes meteorological station.

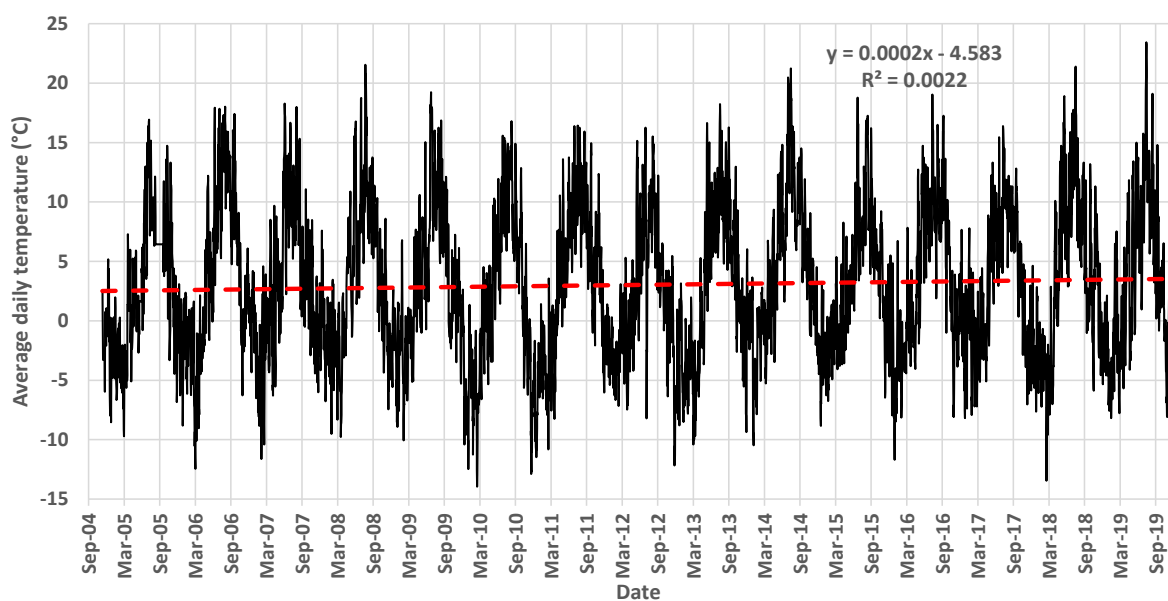


Figure 33. Time-series of average daily air temperature, from November 2004 to September 2019, at the Åknes meteorological station.



UiO : Department of Geosciences
University of Oslo

Åknes rock mass characterization

January – July 2020

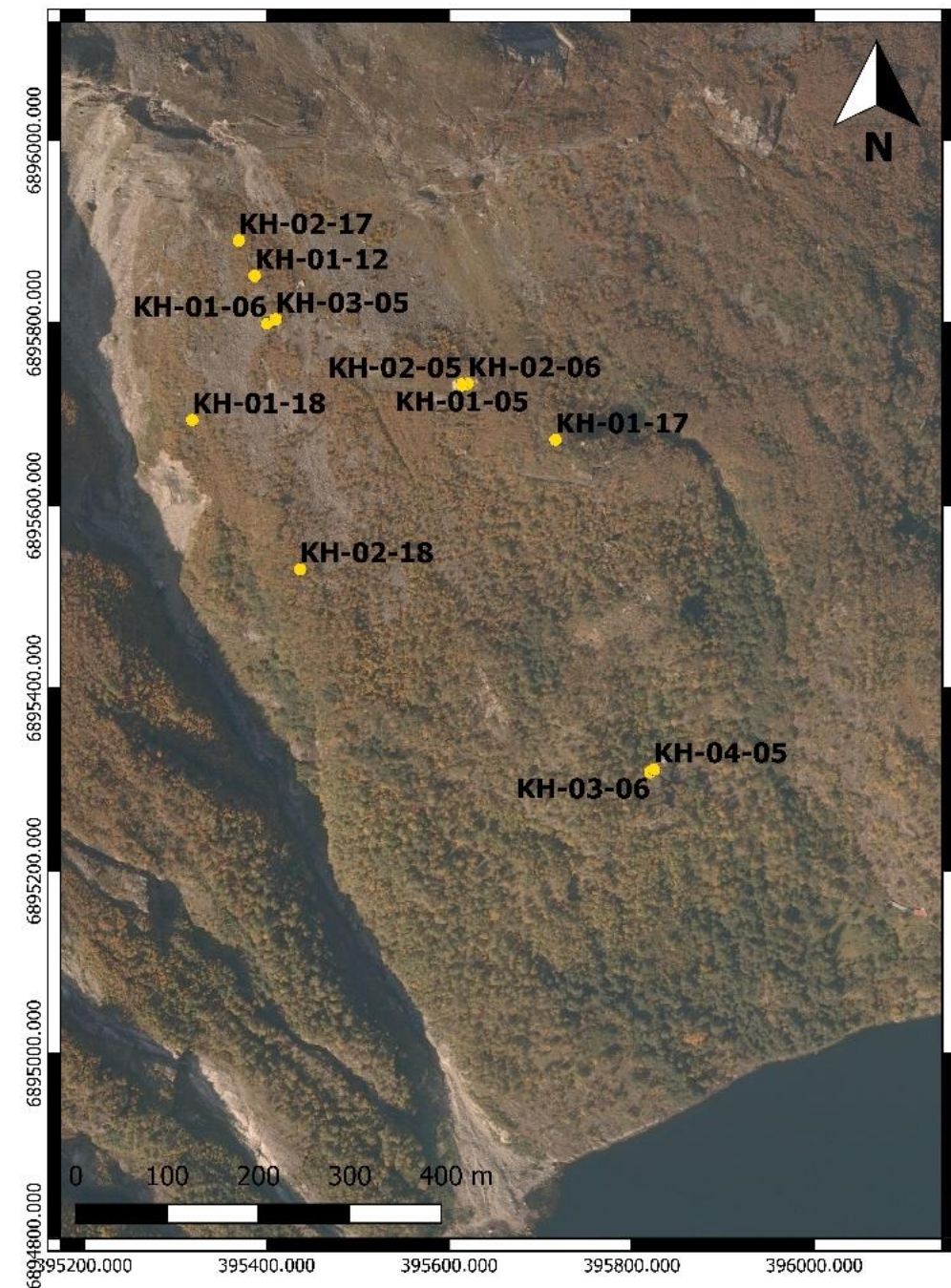
Ioannis Papadimitrakis



The first step towards the definition of the rock mass domains was to process the available fracture frequency data from televiewer and geological logging.

Processing fracture frequencies data:

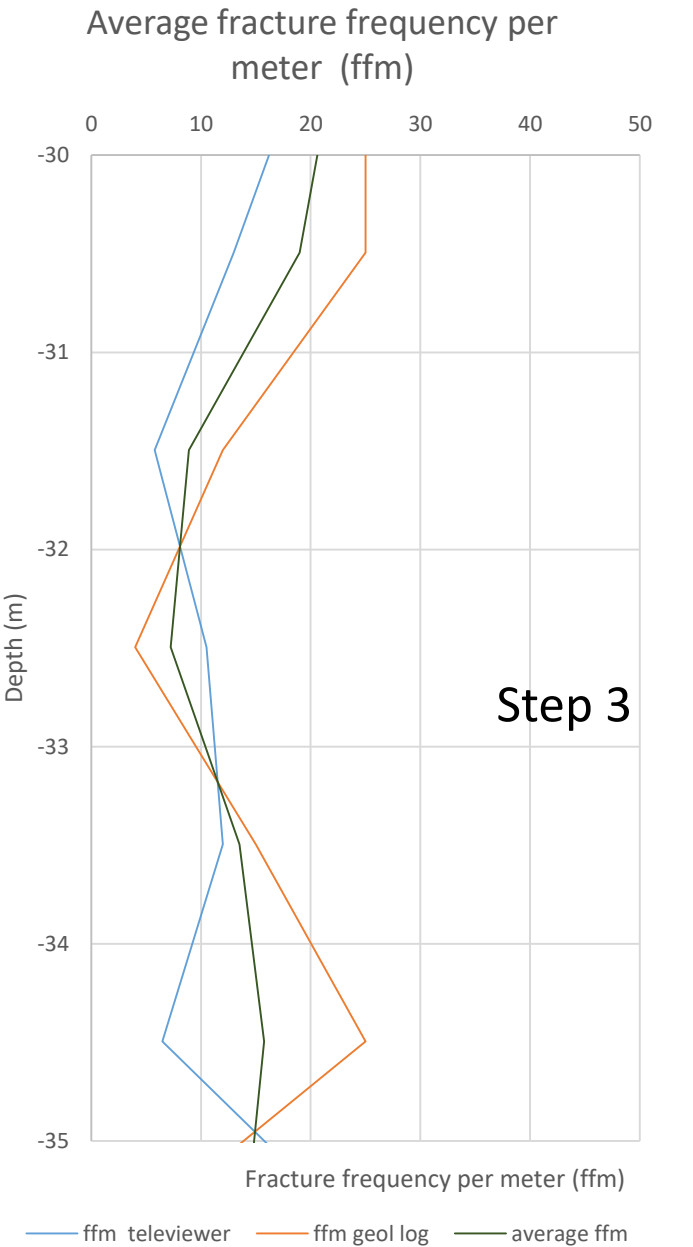
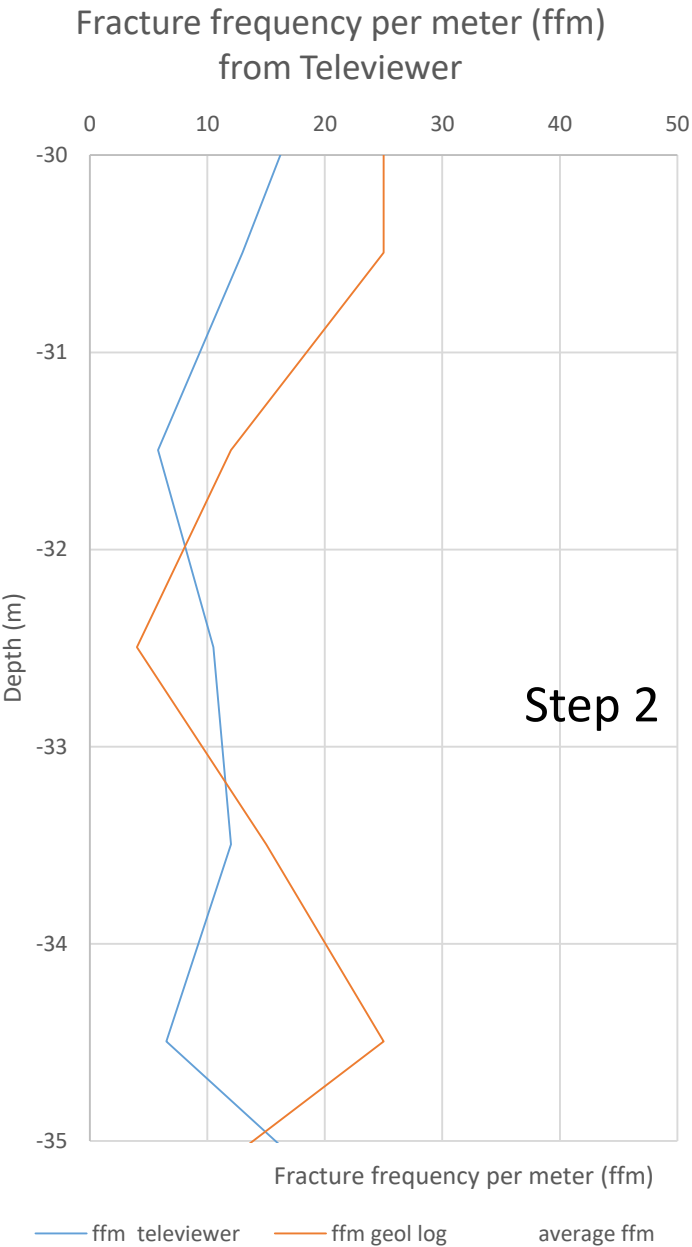
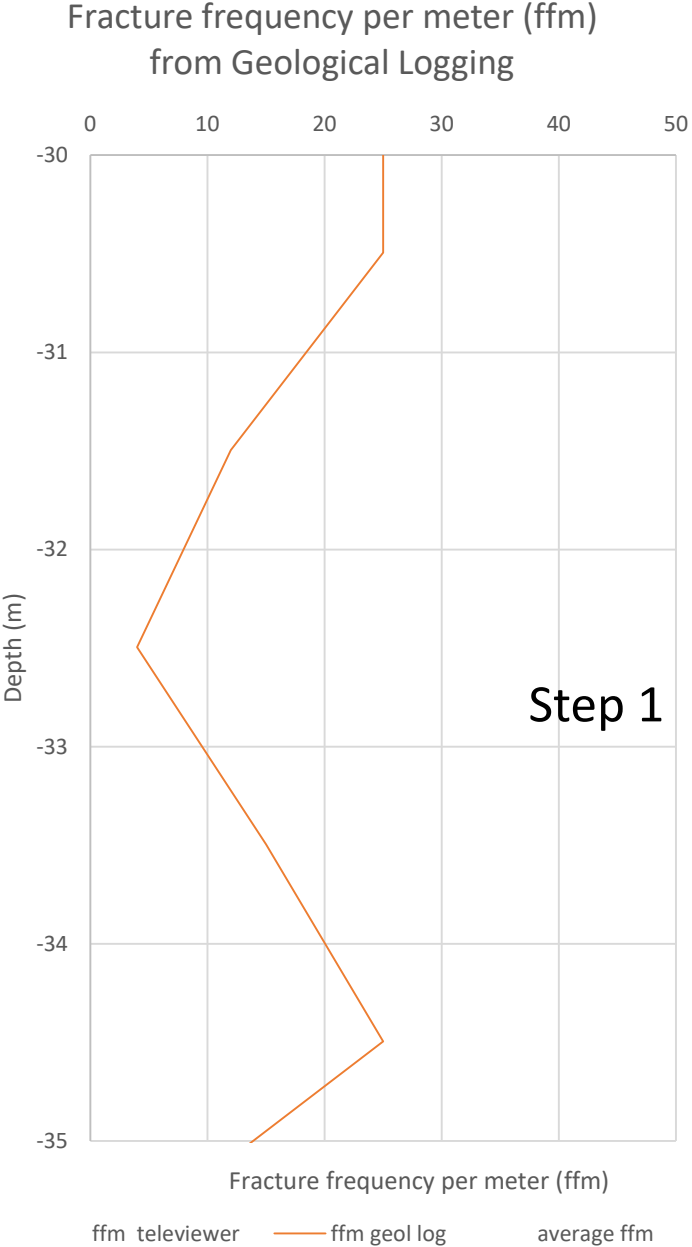
- Logs of fracture frequency data from drill cores
- Logs of fracture frequency data from televiewer
- Processed and adjusted both datasets and calculated the fracture frequencies per meter.
- Main assumption: fracture frequency obtained from the analysis of drill cores (i.e. geological logging) is influenced by drilling-induced fractures. So, an overestimation of the real value is expected. Fracture frequency obtained from televiewer data may be underestimated due to the limit imposed by the resolution and quality of the televiewer image.
- In order to have a value for fracture frequency per meter (ffm) closer to the actual value the average from those two data sets was calculated.
- From the boreholes having both datasets (KH-01-12, KH-01-17, KH-02-17, KH-01-18, KH-02-18) a constant correction factor and a depth-dependent zonal correction factor were calculated and subsequently applied to those boreholes where televiewer data is absent.
- Calculated the running average every 3 meters for the fracture frequency.



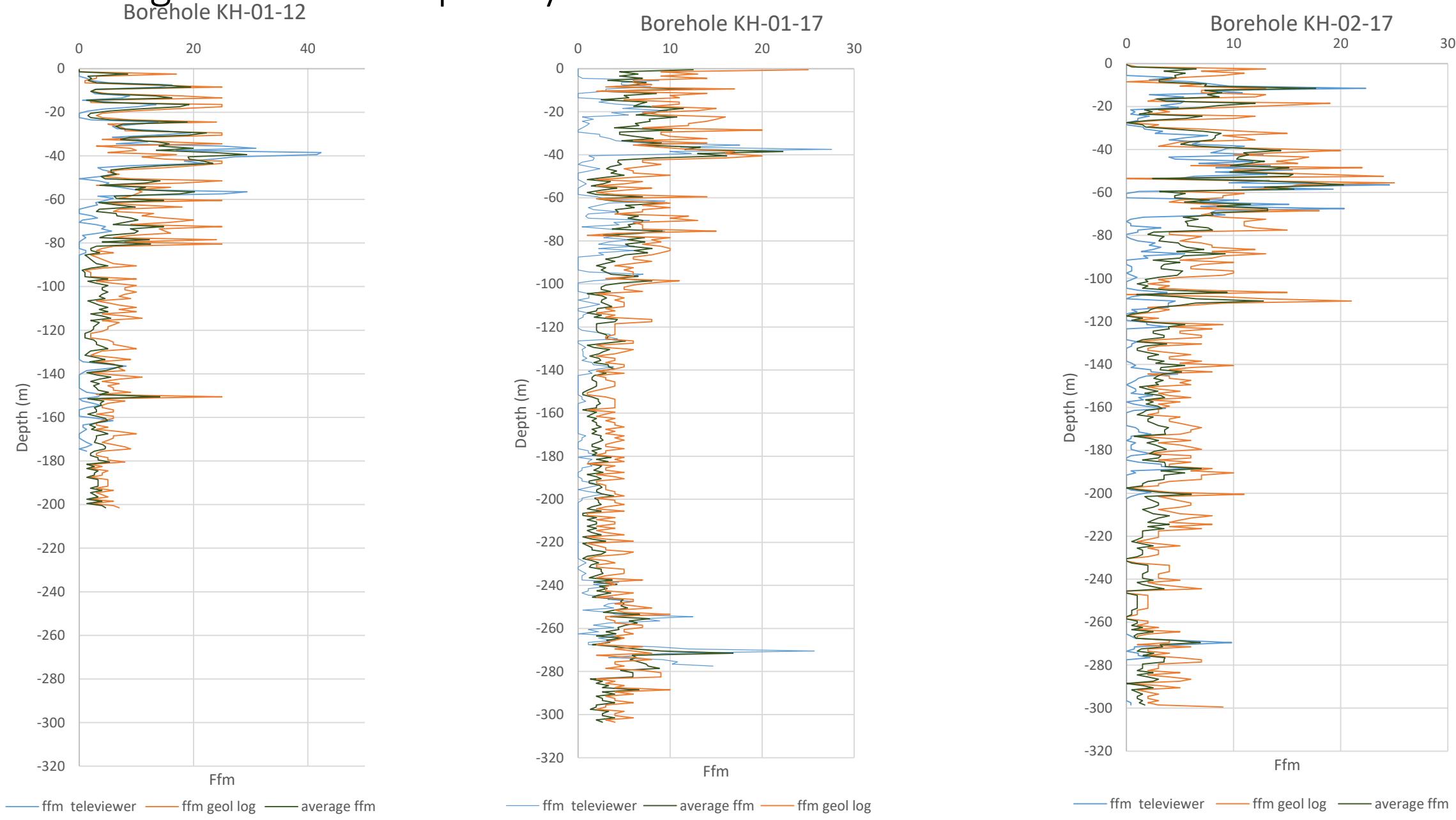
Fracture frequency data from geological logging is available for all the boreholes installed in Åknes.

The boreholes without televiewer data are KH-01-05 , KH-02-05, KH-03-05, KH-04-05, KH-01-06, KH-02-06, KH-03-06

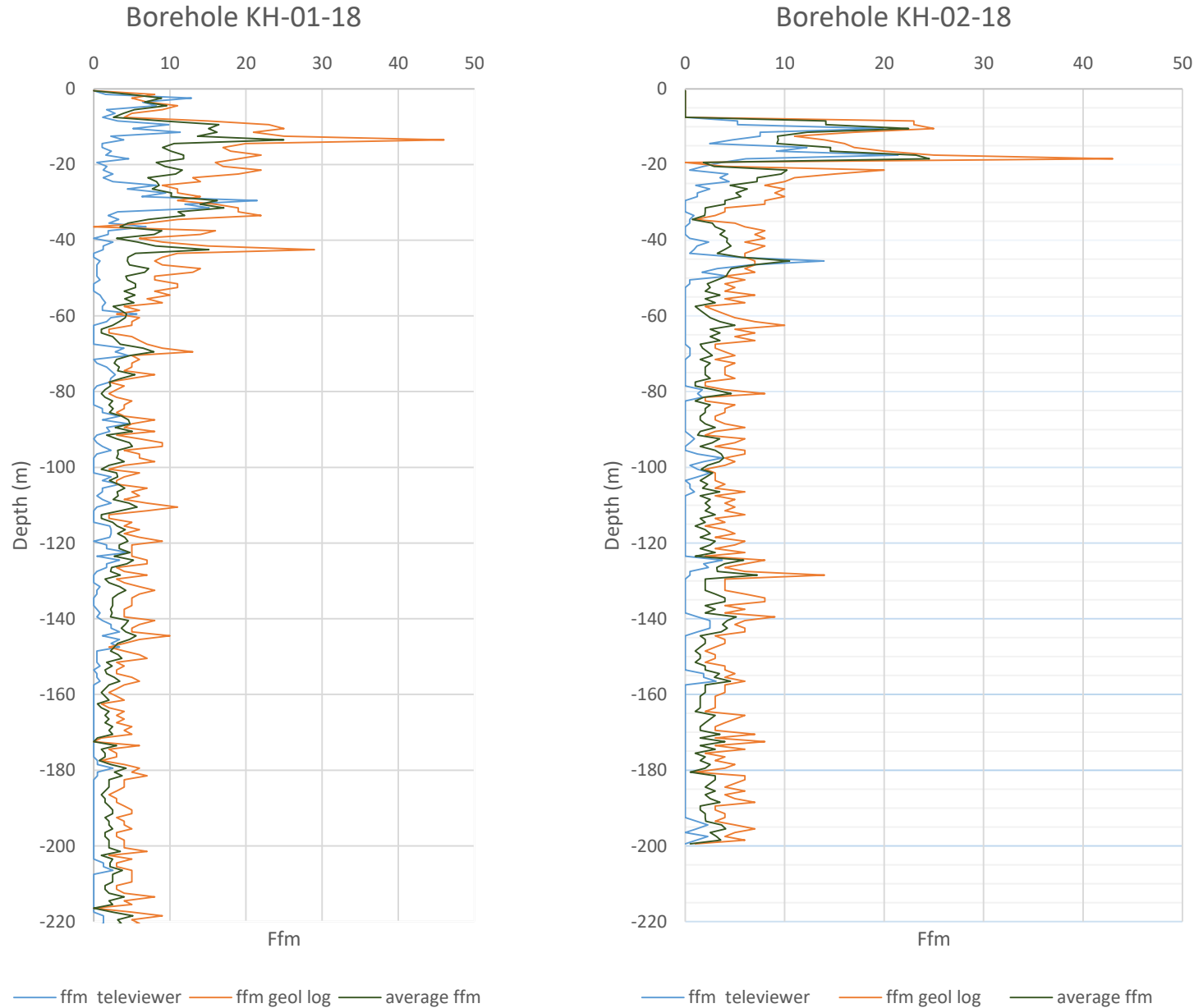
Calculation of the average fracture frequency for the boreholes with both datasets



Average fracture frequency obtained for each borehole with both datasets



Average fracture frequency obtained for each borehole with both datasets



aknes-hydro\data_processing\ioannip\1mBorehole.xlsx data - tab for each borehole

Correction Factor for the fracture frequency

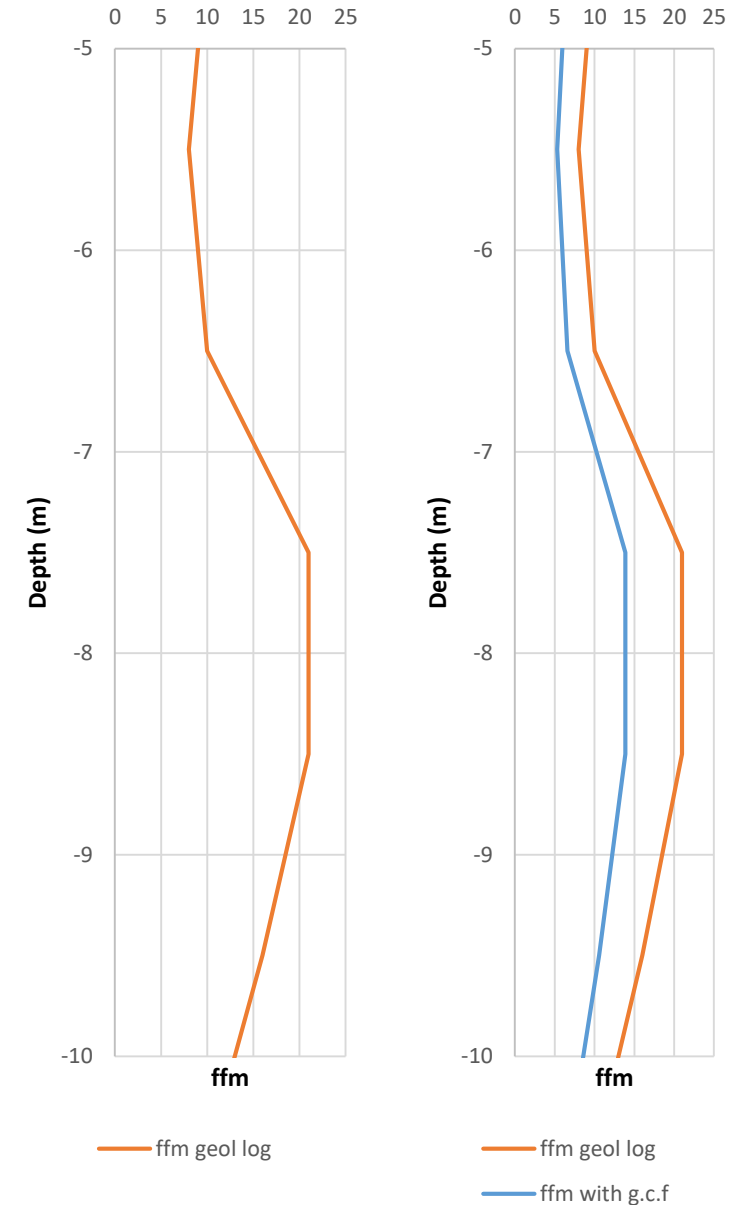
The average fracture frequency was calculated for the boreholes with both Televiwer and geological logging data. In order to have a representative value for the average fracture frequency for the rest of the boreholes with only fracture frequencies from geological logging, a correction factor was calculated. This value multiplied with the fracture frequencies from geological logging gives a representative average fracture frequency per meter for the rest of the boreholes.

$$\text{Average } ffm = \frac{\text{geological logging } ffm + \text{televiwer } ffm}{2}$$

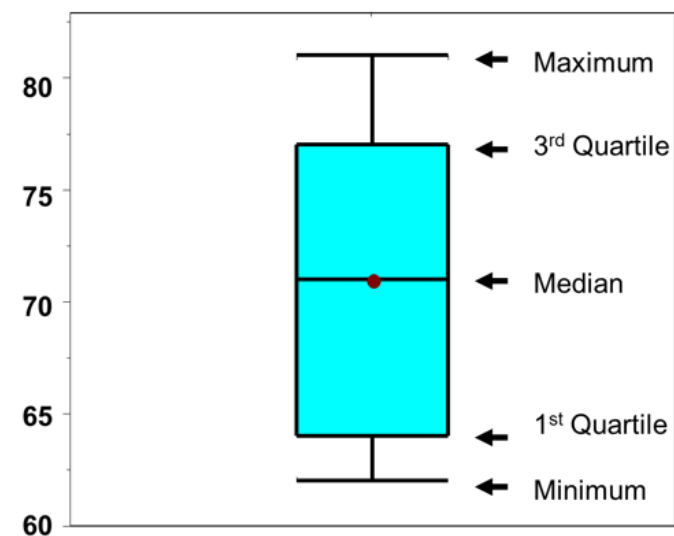
$$\text{General Correction factor}(g.c.f) = \frac{\text{average } ff}{\text{geological logging } ffm}$$



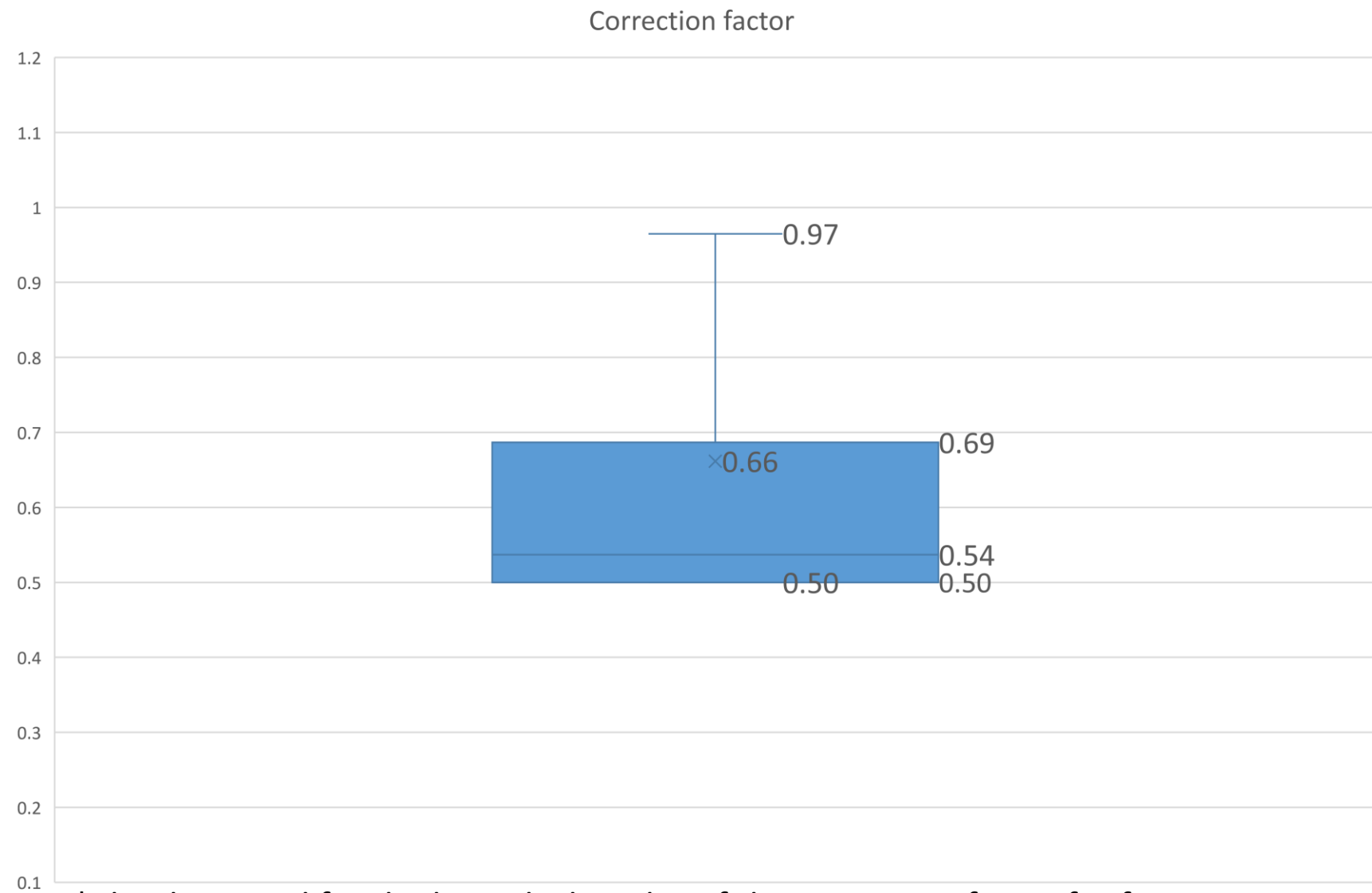
Average ffm for the boreholes without Televiwer = geological logging ffm x general correction factor (g.c.f)



Box-whisker plot of the general correction factor for the fracture frequency

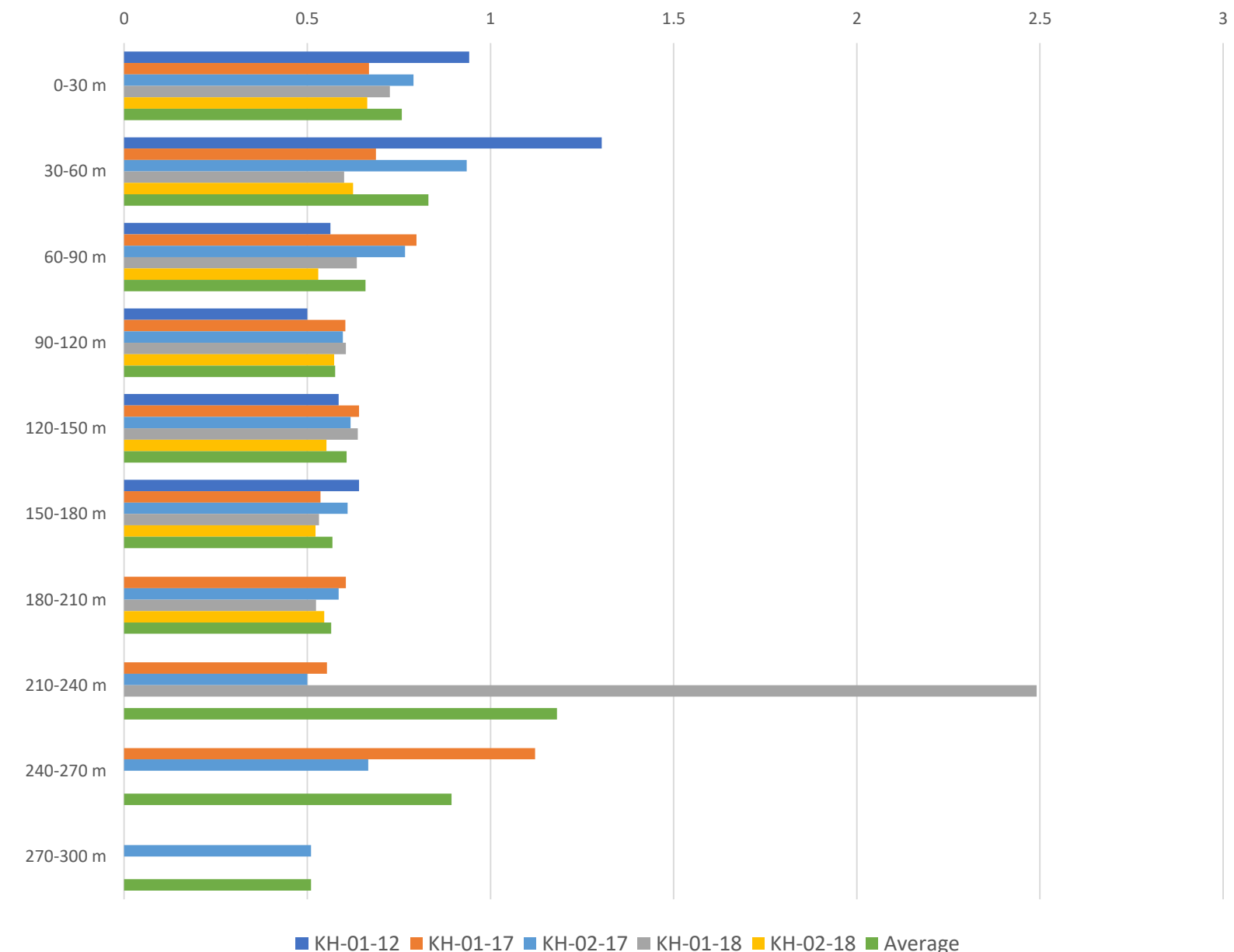


*Explanation of Box-whisker plot



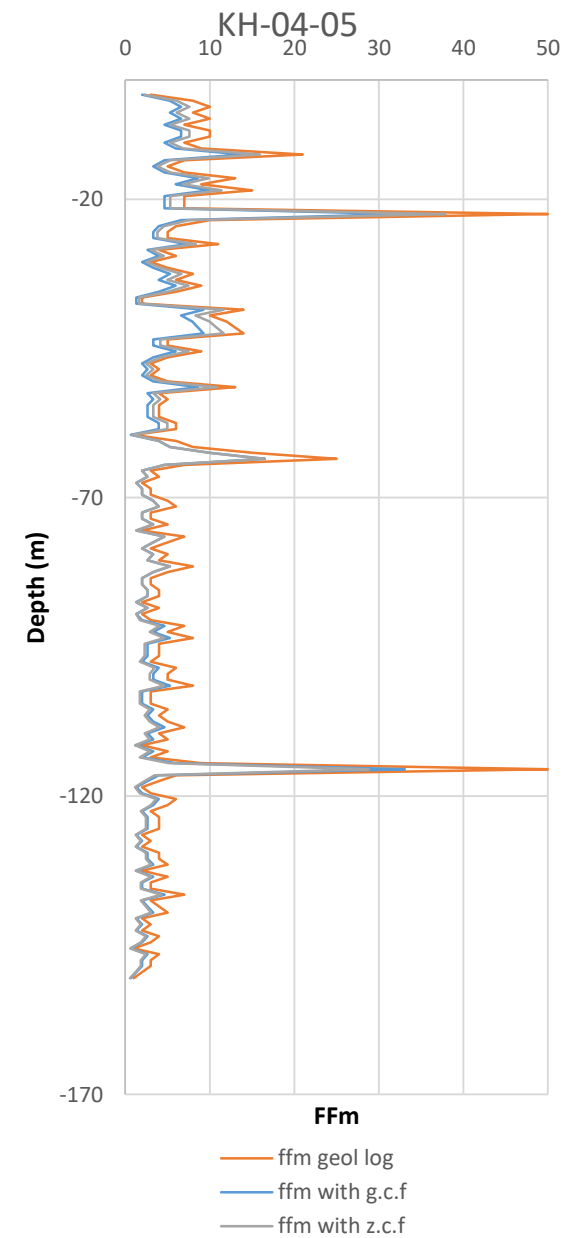
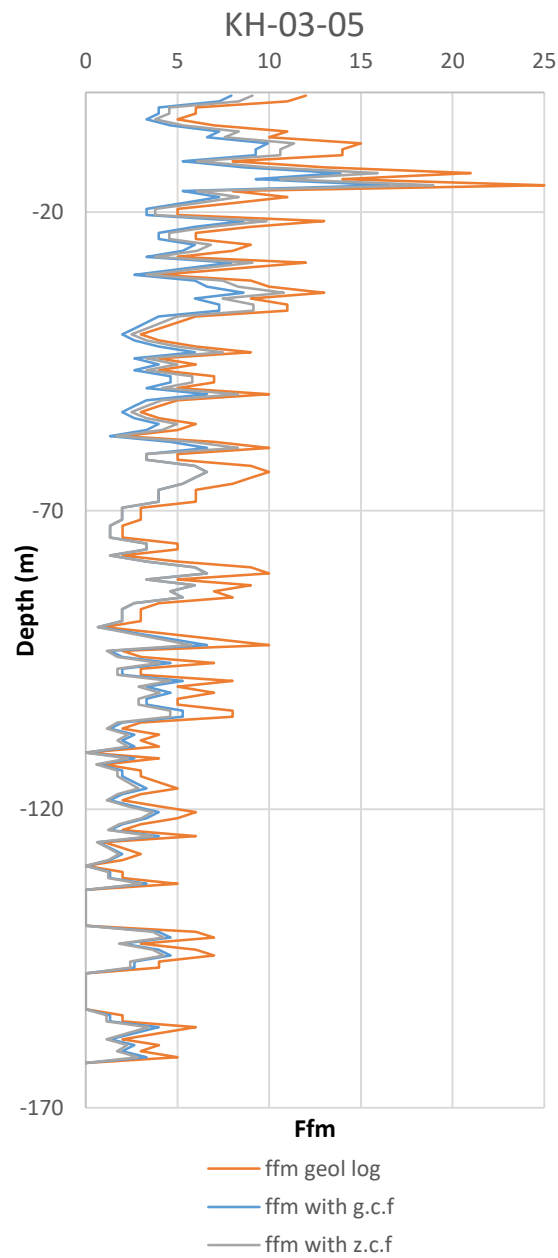
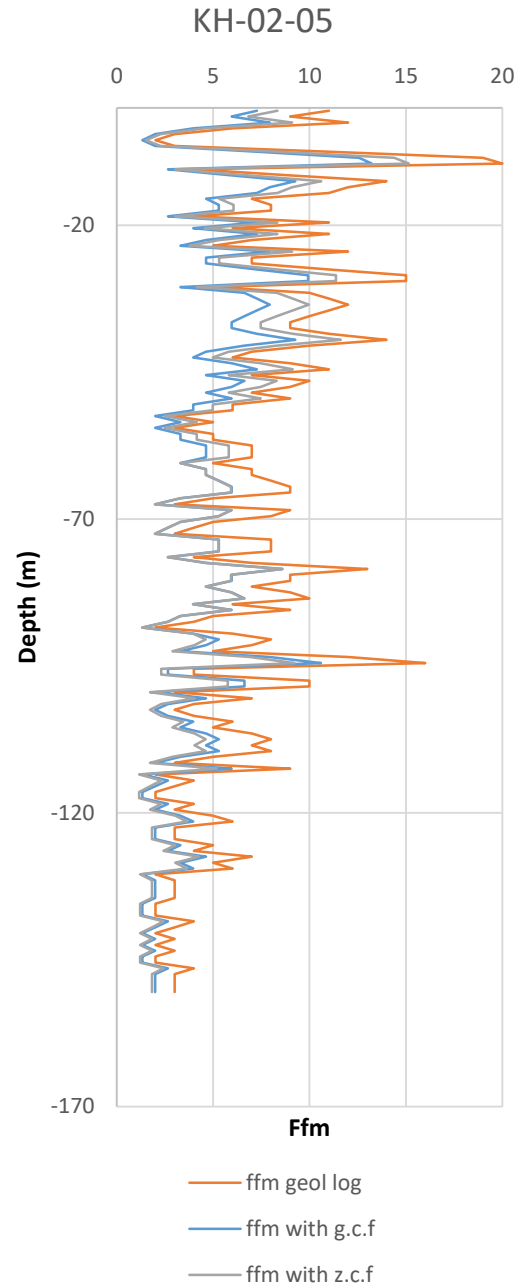
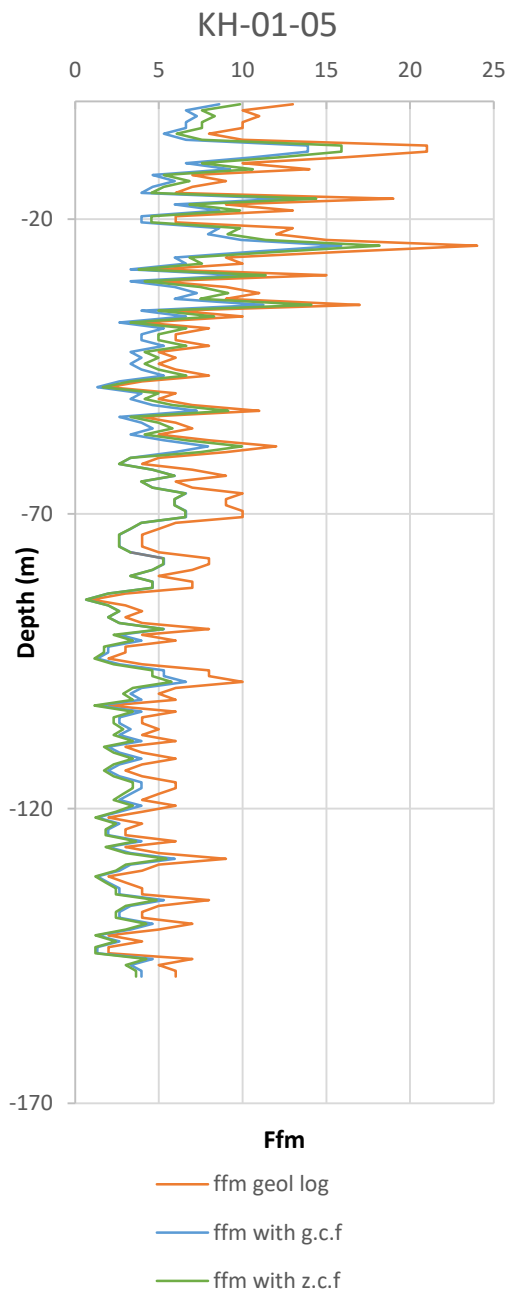
*The data used for the box whisker plot of the correction factor for fracture frequency is based on the 5 boreholes having both of the datasets.

Depth-dependent correction factor for the fracture frequency data



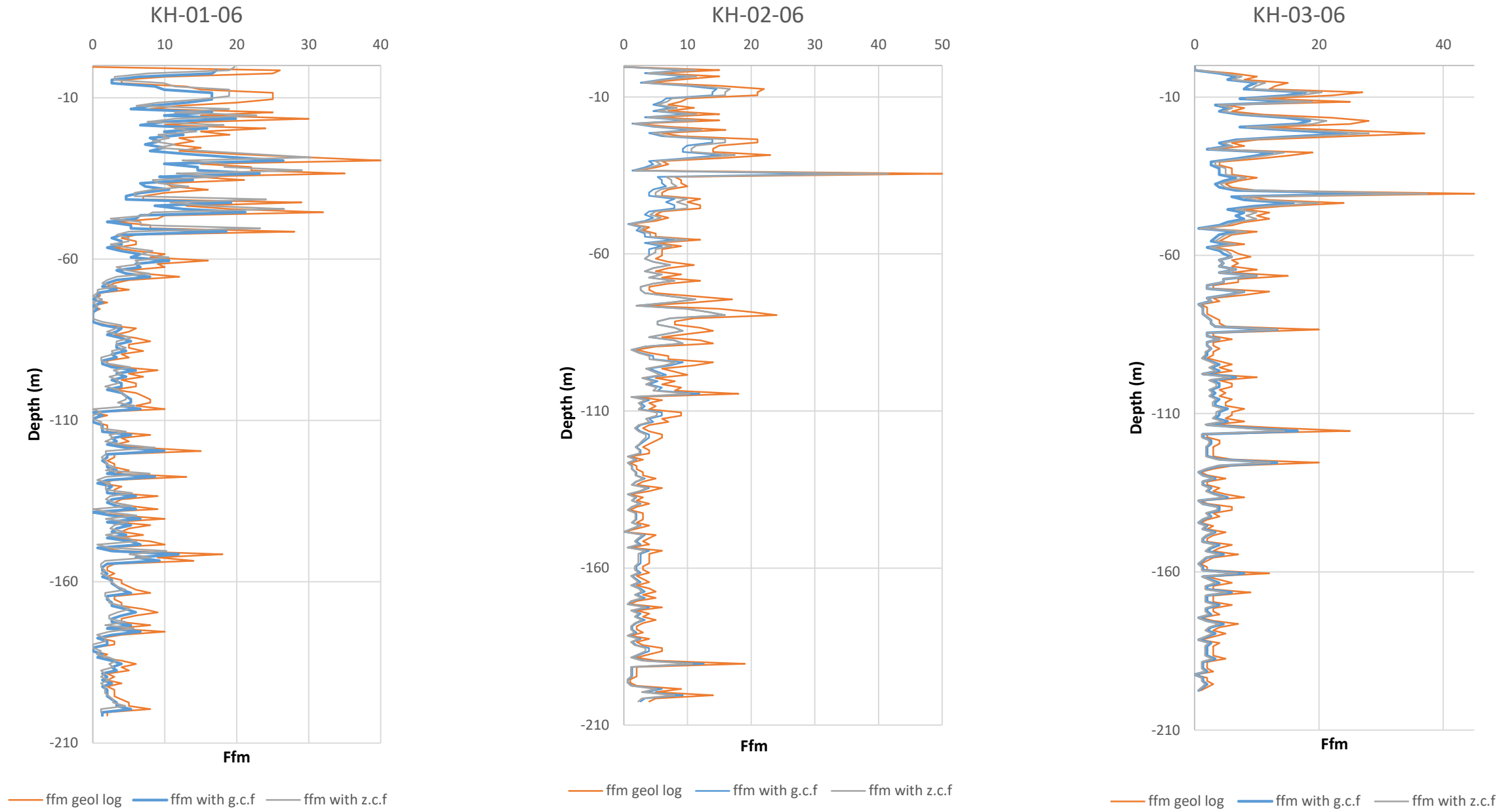
In order to check the possible variations of the correction factor depending depth, a depth-dependent correction factor was calculated. By calculating the moving average correction factor every 30 meters depth it was decided to use this value for the boreholes without televiewer data in order to have a more representative value of fracture frequency. This was called zonal correction factor- zcf.

Assigning correction factor to the boreholes without Televiewer data



gcf: general correction factor; zcf: zonal correction factor






Assigning correction factor to the boreholes without Televiewer data



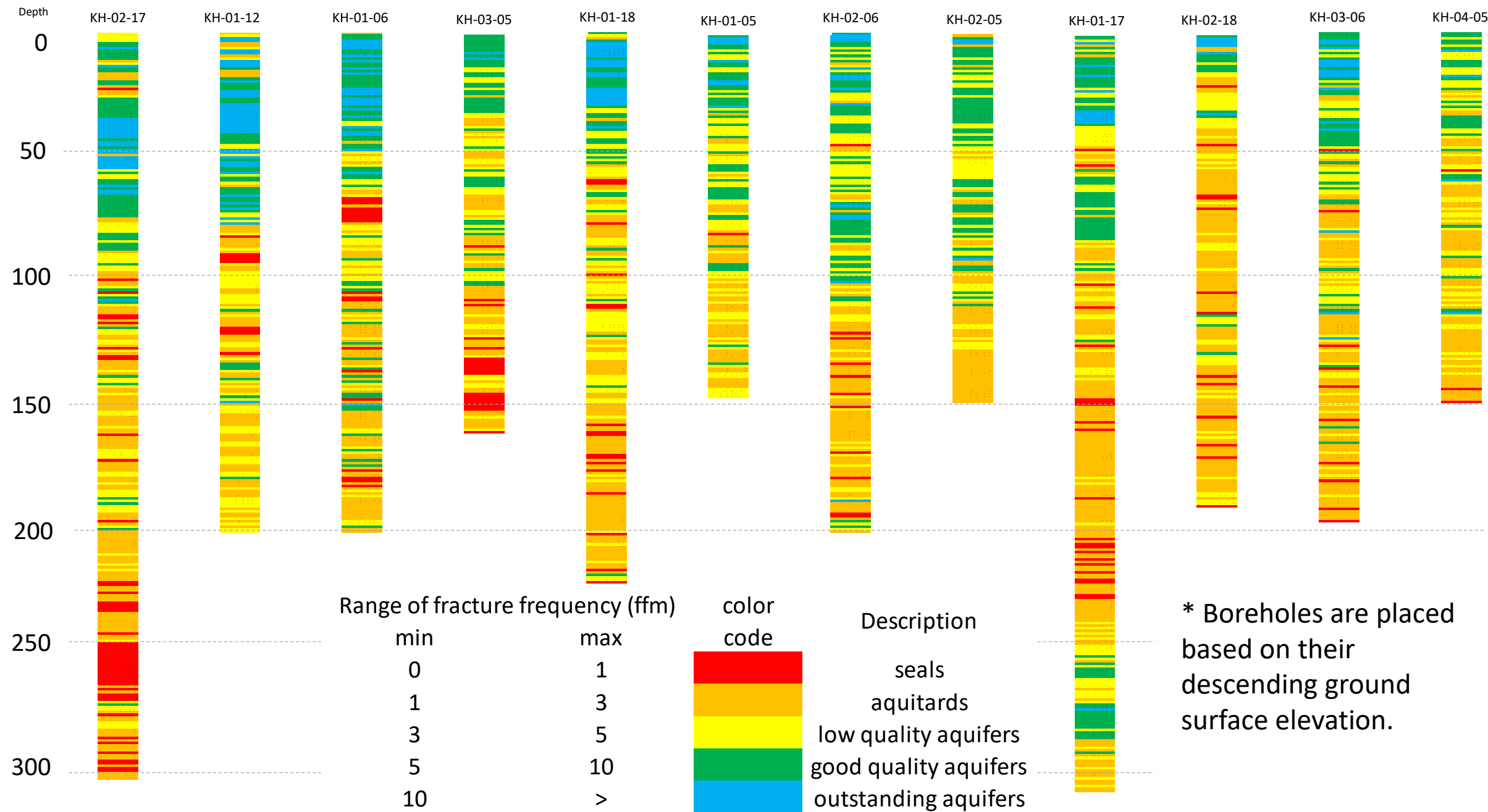
aknes-hydro\data_processing\ioannip\3classes.1mBorehole data.xlsx - tab for each borehole

Fracture data converted to bedrock aquifers potential




- Depending on the number of the fractures it was assigned a color code to every meter of each borehole in order to convert the fracture frequency to bedrock aquifer potential. This is based on the premise that a higher ffm implies a higher bedrock aquifer potential.

Range of fracture frequency (ffm)		color code	Description
min	max		
0	1		seals
1	3		aquitards
3	5		low quality aquifers
5	10		good quality aquifers
10	>		outstanding aquifers

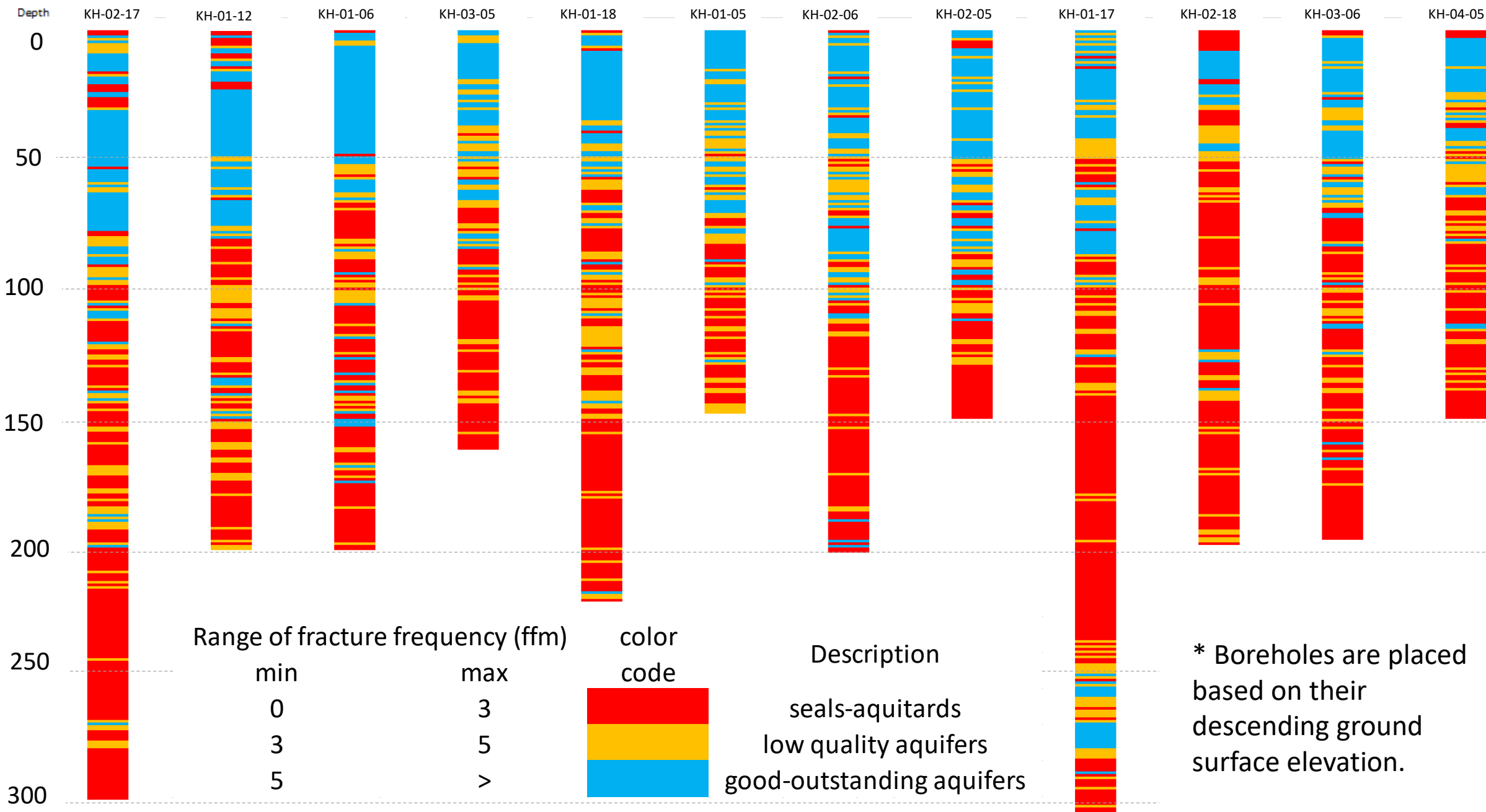
Fracture frequency vs aquifer potential



Eventually the classes were reduced in order to simplify.

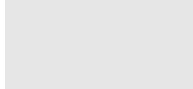

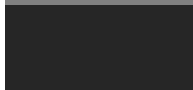
Range of fracture frequency (ffm)		color code	Description
min	max		
0	3		seals-aquitards
3	5		low quality aquifers
5	>		good-outstanding aquifers

Fracture frequency vs aquifer potential




Litho-structural units

- From the existed core photos (KH-01-12, KH-01-17, KH-02-17, KH-01-18, KH-02-18) the color of the rock was noted as a first approach to identify the litho-structural units and the rock masses.

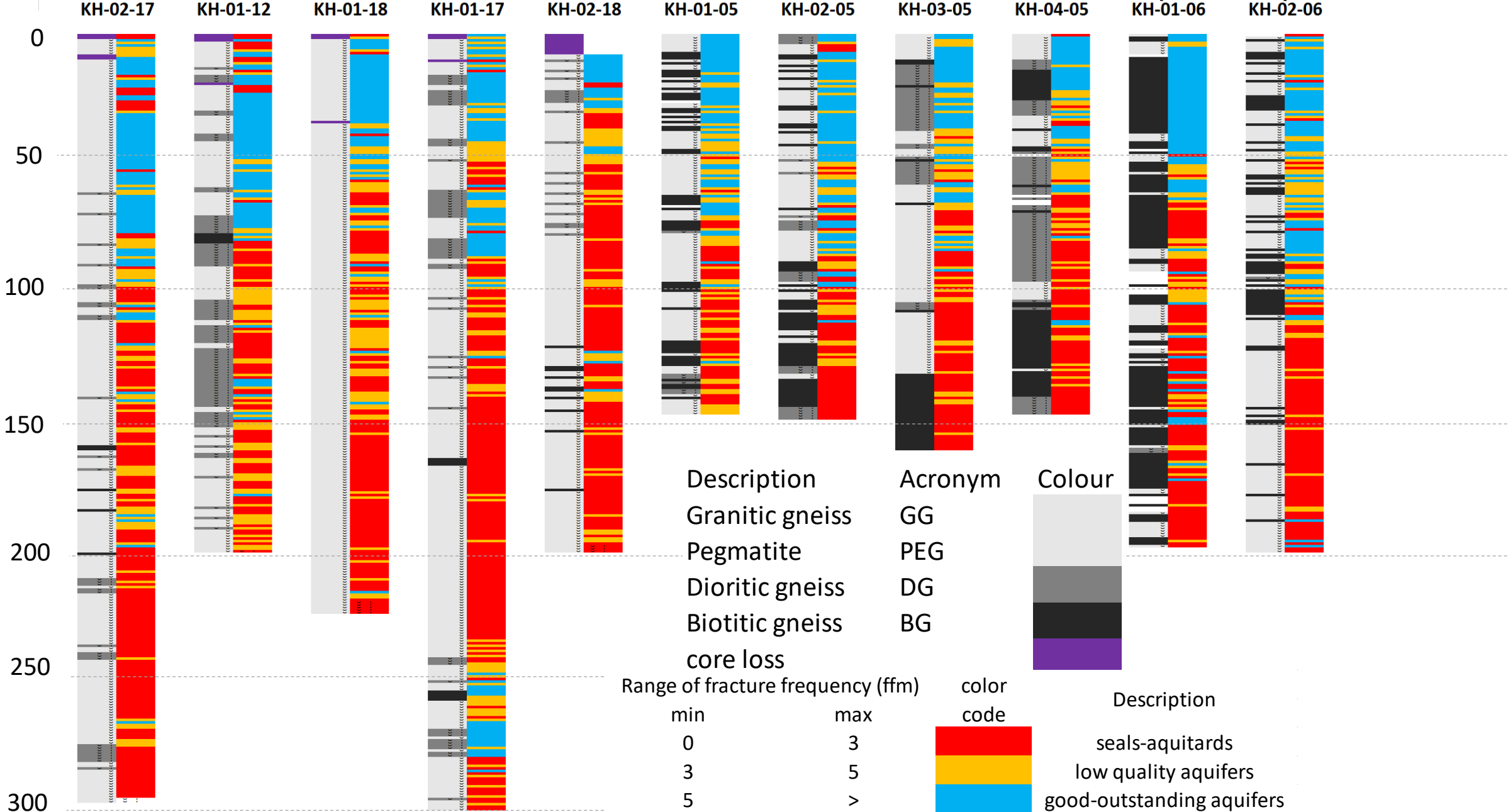
Description	Colour
white-light grey	
dark grey	
black	

- For those boreholes without core photos available (i.e. until 2007) the available geological description was correlated to the color description above.

Description	Acronym	Colour
Granitic gneiss	GG	
Pegmatite	PEG	
Dioritic gneiss	DG	
Biotitic gneiss	BG	

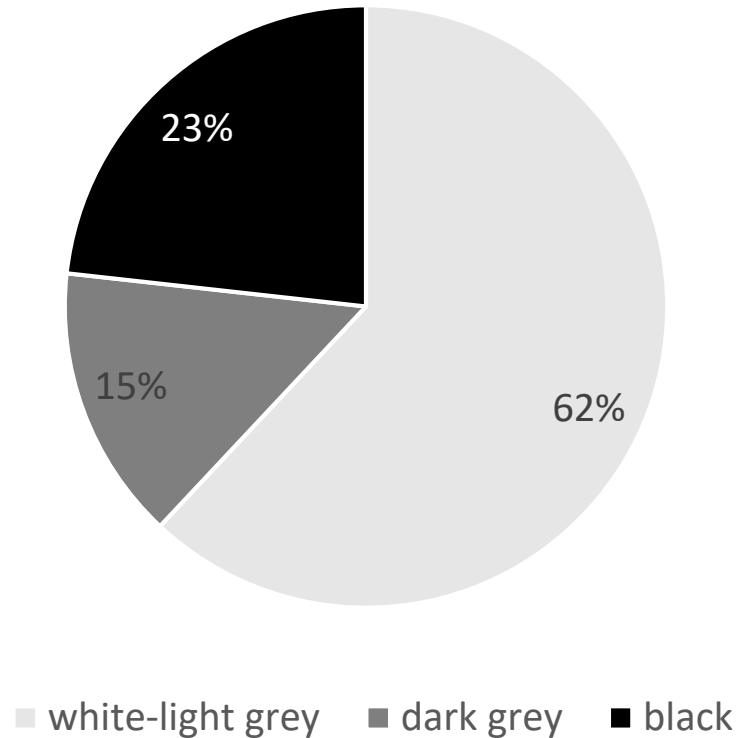
* Granitic gneiss and pegmatite have the same colour because while logging from core photos it was considered only the colour and not the rock type.

Correlation of litho-structural units with bedrock aquifer potential



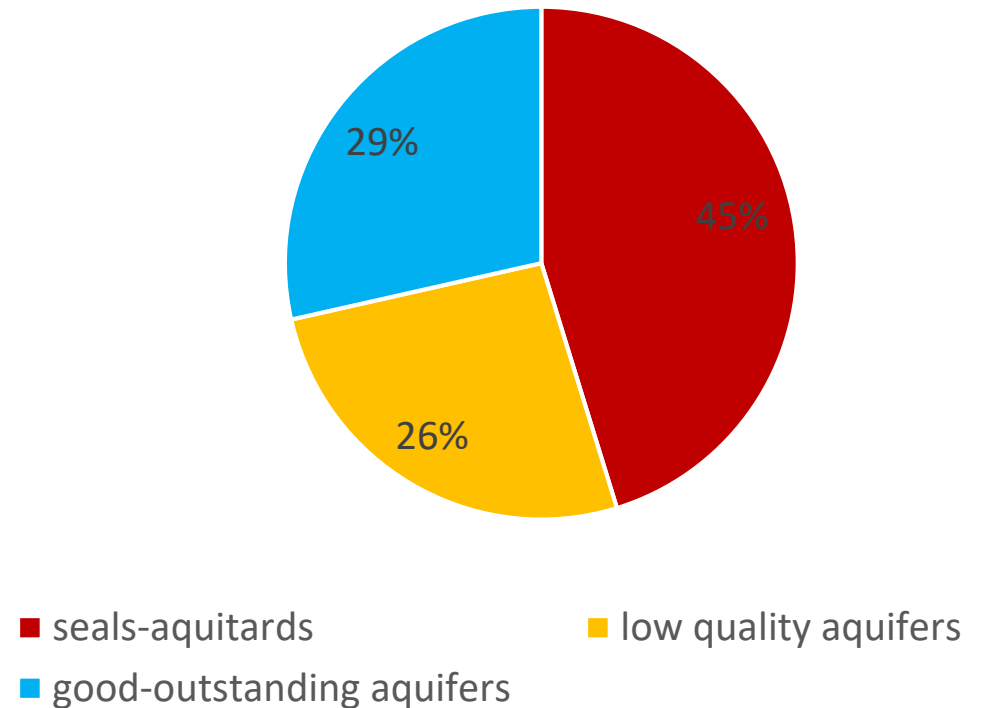
Statistical analysis of the connection between litho-structural units and bedrock aquifer potential

All investigated boreholes



*Borehole KH-01-18 was excluded from the statistical analysis due to poor core photos quality.

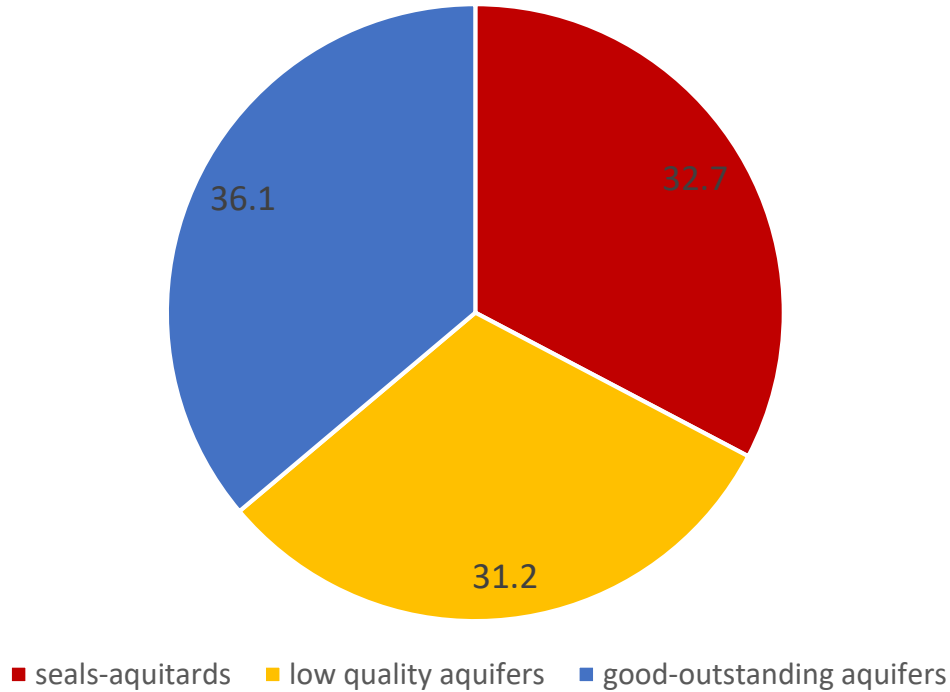
All investigated boreholes



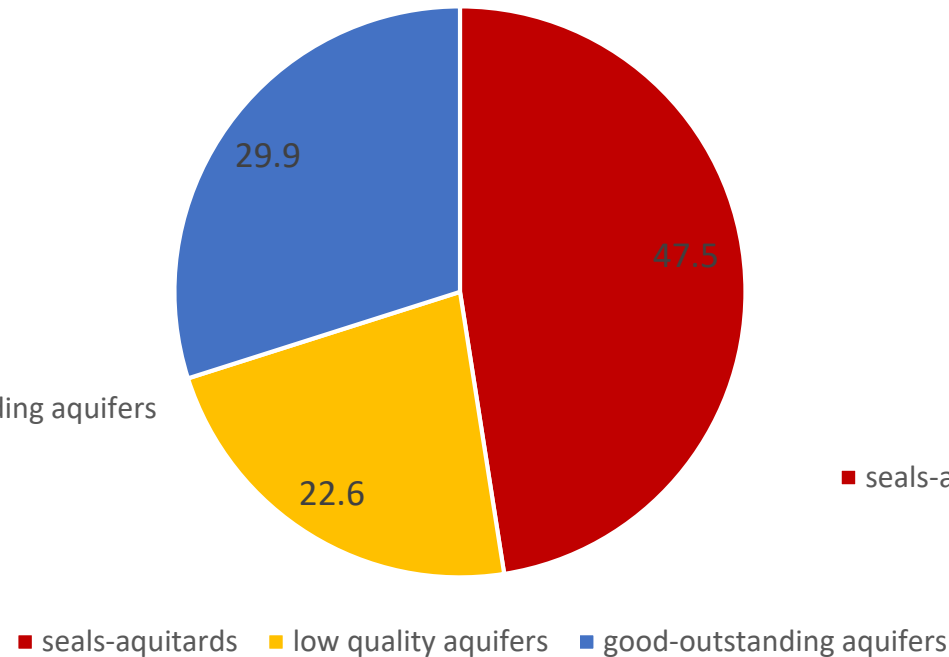
*Pie charts showing the distribution of the bedrock aquifer potential for all the investigated boreholes.

Statistical analysis of the bedrock aquifer potential in each rock type

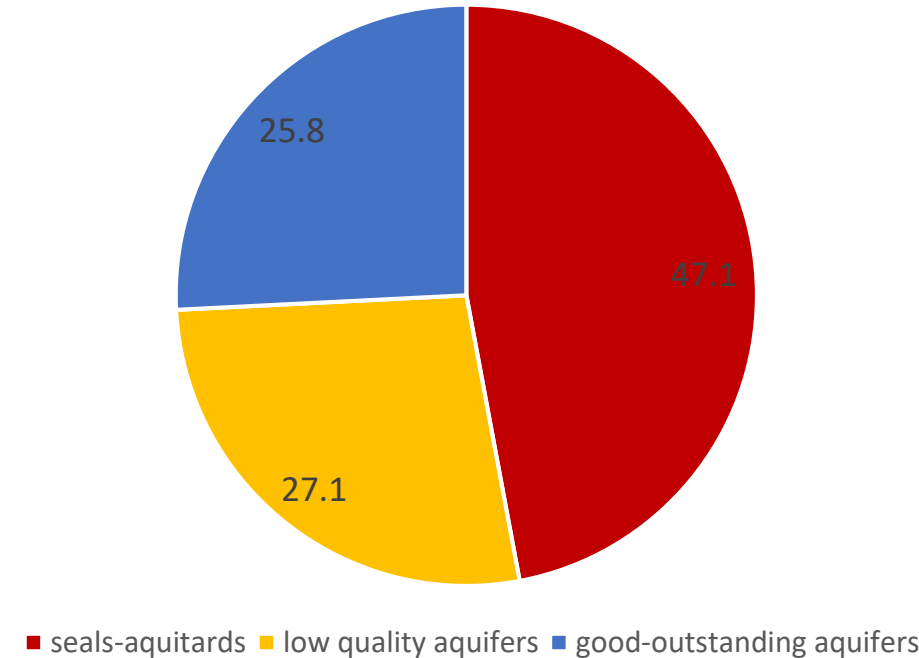
Dioritic Gneiss- dark grey



Biotitic Gneiss - black



Granitic Gneiss-Pegmatite - white-light grey



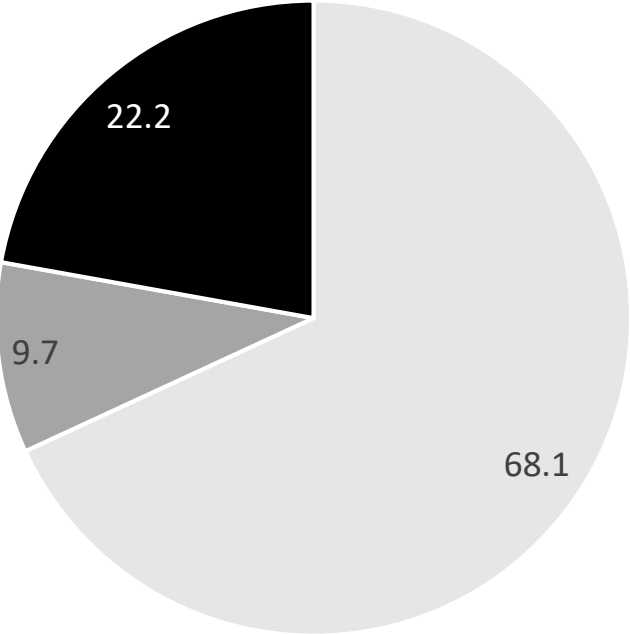
*Borehole KH-01-18 was excluded from the statistical analysis due to poor core photos quality.

aknes-hydro\data_processing\ioannip\3classes.1m.Logging-fracture comparison.xlsx - statistics tab

*Pie charts showing the distribution of the bedrock aquifer potential in each rock type.

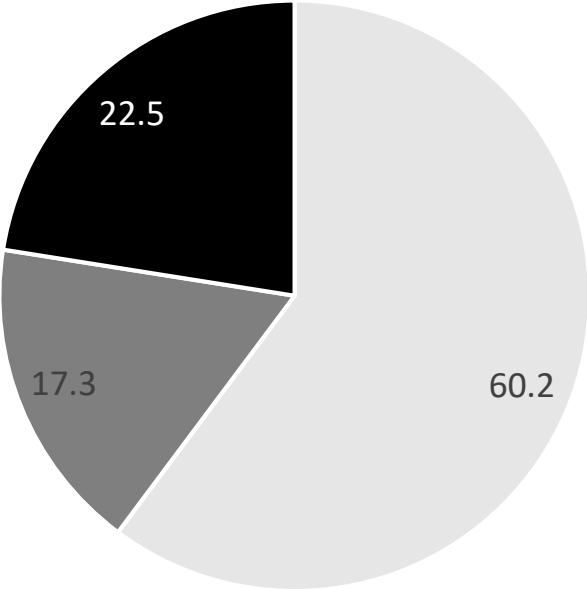
Statistical analysis of the rock type in each bedrock aquifer potential class

Seals - aquitards



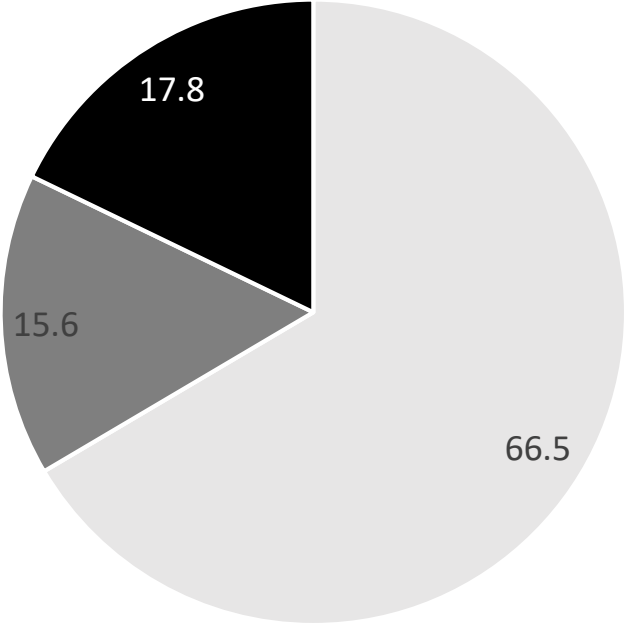
white-light grey dark grey black

Good-outstanding aquifers



white-light grey dark grey black

Low quality aquifers



white-light grey dark grey black

*Borehole KH-01-18 was excluded from the statistical analysis due to poor core photos quality.

*Pie charts showing the distribution of rock types in each bedrock aquifer potential.

Geophysical data

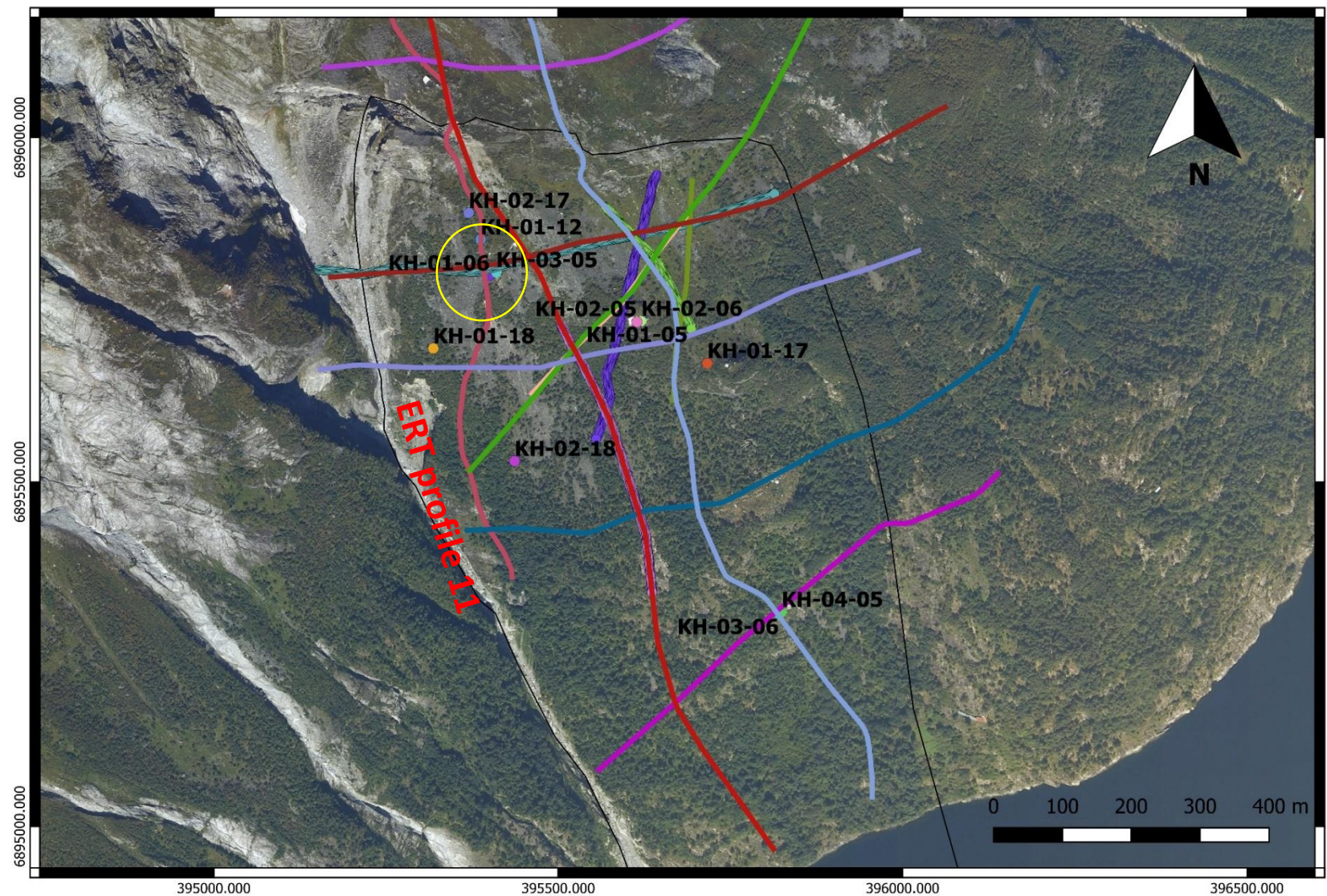
- Interpreted 2D electrical resistivity profiles (ERT).
- Investigated the link between litho-structural units and ERT values.
- Seismic refraction profiles were considered where it was applicable to compare with ERT, type of bedrock and fracture frequency.

Interpretation of the resistivity profiles.

From the NGU REPORT 2019.004 (Tassis and Rønning, 2019) as well as personal discussions and input from Georgios Tassis, the table below was defined in order to characterize the resistivities, i.e the ERT values.

<div>Shallower</div> <div>General trend</div> <div>Deeper</div> <div>↓</div>	Description	Resistivity
	Scree materials - Tallus bedrock	30-35K ohm.m
	Drained - Highly fractured	30-50K
	Water saturated - moderately fractured	12-30K ohm.m
	Water saturated - fractured	1-7.5K / <12K ohm.m
	Massive bedrock - unfractured	15-30K ohm.m

Example of the interpretation of an ERT profile with fracture frequency logs and lithology



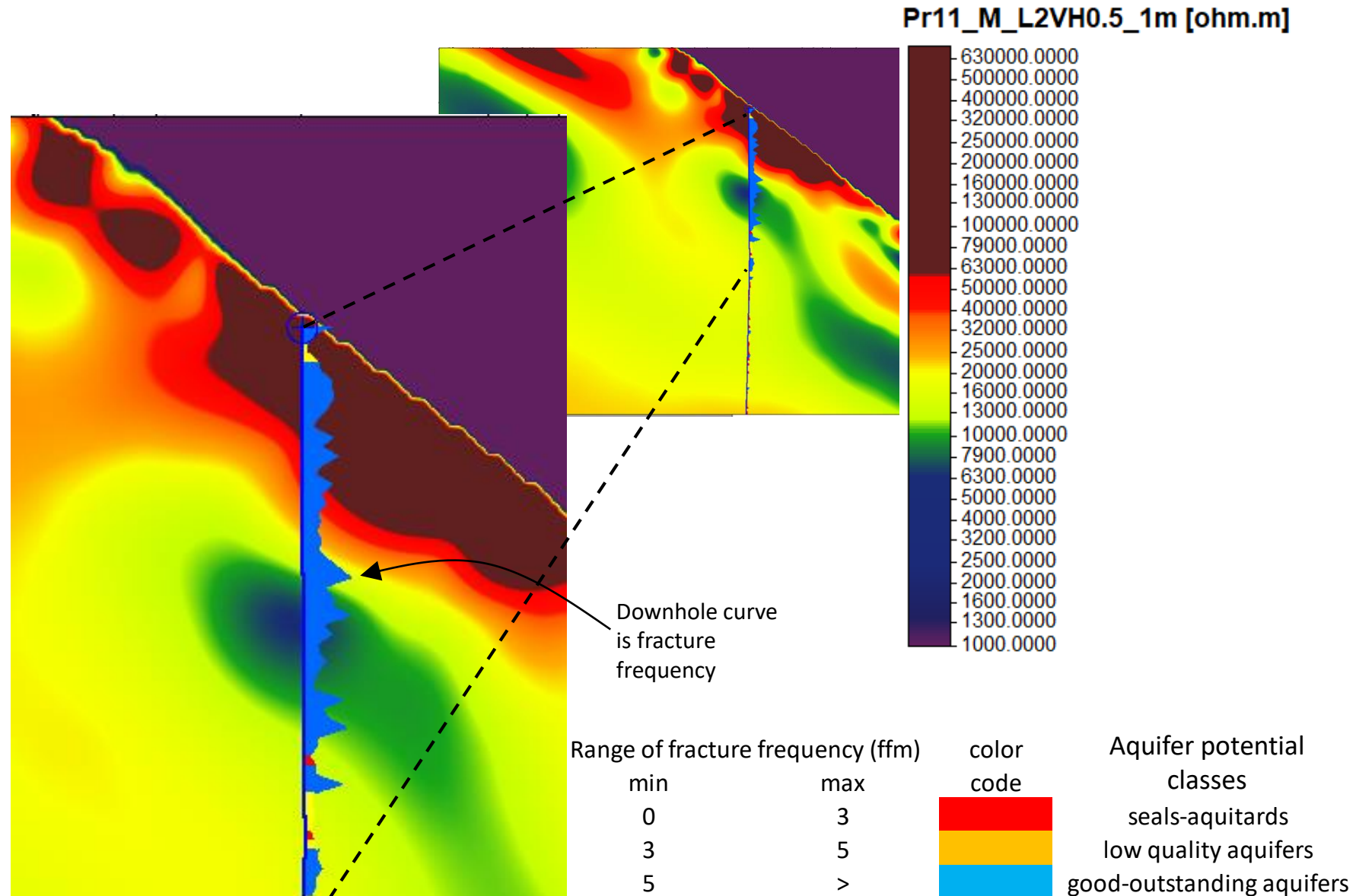
Location of ERT profile 11 and borehole KH-01-06

- | | | | | | |
|-------------------|-------------------|-------------------|--------------------|-------------------|-------------------|
| Resistivity_line1 | Resistivity_line4 | Resistivity_line7 | Resistivity_line10 | Seismic profile 2 | Seismic profile 3 |
| Resistivity_line2 | Resistivity_line5 | Resistivity_line8 | Resistivity_line11 | Seismic profile 4 | |
| Resistivity_line3 | Resistivity_line6 | Resistivity_line9 | Seismic profile 1 | | |

Resistivity profile 11 –borehole KH-01-06

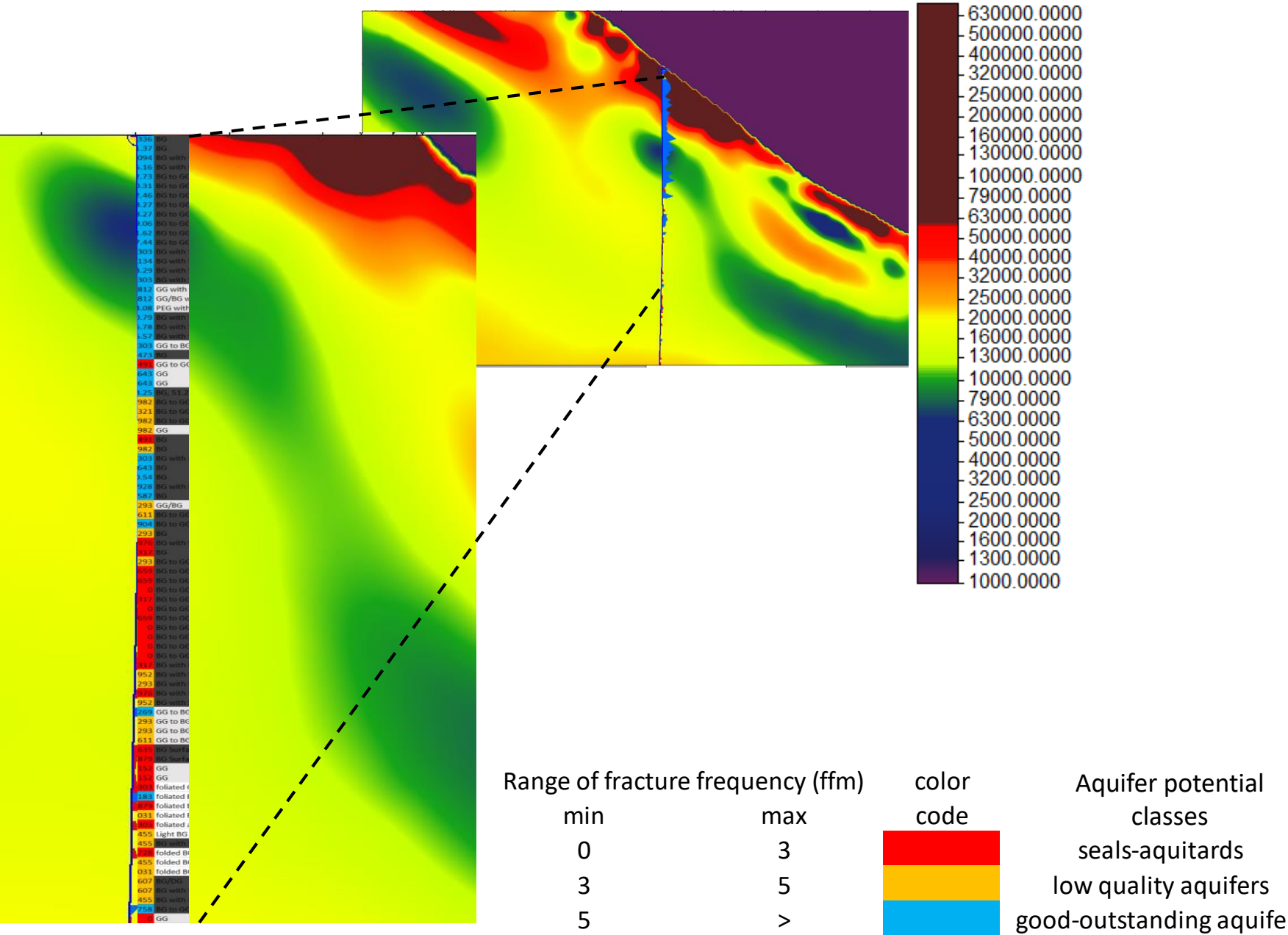
At the current ERT profile, relatively high fracture frequency can be found in both high and very low resistivities. They correlate either with highly fractured-drained areas or scree material but also with water saturated zones. Where the resistivity is very low can be observed that the fracture frequency decreases.

Logs of fracture frequency →
aknes-hydro\data_processing\ioannip\Task
2\fracture logs for petrel



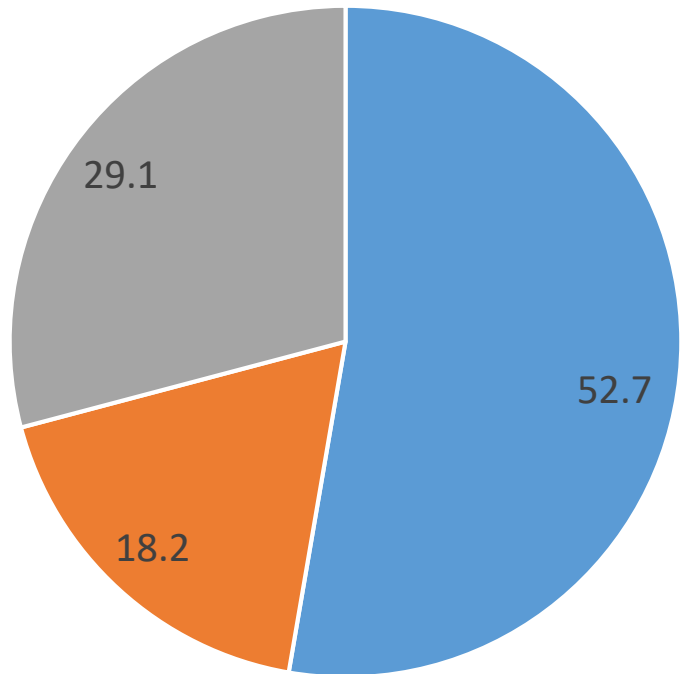
Resistivity profile 11 –borehole KH-01-06

The comparison of the current ERT profile with the lithology shows that there is no obvious connection between the lithology and the electrical resistivity. For instance, biotitic gneiss dominates here at the water saturated zones (low el. resistivity) but also exists at the higher resistivity areas. Moreover, granitic gneiss can be seen at the water saturated areas as well. The statistical analysis in the next page indicates that the majority of biotitic gneiss occurs in massive bedrock ERT areas.



Statistical analysis of the main ERT groups in each rock type

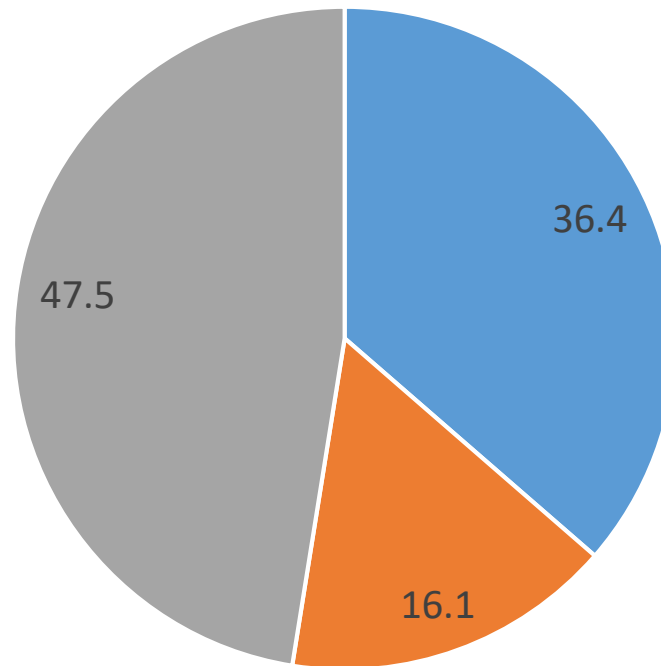
Granitic Gneiss-Pegmatite-white-light grey



■ ws ■ drained ■ massive bedrock

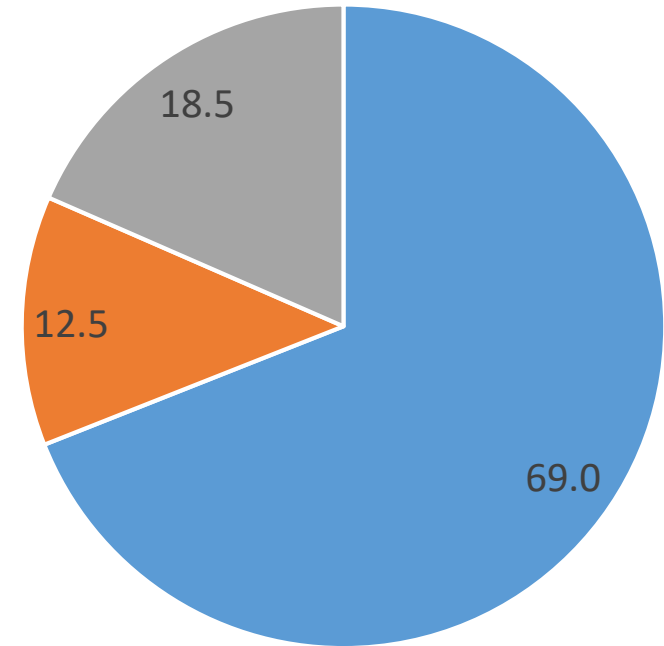
*ws – water saturated

Biotitic Gneiss -Black



■ ws ■ drained ■ massive bedrock

Dioritic Gneiss - dark grey



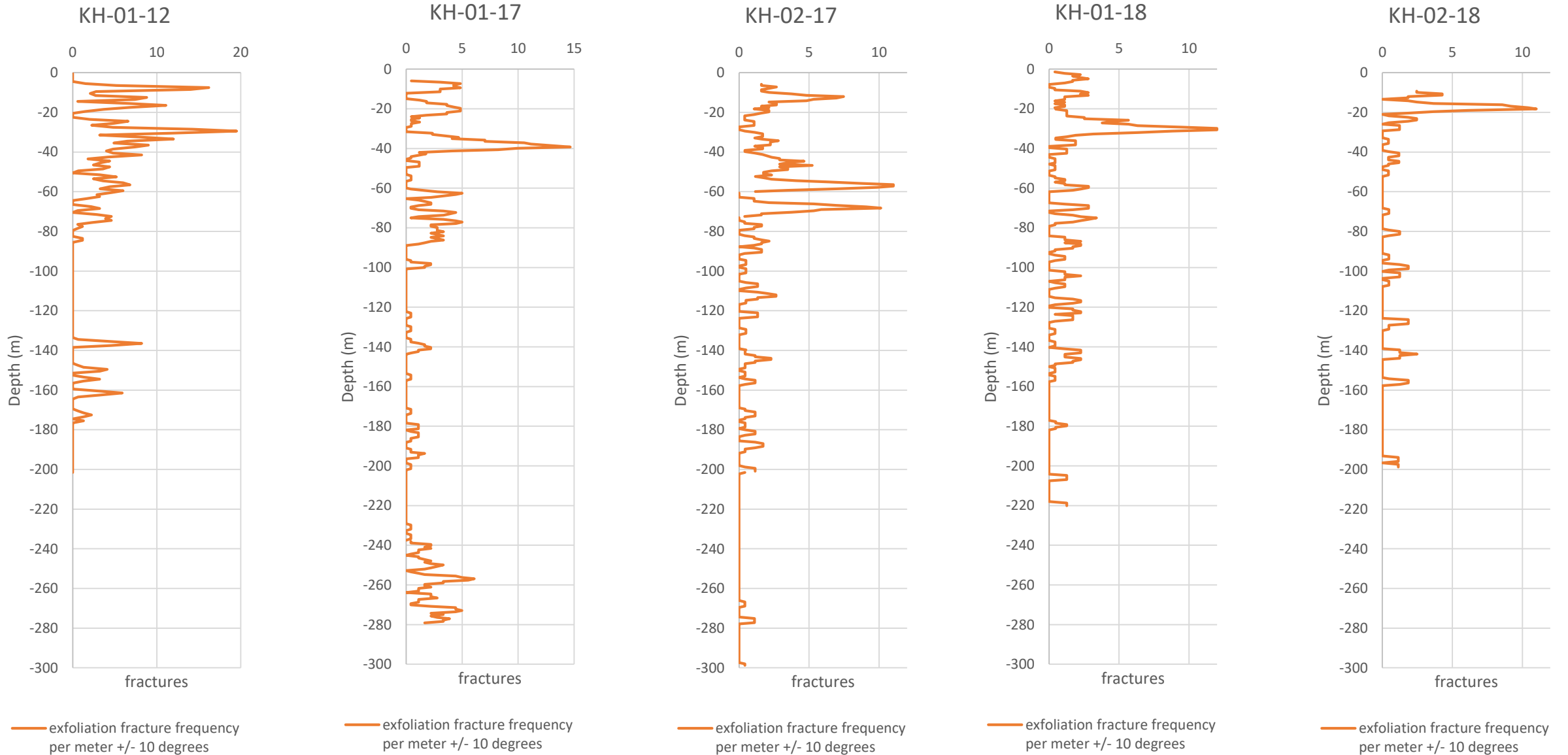
■ ws ■ drained ■ massive bedrock

*Pie charts showing the distribution of ERT groups in each rock type.

Heading to the final interpretation of the rock mass domains.

- For the final interpretation of the rock mass domains all the available data were combined. Nevertheless, it was put more weight to the exfoliation fractures showing the horizontal water movement, the flow measurement graphs from reports and off course the processed fracture frequency data.
- The exfoliation fracture frequencies were taken from the raw files of the Optical Televiwer data. Depending the slope that each borehole was drilled the fractures that were parallel to the surface (+/- 10 degrees) were considered as exfoliation fractures. Below are presented the degrees of the slope for each borehole with televiwer data.
- KH-01-12 – 30 degrees
KH-01-17 – 34 degrees
KH-02-17 – 32 degrees
KH-01-18 – 33 degrees
KH-02-18 – 38 degrees

Exfoliation fracture frequency from Televue



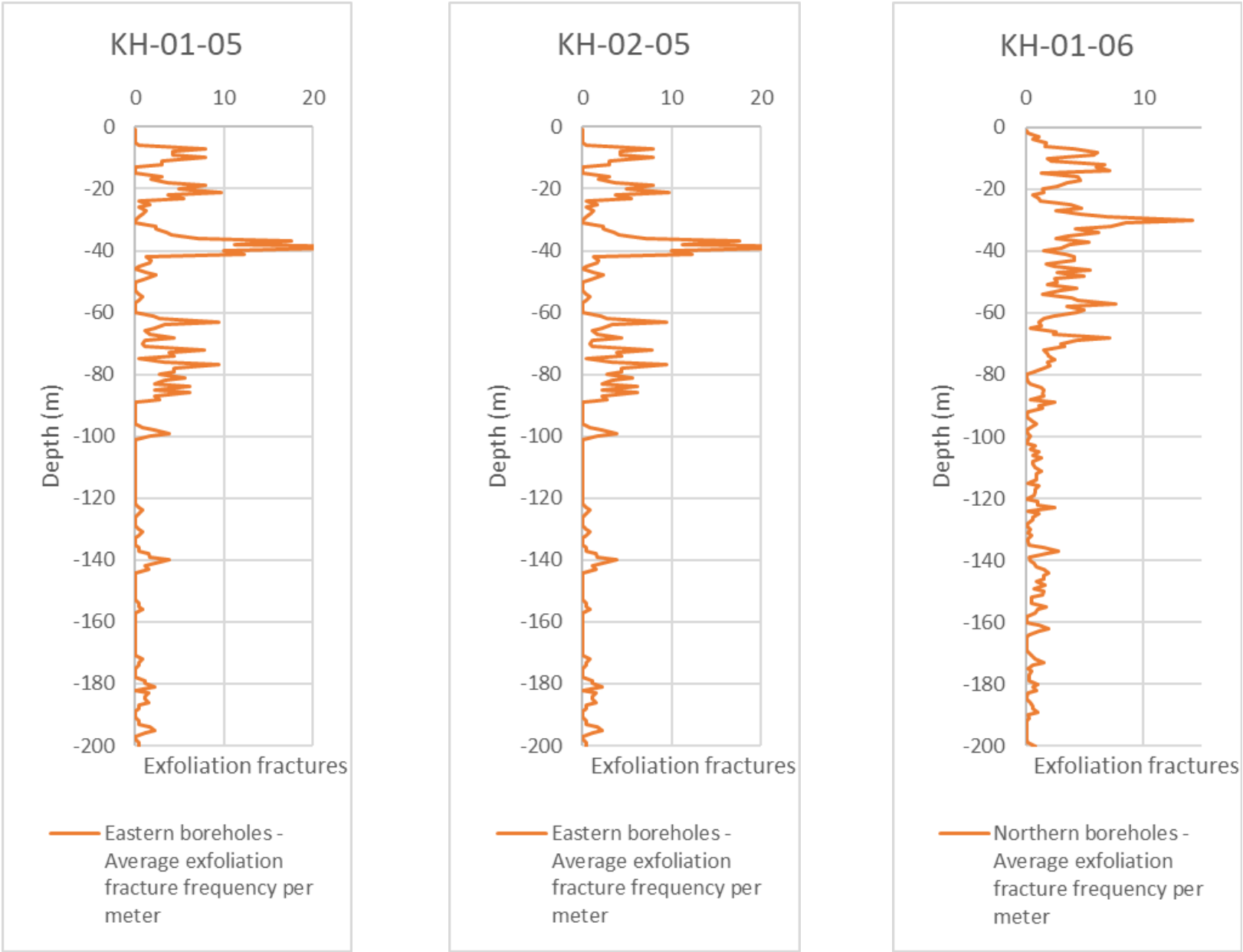
aknes-hydro\data_processing\ioannip\1mBorehole data.xlsx - tab for each borehole

Exfoliation fractures for the boreholes without televiewer data

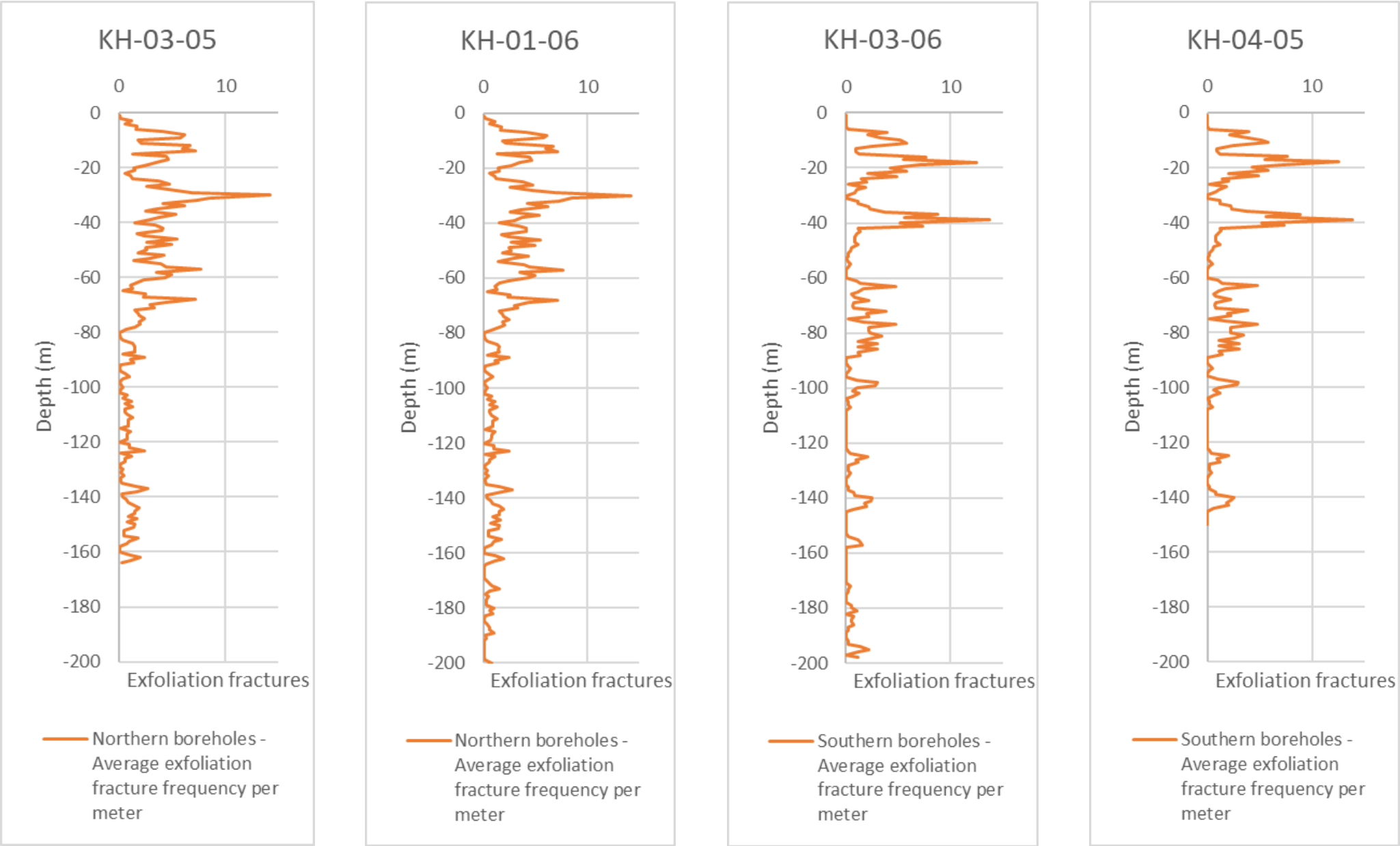
- The average exfoliation fracture frequency per meter was calculated from available televiewer data. Furthermore, the results were color coded in the same way as it was done with the total fracture frequencies.
- The result for the average of all the boreholes was not very clear. Therefore, it was calculated the average for the boreholes divided into 4 clusters depending their location.
- The estimated local average exfoliation fracture frequencies were added to the boreholes depending the location and how well the result was fitting with the frequencies from Televiewer from the nearby boreholes.

	Average exfoliation fracture frequency	
Cluster	Calculated	Estimated
Northern	KH-02-17, KH-01-12, KH-01-18	KH-03-05, KH-01-06
Southern	KH-01-17, KH-02-18	KH-04-05, KH-03-06
Eastern	KH-01-17	KH-02-06, KH-02-05, KH-01-05
Western	KH-02-17, KH-01-12, KH-01-18, KH-02-18	

Exfoliation fracture frequency graphs for the boreholes missing Televiewer



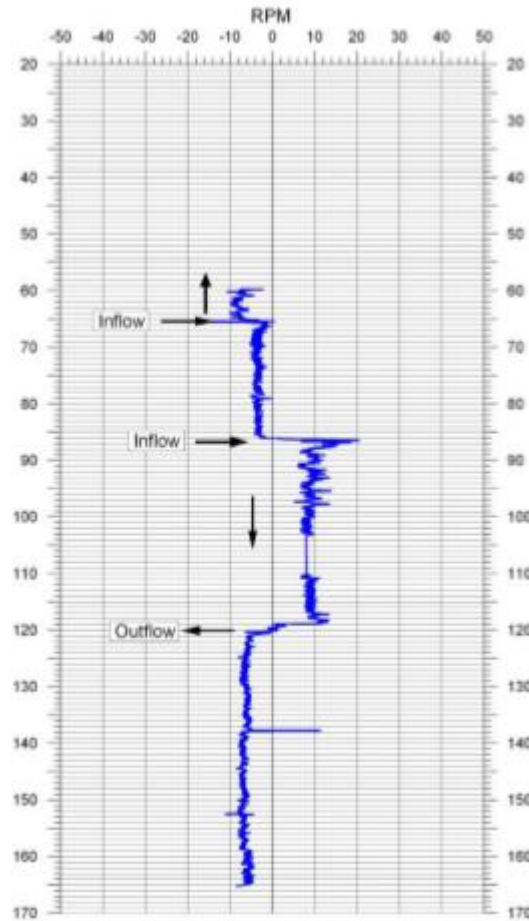
Exfoliation fracture frequency graphs for the boreholes missing Televiewer



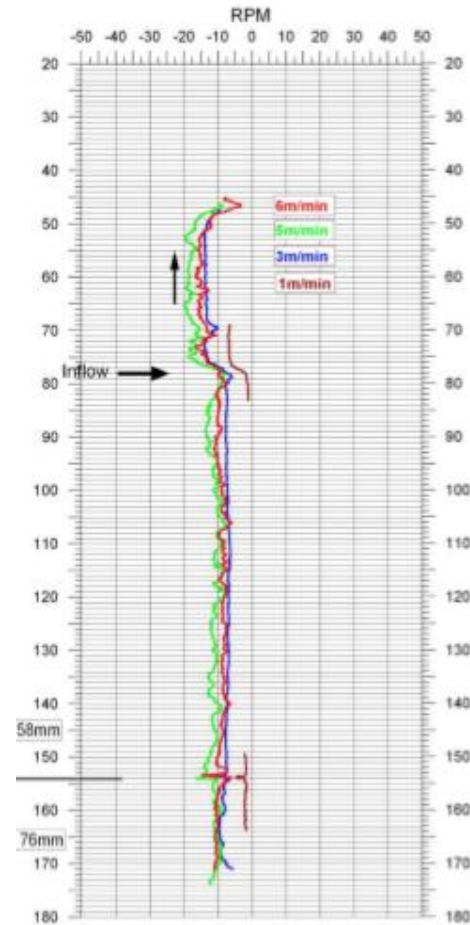
Flow measurements

From the previous NGU reports the depth and the type of the flow measurements were assigned to each borehole. The boreholes drilled in 2005 did not have data for flow measurements.

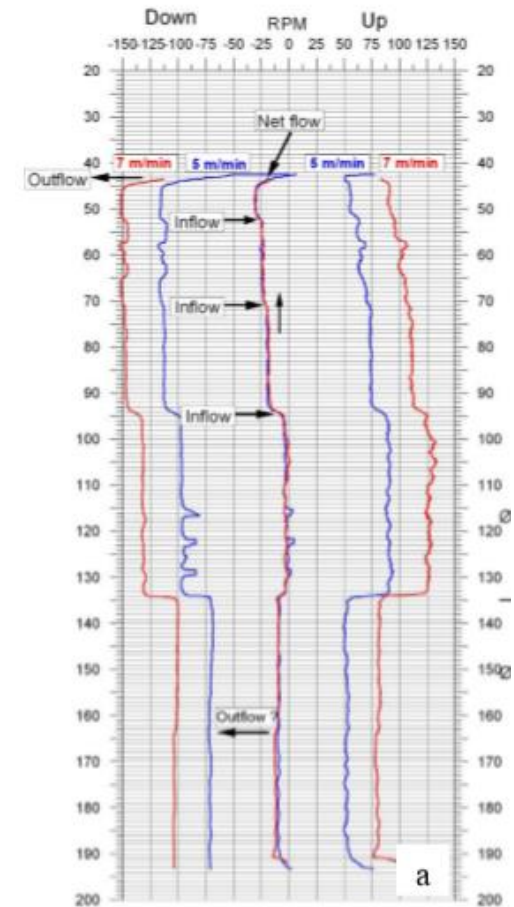
Flow measurements



KH-01-06

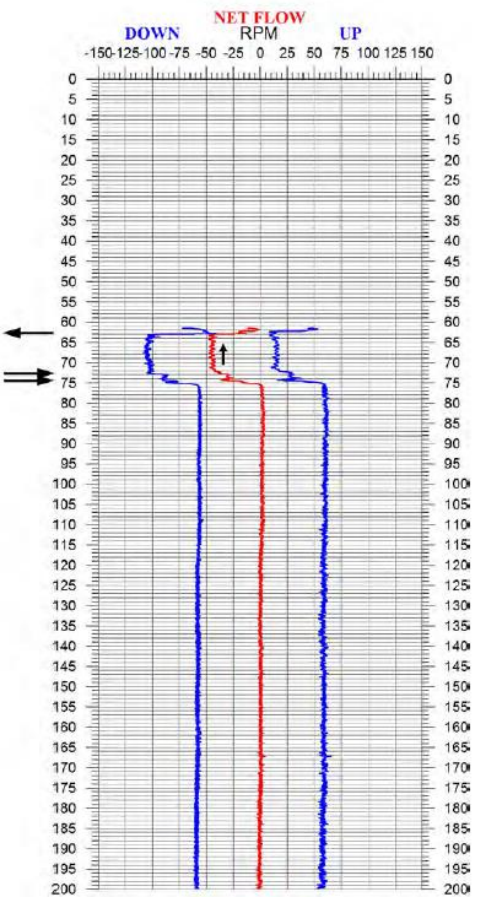


KH-02-06

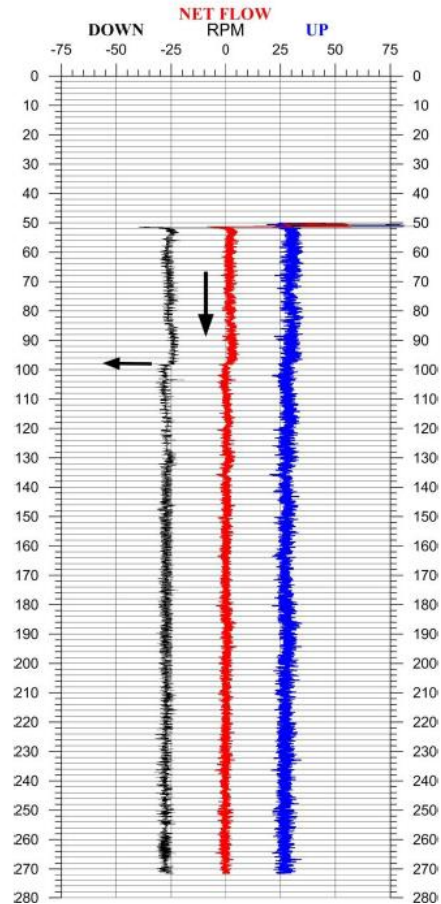


KH-03-06

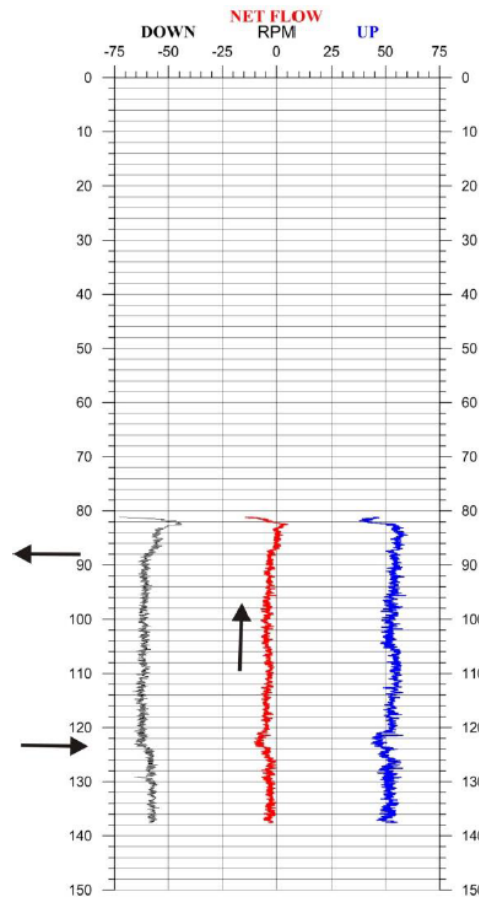
Flow measurements



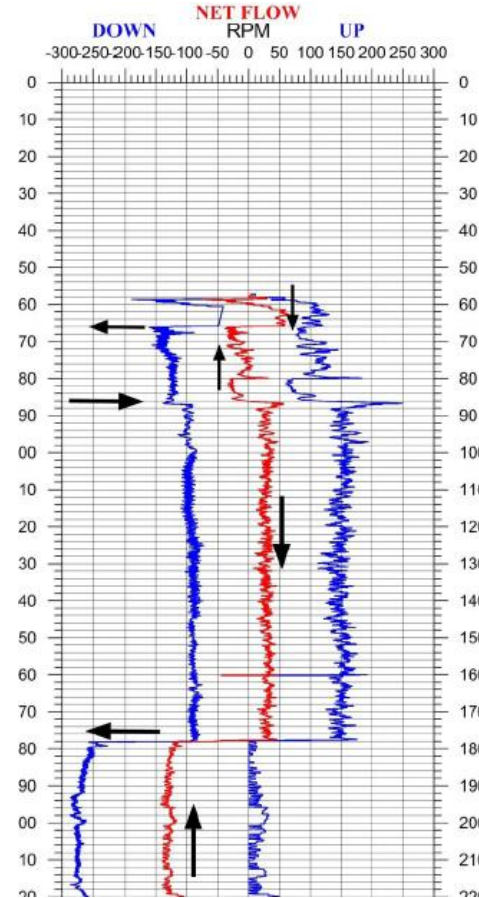
KH-01-12



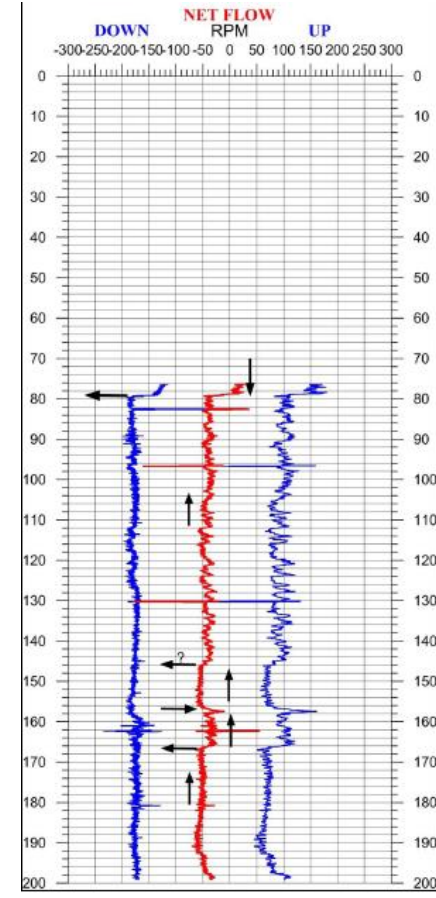
KH-01-17



KH-02-17



KH-01-18



KH-02-18

Final rock mass domain interpretation

- Based on the fracture frequencies, the exfoliation fractures as well as the flow measurements, two sets of bins were defined for each borehole.
- The first set of bins has 5 meters minimum domain length and they have a more local interpretation.
- On the other hand, the second set of bins have 20 meters minimum domain length in order to be able to connect the rock mass domains between different locations and also be compared with the electrical resistivity profiles.

Rock characteristics and flow patterns

Bin with minimum 5 m domain length				
fracture frequencies	exfoliation	fracture frequencies	Flow measurements	bin code bin color
low		low	(-)	a
low		low	inflow	b
low		low	outflow	c
low		low	downflow-upflow	d
low		moderate - high	(-)	f
low		moderate - high	inflow	g
low		moderate - high	outflow	h
low		moderate - high	downflow-upflow	i
moderate - high		low	(-)	k
moderate - high		low	inflow	l
moderate - high		low	outflow	m
moderate - high		low	downflow-upflow	n
moderate - high		moderate - high	(-)	p
moderate - high		moderate - high	inflow	q
moderate - high		moderate - high	outflow	r
moderate - high		moderate - high	downflow-upflow	s

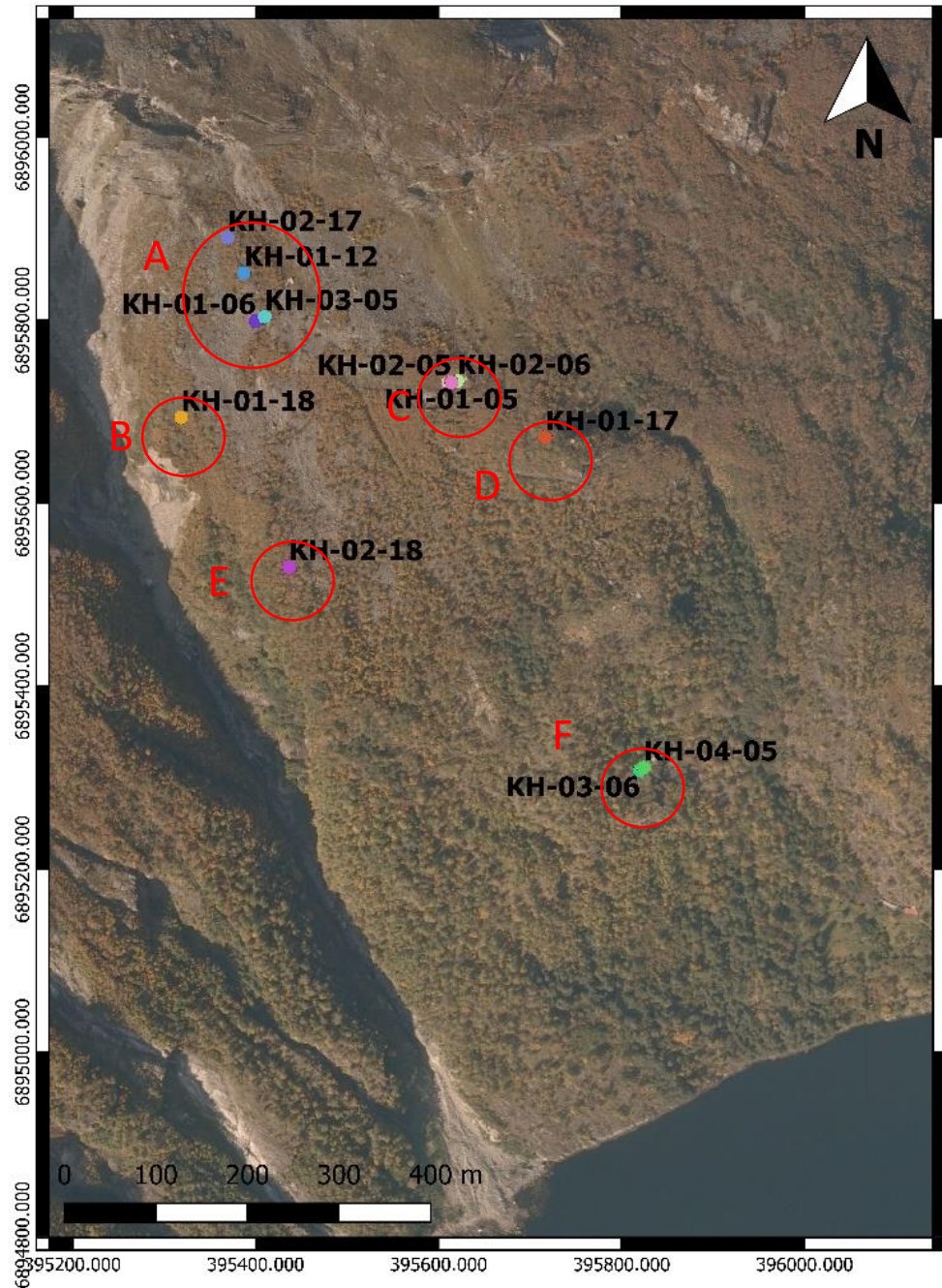
To decrease the number of the bins the downflow and the upflow from the graphs were merged together as it was only showing movement of the water locally at each borehole.

Rock characteristics and flow patterns

Bin with minimum 20 m domain length

fracture frequencies	exfoliation	fracture frequencies	flow measurements	bin code	bin color
low		low	(-)	A	
low		low	inflow-outflow	B	
low		moderate - high	(-)	C	
low		moderate - high	inflow-outflow	D	
moderate - high		low	(-)	E	
moderate - high		low	inflow-outflow	F	
moderate - high		moderate - high	(-)	G	
moderate - high		moderate - high	inflow-outflow	H	
Inflow - Outflow				GQ	

The upflow and downflow were neglected for this bin interpretation and the inflow and outflow were merged together as Inflow – Outflow section with light blue color. This section might indicate good quality aquifers, although this is highly influenced by the local hydraulic gradient at the time the flow measurements took place.



Clusters

The boreholes with their rock characteristics and flow patterns were divided into 5 clusters depending their location on the map.

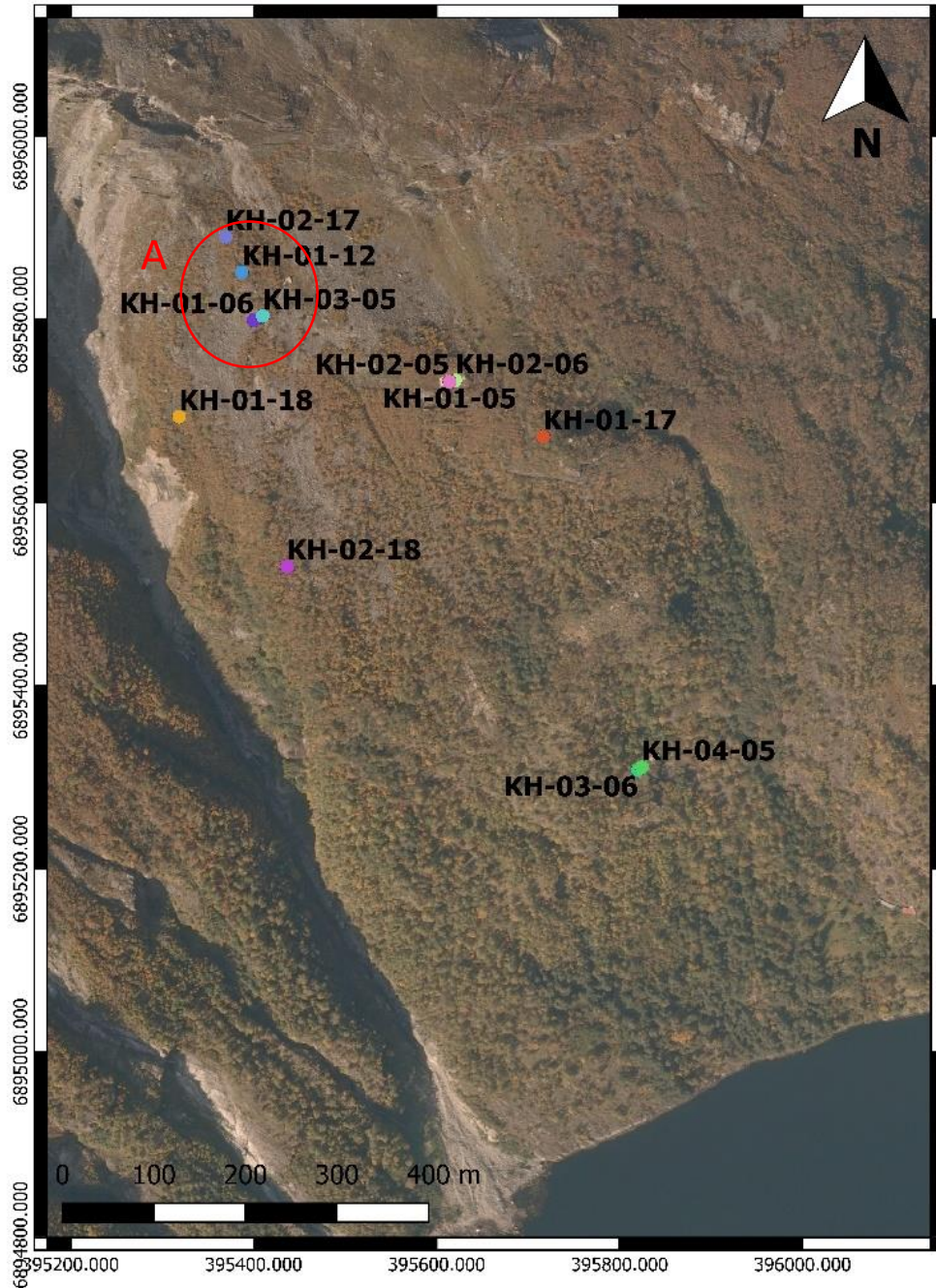
Main rock mass domains

The analysis of the clusters of the rock mass characteristics and flow patterns gave two different interpretations.

The Interpretation A, with 8 rock mass domains, gives a more detailed overview mostly of the deeper domains while Interpretation B, with 4 rock mass domains (plus 2 extra domains in the deeper borehole), gives a more simplified opinion about the deeper part of the rocks.

The characteristics of the domains of both the interpretations are presented in detail in the following slides.

Interpretation Scenario A



Cluster A

Consisted of 4 Boreholes

KH-02-17

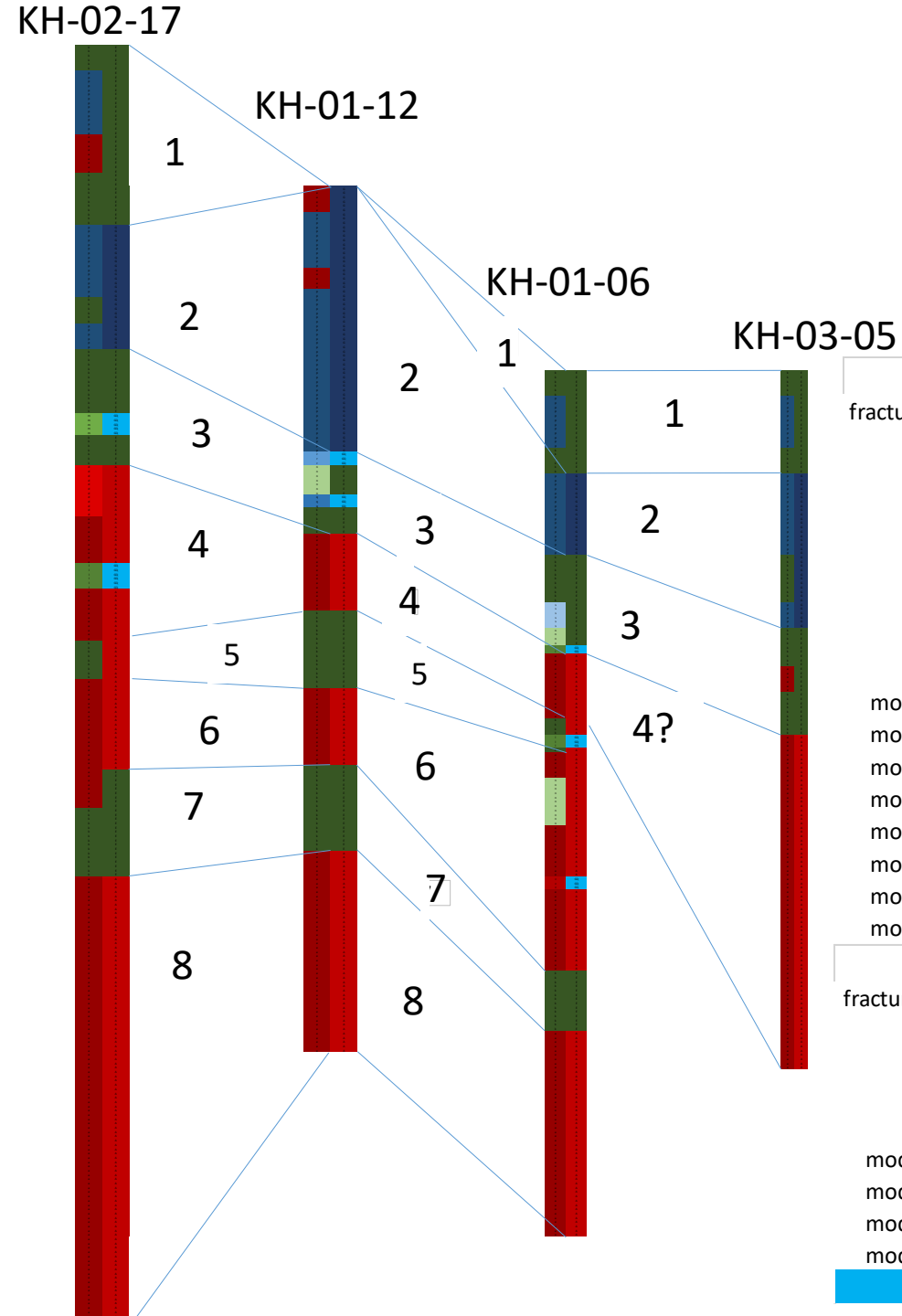
KH-01-12

KH-01-06

KH-03-05

Eight rock mass domains were identified in this cluster

Interpretation
scenario A.
Cluster A



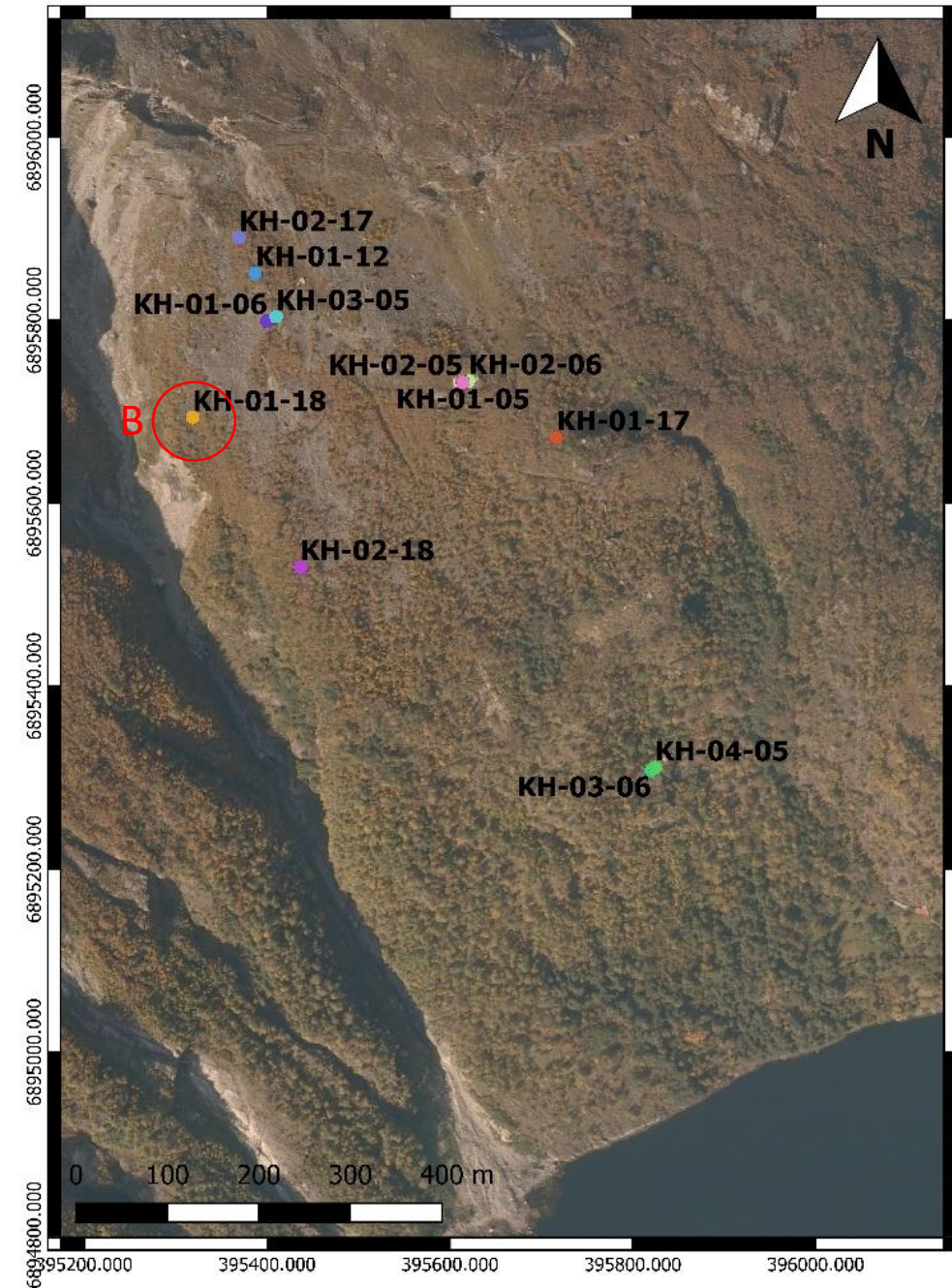
The left half of each borehole represents the rock mass characteristics and flow patterns of the 5 meter domain bins, while the right half the 20 m domain bins.

Interpretation Scenario A

Cluster B

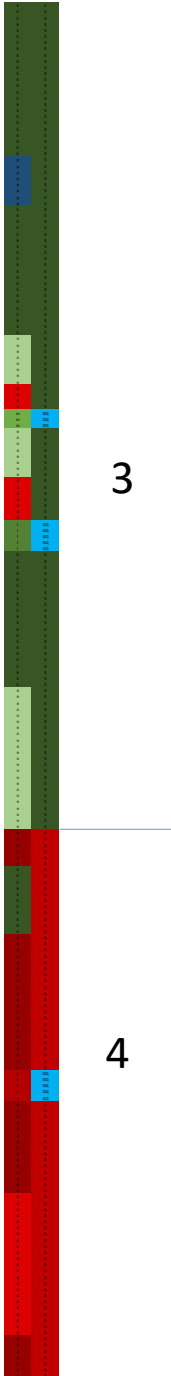
Consisted of 1 Borehole
KH-01-18

Two rock mass domains where identified in this cluster



Interpretation
scenario A.
Cluster B

KH-01-18



The left half of each borehole represents the rock mass characteristics and flow patterns of the 5 meter domain bins, while the right half the 20 m domain bins.

Bin with minimum 5 m domain length					
fracture frequencies	exfoliation	fracture frequencies	Flow measurements	bin code	bin color
low		low	(-)	a	
low		low	inflow	b	
low		low	outflow	c	
low		low	downflow-upflow	d	
low		moderate - high	(-)	f	
low		moderate - high	inflow	g	
low		moderate - high	outflow	h	
low		moderate - high	downflow-upflow	i	
moderate - high		low	(-)	k	
moderate - high		low	inflow	l	
moderate - high		low	outflow	m	
moderate - high		low	downflow-upflow	n	
moderate - high		moderate - high	(-)	p	
moderate - high		moderate - high	inflow	q	
moderate - high		moderate - high	outflow	r	
moderate - high		moderate - high	downflow-upflow	s	

Bin with minimum 20 m domain length					
fracture frequencies	exfoliation	fracture frequencies	flow measurements	bin code	bin color
low		low	(-)	A	
low		low	inflow-outflow	B	
low		moderate - high	(-)	C	
low		moderate - high	inflow-outflow	D	
moderate - high		low	(-)	E	
moderate - high		low	inflow-outflow	F	
moderate - high		moderate - high	(-)	G	
moderate - high		moderate - high	inflow-outflow	H	
Inflow - Outflow				GQ	

Interpretation Scenario A

Cluster C

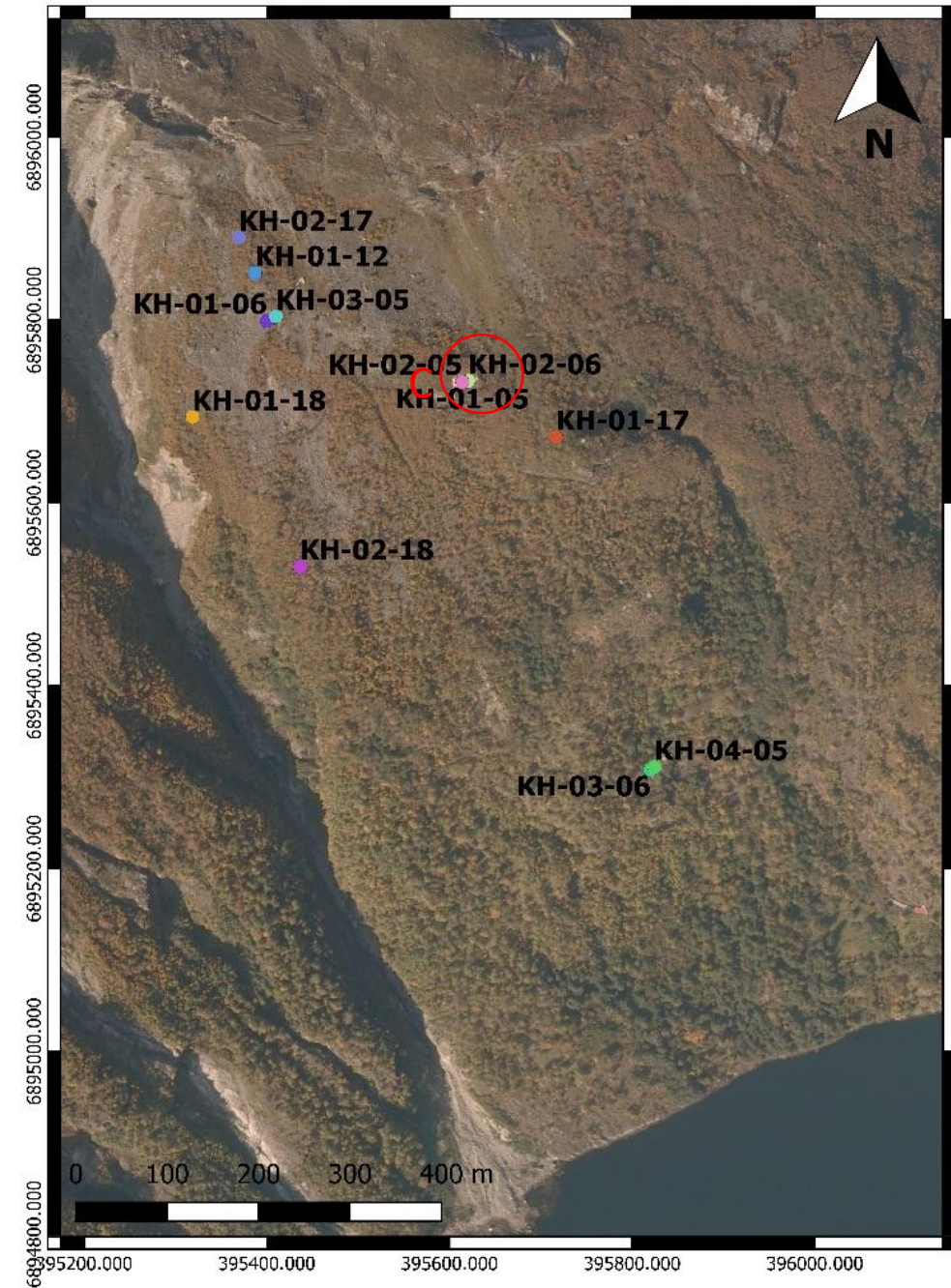
Consisted of 3 Borehole

KH-02-05

KH-02-06

KH-01-05

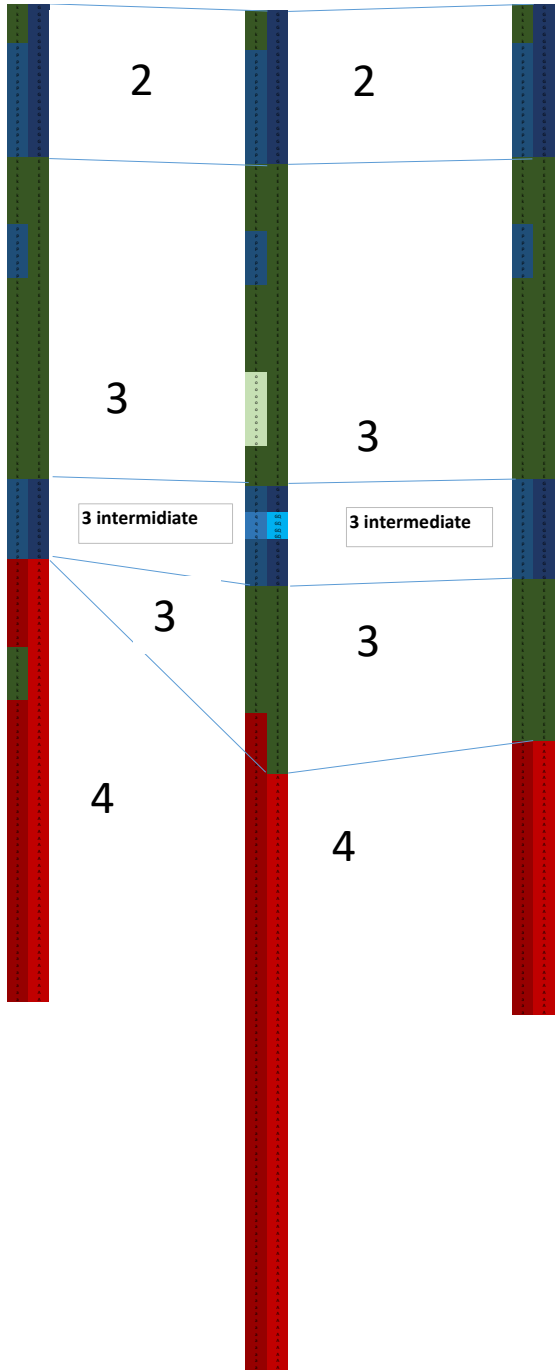
Five rock mass domains where identified in this cluster



Interpretation scenario A. Cluster C

*3 Intermediate domain has both high exfoliation fracture frequency and total fracture frequency, while domain 3 has only high total fracture frequency.

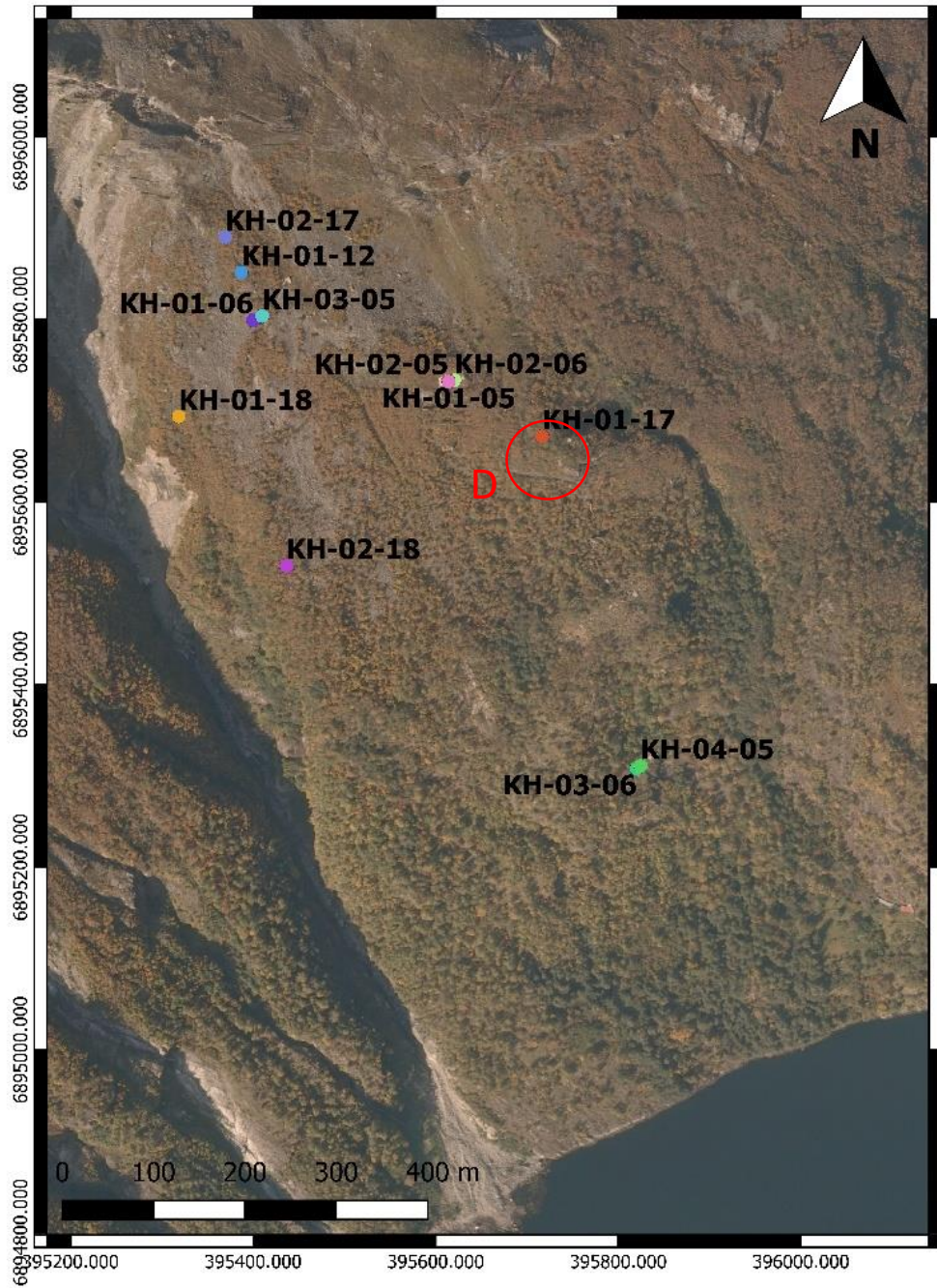
KH-01-05 KH-02-06 KH-02-05



The left half of each borehole represents the rock mass characteristics and flow patterns of the 5 meter domain bins, while the right half the 20 m domain bins.

Bin with minimum 5 m domain length					
fracture frequencies	exfoliation	fracture frequencies	Flow measurements	bin code	bin color
low		low	(-)	a	
low		low	inflow	b	
low		low	outflow	c	
low		low	downflow-upflow	d	
low		moderate - high	(-)	f	
low		moderate - high	inflow	g	
low		moderate - high	outflow	h	
low		moderate - high	downflow-upflow	i	
moderate - high		low	(-)	k	
moderate - high		low	inflow	l	
moderate - high		low	outflow	m	
moderate - high		low	downflow-upflow	n	
moderate - high		moderate - high	(-)	p	
moderate - high		moderate - high	inflow	q	
moderate - high		moderate - high	outflow	r	
moderate - high		moderate - high	downflow-upflow	s	
Bin with minimum 20 m domain length					
fracture frequencies	exfoliation	fracture frequencies	flow measurements	bin code	bin color
low		low	(-)	A	
low		low	inflow-outflow	B	
low		moderate - high	(-)	C	
low		moderate - high	inflow-outflow	D	
moderate - high		low	(-)	E	
moderate - high		low	inflow-outflow	F	
moderate - high		moderate - high	(-)	G	
moderate - high		moderate - high	inflow-outflow	H	
Inflow - Outflow				GQ	

Interpretation Scenario A

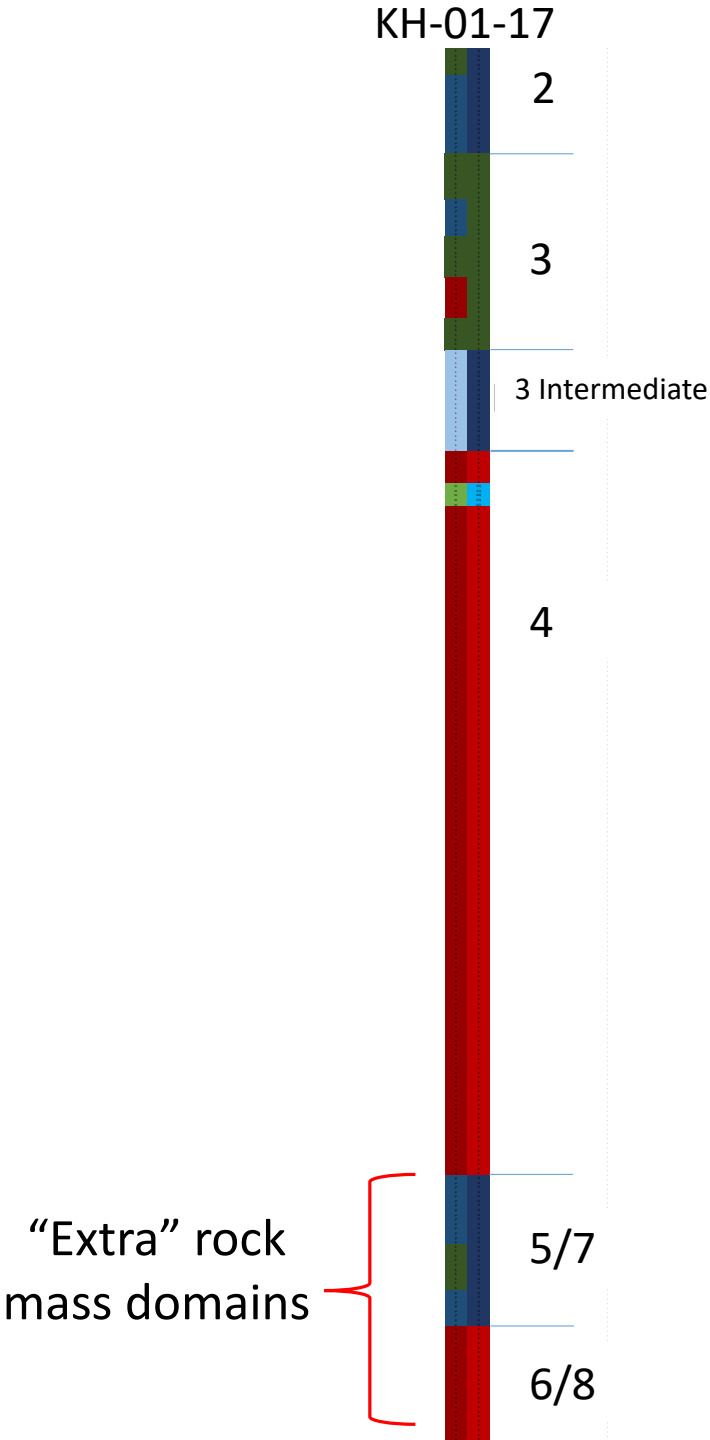


Cluster D

Consisted of 1 Borehole
KH-01-17

6 rock mass domains were identified in this cluster.
Borehole KH-01-17 is the deepest borehole and after the 245
masl there were two “extra” rock mass domains that gave
some uncertainty in terms of their characterization.

Interpretation
scenario A.
Cluster D

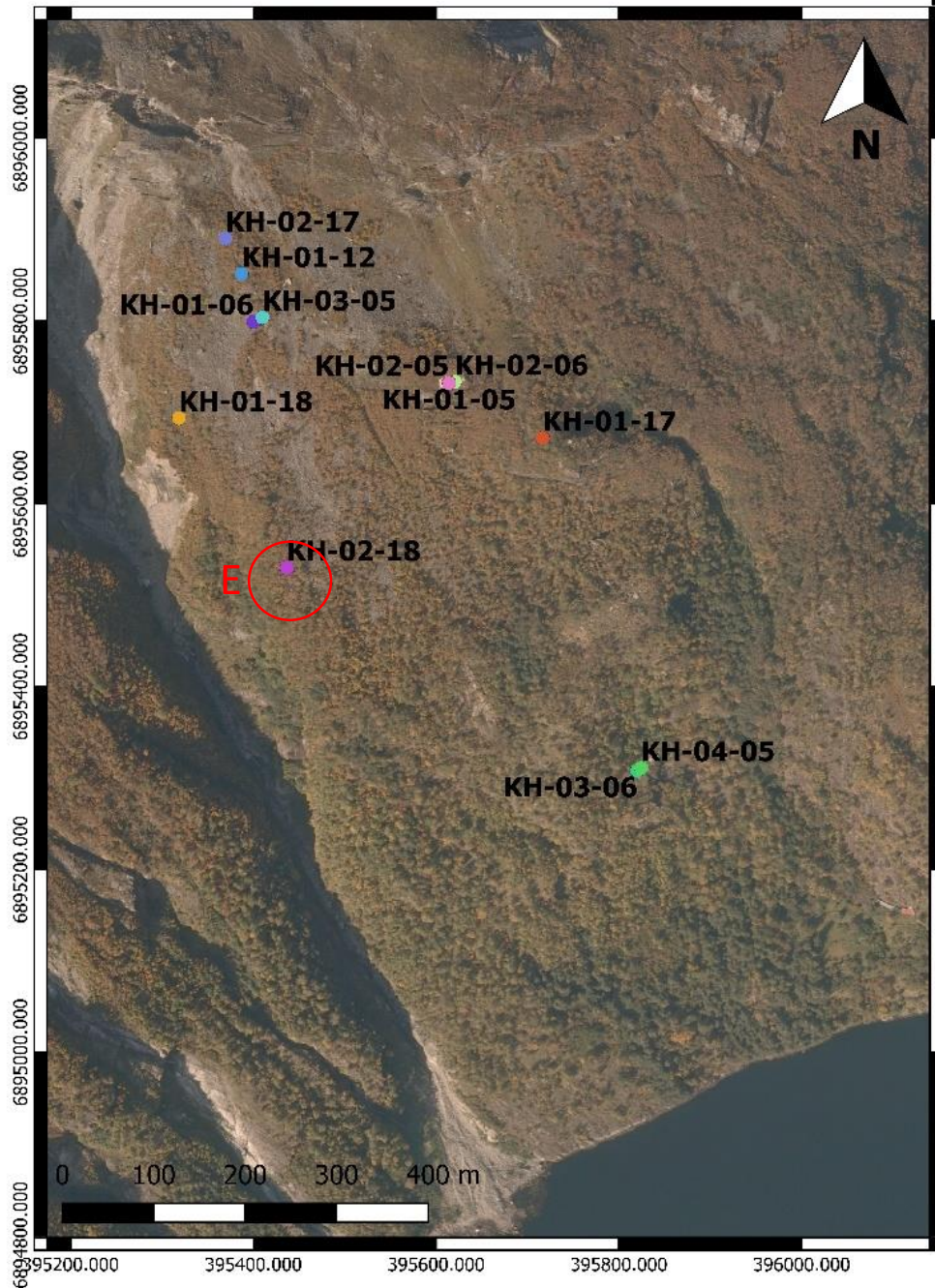


The left half of each borehole represents the rock mass characteristics and flow patterns of the 5 meter domain bins, while the right half the 20 m domain bins.

Bin with minimum 5 m domain length					
fracture frequencies	exfoliation	fracture frequencies	Flow measurements	bin code	bin color
low		low	(-)	a	
low		low	inflow	b	
low		low	outflow	c	
low		low	downflow-upflow	d	
low		moderate - high	(-)	f	
low		moderate - high	inflow	g	
low		moderate - high	outflow	h	
low		moderate - high	downflow-upflow	i	
moderate - high		low	(-)	k	
moderate - high		low	inflow	l	
moderate - high		low	outflow	m	
moderate - high		low	downflow-upflow	n	
moderate - high		moderate - high	(-)	p	
moderate - high		moderate - high	inflow	q	
moderate - high		moderate - high	outflow	r	
moderate - high		moderate - high	downflow-upflow	s	

Bin with minimum 20 m domain length					
fracture frequencies	exfoliation	fracture frequencies	flow measurements	bin code	bin color
low		low	(-)	A	
low		low	inflow-outflow	B	
low		moderate - high	(-)	C	
low		moderate - high	inflow-outflow	D	
moderate - high		low	(-)	E	
moderate - high		low	inflow-outflow	F	
moderate - high		moderate - high	(-)	G	
moderate - high		moderate - high	inflow-outflow	H	
Inflow - Outflow				GQ	

Interpretation Scenario A

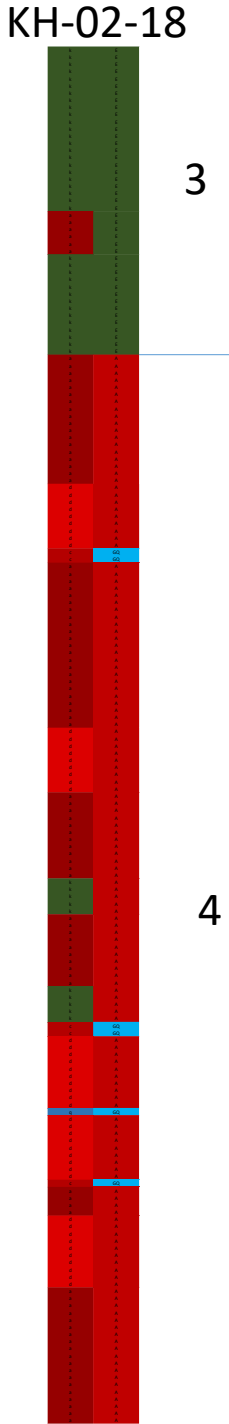


Cluster E

Consisted of 1 Borehole
KH-02-18

Two rock mass domains were identified in this cluster.

Interpretation
scenario A.
Cluster E



The left half of each borehole represents the rock mass characteristics and flow patterns of the 5 meter domain bins, while the right half the 20 m domain bins.

Bin with minimum 5 m domain length					bin code	bin color
fracture frequencies	exfoliation	fracture frequencies	Flow measurements			
low		low	(-)		a	
low		low	inflow		b	
low		low	outflow		c	
low		low	downflow-upflow		d	
low		moderate - high	(-)		f	
low		moderate - high	inflow		g	
low		moderate - high	outflow		h	
low		moderate - high	downflow-upflow		i	
moderate - high		low	(-)		k	
moderate - high		low	inflow		l	
moderate - high		low	outflow		m	
moderate - high		low	downflow-upflow		n	
moderate - high		moderate - high	(-)		p	
moderate - high		moderate - high	inflow		q	
moderate - high		moderate - high	outflow		r	
moderate - high		moderate - high	downflow-upflow		s	

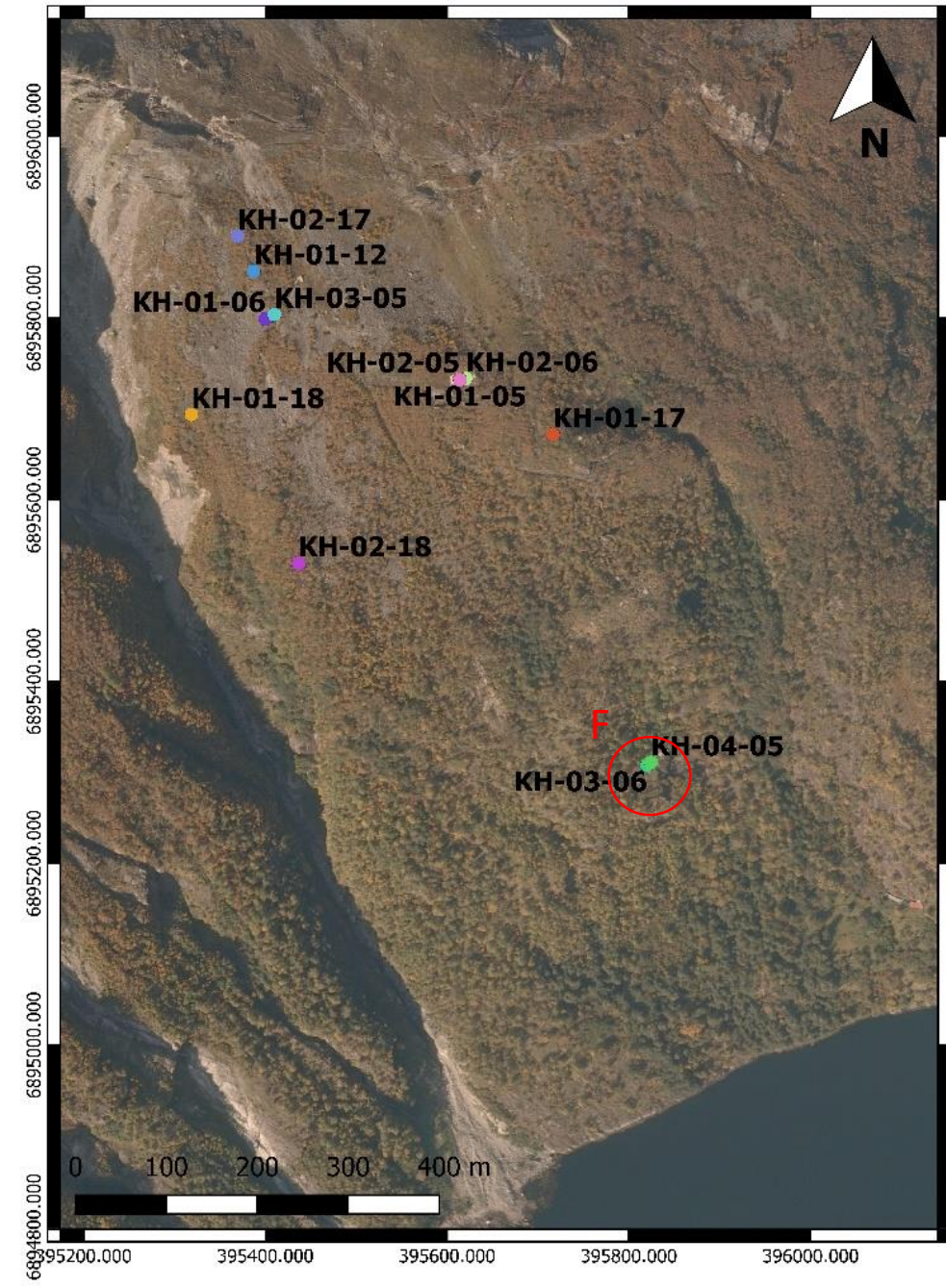
Bin with minimum 20 m domain length					bin code	bin color
fracture frequencies	exfoliation	fracture frequencies	flow measurements			
low		low	(-)		A	
low		low	inflow-outflow		B	
low		moderate - high	(-)		C	
low		moderate - high	inflow-outflow		D	
moderate - high		low	(-)		E	
moderate - high		low	inflow-outflow		F	
moderate - high		moderate - high	(-)		G	
moderate - high		moderate - high	inflow-outflow		H	
Inflow - Outflow					GQ	

Interpretation Scenario A

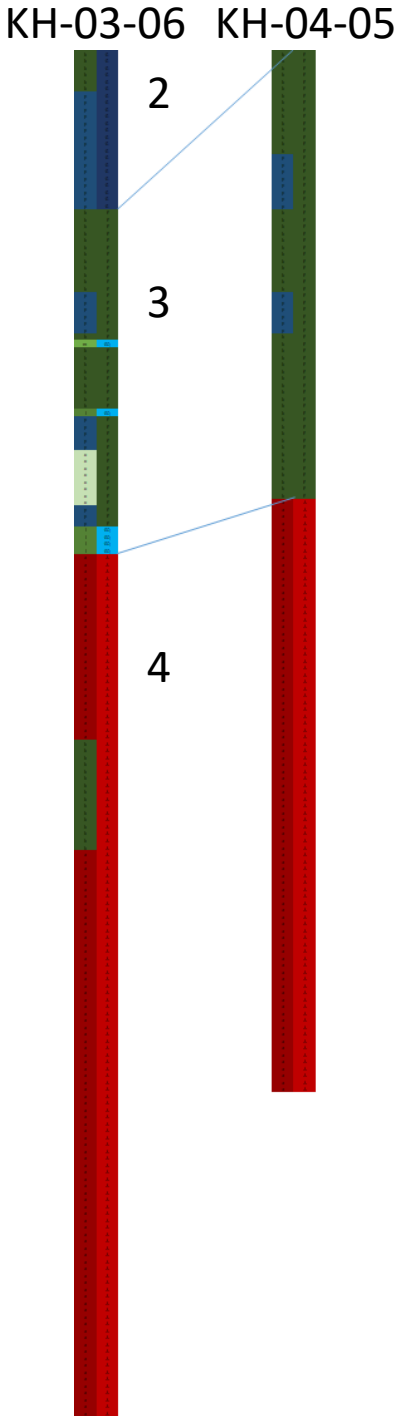
Cluster F

Consisted of 2 Boreholes
KH-03-06 KH-04-05

Three rock mass domains were identified in this cluster



Interpretation
scenario A.
Cluster F



The left half of each borehole represents the rock mass characteristics and flow patterns of the 5 meter domain bins, while the right half the 20 m domain bins.

Bin with minimum 5 m domain length				
fracture frequencies	exfoliation	fracture frequencies	Flow measurements	bin code
low		low	(-)	a
low		low	inflow	b
low		low	outflow	c
low		low	downflow-upflow	d
low		moderate - high	(-)	f
low		moderate - high	inflow	g
low		moderate - high	outflow	h
low		moderate - high	downflow-upflow	i
moderate - high		low	(-)	k
moderate - high		low	inflow	l
moderate - high		low	outflow	m
moderate - high		low	downflow-upflow	n
moderate - high		moderate - high	(-)	p
moderate - high		moderate - high	inflow	q
moderate - high		moderate - high	outflow	r
moderate - high		moderate - high	downflow-upflow	s

Bin with minimum 20 m domain length				
fracture frequencies	exfoliation	fracture frequencies	flow measurements	bin code
low		low	(-)	A
low		low	inflow-outflow	B
low		moderate - high	(-)	C
low		moderate - high	inflow-outflow	D
moderate - high		low	(-)	E
moderate - high		low	inflow-outflow	F
moderate - high		moderate - high	(-)	G
moderate - high		moderate - high	inflow-outflow	H
Inflow - Outflow				GQ

Rock mass domain characteristics of Interpretation scenario A

- **Domain 1 – top domain**

Moderate-high fracture frequency/m

Limited number of exfoliation fractures

- **Domain 2**

Both moderate – high fracture frequency/m and exfoliation fractures

- **Domain 3**

Moderate-high fracture frequency/m

Limited number of exfoliation fractures

Subdomains with inflow-outflow

- **Domain 3 intermediate**

In some occasions the lower part of the domain 3 had moderate to high exfoliation fracture frequency for 15m length. Therefore, it was considered as a separate domain.

- **Domain 4**

Both low fracture frequency/m and exfoliation fractures -probably aquitards-seals

Subdomains with Inflow - Outflow

- **Domain 5**

Limited number of exfoliation fractures

Subdomains with Inflow - Outflow

In some boreholes does not exist while in others 18-20 m

The current domain could have been also considered as an intermediate domain of domain 4

- **Domain 6**

Both low fracture frequency/m and exfoliation fractures -probably aquitards-seals

In some occasions subdomains with Inflow - Outflow

From few to several meters

In some boreholes does not exist

The domain could have been considered as the continuation of domain 4

- **Domain 7**

Moderate-high fracture frequency/m

Limited number of exfoliation fractures

From few to 18-22 meters

In some boreholes does not exist

The current domain could have been also considered as an intermediate domain of domain 4

- **Domain 8**

Hard bedrock or the deepest part of domain 4

Clusters

- Based on common rock mass domain numbering and the observed characteristics, the clusters appear to have the domains below (shown also on the map on the left).

Cluster A: domains 1-8

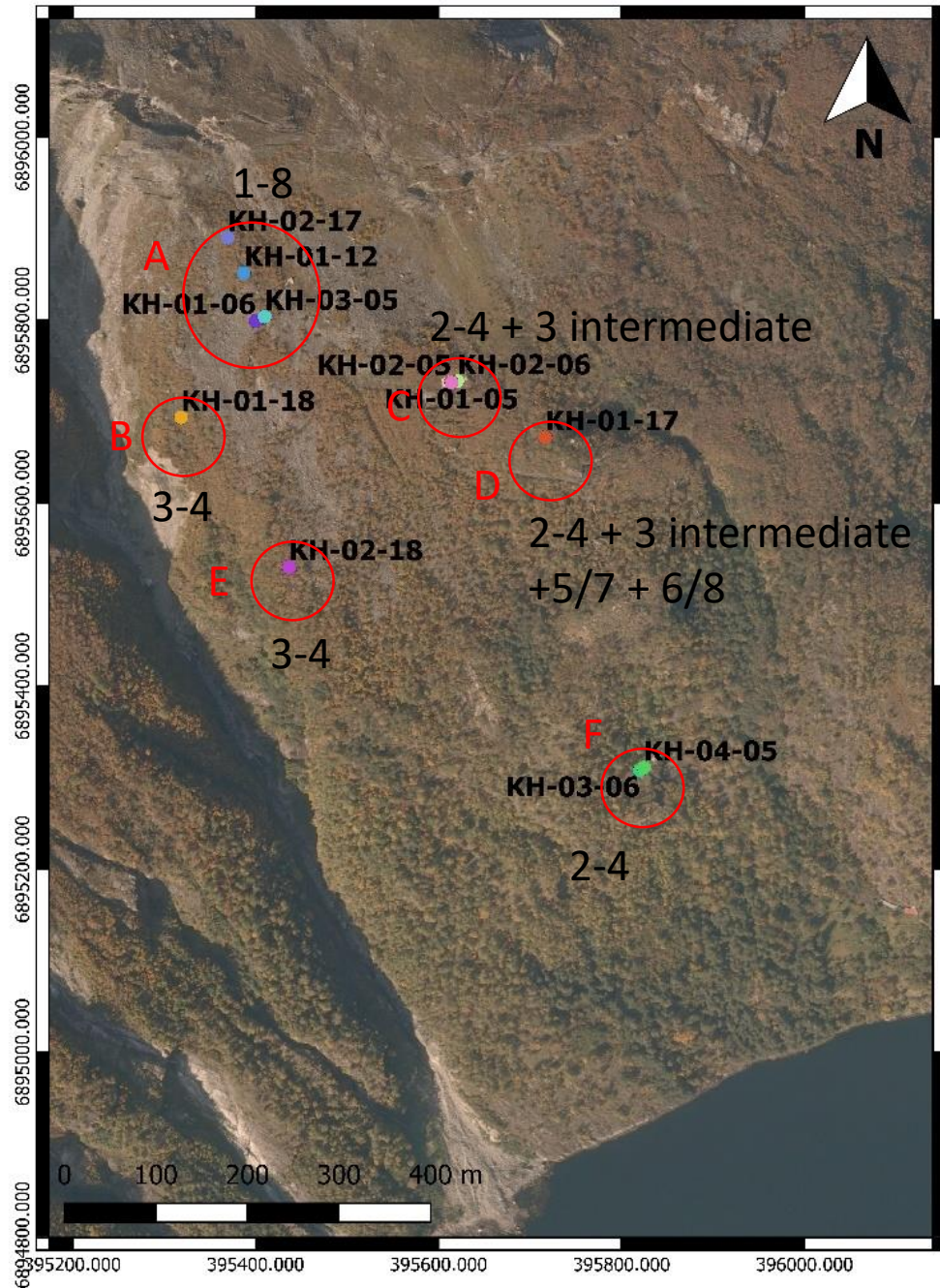
Cluster B: domains 3-4

Cluster C: domains 2-4 + 3 intermediate

Cluster D: domains 2-4 + 3 intermediate + 5/7+6/8

Cluster E: domains 3-4

Cluster F: domains 2-4



Interpretation Scenario A

Clusters

Cluster A: domains 1-8

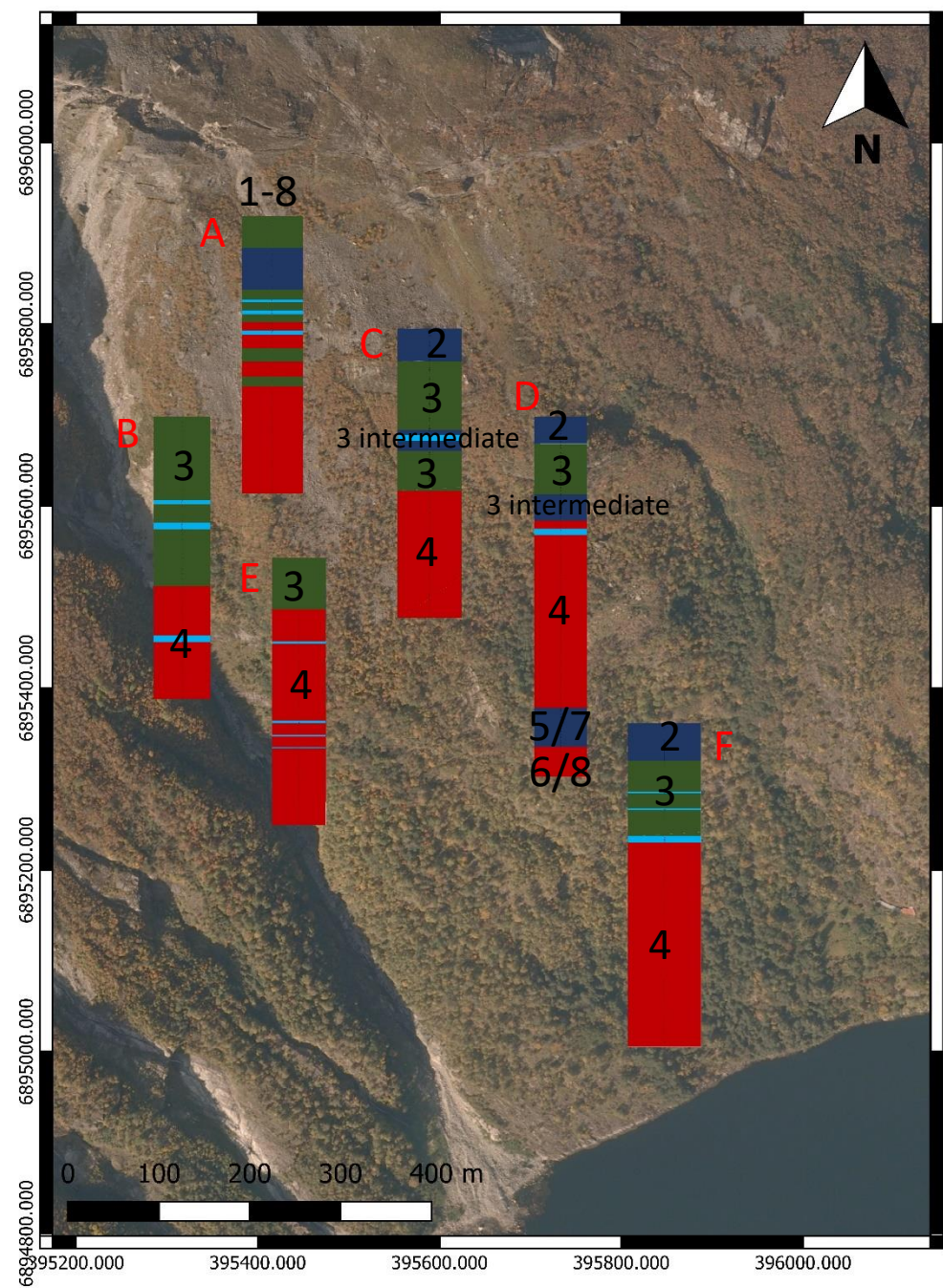
Cluster B: domains 3-4

Cluster C: domains 2-4 + 3 intermediate

Cluster D: domains 2-4 + 3 intermediate + 5/7+6/8

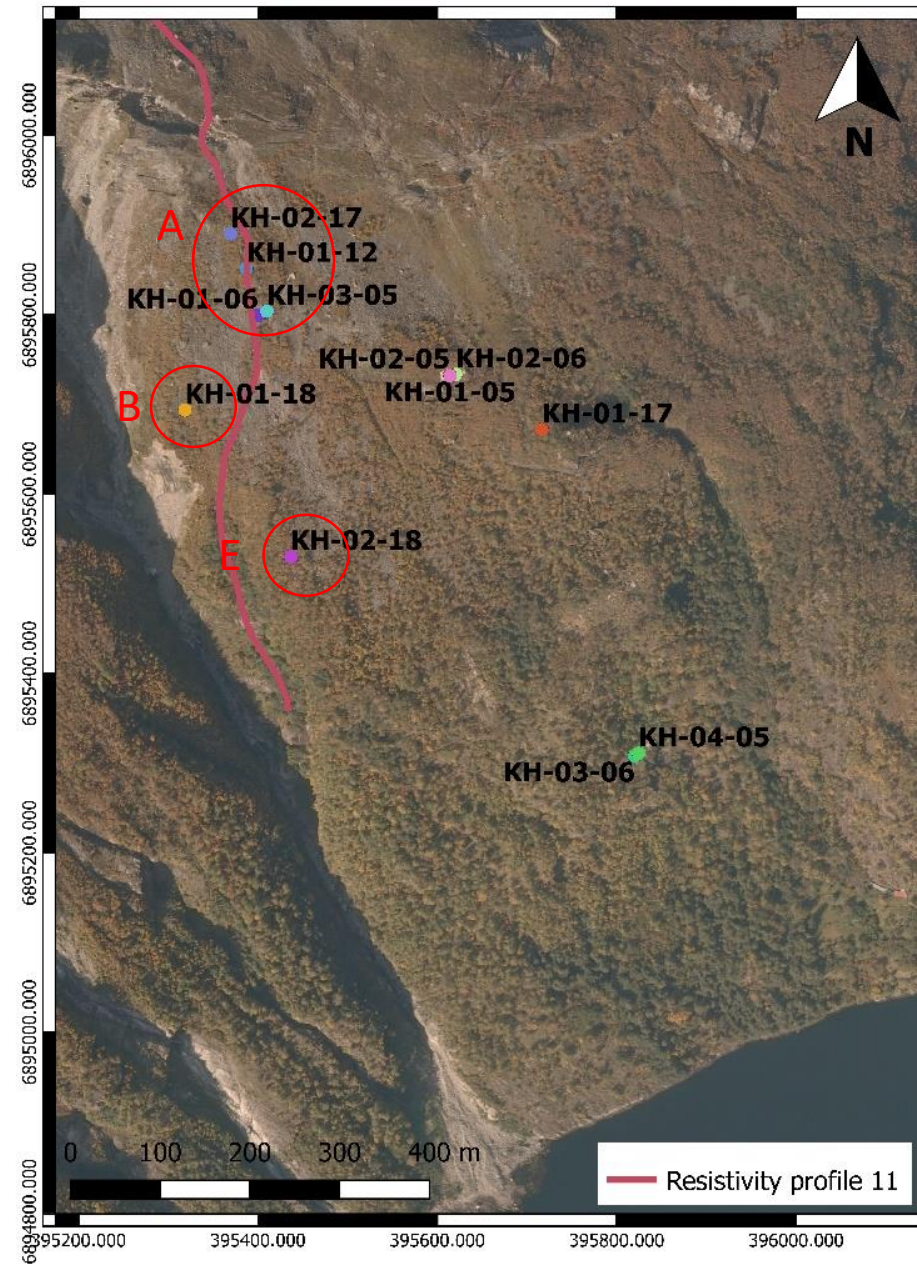
Cluster E: domains 3-4

Cluster F: domains 2-4

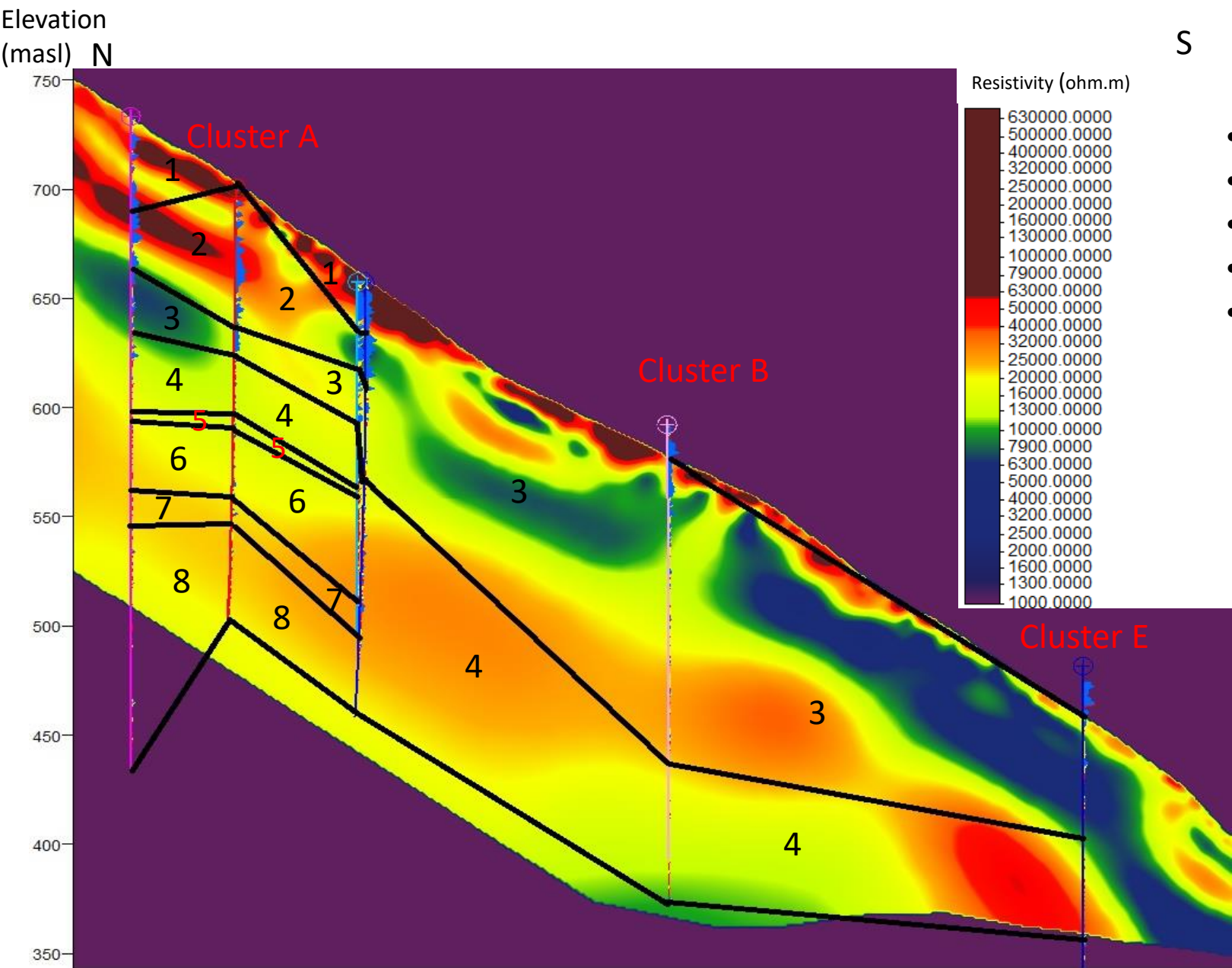


Bin with minimum 20 m domain length					
fracture frequencies	exfoliation	fracture frequencies	flow measurements	bin code	bin color
low		low	(-)	A	
low		low	inflow-outflow	B	
low		moderate - high	(-)	C	
low		moderate - high	inflow-outflow	D	
moderate - high		low	(-)	E	
moderate - high		low	inflow-outflow	F	
moderate - high		moderate - high	(-)	G	
moderate - high		moderate - high	inflow-outflow	H	
Inflow - Outflow				GQ	

Comparison of the rock mass domains in scenario A with ERT profiles



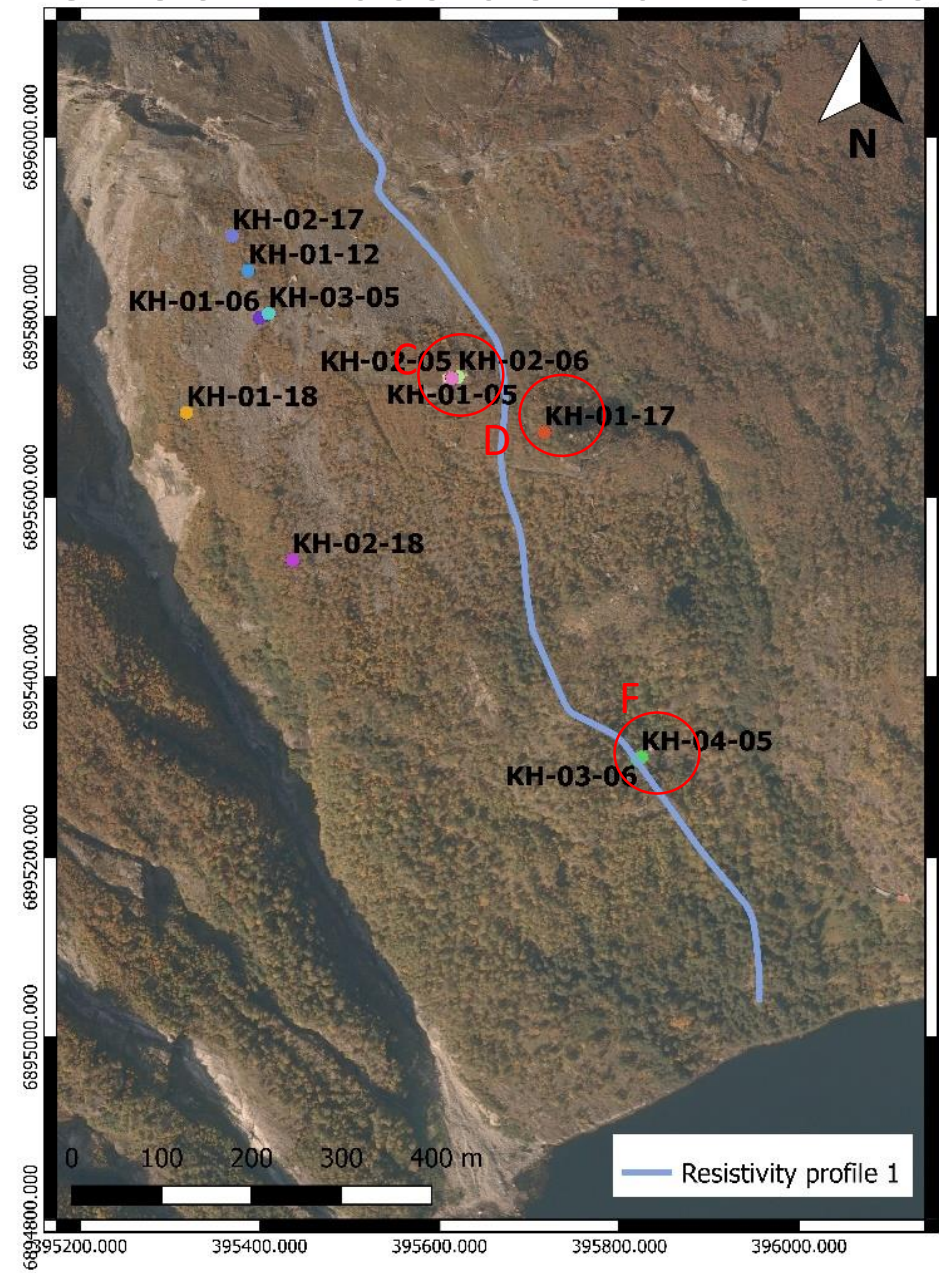
Comparison of the rock mass domains in scenario A with ERT profiles



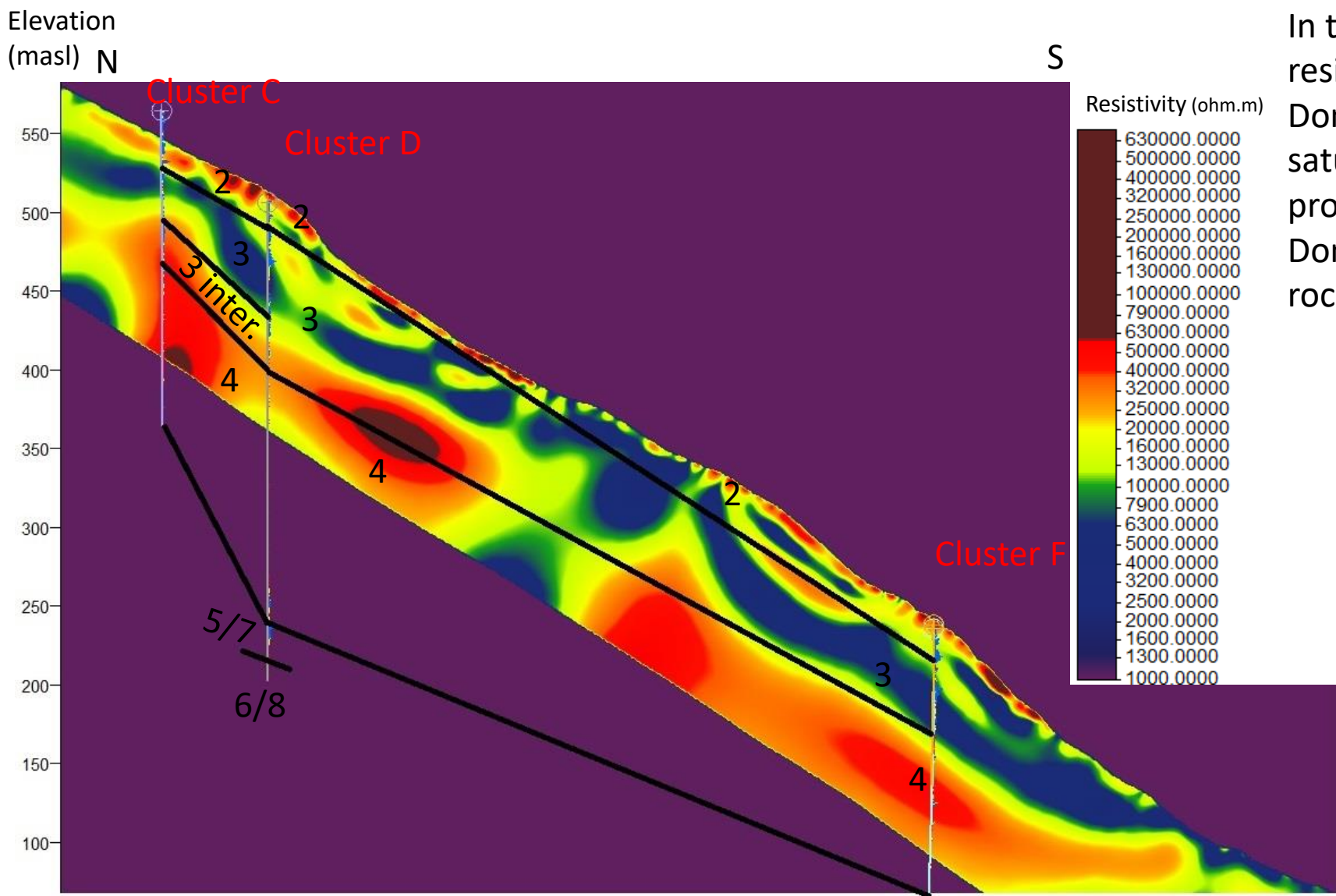
- Domain 1 – scree material
- Domain 2 – drained
- Domain 3 – water saturated zone
- Domains 4-5-6 – water saturated
- Domain 8 – unfractured rock

Description	Resistivity
Scree materials - Tallus bedrock	30-35K ohm.m
Drained - Highly fractured	30-50K
Water saturated - moderately fractured	12-30K ohm.m
Water saturated - fractured	1-7.5K / <12K ohm.m
Massive bedrock - unfractured	15-30K ohm.m

Comparison of the rock mass domains in scenario A with ERT profiles



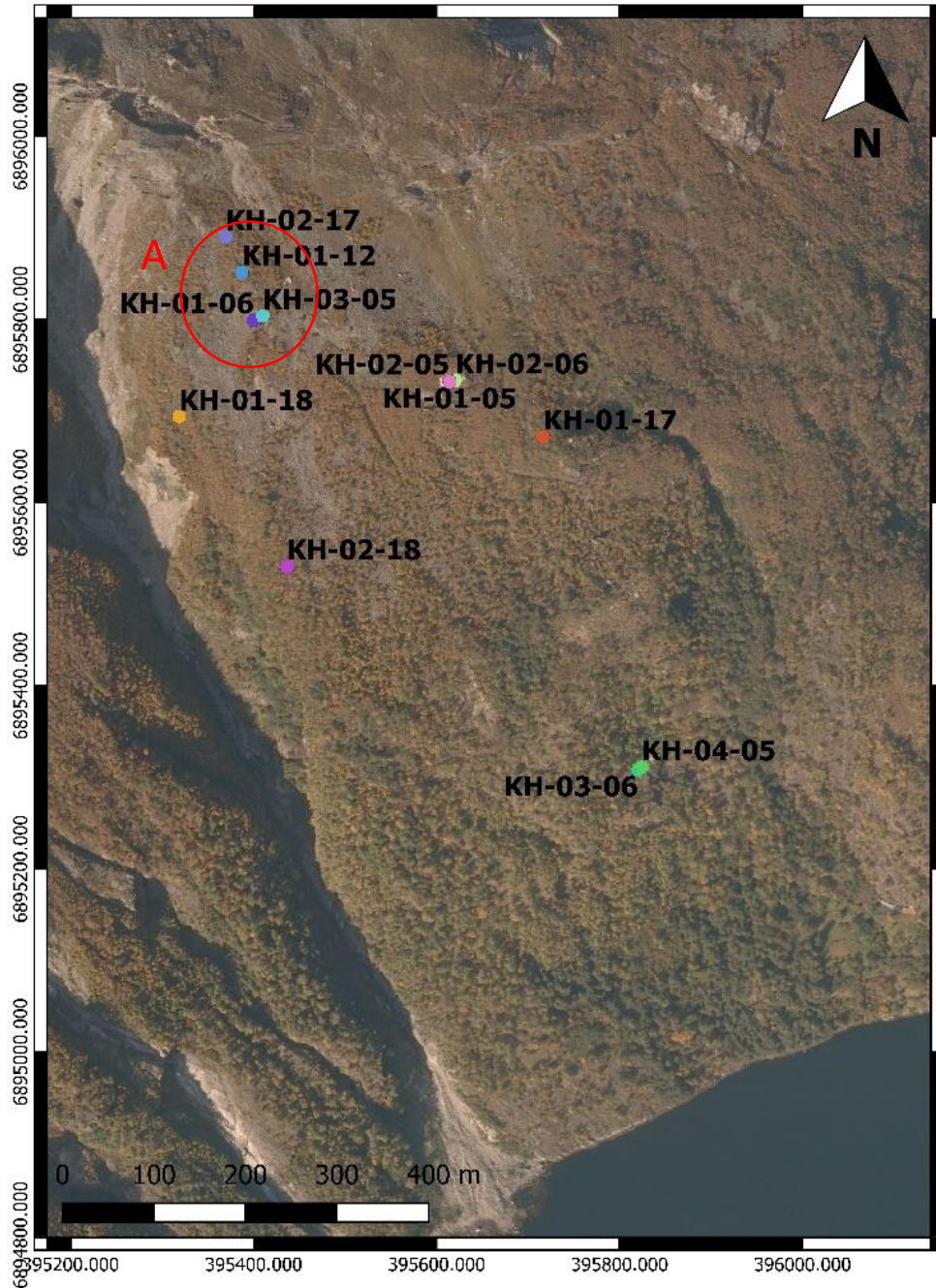
Comparison of the rock mass domains in scenario A with ERT profiles



In this resistivity profile Domain 2 has high resistivity indicating scree material. Domain 3 coincides with the water saturated zone, while 3 intermediate is probably at the drained area (40k ohm.m) Domain 4 can be considered as unfractured rock due to the low rock fracturing.

Description	Resistivity
Scree materials - Tallus bedrock	30-35K ohm.m
Drained - Highly fractured	30-50K
Water saturated - moderately fractured	12-30K ohm.m
Water saturated - fractured	1-7.5K / <12K ohm.m
Massive bedrock - unfractured	15-30K ohm.m

Interpretation Scenario B



Cluster A

Consisted of 4 Boreholes

KH-02-17

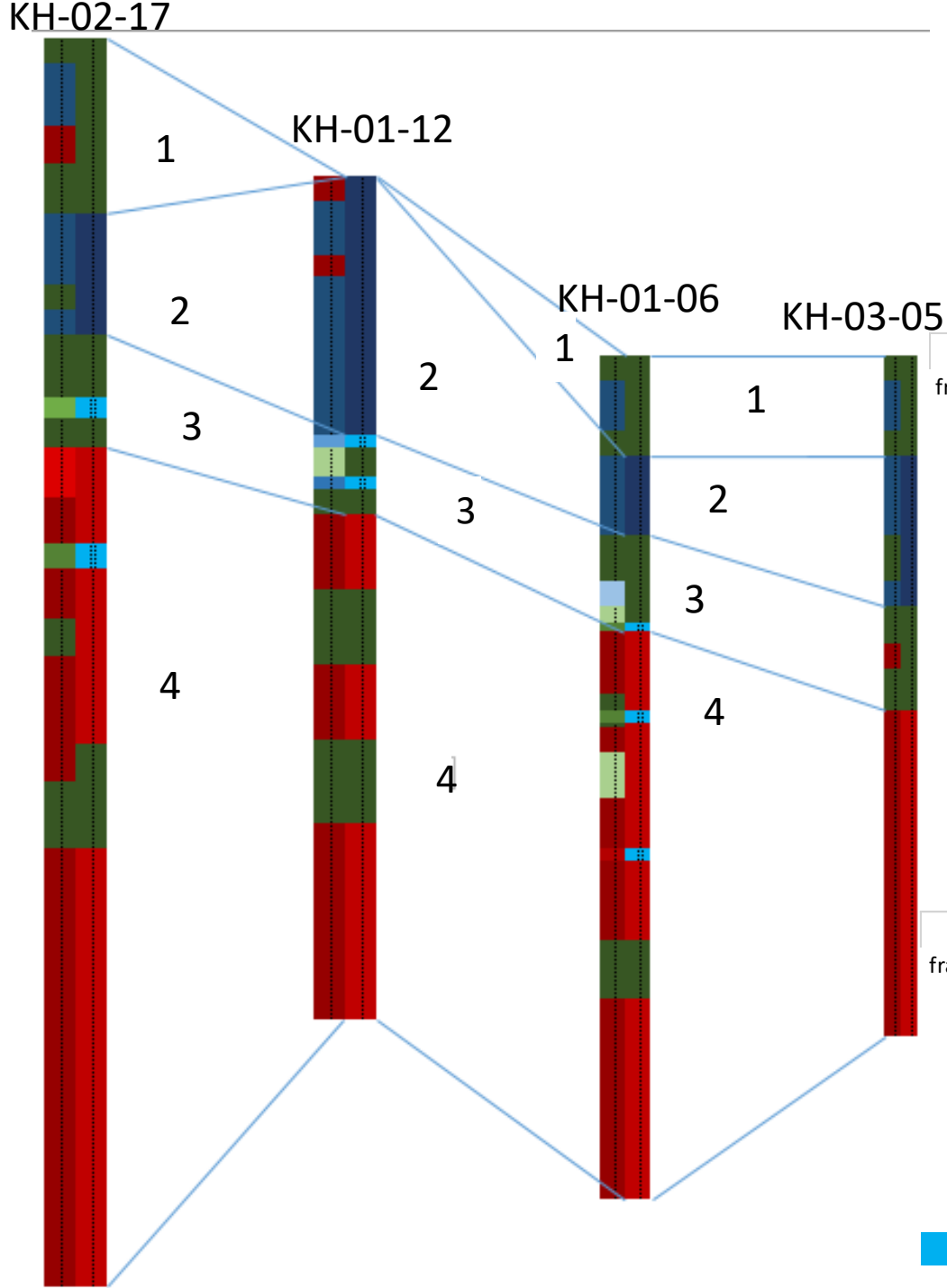
KH-01-12

KH-01-06

KH-03-05

Four rock mass domains were identified in this cluster

Interpretation
scenario B.
Cluster A



The left half of each borehole represents the rock mass characteristics and flow patterns of the 5 meter domain bins, while the right half the 20 m domain bins.

Bin with minimum 5 m domain length					
fracture frequencies	exfoliation	fracture frequencies	Flow measurements	bin code	bin color
low	low		(-)	a	
low	low		inflow	b	
low	low		outflow	c	
low	low		downflow-upflow	d	
low	moderate - high		(-)	f	
low	moderate - high		inflow	g	
low	moderate - high		outflow	h	
low	moderate - high		downflow-upflow	i	
moderate - high	low		(-)	k	
moderate - high	low		inflow	l	
moderate - high	low		outflow	m	
moderate - high	low		downflow-upflow	n	
moderate - high	moderate - high		(-)	p	
moderate - high	moderate - high		inflow	q	
moderate - high	moderate - high		outflow	r	
moderate - high	moderate - high		downflow-upflow	s	

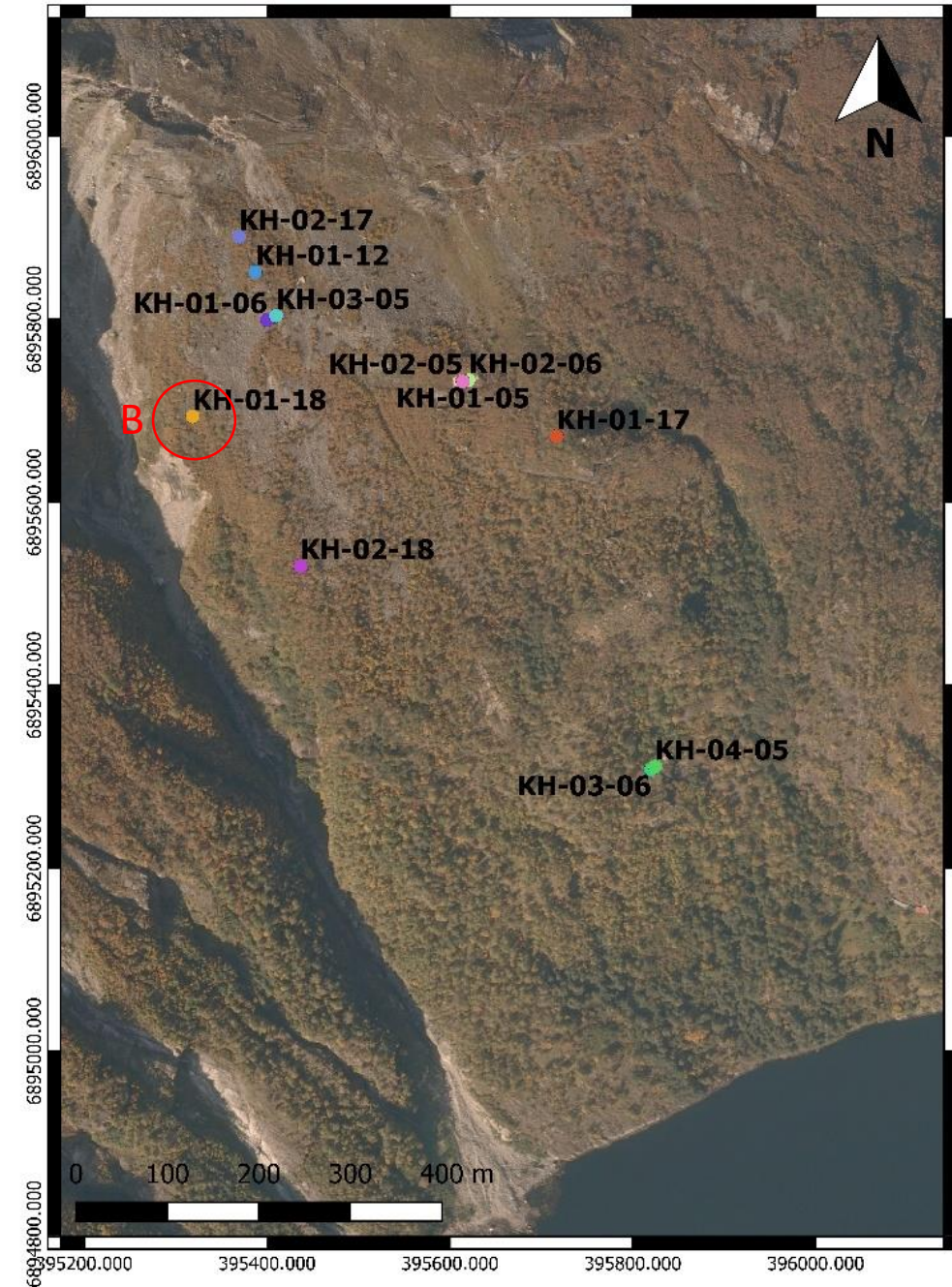
Bin with minimum 20 m domain length					
fracture frequencies	exfoliation	fracture frequencies	flow measurements	bin code	bin color
low	low		(-)	A	
low	low		inflow-outflow	B	
low	moderate - high		(-)	C	
low	moderate - high		inflow-outflow	D	
moderate - high	low		(-)	E	
moderate - high	low		inflow-outflow	F	
moderate - high	moderate - high		(-)	G	
moderate - high	moderate - high		inflow-outflow	H	
Inflow - Outflow				GQ	

Interpretation Scenario B

Cluster B

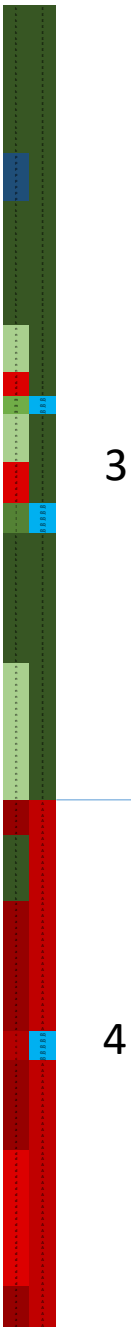
Consisted of 1 Borehole
KH-01-18

Two rock mass domains were identified in this cluster



Interpretation
scenario B.
Cluster B

KH-01-18



The left half of each borehole represents the rock mass characteristics and flow patterns of the 5 meter domain bins, while the right half the 20 m domain bins.

Bin with minimum 5 m domain length				
fracture frequencies	exfoliation	fracture frequencies	Flow measurements	bin code
low	low	(-)	a	
low	low	inflow	b	
low	low	outflow	c	
low	low	downflow-upflow	d	
low	moderate - high	(-)	f	
low	moderate - high	inflow	g	
low	moderate - high	outflow	h	
low	moderate - high	downflow-upflow	i	
moderate - high	low	(-)	k	
moderate - high	low	inflow	l	
moderate - high	low	outflow	m	
moderate - high	low	downflow-upflow	n	
moderate - high	moderate - high	(-)	p	
moderate - high	moderate - high	inflow	q	
moderate - high	moderate - high	outflow	r	
moderate - high	moderate - high	downflow-upflow	s	

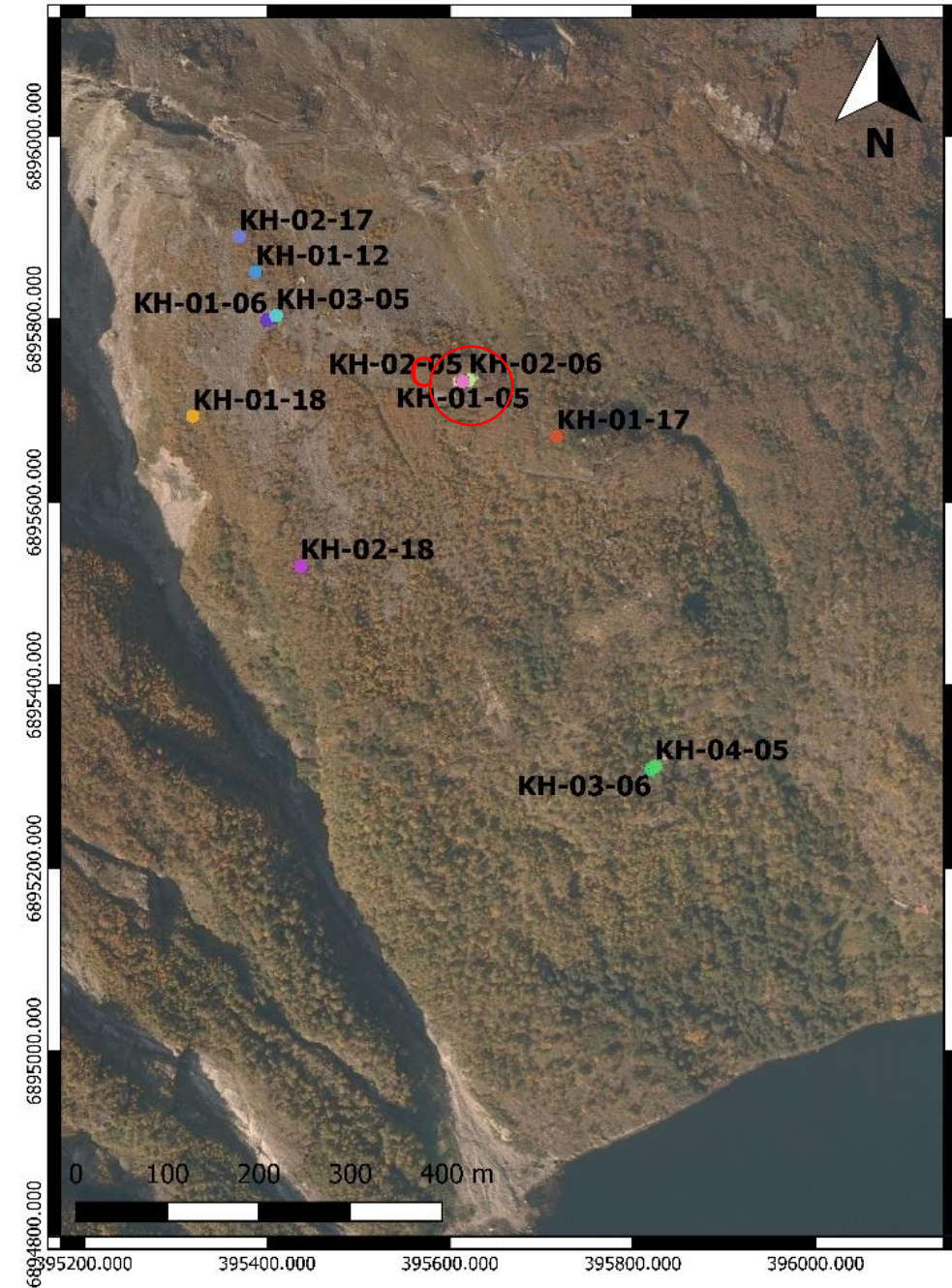
Bin with minimum 20 m domain length				
fracture frequencies	exfoliation	fracture frequencies	flow measurements	bin code
low	low	(-)	A	
low	low	inflow-outflow	B	
low	moderate - high	(-)	C	
low	moderate - high	inflow-outflow	D	
moderate - high	low	(-)	E	
moderate - high	low	inflow-outflow	F	
moderate - high	moderate - high	(-)	G	
moderate - high	moderate - high	inflow-outflow	H	
Inflow - Outflow				GQ

Interpretation Scenario B

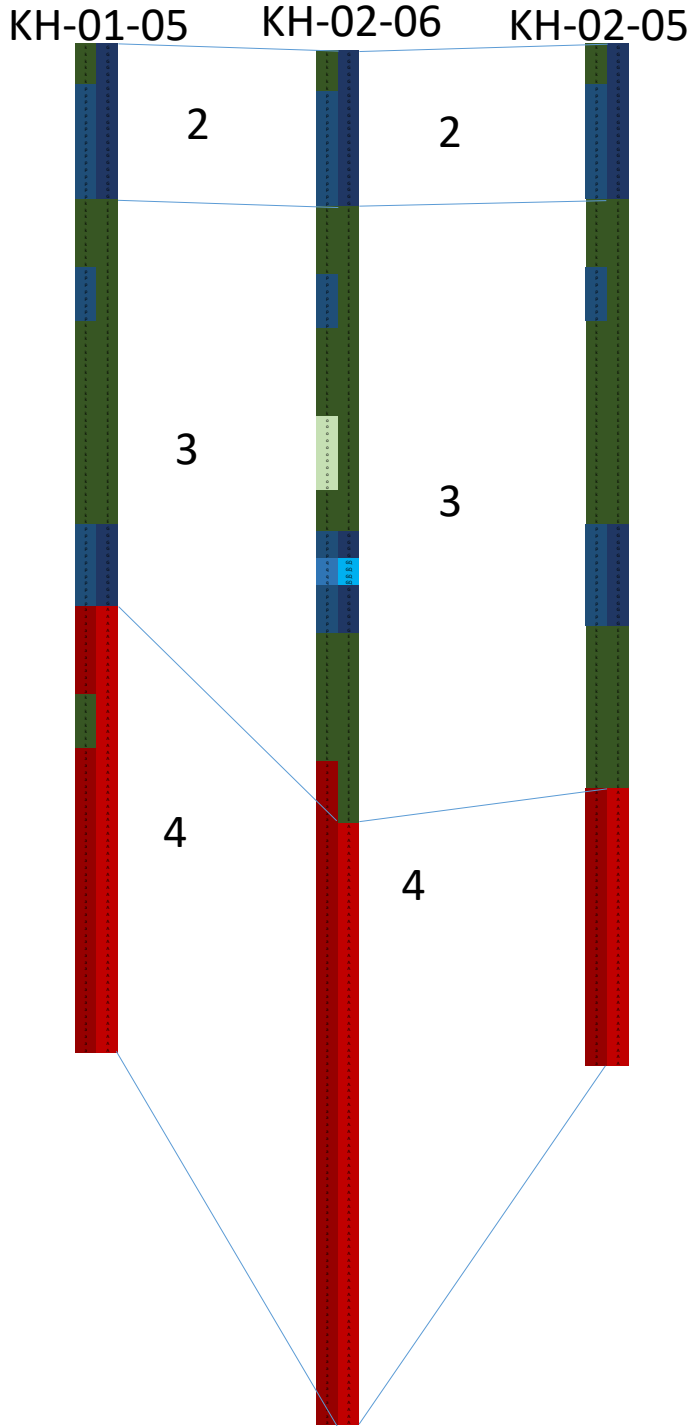
Cluster C

Consisted of 3 Borehole
KH-02-05 KH-02-06
 KH-01-05

Three rock mass domains were identified in this cluster



Interpretation
scenario B.
Cluster C

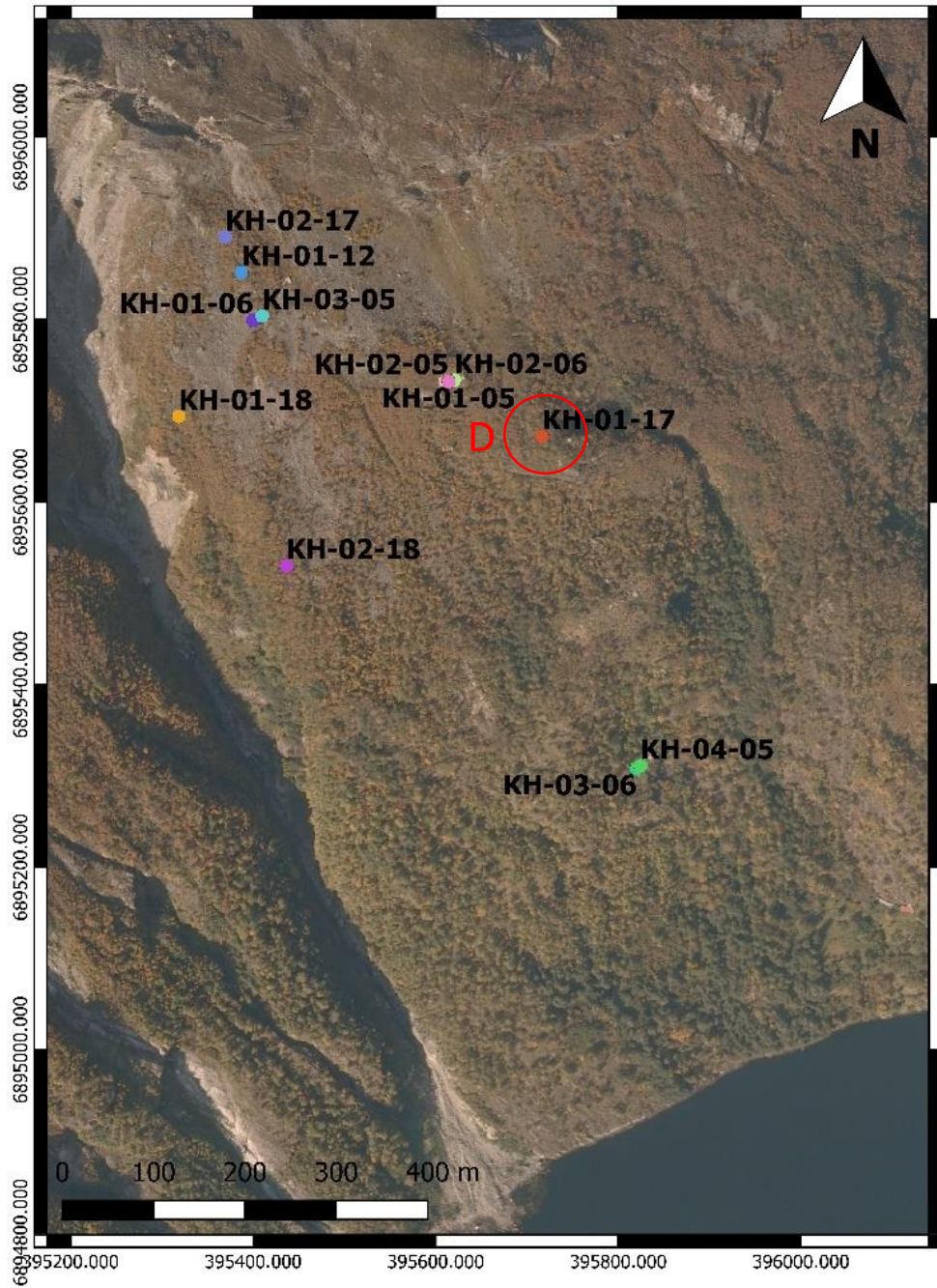


The left half of each borehole represents the rock mass characteristics and flow patterns of the 5 meter domain bins, while the right half the 20 m domain bins.

Bin with minimum 5 m domain length				bin code	bin color
fracture frequencies	exfoliation	fracture frequencies	Flow measurements		
low		low	(-)	a	
low		low	inflow	b	
low		low	outflow	c	
low		low	downflow-upflow	d	
low		moderate - high	(-)	f	
low		moderate - high	inflow	g	
low		moderate - high	outflow	h	
low		moderate - high	downflow-upflow	i	
moderate - high		low	(-)	k	
moderate - high		low	inflow	l	
moderate - high		low	outflow	m	
moderate - high		low	downflow-upflow	n	
moderate - high		moderate - high	(-)	p	
moderate - high		moderate - high	inflow	q	
moderate - high		moderate - high	outflow	r	
moderate - high		moderate - high	downflow-upflow	s	

Bin with minimum 20 m domain length				bin code	bin color
fracture frequencies	exfoliation	fracture frequencies	flow measurements		
low		low	(-)	A	
low		low	inflow-outflow	B	
low		moderate - high	(-)	C	
low		moderate - high	inflow-outflow	D	
moderate - high		low	(-)	E	
moderate - high		low	inflow-outflow	F	
moderate - high		moderate - high	(-)	G	
moderate - high		moderate - high	inflow-outflow	H	
Inflow - Outflow				GQ	

Interpretation Scenario B

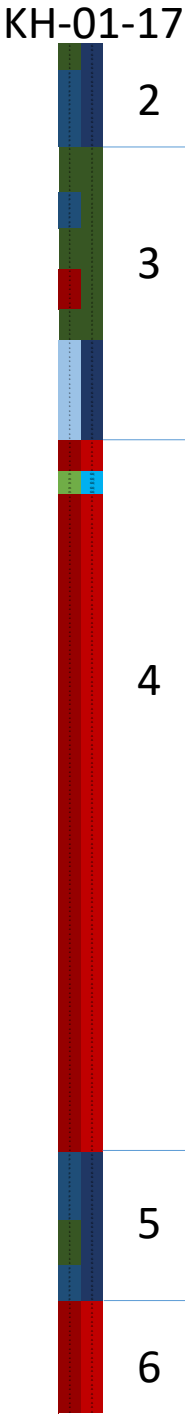


Cluster D

Consisted of 1 Borehole
KH-01-17

6 rock mass domains were identified in this cluster.
Borehole KH-01-17 is the deepest borehole and two extra domains were identified below the 4 rock mass domain trend that rest of the boreholes had.

Interpretation
scenario B.
Cluster D



The left half of each borehole represents the rock mass characteristics and flow patterns of the 5 meter domain bins, while the right half the 20 m domain bins.

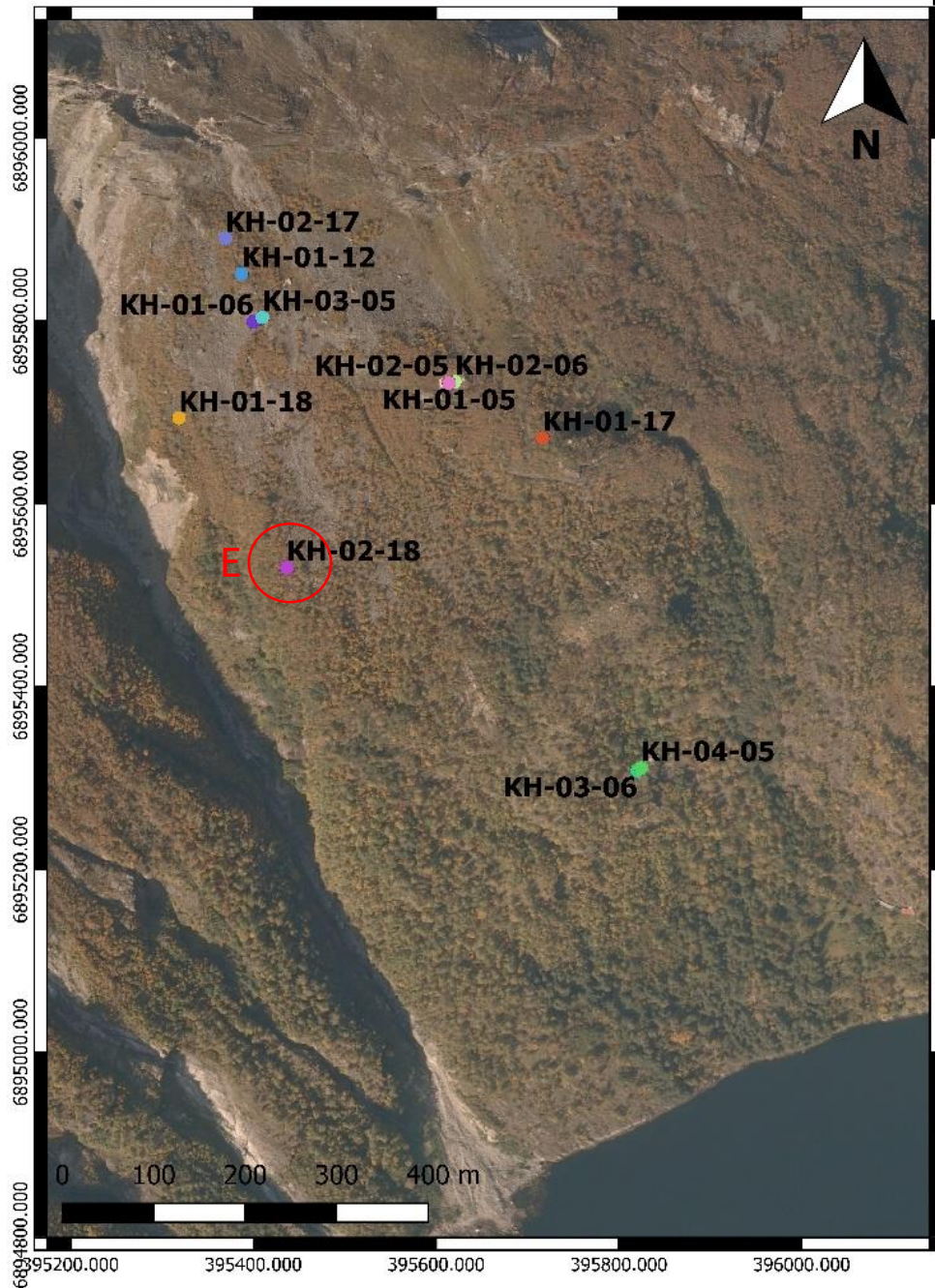
Bin with minimum 5 m domain length					bin code	bin color
fracture frequencies	exfoliation	fracture frequencies	Flow measurements			
low		low	(-)		a	
low		low	inflow		b	
low		low	outflow		c	
low		low	downflow-upflow		d	
low		moderate - high	(-)		f	
low		moderate - high	inflow		g	
low		moderate - high	outflow		h	
low		moderate - high	downflow-upflow		i	
moderate - high		low	(-)		k	
moderate - high		low	inflow		l	
moderate - high		low	outflow		m	
moderate - high		low	downflow-upflow		n	
moderate - high		moderate - high	(-)		p	
moderate - high		moderate - high	inflow		q	
moderate - high		moderate - high	outflow		r	
moderate - high		moderate - high	downflow-upflow		s	

Bin with minimum 20 m domain length					bin code	bin color
fracture frequencies	exfoliation	fracture frequencies	flow measurements			
low		low	(-)		A	
low		low	inflow-outflow		B	
low		moderate - high	(-)		C	
low		moderate - high	inflow-outflow		D	
moderate - high		low	(-)		E	
moderate - high		low	inflow-outflow		F	
moderate - high		moderate - high	(-)		G	
moderate - high		moderate - high	inflow-outflow		H	

Good quality aquifers

GQ

Interpretation Scenario B



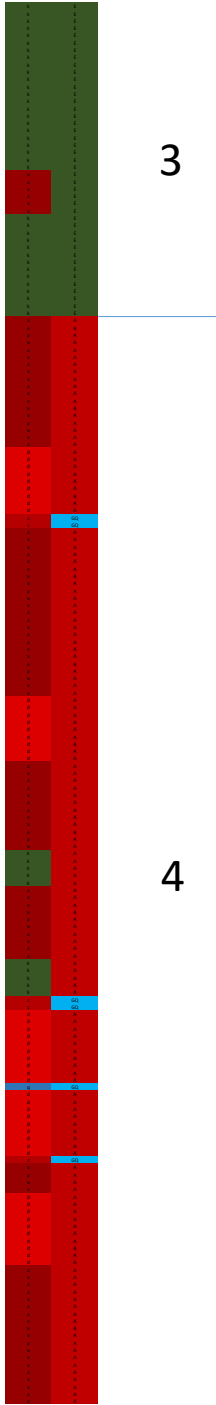
Cluster E

Consisted of 1 Borehole
KH-02-18

Two rock mass domains were identified in this cluster.

Interpretation
scenario B.
Cluster E

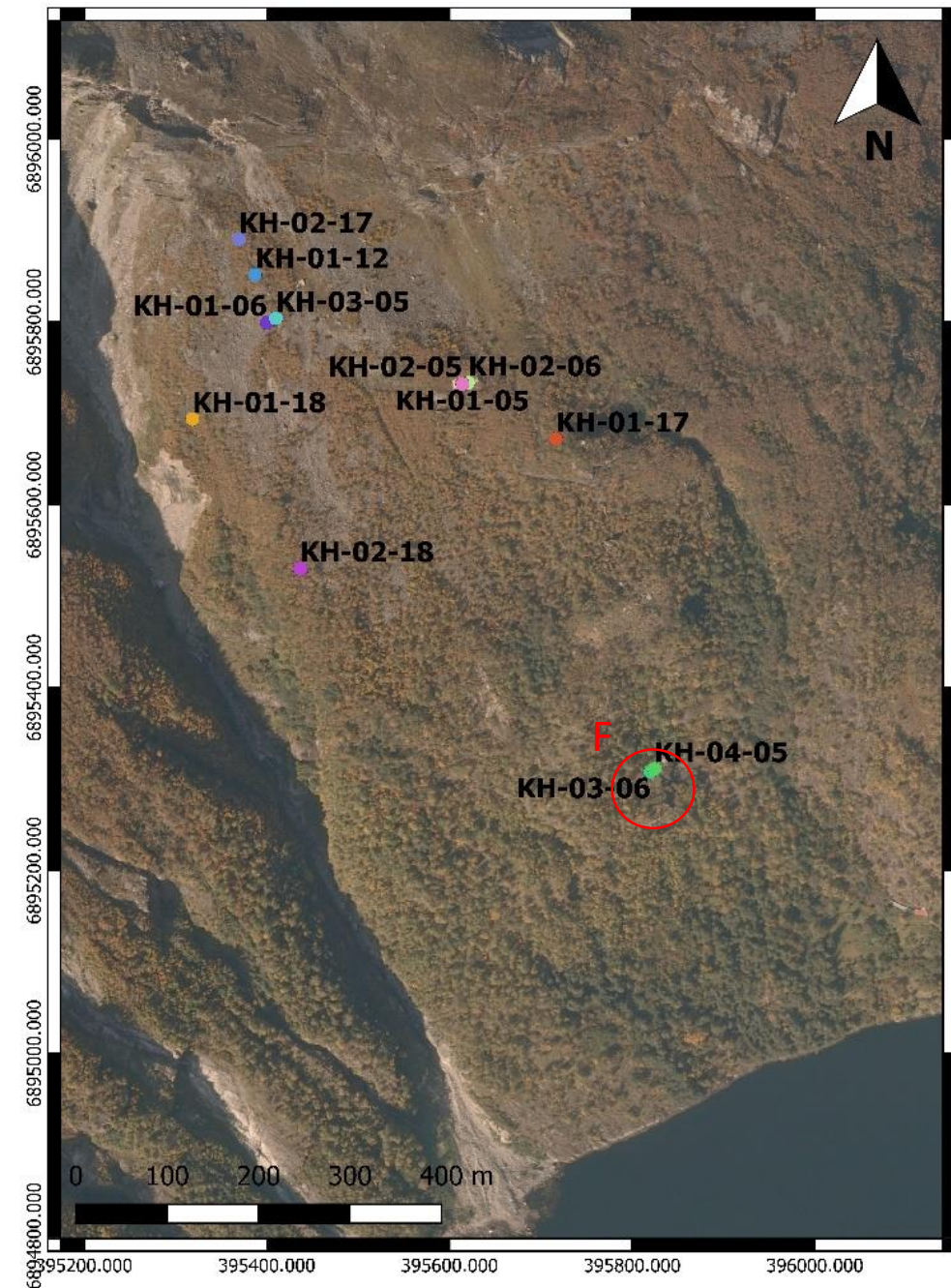
KH-02-18



The left half of each borehole represents the rock mass characteristics and flow patterns of the 5 meter domain bins, while the right half the 20 m domain bins.

Bin with minimum 5 m domain length				
fracture frequencies	exfoliation	fracture frequencies	Flow measurements	bin code
low		low	(-)	a
low		low	inflow	b
low		low	outflow	c
low		low	downflow-upflow	d
low		moderate - high	(-)	f
low		moderate - high	inflow	g
low		moderate - high	outflow	h
low		moderate - high	downflow-upflow	i
moderate - high		low	(-)	k
moderate - high		low	inflow	l
moderate - high		low	outflow	m
moderate - high		low	downflow-upflow	n
moderate - high		moderate - high	(-)	p
moderate - high		moderate - high	inflow	q
moderate - high		moderate - high	outflow	r
moderate - high		moderate - high	downflow-upflow	s
Bin with minimum 20 m domain length				
fracture frequencies	exfoliation	fracture frequencies	flow measurements	bin code
low		low	(-)	A
low		low	inflow-outflow	B
low		moderate - high	(-)	C
low		moderate - high	inflow-outflow	D
moderate - high		low	(-)	E
moderate - high		low	inflow-outflow	F
moderate - high		moderate - high	(-)	G
moderate - high		moderate - high	inflow-outflow	H
Inflow - Outflow				GQ

Interpretation Scenario B

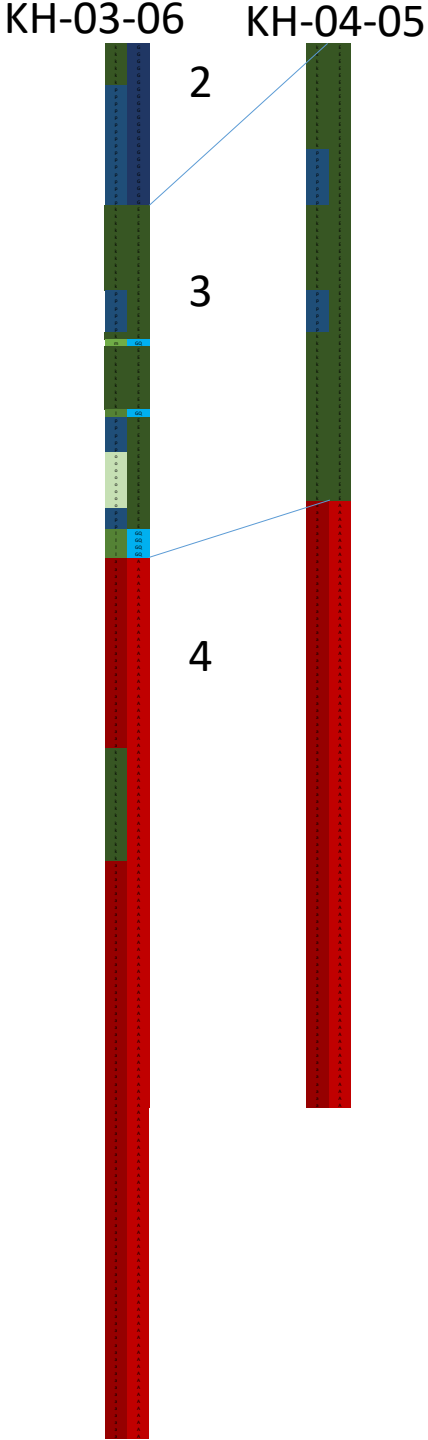


Cluster F

Consisted of 2 Boreholes
KH-03-06 KH-04-05

Two rock mass domains were identified in this cluster

Interpretation
scenario B.
Cluster F



The left half of each borehole represents the rock mass characteristics and flow patterns of the 5 meter domain bins, while the right half the 20 m domain bins.

Bin with minimum 5 m domain length					
fracture frequencies	exfoliation	fracture frequencies	Flow measurements	bin code	bin color
low		low	(-)	a	
low		low	inflow	b	
low		low	outflow	c	
low		low	downflow-upflow	d	
low		moderate - high	(-)	f	
low		moderate - high	inflow	g	
low		moderate - high	outflow	h	
low		moderate - high	downflow-upflow	i	
moderate - high		low	(-)	k	
moderate - high		low	inflow	l	
moderate - high		low	outflow	m	
moderate - high		low	downflow-upflow	n	
moderate - high		moderate - high	(-)	p	
moderate - high		moderate - high	inflow	q	
moderate - high		moderate - high	outflow	r	
moderate - high		moderate - high	downflow-upflow	s	

Bin with minimum 20 m domain length					
fracture frequencies	exfoliation	fracture frequencies	flow measurements	bin code	bin color
low		low	(-)	A	
low		low	inflow-outflow	B	
low		moderate - high	(-)	C	
low		moderate - high	inflow-outflow	D	
moderate - high		low	(-)	E	
moderate - high		low	inflow-outflow	F	
moderate - high		moderate - high	(-)	G	
moderate - high		moderate - high	inflow-outflow	H	
Inflow - Outflow				GQ	

Rock mass domain characteristics of Interpretation scenario B

- **Domain 1 – top domain**

Moderate-high fracture frequency /m

Limited number of exfoliation fractures

- **Domain 2**

Both moderate – high fracture frequency/m and exfoliation fractures

- **Domain 3**

Moderate-high fracture frequency/m

Limited number of exfoliation fractures

Subdomains of Inflow - Outflow

In some occasions the lower part of the domain had moderate to high exfoliation fracture frequency for 15m length. In this scenario this part was not considered as a separate domain as in Scenario A where it was considered as domain 3 intermediate.

- **Domain 4**

Both low fracture frequency/m and exfoliation fractures-probably aquitards-seals

Subdomains with Inflow - Outflow

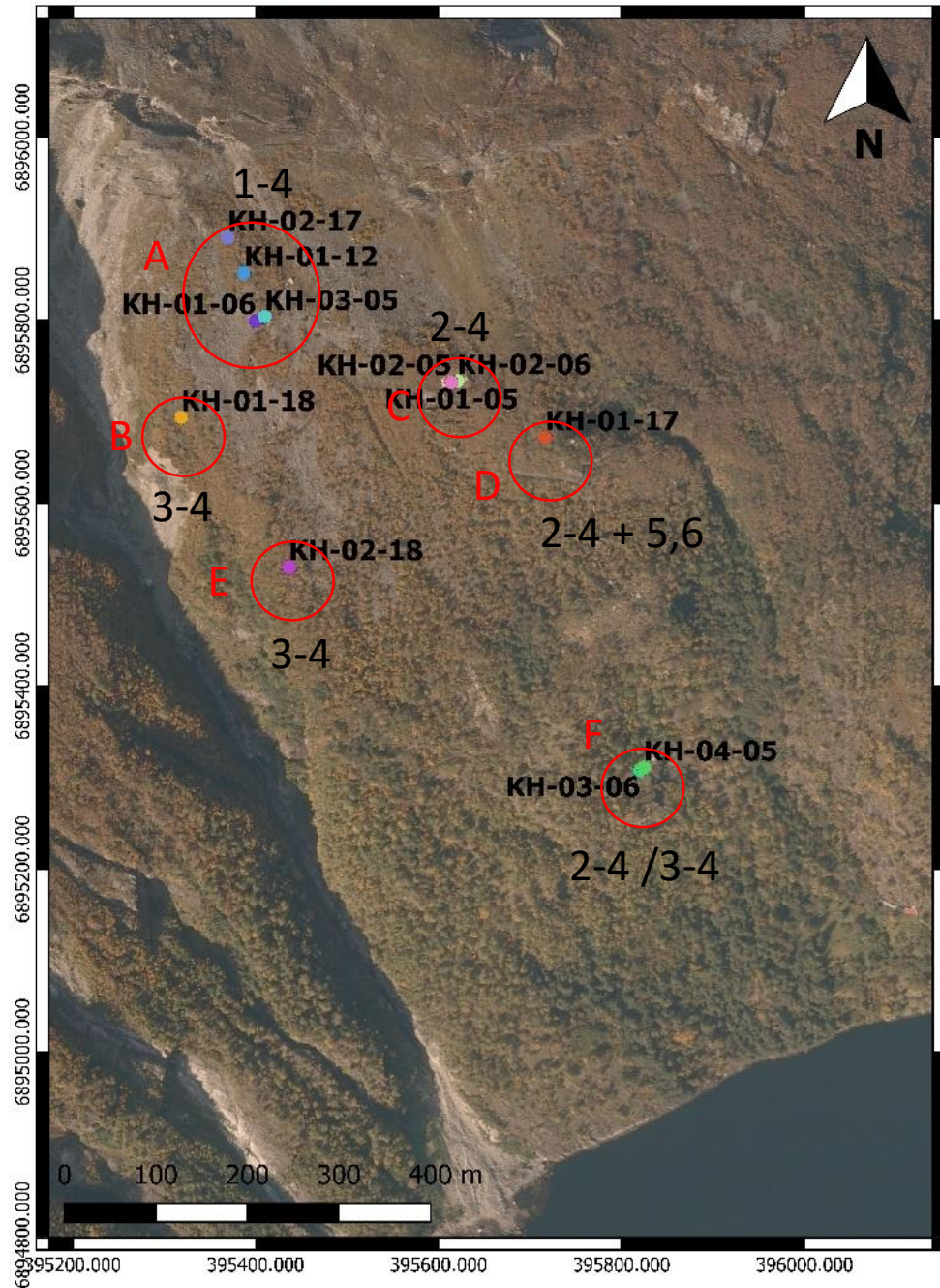
In some boreholes has subdomains of few to 18-25 meters while in others these subdomains do not exist.

- **Domains 5-6**

They appear only at the deepest borehole KH-01-17.

domain 5 has both high fracture frequency/m and exfoliation fractures while domain 6 is unfractured rock.

Clusters



- Based on common rock mass domain numbering and the observed characteristics, the clusters appear to have the domains below (shown also on the map on the left).

Cluster A: domains 1-4

Cluster B: domains 3-4

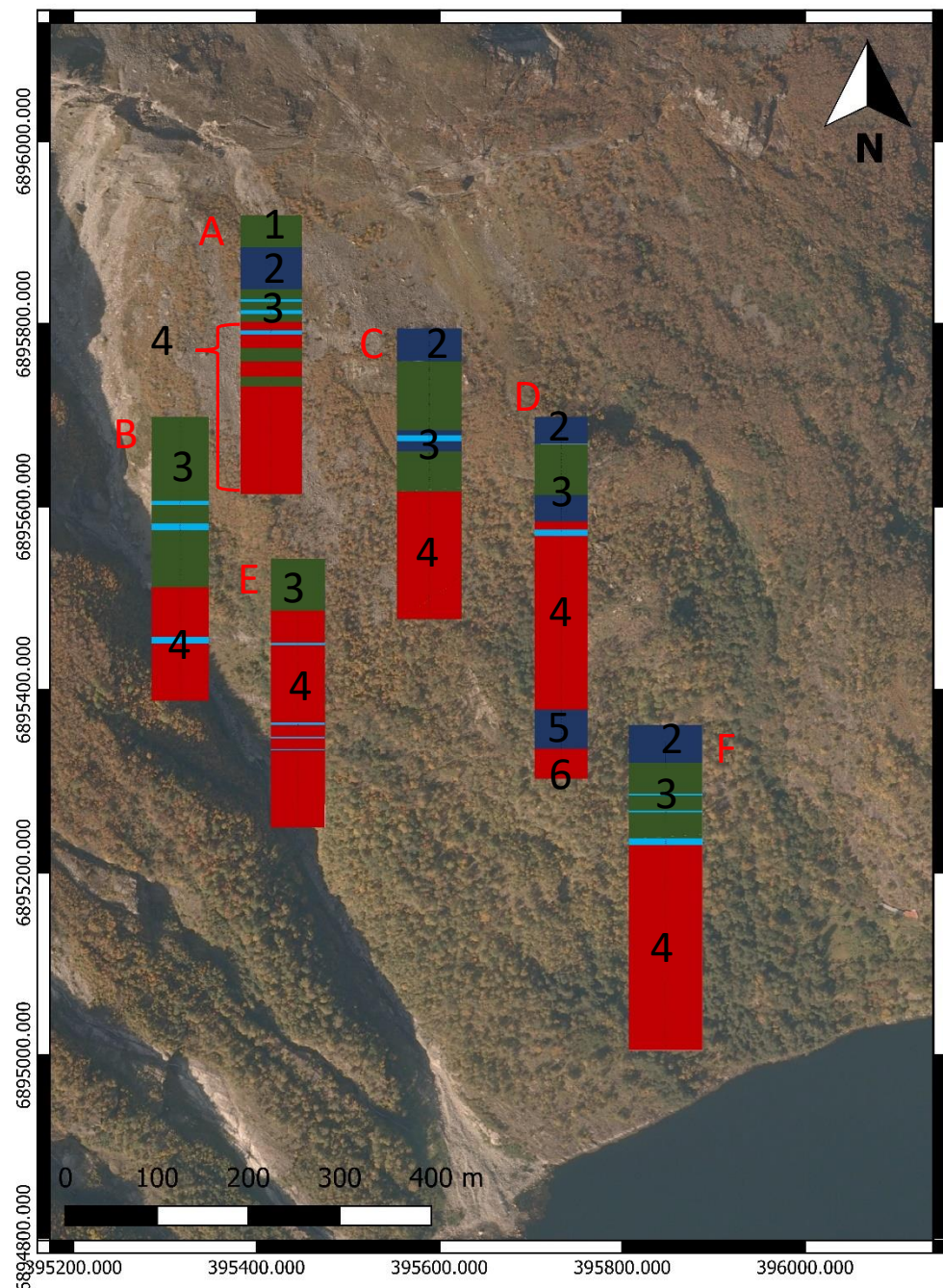
Cluster C: domains 2-4

Cluster D: domains 2-4 +5,6

Cluster E: domains 3-4

Cluster F: domains 2-4

Interpretation Scenario B



Clusters

Cluster A: domains 1-4

Cluster B: domains 3-4

Cluster C: domains 2-4

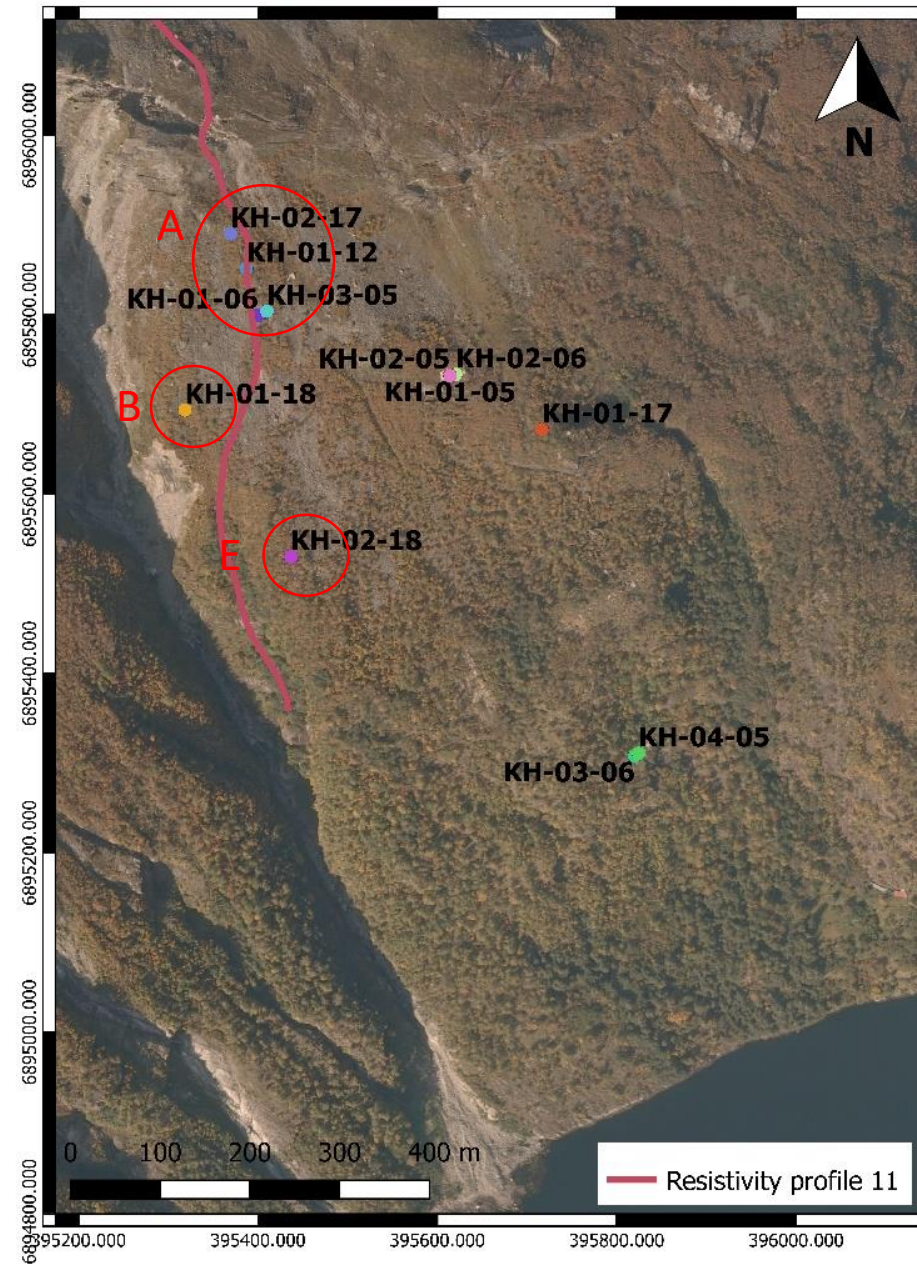
Cluster D: domains 2-4 +5,6

Cluster E: domains 3-4

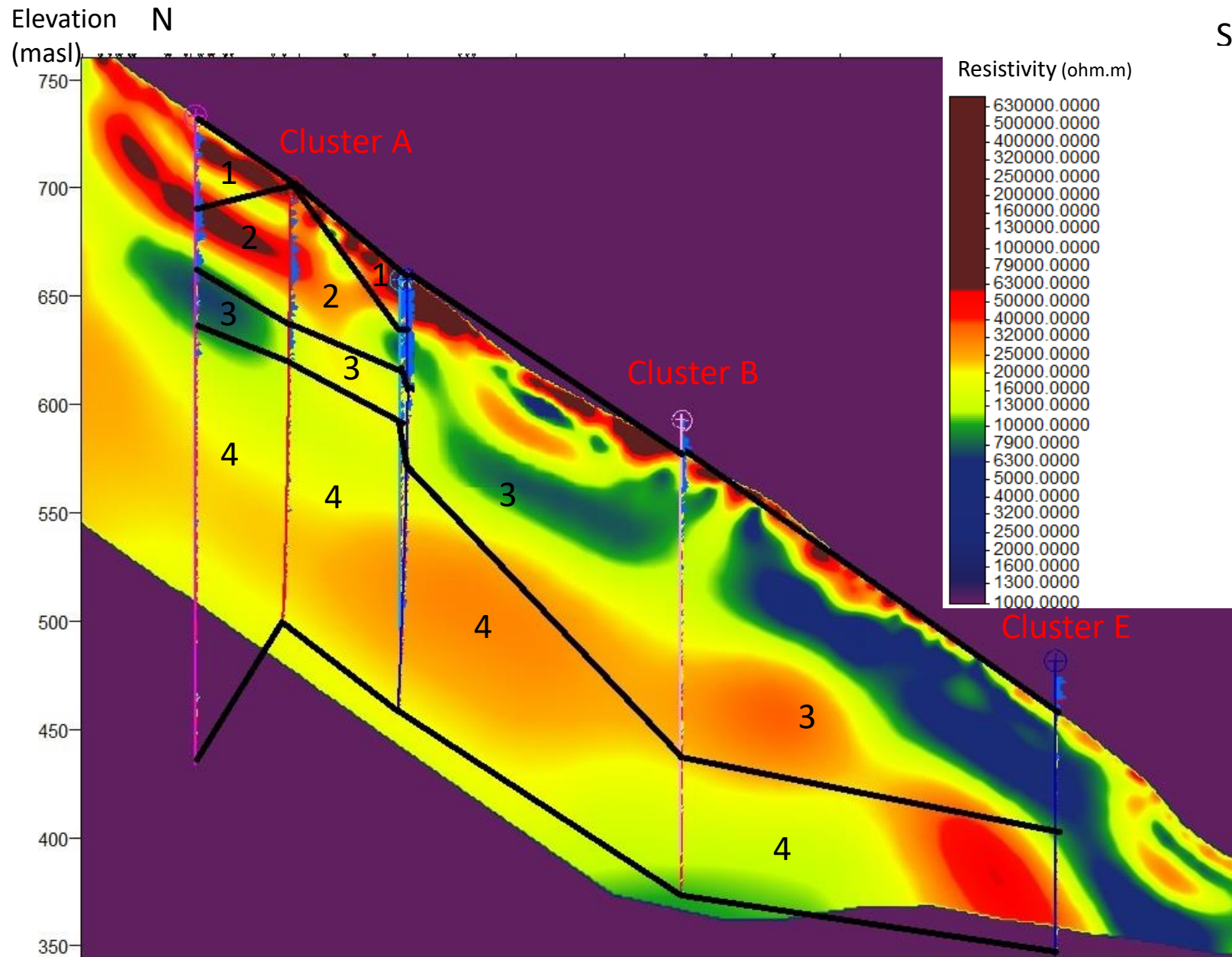
Cluster F: domains 2-4

Bin with minimum 20 m domain length				bin code	bin color
fracture frequencies	exfoliation	fracture frequencies	flow measurements		
low		low	(-)	A	
low		low	inflow-outflow	B	
low		moderate - high	(-)	C	
low		moderate - high	inflow-outflow	D	
moderate - high		low	(-)	E	
moderate - high		low	inflow-outflow	F	
moderate - high		moderate - high	(-)	G	
moderate - high		moderate - high	inflow-outflow	H	
Inflow - Outflow				GQ	

Comparison of the rock mass domains in scenario B with ERT profiles



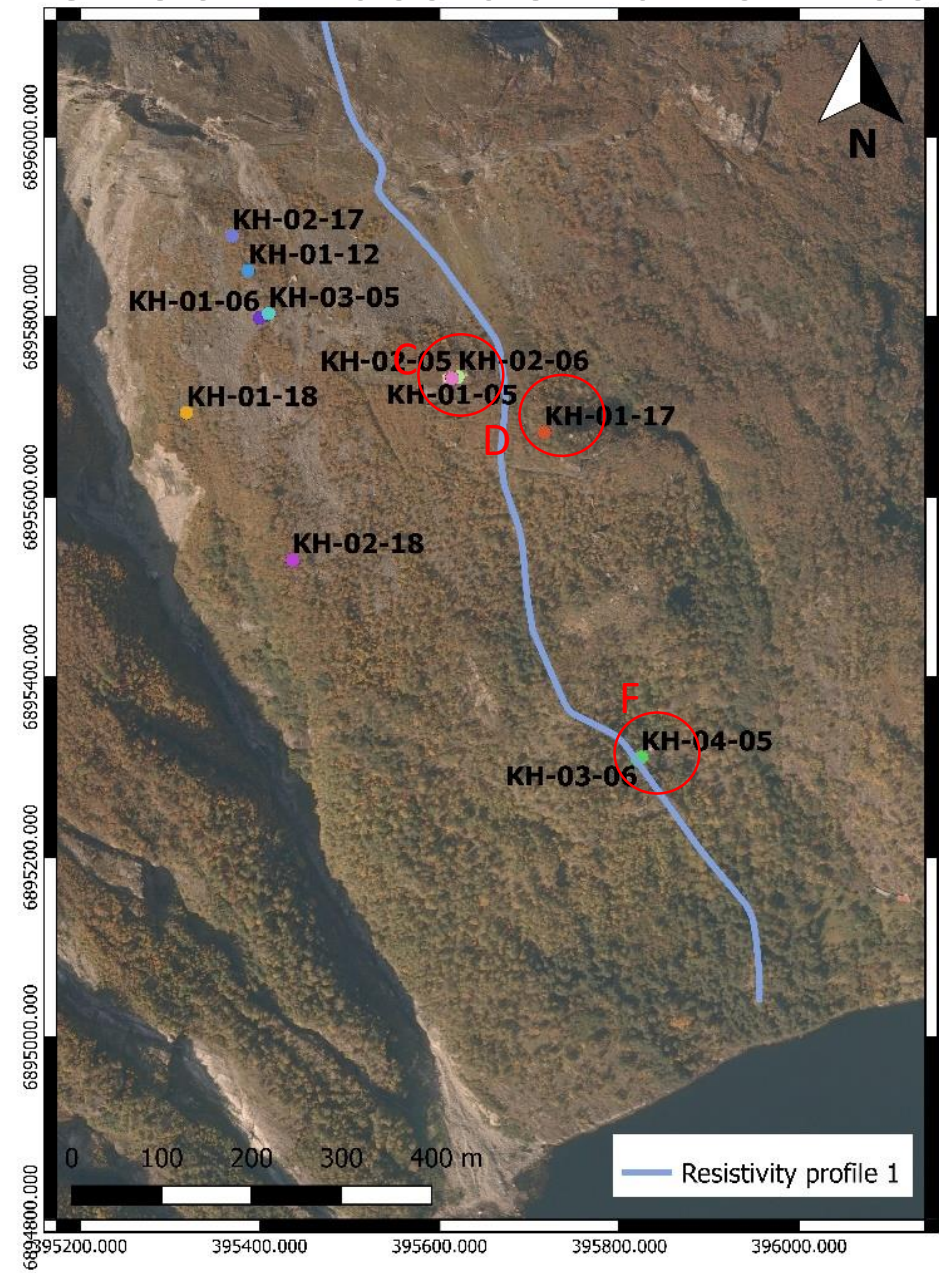
Comparison of the rock mass domains in scenario B with ERT profiles



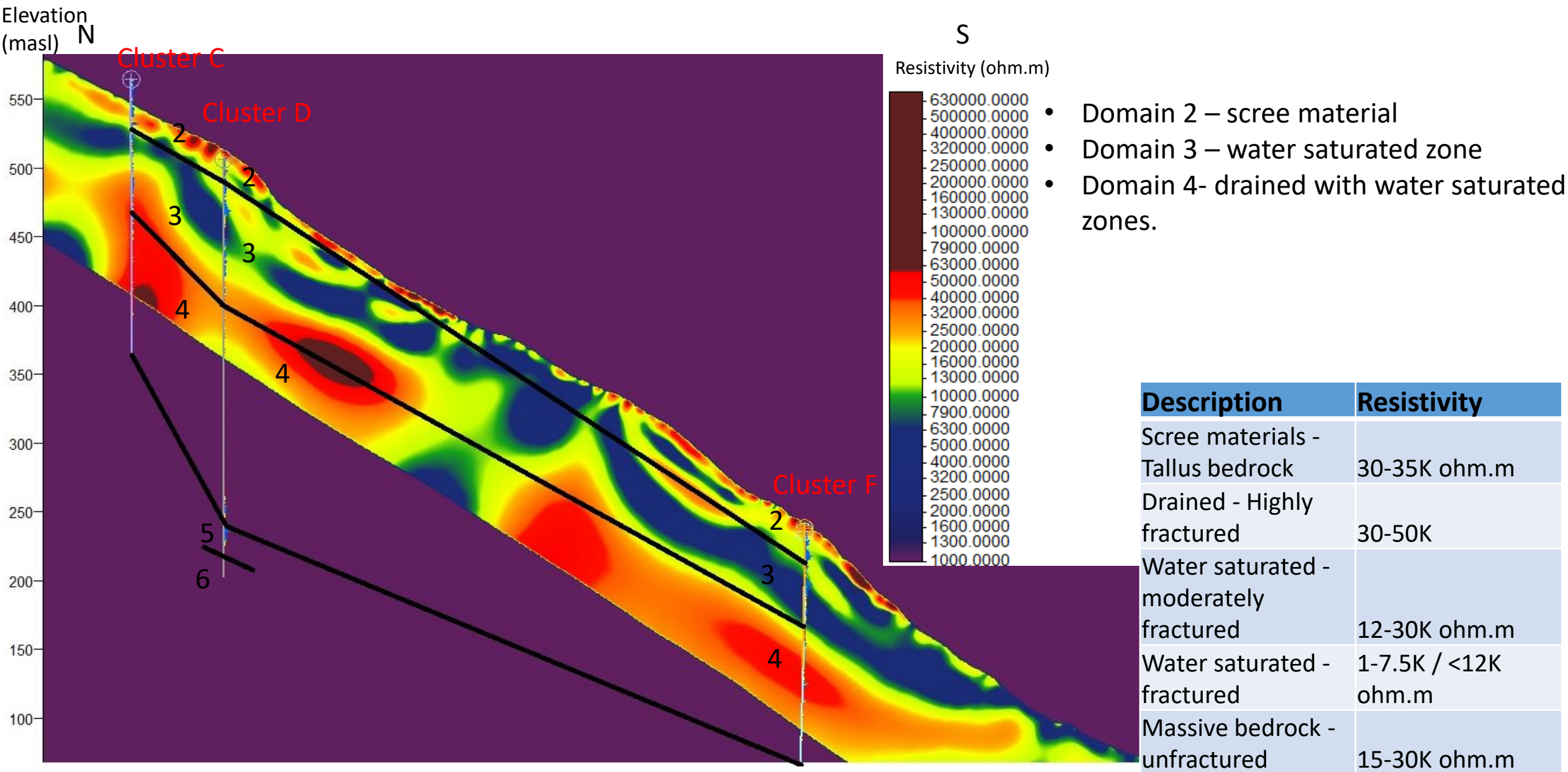
- Domain 1 – scree material
- Domain 2 – drained
- Domain 3 – water saturated zone
- Domain 4 – mostly massive unfractured rock

Description	Resistivity
Scree materials - Tallus bedrock	30-35K ohm.m
Drained - Highly fractured	30-50K
Water saturated - moderately fractured	12-30K ohm.m
Water saturated - fractured	1-7.5K / <12K ohm.m
Massive bedrock - unfractured	15-30K ohm.m

Comparison of the rock mass domains in scenario B with ERT profiles



Comparison of the rock mass domains in scenario B with ERT profiles



Discussions - Conclusions

- The zonal correction factor (zcf) is preferred to the general correction factor (gcf) since it reflects better the variation of fracture frequency with depth (slides 11-12).
- Within biotite, granite gneisses and pegmatite, aquitards seem to prevail (slide 20). Apart from this, no other connection is clear between lithology and aquifer potential.
- For the boreholes drilled in 2005 no netflow measurements were conducted. Therefore, there is no indication (light blue color) of inflow-outflow at these specific boreholes in the clusters.
- Two interpretation scenarios of the rock mass domains are proposed based on the rock characteristics and flow patterns. Both of the interpretations indicate more or less the existence of four main rock mass domains.
- Both of the interpretations of the rock mass domains seem to correlate quite well with the ERT profiles.



NVE

Norges vassdrags- og energidirektorat

Middelthuns gate 29
Postboks 5091 Majorstuen
0301 Oslo
Telefon: (+47) 22 95 95 95